Thesis submitted in fulfillment of the requirements for the degree of Doctor (PhD) in Engineering and Architecture from the Public University of Navarre

Evaluation of the improvement of streamflow prediction through the assimilation of remotely sensed soil moisture observations

Javier Loizu Maeztu

May 2017

Supervisors:

Jesús Álvarez Mozos

Javier Casalí Sarasibar

upna
Universidad Pública de Navarra
Nafarroako Unibertsitate Publikoa

upna
Universidad Pública de Navarra
Nafarroako Unibertsitate Publikoa

ACKNOWLEDGEMENTS

First, I would like to thank my supervisors professor Jesús Álvarez Mozos and professor Javier Casalí Sarasibar from the Projects and Rural Engineering Department of the Public University of Navarre for helping and advising me through this challenging work. I want to thank them for helping me with the technical challenges, for being patient and supportive, and for listening to me in the moments of difficulties and dejection.

I also want to thank all my colleagues at the Laboratory of Hydraulics, for all the laughs we shared during the morning's coffee break, and for putting up with me in times of stress.

Furthermore, I am very grateful to all the team of the Hydrology Group of the Research Institute for Geo-Hydrological protection of the *Consiglio Nazionale delle Ricerche (CNR)*, from Perugia. I want to thank Luca Brocca, Angelica Tarpanelli, Christian Massari, Luca Ciabatta, Stefania Camici, Pamela Maccioni, Silvia Barbetta, and Tommaso Moramarco for kindly sharing their knowledge with me during three months. They all cared about me having a nice experience in Perugia, Assisi or in Amatrice. Thank to you all, I will always keep the best memories of my Italian experience, plenty of *Pasta alla Norcina* and *Tortas al Testo*.

Likewise, I want to thank my professors at the University of Melbourne Andrew Western and Dongryeol Ryu, for inspiring this PhD thesis. Andrew Western for delivering a very ingesting lectures on soil moisture spatial behavior, and to Dongryeol for making Data Analysis Tools my favorite subject of the Environmental Engineering Master.

Of course, I would also like to acknowledge my parents for having always supported me.

Moreover, I want to thank so much Irantzu for being so supportive and patient with me during these years.

This PhD thesis was partially funded by the Spanish Ministry of Science and Innovation (Project CGL2011-24336), the Spanish Ministry of Innovation and Competitiveness (Project CGL2015-64284-C2-1-R MINECO/FEDER) and mainly by the Public University of Navarre through a pre-doctorate research scholarship to the author.

TABLE OF CONTENTS

LIST OF ACRONYMS

1D-Var	One dimensional variational data assimilation
ARG	Arga catchment
ASCAT	Advanced SCATterometer
BEC	Barcelona Expert Center
BF	Baseflow
BP	Best performing parameter set
CAL	Calibration
CATHY	CATchment Hydrology model
CDF	Cumulative Distribution Function
CID	Cidacos catchment
CNR	*Consiglio Nazionale delle Ricerche*
CON	CONventional method
DA	Data Assimilation
DisPATCh	Disaggregation based on Physical and Theoretical Scale Change
DoE	Design of Experiment
EC-JRC	European Commission- Joint Research Center
EE	Elementary effects
EKF	Extended Kalman Filter
EnKF	Ensemble Kalman Filter
ESA	European Space Agency
ESA-CCI	European Space Agency – Climate Change Initiative
ET	Evapotranspiration
EUMETSAT	European Organisation for the Exploitation of Meteorological Satellites
GIUH	Geomorphological Instantaneous Unit Hydrograph
GNSS-R	Global Navigation Satellite Signal-Reflectometry
IP	Initial Points
KF	Kalman Filtering
LAI	Leaf Area Index
LR	Linear Regression technique
LSM	Land Surface Models
LST	Land Surface Temperature

LWR	Long Wave Radiation
MCMC	Markov-Chain Monte-Carlo
MESH	Modelilisation Environmentale-Surface et Hydrologie model
MetOP-A/B/C	Meteorological Operation satellites
MIRAS	Microwave Imaging Radiometer with Aperture Synthesis
MISDc	Modello Idrologico Semi Distribuito in continuo
MOAT	Sampling method for Morris Method (MoM)
MODIS	Moderate Resolution Imaging Spectroradiometer
MoM	Morris sensitivity analysis method
MSPW	Multi-Start Powell Method for model calibration
NIR	Near-infrared
NDVI	Normalized Difference Vegetation Index
NRCS-USDA	Natural Resources Conservation Service - Unites States Department of Agriculture
NRMSE	Normalized Root Mean Square Error
NRT	Near-Real-Time
NSE	Nash and Sutcliffe efficiency
OAT	One-at-a-time
OL	Open Loop run
OP	Optimal parameter values
PEST	Parameter Estimation Software
PF	Particle Filtering
PM	Powell Method
REMEDHUS	Red de Medidas de Humedad del Suelo
RFI	Radio frequency Interference
RMSE	Root Mean Square Error
RND	RaNDom method
RR	Rainfall-Runoff
RT	Re-scaling technique
RZ-SM	Root Zone Soil Moisture
SA	Sensitivity analysis
SAC-SMA	Sacramento Soil Moisture Accounting model
SAR	Synthetic Aperture Radar
SCAN	Soil Climate Analysis Network

SCS	Soil Conservation Service
SM	Soil Moisture
SMOS	Soil Moisture Ocean Salinity Earth Explorer mission
SOBOL	Sampling method for Sobol Sensitivity Analysis method
SoM	Sobol sensitivity analysis method
SR	Surface Runoff
SSM	Surface soil moisture
STD	STandard Deviation
SVAT	Soil-Vegetation-Atmosphere Transfer scheme
SWB	Soil Water Balance model
SWI	Soil Water Index
SZ	Surface Zone
TC	Triple Collocation
TEJ	Tejeria catchment
TI	Topographic Index
TIR	Thermal Infra-red
TOPLATS	TOPMODEL-based Land-Atmosphere Transfer Scheme
TS	Transmission Zone
TU-Wien	*Technische Universität Wien*
TWS	Terrestrial Water Storage
TZ-SM	Transmission Zone Soil Moisture
VAL	VALidation
VI	Vegetation Indices
VIC	Variable Infiltration Capacity model
VIR/IR	Visible infra-red
VM	Variance Matching technique
W3	World Wide Water model
WTD	Water Table Depth

PARAMETER GLOSSARY

Symbol	Parameter details
μ, μ^*	Morris method sensitivity
B	Brooks-Corey Pore Size distribution Index
bs	Bare soils
E	Evaporation
Eff_{OL}	Efficiency of data assimilation compared to open loop run
Eff_{VAL}	Efficiency of data assimilation compared to validation run
ensk	Ensemble skill
ensp	Ensemble spread
f	Hydraulic conductivity decay
g	Drainage
G	Soil heat flux
G_k	Kalman gain
H	Latent heat flux
I	Infiltration
K_c	Correction coefficient for potential evapotranspiration
K_s	Surface saturated hydraulic conductivity
mse	Ensemble mean square error
P	Ensemble background error covariance matrix
P_n	Net precipitation
Pr	Precipitation
Q_0	Subsurface flow at complete saturation
q_{bf}	Baseflow
q_{ie}	Infiltration excess runoff
q_s	Saturation excess runoff
r_{min}	First soil resistance parameter
R_n	Net radiation
S	Potential maximum soil moisture retention
S_i	Individual parameter sensitivity in Sobol method
S_{TI}	Sobol Total Order interaction
T	Parameter controlling SWI oscillation
U_k	Gain updating term for SWI calculation
vg	Vegetated soil
w	Capillary rise
wc	Wet canopy
W_{max}	Maximum water capacity of the soil layer
WTD_m	Water table depth mean value
WTD_{SD}	Water table depth standard deviation

Z	Ensemble representation of the observation error covariance matrix
α	Parameter of the relationship between modeled SM and the S of the SCS-CN method
η	Lag-area relationship parameter
θ	Soil moisture content
θ_m	Soil moisture mean value
θ_r	Residual soil moisture content
θ_s	Saturated soil moisture
θ_{SD}	Soil Moisture standard deviation
λ	Initial abstraction coefficient
ν	Parameter controlling the fraction of drainage that transforms into subsurface runoff
σ	Morris method interaction
ψ_c	Bubbling pressure

LIST OF FIGURES

LIST OF TABLES

ABSTRACT

Hydrological catchment models are useful tools that provide relevant information for the understanding of the water cycle at different time and spatial scales. Models are widely used for flood prediction and awareness, evaluation of environmental impacts or water resources management purposes. They usually incorporate some type of soil moisture modeling and differently defined soil layers, since soil moisture is a key component defining the partition of rainfall into infiltration and runoff. In order to improve the accuracy of soil moisture simulations, Earth observation satellites have emerged as valuable information sources. Some sensors provide surface soil moisture products that can be useful for improving streamflow simulation through its integration into hydrological models. Observed surface soil moisture data can be integrated into models using different types of data assimilation techniques, which include variants of the Kalman Filter, being the Ensemble Kalman Filter (EnKF) the most commonly used for hydrological applications.

This PhD thesis has as its main objective to evaluate whether the assimilation of remotely sensed surface soil moisture data into hydrological models can improve their streamflow prediction. This general objective includes the evaluation of data assimilation with models of different spatial configuration (i.e. lumped, semi-distributed or fully distributed), the use of L-band and C-band microwave remote sensing observations (i.e., ASCAT and SMOS) as assimilation data sources, the use of SSM downscaled products, the application of different re-scaling techniques used for matching observations to simulated surface soil moisture, or the valuation of different observation error estimations. This PhD thesis also aims to evaluate TOPMODEL-based Land Surface-Atmosphere Transfer Scheme (TOPLATS) as a streamflow simulation tool in Mediterranean catchments. This includes performing a sensitivity analysis of the model, with two different methods, and performing model calibration by means of an optimization algorithm.

To achieve these objectives the thesis was structured in three separate studies. On the first study, the statistical mode (semi-distributed) of TOPLATS model was applied on three mediterranean catchments of different size, topography, land use and climate. A sensitivity analysis with two different methods was then performed. The model was afterwards calibrated with an optimization algorithm and a multi-start approach. Hourly and daily time-step simulation results were obtained by applying conventional and random calibration and validation period selection approaches. On the second study, a lumped simple conceptual model (MISDc) and the statistical mode of TOPLATS were used for ASCAT surface soil moisture assimilation in order to evaluate its impact on streamflow simulation. This study was performed in two catchments of similar size, one located in Italy and the other one in Spain. This study also evaluated the influence of the re-scaling technique applied to the observed

data, and also evaluated the influence of the error attributed to the observations on the assimilation results. The EnKF was the assimilation method applied, and discrete ASCAT observations were filtered, transforming them into a Soil Water Index (SWI), prior to their re-scaling. Finally, on the third study, the benefits of assimilating a downscaled product, obtained from SMOS and MODIS and with 1 km spatial resolution, into the fully distributed mode of TOPLATS were evaluated. This study also evaluated the influence of assimilating only over specific areas (i.e. excluding from the assimilation forested areas or areas with steep relief, where SMOS data quality is expected to be lower). This study was performed in a semi-arid catchment located in northern Spain.

This thesis determined that TOPLATS is a suitable model to simulate streamflow in complex climate conditions such as Mediterranean climate catchments. Positive results, in terms of efficiency on simulated total volume were achieved in both hourly and daily time-step simulations. These significant results were obtained after a detailed sensitivity analysis to identify the most influential parameters, and after the application of an intense calibration method based on an optimization algorithm search. Some difficulties were found due to different weather variability contained on calibration and validation periods in one of the catchments. To overcome this issue, calibration data was randomly selected, in such a way that enough wet periods would be contained on it. This notoriously improved streamflow simulated volume results. Furthermore, the assimilation of ASCAT SSM data into a lumped and into a semi-distributed model improved the streamflow simulation accuracy in most of the studied cases. Only on a very well calibrated catchment/model combination no improvement was achieved. The best combination of satellite error estimation and re-scaling method combinations offered efficiency increases in the remaining cases. Assimilation of a downscaled SSM product, derived from SMOS and MODIS also improved distributed modeling of streamflow, when the assimilation was performed over cultivated or flat areas.

Successful application of hydrological catchment models rely on the proper identification of influential parameters, the adequate calibration strategy and the adequate calibration data selection. Afterwards, SSM remotely sensed observations are a valuable source that can improve streamflow simulations in models of different spatial representation of the catchment. This is not a direct and simple task, as it depends on the satellite error estimation, on the selected re-scaling technique or on the area were assimilation is performed when distributed models are used. Assimilation of downscaled products is a promising source to improve models' soil moisture simulation, which may propagate into improved streamflow predictions.

RESUMEN

Los modelos hidrológicos son herramientas de gran utilidad, capaces de aportar información para un mejor entendimiento del ciclo hidrológico en sus diferentes escalas, tanto temporales como espaciales. Estos modelos son ampliamente utilizados en la predicción de inundaciones, en la evaluación de impactos medioambientales o para la adecuada gestión de los recursos hídricos. Generalmente incorporan el cálculo de la humedad del suelo en las diferentes capas en las que se estructuran, ya que dicha variable es un factor determinante y que condiciona, entre otros aspectos, el que el agua procedente de la lluvia se trasforme en escorrentía o quede retenida en las capas del suelo. Los diferentes satélites que actualmente se encargan de observar la superficie terrestre se han mostrado como fuentes de información muy valiosa para mejorar la simulación de la humedad del suelo ofrecida por los diferentes modelos. En efecto, la observación que de la humedad de la capa superficial del suelo llevan a cabo algunos de estos satélites hacen puede ser de gran ayuda para la mejora de la predicción de la caudales de los ríos ofrecida por los modelos. La información obtenida por los satélites puede ser integrada en los modelos a través de técnicas de asimilación de datos, entre las que se incluyen diferentes variantes del Filtro de Kalman, siendo en hidrología la más usada la versión *ensemble* (conjunto) de dicho filtro.

El objetivo principal de esta tesis es evaluar si la asimilación de datos de humedad superficial del suelo obtenidos mediante técnicas de teledetección, en modelos hidrológicos es capaz de mejorar la predicción de caudales en los ríos a la salida de las cuencas. Este objetivo general se concreta en los siguientes objetivos específicos: 1) evaluar la respuesta de modelos de diferente configuración espacial (agregados, semi-distribuidos, distribuidos), a la asimilación de datos, con el fin de conseguir una mejora en la simulación de caudales; 2) evaluar la influencia de las características de cada cuenca (como tamaño, topografía, clima o usos del suelo) en los resultados de la asimilación de datos; 3) evaluar la posible mejora obtenida en la simulación de escorrentía mediante la asimilación de datos de sensores como ASCAT o SMOS, que observan diferentes frecuencias (banda C y banda L); 4) evaluar la mejora en la predicción de escorrentía al asimilar en un modelo distribuido el producto de alta resolución (1-km) desarrollado en el Barcelona Expert Center y obtenido a partir de los datos de los satélites SMOS y MODIS; 5) evaluar la influencia que las diferentes técnicas de re-escalado de la información observada tienen sobre los resultados de la asimilación, y por último; 6) evaluar la influencia que tiene sobre los resultados de la asimilación el valor de error de observación atribuido a cada satélite.

Un segundo objetivo de esta tesis es la evaluación del modelo TOPLATS como herramienta de simulación de caudales en cuencas Mediterráneas, y se concretó en los siguientes objetivos específicos: 1) llevar a cabo una revisión bibliográfica en profundidad de los diferentes trabajos desarrollados con TOPLATS anteriormente, con especial atención a aquellos en los que se trabajó en la calibración del modelo y en el análisis de sus diferentes parámetros; 2) desarrollar un análisis de sensibilidad muy completo del modelo, en el que se analice la sensibilidad de la escorrentía superficial, el flujo base, la evapotranspiración, la humedad del suelo y de la eficiencia enfocada a los diferentes rangos de caudal, a diferentes parámetros; 3) comparar dos métodos de análisis de sensibilidad de diferente complejidad y costo computacional; 4) evaluar la efectividad de un algoritmo de optimización como herramienta de calibración del modelo aplicado a diferentes escalas temporales; 5) comparar la influencia que tiene sobre la calibración de un modelo la selección de periodos de calibración continuos o discontinuos seleccionados en función de la variabilidad climática que contienen; y 6) evaluar la eficiencia del modelo para predecir correctamente los caudales simulados en cuencas mediterráneas de diferente tamaño y diferentes condiciones climáticas, tanto cuando el modelo es aplicado en paso horario como diario.

Esta tesis se estructura en tres estudios separados mediante los que se pretendía alcanzar los objetivos señalados. En el primer estudio se aplicó el modo estadístico, que es una configuración semi-distribuida, del modelo TOPLATS. Este modelo está basado en el modelo TOPMODEL, al que se le añadió un balance de agua y energía entre el suelo, la vegetación y la atmosfera. TOPLATS se aplicó en tres cuencas navarras de diferente tamaño, topografía y climatología, llevando a cabo previamente un análisis de sensibilidad del mismo mediante dos técnicas ampliamente utilizadas en hidrología. Una vez seleccionados los parámetros del modelo con mayor impacto sobre los resultados, el modelo fue calibrado mediante un algoritmo de optimización, iniciando la búsqueda del algoritmo desde diferentes valores iniciales de los parámetros a calibrar. Se obtuvieron resultados óptimos tanto al calibrar el modelo en paso horario, como diario, y se utilizaron periodos de calibración continuos y discontinuos para ello.

El segundo estudio consistió en la asimilación de datos del satélite ASCAT en el modelo agregado y conceptual MISDc, y en el modo semi-distribuido de TOPLATS. El objetivo de este estudio era explorar el efecto de esta asimilación en la predicción de la escorrentía. Los modelos se aplicaron en dos cuencas de similar tamaño, una en Italia y la otra en Navarra (España). En este estudio se analizó también el impacto sobre los resultados de la asimilación del uso de diferentes técnicas de re-escalado de los datos observados por el satélite. Finalmente se analizó la influencia sobre los resultaos del error en la observación atribuido al satélite. En este estudio se utilizó como técnica de asimilación el Filtro de Kalman, en su modo *ensemble*.

Por último, en el tercer trabajo, se estudiaron los efectos sobre la simulación de escorrentía de la asimilación de un producto de humedad superficial del suelo de alta resolución (1-km), obtenido a partir de los satélites SMOS y MODIS. La asimilación se efectuó sobre la simulación del modelo TOPLATS, configurado en modos distribuido con celdas de 1 km. En este estudio también se exploró el efecto de considerar la asimilación de datos únicamente en aquellas celdas ocupadas por suelos agrícolas (es decir, excluyendo zonas boscosas), o situadas sobre áreas de baja pendiente. De esta forma quedaban excluidas de la asimilación zonas de altas pendientes o cubiertas por grandes masas de vegetación, donde la observación del satélite es de peor calidad. Este estudio se desarrolló en la cuenca del rio Cidacos, en la zona media de Navarra (zona norte de España).

En general, los resultados obtenidos nos permiten concluir que hay un importante potencial para la mejora de la simulación de caudales mediante modelos agregados, semi-distribuidos o distribuidos, a través de la asimilación de diferentes productos de humedad del suelo obtenidos mediante teledetección. En cualquier caso, no se trata de un proceso que pueda ser aplicado de forma sencilla y directa en cualquier cuenca, modelo o con cualquier producto de humedad. Este trabajo ha comprobado que la utilización de una u otra técnica para re-escalar los datos observados, o la consideración de diferentes errores atribuidos al satélite, tienen una gran importancia sobre los resultados obtenidos. Del mismo modo, las características de cada cuenca tienen una gran influencia sobre la magnitud de la posible mejora en le predicción de escorrentía. Por otro lado, esta tesis ha conseguido aplicar con éxito el modelo TOPLATS en cuencas mediterráneas de diferente tamaño, topografía y pluviometría. Se han obtenido resultados notables en la mayoría de las cuencas evaluadas, tanto en modelado de paso horario como diario. También ha sido capaz de identificar los parámetros con mayor influencia en los diferentes procesos hidrológicos modelados por TOPLATS. Por último, se ha constatado la necesidad de desarrollar la calibración de modelos hidrológicos en periodos que incluyan una suficiente variabilidad climatológica, en especial referido a la necesidad de contener periodos húmedos.

CHAPTER 1. INTRODUCTION

1.1. STATE OF THE ART

1.1.1. Hydrological modeling

Hydrological catchment models are powerful tools that are currently applied on a wide range of research and decision-making areas, including environmental protection and resource management (Singh and Woolhiser, 2002). These models provide streamflow estimations, useful to different stakeholders including, among others, those working on: water resources management, civil engineering operations, climate change analysis, or bio-diversity conservation requirements (Christensen et al., 2004; Hayashi et al., 2008; Richter and Richter, 2000; Rogger et al., 2012). The intense development in the field of hydrological simulation over the last decades offers today researchers worldwide dozens of models capable of simulating not only streamflow level but also other related processes, at different time and spatial scales (e.g., Burnash et al. 1973; Chiew and McMahon 2002; Brocca et al. 2011a).

Catchment models are usually divided into conceptual and physically–based depending on their underlying structure and the level of simplification of reality they assume. On the latter type, models are more complex, with parameters that are measurable (in principle), have specific units, and are applied on equations representing different hydrological processes (Beven, 1989). Physically based models are intended to minimize the need for calibration by building on parameters, which in principle are measurable. However, the parameters are often difficult to determine at the desired scale and in consequence the physical basis of the models can be debated and some even argue that distributed and physically based models are in reality just complex conceptual models (Stisen et al., 2008). Indeed, it is common to find models that combine both physical and conceptual approaches and parameterization.

Models can also be classified as lumped or fully distributed (Elsanabary and Gan, 2015). Lumped models simplify the description of a spatially distributed system by representing the catchment as a

discrete entity characterized by bulk parameters representing mean catchment response (Li et al., 2015). On the other hand, spatially distributed approaches subdivide the catchment into single elements (grids of cells or subcatchments), considering the spatial variability within the catchment. Distributed hydrological models are commonly physically based and require large amounts of high resolution data (Chaney et al., 2015). These different strategies (i.e., conceptual-physically based, lumped-distributed) can result in models with substantial differences in terms of the complexity of their structure, their level of parameterization, or their input requirements (Demaria et al., 2007).

The principle of parsimony recommends that simple models that require a lower number of parameters and input variables are preferable than more complex ones (Jakeman and Hornberger, 1993; Nash and Sutcliffe, 1970), because the former can be more easily generalized, are computationally more efficient, more robust and less prone to overfitting (Kirchner, 2009; Perrin et al., 2001). This principle needs to be taken into account, along with model goodness-of-fit statistics (Moriasi et al., 2007; Ritter and Muñoz-Carpena, 2013), when selecting a model for a particular application. It is also important to bear in mind that some models might be more suitable for certain specific catchment characteristics than others, for instance depending on the climatology or dominant runoff types in the catchment of interest (Alvarez-Garreton et al., 2013).

Among the many different hydrological models that exist, there has been a significant development of catchment models based on the TOPMODEL concept (Beven and Kirkby, 1979). From this initial conceptualization, Famiglietti and Wood (1994), started the development of a full hydrological catchment model that incorporated a separate computation of water and energy balances. This model was called TOPMODEL-based Land-Atmosphere Transfer Scheme (TOPLATS). TOPLATS can be run at any user-specified time step, from daily (Bormann et al., 2007) to hourly (Loaiza-Usuga and Pauwels, 2008), or even on less than a minute time-step (Seuffert et al., 2002). While this permits the model to be applied for an extensive range of purposes, it can also affect model performance, especially in terms of runoff and soil moisture processes simulation. TOPLATS has been applied on a wide range of locations worldwide, but its use on Mediterranean catchments

was only reported in Loaiza-Usuga and Pauwels (2008) and in Loaiza-Usuga and Poch (2009). Hydrological processes in the Mediterranean environment are largely variable, both in time and space, due to the high variability of rainfall regime, topography, soil and land use. In this context, distributed hydrological models may provide a valid support in water management, as they account for the spatial variability of the catchment characteristics (Milella et al., 2012).

So, even if models can easily be applied on different conditions (in terms of climate, catchment size or time-step), achieving the best simulation results depends largely on the users' knowledge of model structure and suitability, but also on the available tools to maximize the accuracy of the results (Khakbaz et al., 2012). Thus, achieving optimal modelled streamflow values requires, first, detailed sensitivity analyses to provide the modeler with objective criteria to identify the parameters to include on the calibration procedure and next, calibration and validation strategies to find the parameter values that optimize model results (Ritter and Muñoz-Carpena, 2013; Saltelli et al., 2006; Van Werkhoven et al., 2009). Normally, simple models can be more easily evaluated using sensitivity analysis or uncertainty assessment tools (Moradkhani et al., 2005a), and also more easily optimized through calibration and validation approaches (Vrugt et al., 2003), since their number of parameters is lower and are thus less affected by issues such as parameter interdependency and equifinality (Beven, 2006). Ultimately, model performance and optimal parameter values will largely depend on: catchment size, rainfall pattern and climate conditions, modeling time-scale, and the suitability of model structure to all of them (Demaria et al., 2007).

1.1.1.1. Sensitivity analysis

Identifying optimal parameter values on complex hydrological models is not an easy task. Different sources of uncertainty limit users' capability to reach this objective. Those include: observation errors, model formulations and the complexity added by over-parameterization and nonlinearity on parameter interactions. Even on physically based models, where some parameters can be, in principle, measured, they require further investigation to adapt optimal values to

catchment scale performance. As a result of these difficulties, Sensitivity Analysis techniques emerged as complementary tools to hydrological models.

Sensitivity Analysis (SA) techniques can identify influential parameters, i.e. those whose uncertainty reduction will have the most significant impact on improving model performance (Gan et al., 2014) and provide model users with useful information to reduce calibration dimensionality (Garambois et al., 2013). If some insensitive parameters are identified through SA, they can be fixed reasonably at given values over their variation range. Thus, reducing calibration computational cost without decreasing model performance (Ritter and Muñoz-Carpena, 2013). SA methods usually require a large number of model runs in order to cover the whole parameter space and all parameter value combinations. In order to minimize the computational effort on this task, statistical parameter distributions have been developed and tested (Wagener and Kollat, 2007).

Sun et al. (2012) classified SA methods into three types: (1) local, (2) screening and (3) global, depending on the way parameters were perturbed. Local methods quantify the percentage change of outputs due to the change of model inputs relative to their baseline (nominal) values (Tang et al., 2007). These methods, also referred to as One-at-A-Time (OAT), evaluate the response of output variables to fractional changes in one single input parameter and are therefore less efficient on complex models. Even on models where parameters are independent, the combination of single-parameter influences can make local methods to fail on capturing model behavior due to non-linearity of model response (Norton, 2009). Screening methods also analyze the model response to a change in the inputs by varying one parameter at a time, but they provide a global sensitivity measure, since different elementary effects (EE) for each parameter are calculated and averaged (Campolongo et al., 2011). They are commonly applied to cases where a large number of parameters needs to be analyzed, or to computationally expensive models where more demanding quantitative techniques might lead to extended simulation times, because they require a smaller number of model runs. They also offer a suitable option to analyze a larger number of parameters in complex models, as a preliminary test, to select a reduced number of them to be studied with

more complex global SA techniques. Finally, global methods, vary simultaneously all studied parameters within their defined parameter space, thus providing information on both individual sensitivity and parameter interaction degrees (Saltelli et al., 2000). Global methods look at the entire input parameters distribution, using specifically designed Monte Carlo sampling techniques of various levels of sophistication, but their application to computationally demanding models might be constrained due to the large number of model runs required (Song et al., 2015). Global methods are recognized as appropriate for hydrological modeling, as they have to evaluate nonlinear processes and high parameter and data uncertainty due to spatial heterogeneity (Spear et al., 1994). Global methods include the following groups (Tang et al., 2007): (1) Regional SA (Young, 1978), (2) Bayesian SA (Oakley and O'Hagan, 2004), (3) regression based approaches (Spear et al., 1994), and (4) variance decomposition methods (Saltelli et al., 2000). Screening and global SA methods include two steps: first, a strategy is used to sample the parameter space (i.e. Design of experiment, DoE) and next a numerical measure is used to quantify the impacts of sampled parameters on model output (Wagener and Kollat, 2007). Some of the most commonly used SA techniques include (to name a few) Morris method (MoM) (Morris, 1991), the Generalized Likelihood Uncertainty Estimation (GLUE) method (Beven and Binley, 1992) and Sobol method (SoM) (Sobol, 1993). Different variants of these already classical techniques have been proposed more recently (e.g., Saltelli et al. (2010) or Gan et al. (2014)).

1.1.1.2. Model calibration and optimization algorithms

Once the most sensitive parameters of a model have been identified through SA procedures, they need to be calibrated, i.e. estimated through an inverse method so that observed and predicted output values are in agreement (Zhang et al., 2009). Therefore, successful application of any hydrological model depends on how accurately the model is calibrated (Duan et al., 1992). Although model calibration used to be a labor intense task that depended largely on modeler knowledge and experience, nowadays computers allow automatic calibration techniques. These are commonly optimization algorithms that search for a set of parameters values that minimize the model prediction

error relative to available measured data for the system being modeled (Tolson and Shoemaker, 2007).

Gupta et al. (1998) pointed out that automatic calibration success depends largely on three aspects: 1) adequate calibration data (mainly in terms of data length and climate variability contained), 2) the objective function (maximum likelihood functions for measuring the "closeness" of the model and the data), and 3) the selected optimization algorithm. However, some studies reported difficulties in finding unique (global) optimum parameter values due to parameter non-uniqueness or equifinality, parameter correlation, or other limitations (Duan et al., 1992). Other challenges of parameter optimization are (Vrugt et al., 2003): the existence of multiple local optima with both small and large domains of attraction (a sub-region of the parameter space surrounding a local minimum), discontinuous first derivatives and curving multidimensional ridges. Recently, optimization algorithms started to shift from simple to multiple objective optimizations (Yapo et al., 1998; Ye et al., 2014).

Calibration of hydrological models for areas with irregular rainfall patterns, such as Mediterranean ones, implies an extra effort in terms of model adaptability and data availability (Loaiza-Usuga and Pauwels, 2008). Several authors (Gan and Biftu, 1996; Li et al., 2010; Perrin et al., 2007) noted that arid catchments were generally more difficult to model than humid ones due to the complexity and variability of hydrological processes there. This can be related to model's response to intense rainfall events and to large inter-annual rainfall variability.

Conventional continuous calibration and validation period selection (i.e., selection of a calibration period of *n* years, followed by a validation period of *m* years) may be a limitation when large differences on climate variables are found among both periods. Thus, alternative (random and discontinuous) period selection methods that lead to a similar calibration and validation climatological conditions and to a minimum of high flows included on the calibration period are worth being explored (Kim and Kaluarachchi, 2009). As stated by Sorooshian and Gupta, (1983) it is not the length of the data series used but the information contained in it and the efficiency with

which that information is extracted that are important. Random sampling approaches are expected to overcome different difficulties, which could include: 1) data availability discontinuity (i.e. Kim and Kaluarachchi, 2009), 2) lack of data series long enough to achieve proper calibration and validation results, or 3) large climate variability between calibration and validation periods.

Optimization algorithms used on hydrological model calibration are divided into local (Tolson and Shoemaker, 2007) and global search methods (Duan et al., 1993). One of the first optimization algorithms was proposed by Powell (1964), and was applied for the first time to hydrological modeling by Kobayashi and Maruyama (1976). This algorithm is a local, derivative-free method where one parameter value is changed at-a-time. Chen et al. (2005) applied a modified multi-start version of the Powell method for model calibration, which is also implemented on this thesis.

1.1.2. Soil moisture remote sensing

A key issue affecting the efficiency of model predictions, regardless of the particular model type, is that they rely strongly on the optimal simulation of soil moisture conditions within the modeled catchment (Crow and Ryu, 2009). Surface soil moisture (SSM) is an important variable in the hydrological cycle that determines the partitioning of incoming water into infiltration and runoff, thus controlling runoff and baseflow generation from the soil profile and determining river flows and flooding (Han et al., 2012). SSM also influences the energy balance at the land-atmosphere interface, and thus controls the partition between sensible and latent heat flux. As such, SSM may also impact atmospheric processes, such as temperature, cloud cover and precipitation (Tuttle and Salvucci, 2016), with consequences in weather dynamics and climate processes across several scales, from local to global (Seneviratne et al., 2010). SSM has been recognized as a key variable for making operational weather forecasts both at the short (Cassardo et al., 2002) and long term (Berg and Mulroy, 2006), in particular over mid latitudes in the Northern Hemisphere and during spring and summer (Koster et al., 2010, 2004). SSM also impacts biogeochemical processes, such as C and N mineralization, with consequences in the C and N cycle (Borken and Matzner, 2009).

Finally, SSM also influences the water available for plants on the soil profile, and consequently is a key factor for the growth and development of crops, and thus for an accurate forecast of agricultural drought and food security (Heim Jr., 2002).

Currently, quantitative information on SSM can be obtained through in situ measurements (Dobriyal et al., 2012) and remotely sensed observations (Jeu et al., 2008; Li et al., 2016). In situ measurements can be carried out using either direct or indirect methods. The direct, or thermo-gravimetric, method consists of collecting soil samples and evaluating its moisture content in the laboratory through weighting and drying (Hillel, 1998). Normally, moisture needs to be quantified in volumetric units, and this requires a known soil volume to be collected, what is not always easy to do. Furthermore, the definition of dry soil (duration of drying and temperature) and eventual experimental errors add uncertainty to this technique, not to mention the inconvenience of being destructive and very time consuming. Nevertheless, the thermo-gravimetric method is still considered the most accurate approach for in situ SSM measurement, and it is commonly used as a reference to calibrate other methods against.

Indirect methods measure soil properties that can be related back to soil moisture, namely dielectric constant, capacitance, neutron thermalization or soil suction (Dobriyal et al., 2012; Muñoz-Carpena et al., 2004). These properties are normally sensed using probes that are inserted in the soil and provide undisturbed and repeatable measurements of a small soil volume around the probe. Some of these methods have been already used for a long time (e.g., Time Domain Reflectometry and Capacitance sensors) (Topp et al., 1980), and proven to be sufficiently accurate and reliable for most applications once correctly calibrated (Bogena et al., 2017). Besides, their costs have substantially decreased in the last years and therefore they are of widespread use. However, along with calibration issues (Evett et al., 2012), the main drawback of this technology is that point measurements only reflect the wetness status of a very small soil volume, and given the large spatial variability of SSM it is difficult to upscale these measurements to larger areas. Recent advances in telemetry and data transmission technologies have enabled the integration of many in

situ probes into sensor networks, providing more reliable areal estimates (Dorigo et al., 2011). Some of these networks, e.g., Soil Climate Analysis Network (SCAN) (Schaefer et al., 2007) or Red de Medidas de Humedad del Suelo (REMEDHUS) (Martínez-Fernández and Ceballos, 2003), have already been operational for a considerable period of time (~20 years), providing extremely valuable information on spatial and temporal SSM trends and their response to long term processes, such as climate change. A global map of ground-based soil moisture testbeds and field campaigns was recently presented by Mohanty et al. (2017).

Advances in sensor technologies have enabled the development of indirect approaches that sense the SSM state of larger areas. For instance, Global Navigation Satellite Signal reflectometry (GNSS-R) (Rodriguez-Alvarez et al., 2009), Cosmic-ray neutron reflection (Zreda et al., 2012) and fiber-optics (Sayde et al., 2010) are very promising techniques that provide areal measurements of different sizes. Although very recent, some of these technologies are already being used in operational research networks (Shuttleworth et al., 2010), and will surely play an important role in the future.

At present, the main limitation of in situ SSM measurement is the difficult generalization of point based measurements to larger areas, mainly due to the high spatial variability of meteorological forcings, soil hydraulic properties and other land features (e.g., topography, vegetation) that influence SSM distribution and dynamics (Ochsner et al., 2013). Some interesting research has been done on the understanding of spatial patterns and temporal stability of SSM and their relation with precipitation and land features (Grayson et al., 1997). Vachaud et al. (1985) prosed the temporal stability analysis, where SSM time series acquired at different sampling locations on a catchment were compared with the catchment average over time in order to detect sites that were normally wetter or dryer than the average (using the mean relative difference indicator), and also to evaluate whether wetness states were stable across time or instable and strongly fluctuating due to fast wetting and drying cycles (using the standard deviation of the relative difference). This approach has been widely used afterwards identifying complex patterns and dynamics in response to multiple factors, including seasonality, wetting or drying cycles, topographical position and morphology of the

catchment, soil properties and vegetation (e.g. Brocca et al., 2009c; Jacobs et al., 2004; Mohanty and Skaggs, 2001; Rosenbaum et al., 2012).

The development of satellite remote sensing over the past decades enables the estimation of different land surface variables over spatial areas at a range of scales (from regional to global) and with a given periodicity (Fang and Lakshmi, 2014), some of which can be of large interest for hydrology (McCabe et al., 2017). Currently, quantitative information on SSM can be best obtained from passive and active microwave instruments (Mohanty et al., 2017; Petropoulos et al., 2015), since microwave emission and scattering depend on the dielectric constant of the soil surface, and besides these instruments are not affected by cloud cover nor atmospheric conditions and do not required solar illumination to operate. Existing sensors differ in their design, sensing mode (active or passive), frequency, polarization and the retrieval algorithm implemented (Rötzer et al., 2014). But all of them operate in the low frequency microwave region from 1 to 10 GHz (Albergel et al., 2012). The actual frequency they use impacts the depth of the sensed SSM layer, with L-band sensors reaching the top 5 cm of the soil column and C- and X-bands even less than that (~2 cm) (Rötzer et al., 2014). On the other hand, C- and X- bands can normally provide higher spatial resolution data and are less affected by radiofrequency interferences.

Passive sensors (radiometers) measure the microwave emission of soils (brightness temperature) and are less sensitive to the effects of surface roughness and vegetation structure than active ones (Rötzer et al., 2014). Different passive microwave sensors have been observing the Earth for the last decades, providing a quasi-continuous global dataset since 1978 (Liu et al., 2012). Although initially designed for ocean wind estimations, scatterometers are the active microwave sensors mostly used for SSM retrieval. Scatterometers transmit a microwave pulse towards the Earth surface and measure the echo that returns back (i.e., backscatter). Microwave backscatter is also dependent on the dielectric properties of the soil surface (and hence, SSM) but is more strongly influenced by disturbing factors, such as vegetation, surface roughness or topography than brightness temperature. Yet,

retrieval algorithms exist that provide operational SSM estimates globally, except for areas of dense vegetation.

Radiometers and scatterometers provide observations with very similar spatial and temporal resolutions, with coarse spatial detail (~20 km) but short revisit times (~daily). At present four operational SSM products exist (Table 1.1). But earlier sensors provided continuous global datasets since 1978 (radiometers) and 1991 (scatterometers). Among these, the Advanced Scatterometer (ASCAT) was the first to provide an operational, near real-time (NRT) Level 2 SSM product (Albergel et al., 2012). It is also important to mention the recent initiative by the European Space Agency Climate Change Initiative (ESA-CCI) SSM product, which is a reanalyzed SSM product based on merging six microwave products that provides global data since 1978 (Liu et al., 2011).

Table 1.1. Main remote sensing surface soil moisture observing missions

Sensor	Type	Band	Available since	Spatial resolution (km)	Revisit time (d)	Reference
ASCAT	Scatterometer	C	2007/01	25	1	(Wagner et al., 2013)
SMOS	Radiometer	L	2010/01	36	2	(Kerr et al., 2012)
AMSR2	Radiometer	C, X	2012/07	50	1	(Kim et al., 2015)
SMAP	Radiometer	L	2015/04	36	2	(Entekhabi et al., 2010)

The coarse spatial resolution of these SSM products remains a challenge for certain applications that require higher spatial detail. Advances in sensor technology will probably improve this in the future, but meanwhile significant progress is being made on the development of downscaling algorithms that enhance the spatial resolution of these products by using complementary higher resolution datasets. Optical multispectral sensors can provide complementary information related to soil moisture patterns at higher spatial resolutions. Observations in the visible and near-infrared (NIR) bands allow for the computation of vegetation indices (VI) that are indirectly related to soil moisture through vegetation condition status (Lobell and Asner, 2002). On the other hand, thermal infrared

(TIR) observations measure the surface radiant temperature (T_S) which is partly dependent on SSM (Quattrochi and Luvall, 1999). When T_S is plotted against VI a scatterplot of triangular or trapezoidal shape emerges. This triangle has been the base for the derivation of different indices related to SSM and vegetation condition (e.g., Sandholt et al., 2002), and also for developing methods to estimate SSM and ET (Carlson, 2007; Petropoulos et al., 2009). From this concept, different T_S/VI based SSM retrieval methods have been proposed ranging from simple empirical relations to more physically based algorithms (Petropoulos et al., 2009).

Following this complementarity between microwave and optical sensors, Piles et al. (2011) proposed a downscaling strategy to improve the spatial resolution of SMOS observations from 40 km to 1 km by using MODIS derived NDVI and T_S values. Their approach was based on a second order polynomial equation to estimate SSM from SMOS normalized brightness temperature and MODIS normalized surface temperature and fractional vegetation cover (obtained from NDVI as in Gutman and Ignatov, 1998). The empirical coefficients of this equation were empirically fitted at 40 km resolution using aggregated MODIS data, and then the equation was applied at the original MODIS resolution to obtain SSM at 1 km resolution. Their results showed that the SSM variability was effectively captured in the downscaled product without a significant degradation of the root mean square error. This 1 km SMOS/MODIS SSM product was later validated in separate studies (Piles et al., 2014; Sánchez et al., 2012) with successful results. Furthermore, this algorithm was implemented to provide an operational fine-scale level 4 SSM product at the SMOS Barcelona Expert Center (BEC) for the Iberian Peninsula, South Africa and Ghana (SMOS-BEC Team, 2016). The topic of coarse scale SSM downscaling is a very active one, with new algorithms and improvements being proposed very recently (Wu et al., 2017). Therefore, it is expected that in the near future more and more downscaled level 4 products will be operationally released by the major space agencies.

Another approach to circumvent the coarse spatial resolution of radiometer or scatterometer based operational SSM products is to resort to high resolution Synthetic Aperture Radar (SAR) observations, with spatial resolutions of 10-100 m. So far, the main drawback of SSM estimation

from SAR data has been related to their poor revisit time (typically ~30 days) and the stronger influence at this scale of disturbing factors, such as soil roughness and vegetation, that limited the development of robust retrieval algorithms ready to use operationally (Kornelsen and Coulibaly, 2013; Verhoest et al., 2008). Today, with the advent of the satellite constellation concept (e.g., Sentinel-1, Radarsat Constellation Mission) a new era has recently started with improved revisit times of only several days (3-6 days for Sentinel-1 over European mainland) at spatial resolutions of 10-20 m. This temporal resolution is now much more attractive for hydrological applications, and what is more, enables the development of simplified SSM retrieval algorithms based on change detection techniques or time series analysis (Balenzano et al., 2011; Paloscia et al., 2013), based on the assumption that disturbing factors (mainly surface roughness and vegetation) change slower than SSM does, so short-term backscatter variations can be attributed to SSM dynamics. These methods have still to be tested and validated, so that high resolution SSM products are operationally available.

1.1.3. Data assimilation

1.1.3.1. General description of methods and their application

As explained in the previous section remote sensing can be considered more and more to be a viable source of SSM information. However, any remotely sensed SSM product has some limitations that need to be recognized. First, remote sensing systems provide observations at a given sampling interval (i.e., revisit time), and although this interval can be as short as 1 or few days, some hydrological applications require temporally continuous information (e.g., flash floods). More importantly, microwave sensors provide at best information of the top 5 cm of the soil profile, where most hydrological and agricultural applications require root zone information (RZSM). Not to mention the limitations of some of the retrieval algorithms used, with their various issues regarding simplifications, assumptions, parameters and validity conditions. Therefore, the usefulness of remotely sensed SSM products alone is limited, but this limitations can be largely overcome if

combined adequately with hydrological or land surface models. If the potentialities of both techniques are exploited, soil moisture and its variations in time and with depth can be estimated.

SSM Data assimilation (SSM-DA) techniques merge observations (obtained either through remote sensing or in situ sensors) with continuous information provided by models to generate an improved product of soil moisture (Houser et al., 1998). SSM-DA techniques correct SSM model predictions towards the observations, by taking into account the uncertainty of both sources of information. Thus, SSM-DA is expected to provide a more realistic catchment simulation, with better state variable modelization and leading to enhanced model output predictions (e.g., streamflow, ET, etc.).

SSM-DA studies have shown to effectively update moisture states at deeper soil layers and improve RZSM estimates when compared to ground observations used as reference (e.g., Crow et al. (2008); Draper et al. (2012); Renzullo et al. (2014); Sabater et al. (2007)). These enhancements are normally translated into more accurate streamflow forecasts, mostly due an improved characterization of antecedent moisture conditions before rainfall events (Alvarez-Garreton et al., 2015, 2014, 2013, Brocca et al., 2012, 2010b; Chen et al., 2014; Crow and Reichle, 2008; Francois et al., 2003; Lievens et al., 2015; Wanders et al., 2014b). However, some studies reported none or minor improvements in streamflow estimations after SSM-DA (Han et al., 2012; Lievens et al., 2016), as explained in the next paragraphs, different options regarding the data preprocessing and SSM-DA set up might partly explain these differences. A further detailed review of SSM-DA studies for improved flood forecasting was reported in Li et al. (2016).

Data assimilation algorithms can be classified into hard updating (direct insertion or initialization), statistical correction, nudging, sequential assimilation, and variational assimilation (Li et al., 2016). DA comprises different techniques applied to hydrology and other fields of science over a period of decades (Rafieeinasab et al., 2014), such as variational assimilation (VAR) (Jazwinski, 1970), particle filtering (PF) (Gordon et al., 1993), or Kalman filtering (KF) (Kalman, 1960). Among them, the sequential type KF (Zhang et al., 2015) and its variants are the DA methods most commonly used in SSM−DA. Here model states are corrected towards observations by weighting the strength of the

correction based on the relative uncertainty of model and observations, using a factor known as the Kalman Gain (Trudel et al., 2014). Several variants were developed from the original KF method to adapt it to different systems. For instance, the extended Kalman filter (EKF) (Maybeck and Siouris, 1980), which involved linearizing the model dynamics using the first-order Taylor series approximation, was proposed for nonlinear systems. Furthermore, the ensemble Kalman filter (EnKF) (Evensen, 1994) was developed to address nonlinear model dynamics without linearizing model equations (Moradkhani et al., 2005b). The EnKF has been frequently used to assimilate observations into hydrological models because it is extremely flexible in treating model and parameter errors, it is well-suited to highly dimensional nonlinear systems (Wanders et al., 2014b) and is computationally affordable and easy to implement (Weerts and El Serafy, 2006).

The EnKF propagates an ensemble of model realizations generated by perturbing model input values (meteorological forcing and input parameters) through time. The error background covariance matrix is then estimated from the ensemble statistics (Trudel et al., 2014), where the probability density of the model states is represented by an ensemble where the mean is the best estimate (Gaussian assumption), and the ensemble spread defines the error variance (Xu et al., 2015). The estimation and propagation of the often large covariance matrices is the most computationally demanding process of EnKF, and makes this DA technique less computationally efficient than variational methods (Reichle et al., 2001).

The added value of EnKF DA strongly depends on the adequate representation of model and observation uncertainties (Reichle et al., 2008). In particular, an incorrect estimation of model error is expected to translate into inaccuracies in the DA outputs (Crow and Van Loon, 2006). Normally, input parameter values are perturbed by adding a simple additive noise (Massari et al., 2015), while precipitation forcing is perturbed using multiplicative error models (Chen et al., 2011; Reichle et al., 2007). However, an adequate perturbation of precipitation forcing is particularly difficult to achieve, since precipitation error characterization depends on factors such as temporal and spatial error correlations, missed rain events, etc. that often show strong scale effects (Hossain and Anagnostou, 2006; Maggioni et al., 2011). Nevertheless, soil moisture was found not to be very sensitive to the

complexity of the rainfall error model implemented and only slights improvements were obtained when more complex rainfall error models were implemented (Maggioni et al., 2012). This could be due to the dissipative and nonlinear nature of soil moisture dynamics (Maggioni and Houser, 2017). The perturbations added to the meteorological forcing and model parameters need to be tuned, so that the obtained ensemble adequately represents model uncertainty, i.e. the ensemble is meaningful (Matgen et al., 2012a). For this, the ensemble mean has to differ substantially from the observed time series, while maintaining the latter statistically undistinguishable from a member of the ensemble (De Lannoy et al., 2006). That is, for an ensemble to be meaningful, its bounds need to capture the observed trend, but also this observed trend needs to be significantly different than the ensemble mean. To verify this, the ensemble spread, its skill and its mean square error need to be evaluated (De Lannoy et al., 2006).

The observation error assumed for SSM products also has a strong influence on SSM–DA results, and its magnitude needs to be adjusted to each specific catchment and model condition (Massari et al., 2015). Although operational SSM products have a nominal observation error, this value may vary largely depending on the area and daily conditions of observation (Albergel et al., 2009; Bhimala and Goswami, 2015; Brocca et al., 2010a; Hahn et al., 2012; Leroux et al., 2014; Paulik et al., 2014). For instance, the ASCAT–SSM product has already been validated over several extensively instrumented test sites located in different climatic regions with different land cover (Wagner et al., 2013). Validation studies found root mean square error (RMSE) values below 0.04 $m^3 m^{-3}$ (Matgen et al., 2012b; Wagner et al., 2013), which correspond with the accuracy goal of both the SMOS and SMAP missions. Using this error estimation as a reference, unless a detailed error characterization is available for a particular site, the observation error rate should be best optimized (Massari et al., 2015).

One of the main challenges faced by SSM–DA is that model simulations and satellite retrievals often exhibit differences in SSM patterns, mainly in terms of different time series mean values and variation ranges (Chen et al., 2011). These have mostly been attributed to the coarse spatial

resolution and shallow penetration depth of the microwave observations (Lievens et al., 2015). Thus, prior to DA, any biases or systematic differences between model simulations and SSM observations need to be mitigated through re-scaling techniques (RTs), so that these representativeness issues are solved (Lievens et al., 2016). Thus, the usual approach is to re-scale the observations to the model response and only take advantage of the resulting SSM time-series in terms of variability (not absolute values) (Kumar et al., 2012). Re-scaling strongly affects the outcome of SSM–DA, and a number of techniques have been proposed in the last few years, constituting a very active field of research (Alvarez-Garreton et al., 2014; Paulik et al., 2014; Ryu et al., 2009; Wanders et al., 2012; Xu et al., 2015).

In the few last years, SSM–DA techniques have been applied to catchments of contrasting rainfall regimens, ranging from semi-arid (<400 mm/year) (Alvarez-Garreton et al., 2015, 2014; Lievens et al., 2015) to intermediate (Brocca et al., 2012) or humid (> 1000 mm/year) (Brocca et al., 2010a). In addition, different model types have been used for SSM–DA, ranging from simple lumped conceptual models (Aubert et al., 2003; Francois et al., 2003; Brocca et al., 2012) to complex, physically based models (Chen et al., 2011; Pauwels et al., 2002) and fully distributed models of different levels of complexity (Lievens et al., 2015; Wanders et al., 2014b). However, the degree of improvement in streamflow predictions varied significantly, from no improvement (Han et al., 2012), to limited improvement (Lievens et al., 2015; Matgen et al., 2012a), and up to 10-30 % improvement (Brocca et al., 2012; Francois et al., 2003; Massari et al., 2015). ASCAT SSM–DA in Mediterranean catchments was also successfully shown in Cenci et al. (2016). All of these studies are difficult to compare, interpret and generalize because their results depend largely on model structure and catchment characteristics, mainly rainfall regime, and thus on the dominant runoff mechanisms (Lievens et al., 2015). It would be therefore interesting to replicate SSM-DA techniques in exactly the same way on models of different types or catchments of different conditions to ascertain the added-value of SSM-DA for each case. Similar efforts have been carried out on a streamflow DA study (Randrianasolo et al., 2014), where two models of different conceptualization (distributed and physically based vs lumped) has been tested using the same catchments.

1.1.3.2. Data assimilation with distributed models

So far most SSM-DA studies oriented to streamflow prediction have been based on lumped hydrological models (Aubert et al., 2003; Pauwels and De Lannoy, 2009), but an increasing number of researchers are paying attention to the capabilities of data assimilation to improve semi-distributed and fully distributed hydrological and Land Surface Models (LSM) at different spatial scales (Brocca et al., 2017). Fully distributed models employed for SSM-DA include: Variable Infiltration Capacity model (VIC) (Lievens et al., 2016, 2015), LISFLOOD (Wanders et al., 2014a, 2014b), Noah (Lin et al., 2017), World Wide Water (W3) (Tian et al., 2017), Sacramento Soil Moisture Accounting (SAC-SMA) model (Yan and Moradkhani, 2016), CATHY (CATchment HYdrology) model (Trudel et al., 2014) and Continuum model (Cenci et al., 2016; Laiolo et al., 2016). Different spatial scales have been applied on those works, but most of them focused on large-scale applications (Lin et al., 2017; Tian et al., 2017).

Assimilation techniques applied into distributed catchment modelization varied from Nudging-based techniques (Cenci et al., 2016; Laiolo et al., 2016), to the one-dimensional variational data assimilation (1D-Var) scheme (Lin et al., 2017) or to the recently developed particle-filter Markov chain Monte Carlo (PF-MCMC) method (Yan and Moradkhani, 2016). But in most cases, Ensemble Kalman Filter emerged as the most applied method for improved hydrological simulation (Abaza et al., 2015; Lievens et al., 2016; Trudel et al., 2014; Wanders et al., 2014a, 2014b; Xu et al., 2015). Other studies have also employed similar techniques, such as Ensemble Kalman Smoother (Tian et al., 2017).

Assimilation research into distributed models have taken advantage of different SSM remote sensing sources, including ASCAT (Cenci et al., 2016; Yan and Moradkhani, 2016), or SMOS (Kornelsen et al., 2016; Lievens et al., 2015; Lin et al., 2017; Tian et al., 2017; Xu et al., 2015), while some other studies have compared the performance of different satellites observations, i.e. Wanders et al. (2014b) tested ASCAT, AMSR-E and SMOS products assimilation. Also, a soil moisture fine-scale product data assimilation study was developed by Lievens et al. (2016), who used

the level 4 fine-scale soil moisture data produced through the DisPATCh (Disaggregation based on Physical And Theoretical scale Change) downscaling algorithm specifically developed for SMOS (Merlin et al., 2012). In any case, that product was up-scaled to a larger scale prior to assimilation. This down-scaled product was also validated for northern Spain location, where it was found the product offered lower correlation values with simulated values for forested and step relief areas (Escorihuela and Quintana-Seguí, 2016). Other authors also pointed out the limitations of L-band observing missions, including SMOS, to provide accurate SSM observations of forested areas (Grant et al., 2007; Kurum et al., 2012; Rahmoune et al., 2013). Topography, specifically areas with steep relief also seem to deteriorate the ability of SMOS to observed SSM adequately (Pellarin et al., 2015; Utku and Le Vine, 2011).

Assimilation studies were proposed with different objectives, including the estimation of terrestrial water storage (TWS) components (Tian et al., 2017), model calibration (Wanders et al., 2014a), improving flood prediction systems (Cenci et al., 2016; Wanders et al., 2014b), improving soil moisture simulation (Lin et al., 2017), or to improve both soil moisture and streamflow simulation (Lievens et al., 2015; Yan and Moradkhani, 2016). Although some studies have proved the ability of SMOS to improve soil moisture predictions obtained with distributed models (Blankenship et al., 2016), also performing SSM assimilation into high spatial resolution land surface models with down-scaled products (Dumedah et al., 2015), there is still a need for further research on the analysis of down-scaled SSM assimilation impact into streamflow simulations (Wanders et al., 2014a).

SSM-DA on distributed models can be more challenging due to the mismatch between the spatial resolution of the model and observations (Lievens et al., 2015). In most cases observations are of coarser resolution, and this mismatch needs to be accounted for in the assimilation algorithm itself (Reichle et al., 2014) or earlier in the preprocessing of the remotely sensed SSM observations (Verhoest et al., 2015). The arising concept of hyperresolution in the hydrological modeling community (Wood et al., 2011) is certainly going to determine the progress of SSM-DA investigations in the near future. In effect, improvements in computing capacities make nowadays possible to simulate global hydrological processes with resolutions of 1 km or less, so the ways to couple remote

sensing datasets to a model grid of such resolution and to effectively assimilate observations need to be intensely investigated. Ultimately this will lead to a better understanding of the water cycle, with consequences on important hydrological applications such as flood and drought predictions, assessing water resources and ensuring a sustainable food production in the context of climate change.

1.2. OBJECTIVES

The main objective of this PhD thesis was to evaluate whether the assimilation of remotely sensed surface soil moisture data into hydrological catchment models was able to improve streamflow simulation.

This general objective expanded into the following specific objectives:

Firstly, before data assimilation can be performed, the model needs to be properly calibrated, for that the following specific objectives were defined:

- To evaluate TOPLATS model streamflow simulation performance on Mediterranean catchments of varying size and climate conditions (at daily and hourly time-step).
- To develop a sensitivity analysis of TOPLATS selected parameters on: surface runoff, baseflow, evapotranspiration, soil moisture patterns and streamflow simulation (discriminating between peaks, average and low flows).
- To compare two SA methods of different complexity and computational requirements.
- To evaluate the performance of an optimization algorithm for model calibration at different time-scale simulations (daily and hourly).
- To appraise the influence of continuous or random period selection for calibration and validation purposes.

Once the models were calibrated, the following data assimilation-related specific objectives were tackled:

- Perform data assimilation with hydrological catchment models of different spatial representation complexity i.e. lumped, semi-distributed or fully distributed with the objective of improving streamflow simulation.
- Perform surface soil moisture data assimilation with different remote sensing sensors, specifically L-band and C-band observing systems that estimate soil moisture at different soil depths.
- Take advantage, trough data assimilation, of surface soil moisture down-scaled products for improved streamflow simulation.
- Perform data assimilation in catchments of different size, topography and climate conditions.
- Evaluate the Ensemble Kalman Filter as useful technique for data assimilation.
- Study the influence of the different techniques to re-scale remotely observed soil moisture data on assimilation results.
- Study the influence of observation error estimation on assimilation results.

1.3. STRUCTURE OF THE THESIS

This thesis is divided on three separate studies, which are expected to be in three different scientific journals. This section details briefly the objectives, materials, methods and publication status of each study.

1. Sensitivity analysis and calibration of TOPLATS on three catchments
   - **Objective:** The main objectives of this study were to perform a detailed sensitivity analysis of TOPLATS model with two SA method of different computational requirements, and to use an optimization algorithm to calibrate the model.
   - **Catchments:** La Tejeria, Cidacos and Arga (Navarre, Spain)
   - **Model:** TOPLATS (Statistical mode)

- **Journal of publication:** Article title: *Evaluation of TOPLATS on three mediterranean catchments*. Published on Journal of Hydrology (JoH) in 2016.
- **Results shown in this document:** in sections 4.1 and 4.2.

2. Assimilation of ASCAT data with lumped and semi-distributed models
   - **Objective:** main objective of this part of the thesis was to evaluate the possible improvement on hourly streamflow prediction that could be achieved by the assimilation of ASCAT data into two models of different spatial representation and parameterization complexity. Different configurations to apply the Ensemble Kalman filter were also tested on both semi-distributed models.
   - **Catchments:** Arga (Spain) and Nestore (Italy)
   - **Models:** TOPLATS (statistical mode) and MISDc (lumped)
   - **Remote sensing source:** Advanced SCATterometer (ASCAT) surface soil moisture data
   - **Data assimilation technique:** Ensemble Kalman Filter (with Soil Water Index calculation). Three re-scaling techniques were evaluated. Different satellite observation error values were analyzed.
   - **Journal of publication:** Submitted to Advances in Water Resources (AWR) on December 15th, 2016. Title: *On the assimilation set-up of ASCAT soil moisture data for improving streamflow catchment simulation*. Received a major review on March 2017. Expected to be accepted on the coming months. Review to be submitted due to the 28th of June, 2017.
   - **Results shown in this document:** in sections 4.3.

3. Assimilation of SMOS/MODIS data with a fully distributed model
   - **Objective:** The objective of this last study was to evaluate the impact on streamflow prediction generated by the assimilation of a 1-km down-scaled SMOS product into a fully distributed hydrological catchment model.

- **Catchments:** Cidacos (Spain)
- **Model:** TOPLATS (distributed mode)
- **Remote sensing data sources:** Soil Moisture Ocean Salinity (SMOS) Earth Explorer surface soil moisture data (1-km resolution product)
- **Data assimilation technique:** Ensemble Kalman Filter (without Soil Water Index calculation). Three re-scaling techniques were evaluated. Satellite observation error was considered as a fixed value.
- **Journal of publication:** Will be submitted to Water Resources Research. Expected submission date, July 2017.
- **Results shown in this document:** in sections 4.4.

CHAPTER 2. DESCRIPTION OF STUDY SITES, HYDROLOGICAL MODELS AND SOIL MOISTURE REMOTE SENSING SOURCES

This chapter of the thesis includes the description of the four catchments where the hydrological models have been applied, of the different models used, and lastly of the technical properties of the soil moisture remote sensing sources considered.

2.1. STUDY SITES

In this thesis four different catchments, ranging from a very small experimental catchment (1.59 km^2) to medium size catchments ($\approx$ 750 km^2) have been selected for our analysis. Three of them are located in northern Spain, while the remaining one is located in central Italy.

The three Spanish catchments are located in the province of Navarre. These catchments are: La Tejeria, Cidacos and Arga (Fig. 2.1). They all are located within the Ebro river basin (86,000 km^2), one of the major Spanish rivers, which flows into the Mediterranean Sea. They were selected with the objective of covering a range of catchment sizes, climate conditions, and contrasting topography. Navarre is divided into Atlantic (10% of the area) and Mediterranean basins (90%). In the latter, where the predominant climate is sub-humid Mediterranean, rainfall decreases notably as one heads south. Spanish study sites and the location of their meteo and gauging stations are shown in Fig. 2.1.

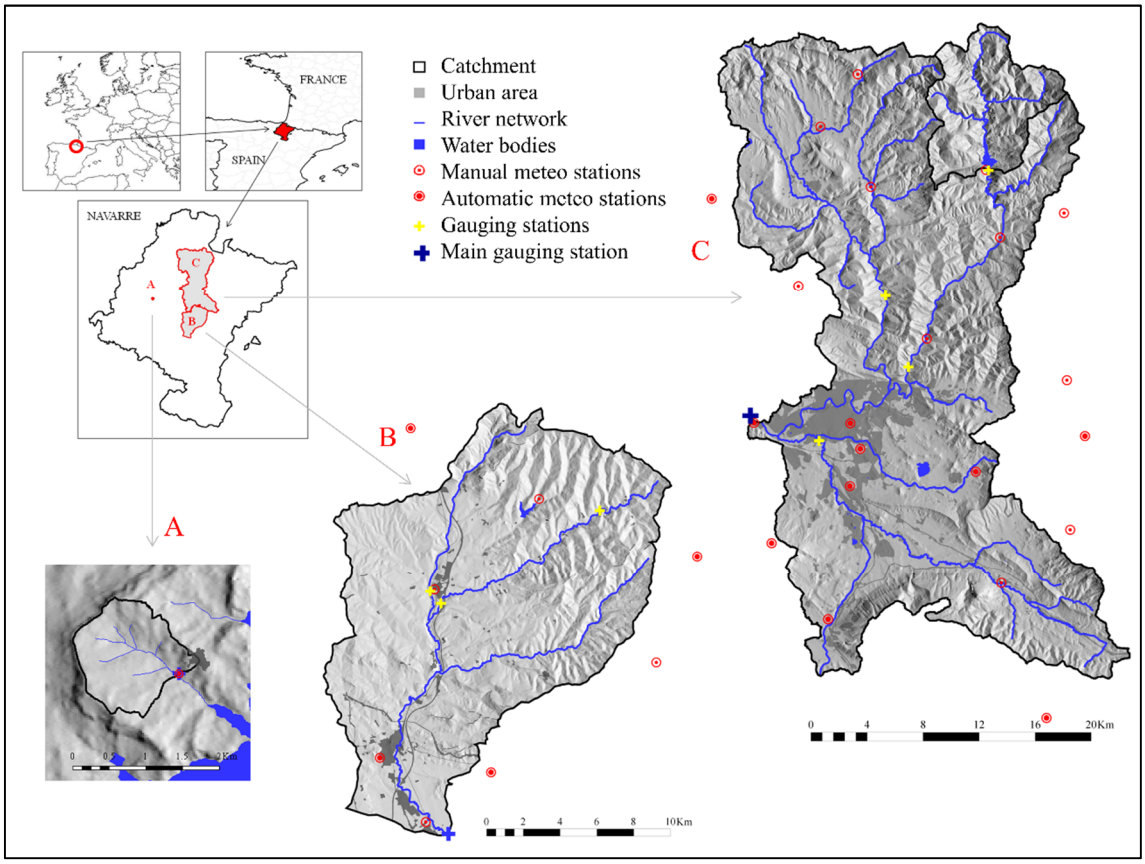

Fig 2.1. Location, topography, hydrological features and instrumentation of the three Spanish studied catchments: A) La Tejeria, B) Cidacos, and C) Arga.

2.1.1. La Tejeria catchment

La Tejeria is a micro-catchment, part of the Agricultural Experimental Catchment Network developed and maintained by the Government of Navarre (http://cuencasagrarias.navarra.es/index.cfm). It has a total extension of 1.59 km^2, with a gauging station and an automatic meteorological station (10 minutes basis) installed at the outlet. Elevation ranges from 496 to 649 m. The main flow channel has a length of 1.9 km, and the average slope within the catchment is 12%. Climate conditions in this catchment are intermediate between the other two catchments. In La Tejeria, average rainfall during the 2000 – 2012 period was 744 mm/year, although the annual rainfall can vary significantly from year to year. During the study period, mean

daily temperature was 12.5 °C and relative humidity 73%. The watershed is underlined by marls and sandstones of continental facies. The prevailing soil class is *Typic Calcixerepts* (NRCS-USDA, 2014), covering 41% of the watershed and located on eroded hillslopes. These soils are relatively shallow (0.5–1.0 m deep) and their upper horizon has a clayey-silty texture (Casalí et al., 2008). Catchment's major land uses are: winter cereals, sunflower, and fallow land (total 92%), riparian vegetation (7%) and urban areas (1%). Further details on the catchment's instrumentation, soil type, land use and hydrological behavior can be found in (Casalí et al., 2008). Previous research works on this catchment focused on soil moisture retrievals (Alvarez-Mozos et al., 2006) and soil erosion evaluation (Casalí et al., 2008).

2.1.2. Cidacos catchment

Cidacos river flows into the Aragón river, one of the main tributaries of Ebro river. At the main hydro station, located in the municipality of Olite, Cidacos has a catchment area of 258 km^2. Elevation ranges from 380 m to 1,156 m. Main river's length is approximately 25 km, and catchment's mean slope is 18%. 35% of the catchment presents flat-gentle slope areas (< 10%) and 19% of the catchment is characterized by steep slopes (> 30%). Climate in the area is defined as mild-Mediterranean, with high rainfall variability that caused dramatic oscillations in the annual water yield between 0.4 and 39 hm^3, with an average value of 19.65 hm^3 in the historic observed series (since 1989). The annual mean precipitation was 639 mm. The catchment is equipped with 8 weather stations: 4 automatic stations (10 min basis) and 4 manual (daily). Highest rainfall rates occur on the North-Eastern mountainous area (809 mm/year), which contrasts with the low 453 mm/year measured in the South. Daily mean temperature is higher than in the adjacent Arga catchment (12.6 °C), while relative humidity is lower (69%). Predominant soil type is *Typic Calcixerepts,* but *Typic Xerorthents* are also found in the North-Eastern mountainous area, and *Typic Xerofluvents* are predominant on the river network paths (NRCS-USDA, 2014). Predominant textures are clay-loam on accumulation hillslopes and silty-clay and loam on eroded hillslopes.

Approximately half of the catchment is used for cereal cultivation (47%, including some minor irrigated areas), while the other half is divided into forest (27%) and dispersed bushes (22%) land covers. Urban areas account for the remaining 4%. Further description of the catchment for its distributed hydrological modelization is given in section 3.5.3.

2.1.3. Arga catchment

Arga river is also one of the main tributaries of Ebro river. Only its upper part has been used on this studies, specifically the 810 km^2 defined by the gauging station at the municipality of Arazuri, being the main river channel 53 km long. Elevation descends from 1,400 m to 400 m at the outlet, with a mean slope of 24%. Flat and gentle-slope areas (< 10% slope) represent 29% of the catchment, and steep slopes (> 30%) are found on 37% of the area. These slope values represent the steepest relief of the four studied sites. In this study, a 69 km^2 subcatchment feeding a reservoir (Eugi) in the Northern boundary of the catchment has been subtracted and both rainfall and streamflow measured at the reservoir's outlet were removed from the analysis. Thus an effective catchment area of 741 km^2 was finally used. Historical streamflow records indicate an average annual contribution of 423 hm^3 at Arazuri station. Arga catchment is heavily instrumented with 20 measuring stations, but somehow limited in temporal resolution since most of them (12) are manual stations working on daily basis. The catchment's average annual rainfall measured for the 2000-2012 period was 956 mm. Average daily temperature and relative humidity were 11.7 °C and 76% respectively. In the southern half of the catchment predominant soils belong to *Aquic* and *Typic Xerorthent* groups of USDA's Soil Taxonomy (NRCS-USDA, 2014), and are silty-clay-loam in texture. Geologically this southern part is underlined by clay marls and Pamplona grey marls. In the Northern area of the catchment the prevailing soil classes are distributed according to the landscape's position. While steeper areas are mainly occupied by *Typic Xerorthents*, *Typic Haploxerepts* prevail on the valley plains. Soils are fine and more than 1 m deep except for those in the eroded hillslope that are shallow. The predominant land covers in the catchment are forest (46%, mostly in the

Northern part), rainfed cereal crops (33%), bushes (12%) and urban areas (10%, including the city of Pamplona).

2.1.4. Nestore catchment

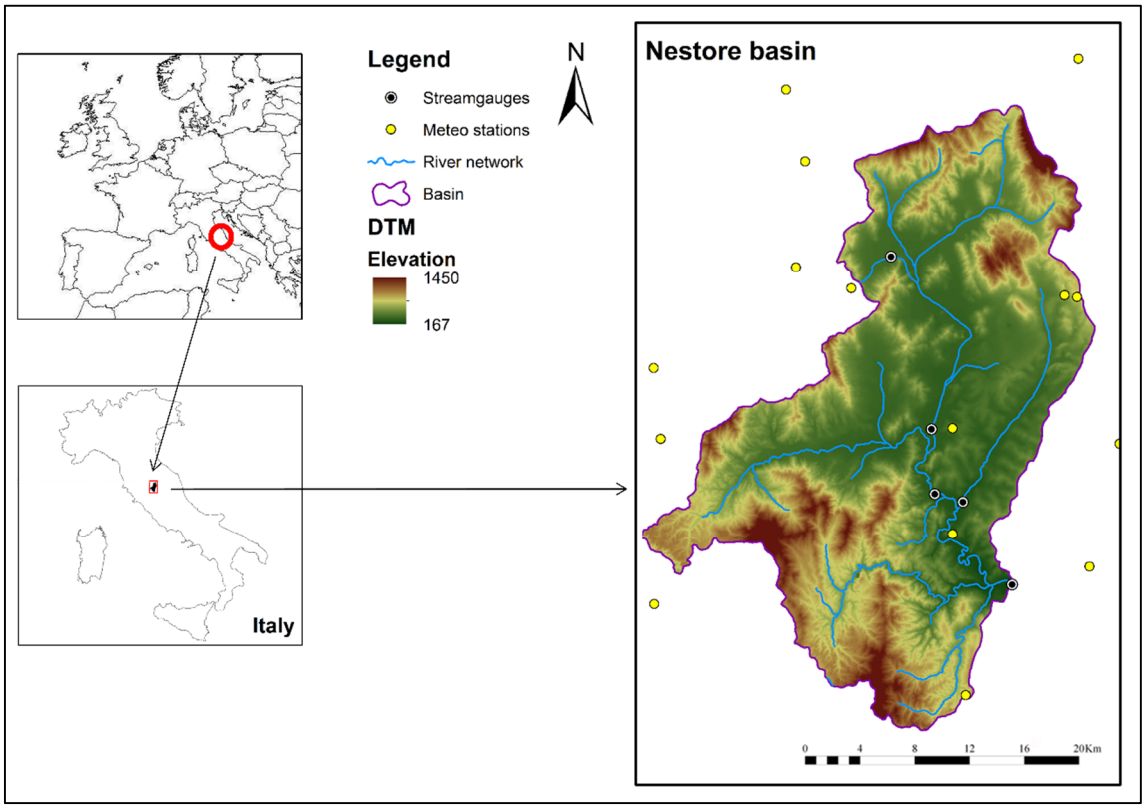

Fig 2.2. Location, topography, hydrological features and instrumentation of the Italian studied catchment of Nestore river, measured at Marsciano.

The Nestore catchment (725 km^2) is located in the Upper Tiber River catchment (Fig. 2.2), an area with a complex topography that can significantly affect the widespread frontal rainfall that causes major flood events. The main land uses are grasslands (54 %) and woods (38 %), whereas urban areas cover only a small part (5 %) of the territory. The geology is characterized by terrigenous facies and flysch deposits. The soil, overlying practically impervious rocks, contains clay and sandy silt. Further information on the soil hydrological properties can be found in Massari et al. (2015). The climate is Mediterranean, with mean annual rainfall of 740 mm. The mean slope of the

catchment is 17 %. The highest monthly rainfall values generally occur during the autumn-winter period, when floods, caused by widespread rainfall, normally occur. A dense, real-time hydrometeorological network (1 station every 150 km^2) has been operating in the area for more than 20 years, and the data are recorded with a time interval of 30 min. Discharges are measured at the hydrometric site of Marsciano (Fig. 2.2), which is characterized by a stage-discharge relationship that is frequently updated to provide reliable discharge estimates.

2.2. HYDROLOGICAL MODELS

2.2.1. TOPLATS

TOPLATS was developed as a water and energy balance model to be used at local and catchment scales. For that, a simple soil-vegetation-atmosphere transfer scheme (SVAT) was implemented onto a TOPMODEL framework (Famiglietti and Wood, 1994). This was afterwards improved by Peters-Lidard et al. (1997) to correct deficiencies in the representation of energy fluxes (i.e. soil evaporation and ground heat flux). Also, some additional modifications were carried out by Pauwels and Wood (1999), who adapted it to high latitude areas, and by Crow et al. (2005b) who tested an expansion of the model to a soil water balance of four layers, and separated soil and canopy contributions to evapotranspiration. The basic concept underlying the model is that shallow groundwater gradients, estimated from the local topography through a Topographic Index (TI) (Sivapalan et al., 1987), set up spatial patterns of soil moisture. Those patterns are considered key factors of simulation control on: 1) storm events, influencing infiltration and runoff generation and 2) inter-storm events, being responsible for evaporation and drainage patterns. TOPLATS incorporates a soil vegetation atmosphere transfer scheme (SVAT) to represent local scale vertical water fluxes within the catchment scale TOPMODEL approach.

2.1.1.1. TOPLATS statistical and distributed modes

TOPLATS can be run in either a fully distributed mode or in a statistical mode (Seuffert et al., 2002). In the fully distributed mode the catchment is subdivided into a grid of regular size cells, where each of those model units (cells) has its own specific soil-vegetation parameterization, soil-topographic index value (TI) and meteorological input data (Pauwels et al., 2002). The land-atmosphere scheme is then applied to each cell. The second mode, named statistical mode, works as a semi-distributed model. Both modes have been applied in this research. The statistical mode in was applied in La Tejeria, Cidacos, Arga and Nestore, while the fully distributed mode was used for Cidacos. In the statistical mode, TI is represented through its statistical probability distribution given a fixed bin-size (Fig. 2.3), thus reducing the computational demand. This mode was developed under the similarity concept, that is, locations with the same TI and soil type, are assumed to respond similarly (Pauwels et al., 2002), performing a semi-distributed catchment representation.

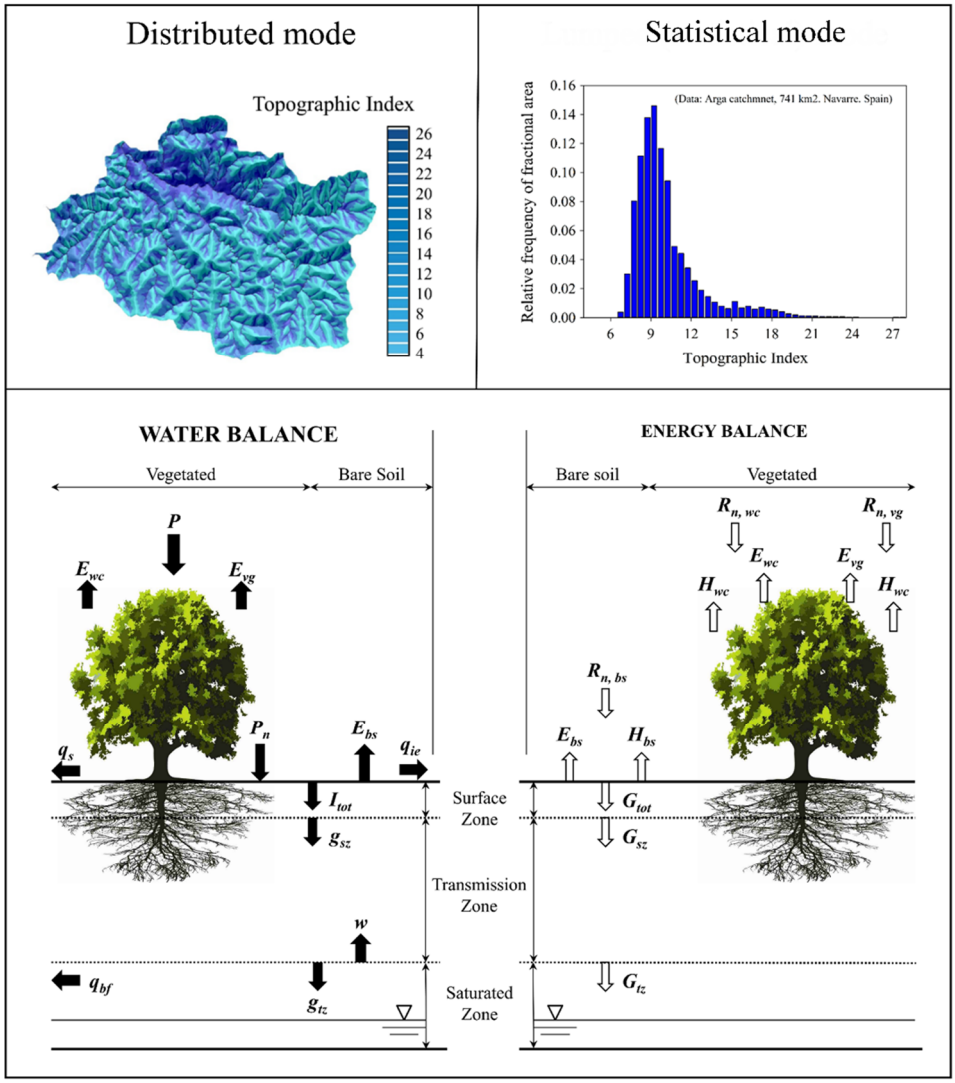

Fig 2.3. TOPLATS model schematic representation: statistical and distributed Topographic Index representation, and SVAT balances (Water and Energy) of vegetated soil (vg), wet canopy (wc) and bare soils (bs). Water balance budgets: precipitation (Pr), net precipitation (P_n), evaporation (E), infiltration excess runoff (q_{ie}), saturation excess runoff (q_s) baseflow (q_{bf}), infiltration (I), drainage (g) and capillary rise (w). Energy balance budgets: net radiation (R_n), latent heat flux (H) and soil heat flux (G).

In both modes, water and energy balances are applied similarly. In TOPLATS, the soil column is divided into two layers (Fig. 2.3): a thin surface zone (SZ) and the deeper transmission zone (TZ). Furthermore, the land surface is partitioned into bare and vegetated areas. Separate water balances (Fig. 2.3) are formulated for the different water reservoirs: the surface zone, the transmission zone, the water table and the canopy. Infiltration is calculated as the minimum of the soil infiltration capacity (Milly, 1986) and net precipitation. The exchange of soil water between the upper and lower

layers is calculated assuming diffusive flux (Peters-Lidard et al., 1997), where diffusivity is given as a function of Brooks and Corey (1964) parameters. Evaporation is calculated with a soil resistance formulation (Passerat De Silans et al., 1986) as the minimum of a soil controlled and an atmospherically controlled evaporation rate. Similarly, canopy transpiration is calculated as the minimum of a plant and an atmospherically controlled transpiration rate, where the canopy resistance to transpiration (Jarvis, 1976) is a function of a minimum: 1) stomatal resistance, 2) LAI, and 3) stress factors (i.e. solar radiation, vapor pressure deficit, air temperature and soil moisture) (Jacquemin and Noilhan, 1990). Plant growth is not directly simulated by TOPLATS, but the seasonal development of plant properties is described by user defined time-step updates of plant parameters, i.e., leaf area index, plant height and stomatal resistance (Bormann, 2006a). A runoff-routing routine based on the unit hydrograph method proposed by the (SCS - Soil Conservation Service, 1972) was written in FORTRAN and added to TOPLATS.

TOPLATS has been applied with different objectives, on a broad range of time and space-scale conditions (Table 2.1). Some researchers used the model to analyze the effects of land use changes and soil classification uncertainty at the catchment scale (Bormann et al., 2007; Breuer et al., 2005; Crow and Wood, 2002; Loaiza-Usuga and Poch, 2009; Loosvelt et al., 2015, 2014a). The spatial resolution of input data, and its influence on different model outputs, such as water balances and flow components, were also investigated (Wood et al. 1988; Endreny et al. 2000; Bormann 2006a, Bormann 2006b). TOPLATS has also been used for discrete observations up-scaling (Crow et al., 2005b), local weather prediction (Seuffert et al., 2002) or crop growth analysis (Pauwels et al., 2007). Different types of remotely sensed information have been integrated with TOPLATS trough data assimilation (DA) procedures for improving streamflow simulation (Pauwels et al., 2002, 2001), soil moisture simulation (Crow et al., 2001; Houser et al., 1998; Lucau-Danila et al., 2005) or latent heat fluxes estimation (Crow and Wood, 2003).

2.1.1.2. Previous sensitivity analysis and calibration studies

The model's behavior and performance has also been explored, for instance, to evaluate its sensitivity to soil parameters (Loosvelt et al., 2014b, 2011) or to analyze different calibration strategies (Goegebeur and Pauwels, 2007; Loaiza-Usuga and Pauwels, 2008; Pauwels et al., 2009). Table 2.1 presents a compilation of the most relevant works carried out with TOPLATS where parameter values were investigated with different objectives and degrees of complexity. On this thesis, parameters selected for TOPLATS sensitivity analysis and calibration were chosen principally according to information extracted from these works.

Calibration related researches (Table 2.1) focused in some cases on obtaining optimal streamflow values at catchment outlet (Crow and Wood, 2002), while some others aimed to obtain accurate soil moisture simulations (Goegebeur and Pauwels, 2007). Pauwels et al. (2009) pointed out that the three most important soil parameters in the determination of the soil moisture content were the saturated hydraulic conductivity (K_s), the pore size distribution index (B), and the bubbling pressure (ψ_c).

Table 2.1. Most relevant TOPLATS parameter calibration (C), Evaluation (E) and Uncertainty (U) analyses published in the past. The type of study, observed variables of interest, catchment or area size and parameters studied are given. Parameter abbreviations are as follows: Leaf Area Index (LAI), stomatal resistance (STr), crop height (h), Brooks-Corey pore size distribution index (B), bubbling pressure (ψc), saturated soil moisture (θs), residual soil moisture (θr), surface saturated hydraulic conductivity (Ks), first soil resistance parameter (rmin), subsurface flow at complete saturation (Q0), hydraulic conductivity decay (f), and initial water table (WTi).

Reference	Type of study	Observed variable	Catchment or Area size	Evaluated TOPLATS parameters											
				Vegetation			Soil						Baseflow		Water table
				LAI	ST_r	h	B	ψ_o	ϑ_o	ϑ_r	K_o	r_{min}	Q_0	f	WT_r
Crow & Wood (2002)	Surface energy fluxes prediction	*Soil moisture / Streamflow /heat fluxes*	*575,000 km²*	E	E	E						E			
Seuffert et al. (2002)	Model coupling	*Streamflow*	*2,000 / 750 / 65 km²*										C	C	
Crow & Wood (2003)	Data assimilation	*Latent heat flux*	--	C									C	C	C
Crow et al. (2005)	Measurements upscaling	*Soil moisture*	*6,400 km²*		E							E	E	E	
Lucau-Danila et al. (2005)	Parameter retrieval from SAR	*SAR data / soil moisture / plant height/ LAI*	*18 agricultural fields (area)*	E		E					C		C	C	C
Bormann (2006b)	Spatial data resolution	*Streamflow*	*134 / 81 / 63 km²*		C								C	C	
Goegebeur & Pauwels (2007)	Calibration	*Soil moisture*	*2.26 km²(area)*				C				C				
Bormann et al. (2007)	Land use change	*Streamflow*	*693 km²*		C		E	E	E	E			C	C	
Loaiza-Usuga and Pauwels (2008)	Calibration	*Soil moisture*	*222 km²(area)*	E		E	C	C			C		E	E	
Pauwels et al. (2009)	Calibration	*Soil moisture*	*250 km² (area)*				C	C			C				
Loosvelt et al. (2011)	Soil Hydraulic Parameter (SHP) uncertainty	*Soil moisture*	*point-scale*				U	U	U	U	U				
Loosvelt et al. (2014a)	Prediction uncertainty	*Streamflow*	*91 km²*										C	C	C

Bormann et al. (2007) proposed a calibration procedure based on first, reproducing the long-term water balance tuning vegetation parameters (stomatal resistances) and secondly, on optimizing the model efficiency by fitting the baseflow recession: adjusting baseflow at complete saturation (Q_0) and the hydraulic conductivity decay (f) parameters. Seuffert et al. (2002) and Bormann (2006b) also worked on the manual calibration of Q_0, f and stomatal resistance (ST_r), while Goegebeur and Pauwels (2007) evaluated PEST and Extended Kalman Filter methods performance in K_s and B calibration. In Loosvelt et al. (2015) automatic calibration was performed based on a weight-adaptive recursive parameter estimation method, which is in concept a multi-start calibration approach.

2.2.2. MISDC

MISDc is a conceptual and semi-distributed model that consists of two main components, a soil water balance model (SWB) (Brocca et al., 2008) to simulate the soil moisture temporal pattern and a routing module (Melone et al., 2001) for transferring the rainfall excess to the catchment outlet (Fig 2.4). The two models are linked through an experimentally derived linear relationship (Brocca et al., 2009b) between the potential maximum soil moisture retention S of the Soil Conservation Service-Curve Number (SCS-CN) and the relative soil moisture at the beginning of the event. The SWB model is a simple water balance model that simulates the main processes in a single soil layer (i.e., infiltration, percolation and evapotranspiration). In particular, infiltration is modeled through the Green–Ampt equation, drainage is modeled using a gravity-driven non-linear relationship, and actual evapotranspiration is modeled using a linear relationship with potential evapotranspiration, calculated using a modified Blaney and Criddle method.

Once the S parameter is estimated, the routing to the catchment outlet is obtained from the convolution of the rainfall excess and the geomorphological instantaneous unit hydrograph (GIUH), proposed by Gupta et al. (1980). The model was initially developed as a single layer soil simulation structure but was later implemented with a second layer to improve the soil water balance simulation,

with the objective of making it a suitable tool to adequately assimilate satellite SSM observations. However, the 2 layers configuration did not improve DA performance (Brocca et al., 2012). Therefore, the initial MISDc configuration where the soil is modelled as a single layer (deposit) has been used on this study (Fig. 2.4).

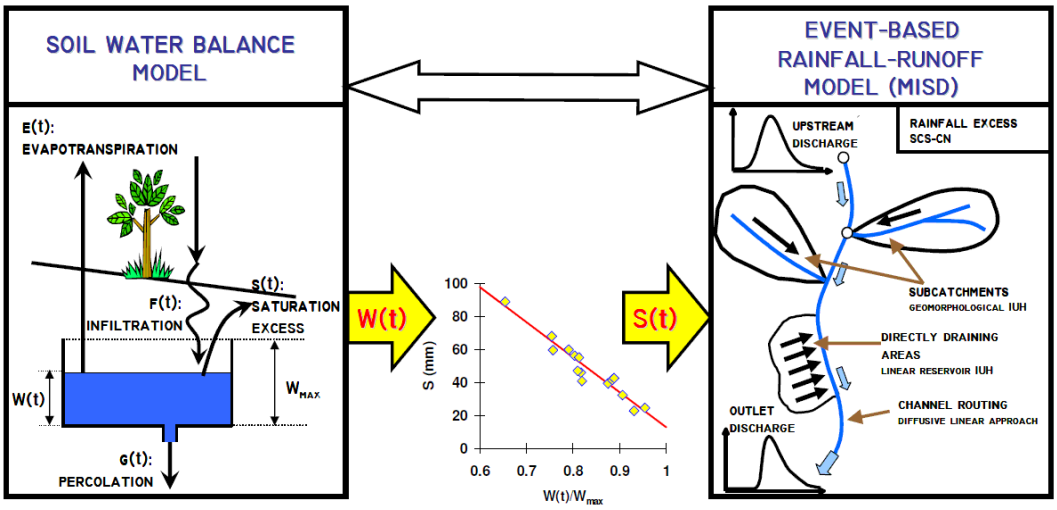

Fig 2.4. MISDc model conceptual scheme (Model developed by the Hydrology Group of the Research Institute for Geo-Hydrological protection. CNR. http://hydrology.irpi.cnr.it/)

The MISDc model requires meteorological variables that are routinely measured (rainfall and air temperature) as input data, and it provides the soil saturation degree and the discharge as output data. To run the continuous rainfall-runoff (RR) model, 9 physical and empirical parameters have to be estimated. The physical parameters include the saturated hydraulic conductivity (K_s), pore size distribution index (β), and maximum water capacity of the soil layer (W_{max}). The main empirical parameters are the parameter controlling the fraction of drainage that transforms into subsurface runoff (ν), the correction coefficient for potential evapotranspiration (K_c), the lag-area relationship parameter (η), the initial abstraction coefficient (λ) and the parameter of the relationship between modeled SM and the S of the SCS-CN method (α). While the model was developed following a semi-distributed approach, in this study a lumped modified version of the model was used.

MISDc has been successfully applied to many catchments worldwide (Brocca et al., 2011b) and also to the Tiber River in central Italy (Brocca et al., 2011a) for flood prediction and operational purposes. Further description of the model and its performance under Mediterranean conditions can be found in Brocca et al. (2013), Camici et al. (2011), and in Massari et al. (2015). Specific DA studies using the MISDc model include Brocca et al. (2012, 2010b). In this research, MISDc calibration was performed using a standard gradient-based automatic optimization search function (Brocca et al., 2011a), tuning four parameters (W_{max}, K_s, K_e and η).

2.3. SOIL MOISTURE REMOTE SENSING

Among the wide range of active and passive microwave devices onboard different satellites used for SSM estimation, two currently operational sensors and probably the most important at present were selected for this research work (i.e., ASCAT and SMOS), as they were deemed suitable for the objectives of the thesis. These two sensors were also selected to compare the suitability of both L-band and C-band observing systems, so the study gives a glimpse on the applicability of different remote sensing data sources for DA tasks. The sensor selected at C-band was ASCAT, while SMOS was the one selected at L-band. Both are described in this chapter, including their spatial and temporal resolutions, as well as other technical details on the instruments themselves and the algorithms used to retrieve SSM from their observations.

2.3.1. ASCAT

The Advanced SCATterometer (ASCAT) is an active microwave sensor that operates in C-band (5.255 GHz) at VV polarization, which measures the backscatter of the Earth surface, a magnitude that is sensitive to the dielectric properties of the soil surface, and hence SSM. ASCAT was first launched in October 2006 onboard the Meteorological Operation-A (MetOp-A) satellite, the first

of the MetOp series that consists of three satellites: MetOp-A, MetOp-B (available since 2012), and MetOp-C (scheduled for launch in 2018), which are expected to provide an uninterrupted stream of ASCAT observations well into the 2020s (Wagner et al., 2013). The MetOp-A satellite follows a near-polar sun-synchronous orbit at an altitude of approximately 817 km with a repeat cycle of 29 days, completing 14 orbits per day and providing a daily global coverage of approximately 82 % of the Earth due to its 550-km wide observation swath. The satellite follows a near-polar orbit, scanning the Earth's surface in both descending and ascending overpasses, corresponding in Western Europe with one acquisition in the morning (descending pass) and once in the evening (ascending pass), between 08-11 and 17-21 UTC, respectively (Brocca et al., 2010b).

The ASCAT-SSM product has a spatial resolution of 50 km and 25 km (resampled to 25-km and 12.5-km grids in the swath geometry), and represents the degree of saturation of the topmost soil layer, ranging from 0 % (dry) to 100 % (wet) (Albergel et al., 2012). To retrieve SSM, the backscattering coefficients are first normalized to a reference incidence angle of 40° and then scaled between the lowest and highest values measured over a long period (Parrens et al., 2012). The soil moisture retrieval scheme uses a change detection approach that is very similar in functionality to the Water Cloud Model (Attema and Ulaby, 1978) but less complex from a mathematical point of view (Bartalis et al., 2007). Two ASCAT−SSM products are available: the first is a NRT product, generated by the European Organization for the Exploitation of Meteorological Satellites (EUMETSAT) (Wagner et al., 2013), and the second is an enhanced product reprocessed and updated by TU Wien, where the most recent algorithmic updates are included (Naeimi et al., 2009). The latter was used in this study and consists of a 6-year (2007-2012) time series at a 12.5-km resolution. The RMSE of this ASCAT−SSM product is estimated to range between 0.014 and 0.06 $m^3 m^{-3}$ (Albergel et al., 2009; Brocca et al., 2010a; Matgen et al., 2012b), with an expected mean value of 0.04 $m^3 m^{-3}$ (Matgen et al., 2012b).

2.3.2. SMOS

The ESA's Soil Moisture and Ocean Salinity (SMOS) mission is in orbit since 2009, providing estimates of salinity over the oceans and of SSM over continental surfaces (Polcher et al., 2016). SMOS is a sun-synchronous orbiting satellite operating at an altitude of 755 km (Rötzer et al., 2014). It is the first dedicated soil moisture mission and its measuring principle is based on the relationship between soil emissivity at microwave frequencies (i.e., brightness temperature) and its dielectric properties, and hence soil moisture (Kerr et al., 2001). SMOS operates at L-band (1.4 GHz) with varying incidence angles, its observation depth then is estimated to be ~5 cm with a spatial resolution of 35-50 km depending on the incident angle and the deviation from the satellite ground track (Wanders et al., 2014b). SMOS mission is equipped with a Microwave Imaging Radiometer using Aperture Synthesis (MIRAS), a 2D interferometric sensor with 69 antenna receivers distributed on a Y-shaped deployable array and a central hub. Due to its operating frequency, SMOS data are potentially affected by radio frequency interference issues (RFI), although the level of affection varies significantly depending on the region of the World (Asia is the most affected continent). Nowadays these RFI are systematically detected and flagged from the data (Oliva et al., 2016). Altogether, the nominal revisit time of SMOS is of 1-3 days depending on the latitude, for both ascending (06:00 LST) and descending (6:00 pm LST) passes (Xu et al., 2015).

The SMOS soil moisture retrieval algorithm consists in iteratively minimizing the differences between measured and modelled brightness temperatures for a variety of incidence angles (Array Systems Computing Inc, 2014). The forward modelled values are a function of polarization, incidence angle, soil moisture (through the soil dielectric constant) and other physical parameters influencing land emissivity at L-band, namely land surface temperature, soil roughness, vegetation optical depth and volume scattering albedo. Ancillary information on land-cover and soil properties (e.g. clay fraction, bulk density, field capacity and wilting point) is also used in the forward modelling. The inversion (retrieval of geophysical variables) is performed by minimizing a cost function that

accounts for the weighted squared differences between modelled and measured data (Kerr et al., 2012).

In this study, a SMOS-based high resolution SSM product (1-km) was used for data assimilation into a distributed model. The so called SMOS-BEC L4 product, developed by Piles et al. (2011), has been applied over a northern Spanish catchment of 258 km^2. This product was obtained at 10 and 1 km resolutions resulting from the application of a downscaling approach to improve spatial resolution of original SMOS data with the use of higher resolution visible/infrared (VIS/IR) satellite data. The algorithm is based on the so-called "universal triangle" concept that relates VIS/IR parameters, such as the Normalized Difference vegetation Index (NDVI), and Land Surface Temperature (*Ts*), to the soil moisture content. This downscaled product was thus achieved in practice by combining SMOS and MODIS VIS/IR data from both the Terra and Aqua spacecrafts.

In short, this downscaling approach combines highly–accurate, but low resolution SMOS radiometric information with high resolution, but low sensitivity, VIS/IR imagery to provide SSM data across spatial scales (Piles et al., 2011). The methodology was first tested with a set of SMOS and MODIS data over the Oznet network, in South-East Australia. Later (Piles et al., 2014), the fine-scale product quality was improved by the inclusion of SMOS polarimetric and multi-angular information (Piles et al., 2015). The latest L4 product (the one used in this research) is the version 3.0 or "all weather". In this version, high resolution soil moisture is estimated under all-weather conditions, greatly enhancing the potential applicability of the data. The downscaling approach is also based on the methodology presented in (Piles et al., 2014), and on the further studies by (Sanchez-Ruiz et al., 2014) who tested the impact of using different vegetation indices from MODIS with higher spatial and temporal resolution (Piles et al., 2015). The novelty of the "all-weather" product is the introduction of ERA-Interim Land Surface Temperature (LST) data in the MODIS LST/NDVI space (Piles et al., 2015).

The data, produced for both ascending and descending passes, is available since December 2016 for the Iberian Peninsula, South Africa and Ghana, and can be freely accessed at the

Barcelona Expert Center data distribution and visualization service (http://cp34-bec.cmima.csic.es/data/data-access/).

CHAPTER 3. METHODS

3.1. SENSITIVITY ANALYSIS

A general description of SA methods is given in the Introduction chapter of this thesis, thus, this section covers only two relevant aspects: Design of Experiment sampling techniques (DoE), and the specific SA methods used in this study: Morris (1991) and Sobol (1993). Both Morris Method (MoM) and Sobol Method (SoM) follow approaches based on DoE techniques, which have a large influence on SA efficiency (Song et al., 2015).

Some SA methods require specific DoE sampling techniques designed ad hoc. This is the case of MOAT sampling for MoM (Morris, 1991) and the sampling technique proposed by Saltelli (2002) (denoted as SOBOL) for SoM (Gan et al., 2014). These sampling techniques are both based on simple random sampling, but different conditions need to be satisfied for their sample sizes (Song et al., 2015). A detailed description on both sampling methodologies can be found in Gan et al. (2014). Substantial differences in the number of required model runs (N_R) are found between both MOAT and SOBOL sampling methods. In the first case (Morris, 1991):

$$N_R = (k + 1) * n \tag{3.1}$$

where k is the number of parameters whose sensitivity is evaluated and n is the number of samples.

On the other hand, Saltelli (2002) proposed two efficient approaches to reduce the computational cost of SoM. The one applied on this study requires a larger number of model runs, but provides more consistent results:

$$N_R = [(2 * k) + 2] * n \tag{3.2}$$

3.1.1. Morris method

The screening-type Morris Method (Morris, 1991) takes advantage of elementary effects (EE) computed at evenly spaced values of each parameter over its entire range. The final effect is then calculated as the average of a set of partial effects. Therefore, it provides a global sensitivity measure

with lower computational cost compared to most global methods. In this way, local sensitivities are integrated to a global sensitivity measure and the presence or absence of nonlinearities or correlation interactions with other parameters can also be identified (Van Griensven et al., 2006). Screening methods, such as MoM, aim to identify the subset of non-influent factors in a model using a small number of model runs (Campolongo et al., 2011).

MoM has a low computational cost, is simple to implement and its results are easy to interpret (Saltelli et al., 2000), but individual interaction between parameters cannot be detected, since MoM only calculates the overall interaction of a parameter with the rest (Saltelli et al., 2000). It measures qualitatively relative sensitivity by ranking input parameters in order of sensitivity but cannot quantify in absolute terms how much one parameter is more important than another (Campolongo and Saltelli, 1997).

Considering that $y(X)$ is the objective function (goodness-of-fit of the model or model output of interest) and $X = (X_1,\ldots, X_k)$ is the parameter set, then

$$y(X) = f(X_1, \ldots, X_k) \tag{3.3}$$

In MoM, $y(X)$ is calculated for each parameter set, where parameter values (X) are changed OAT. The difference resulting of both $y(X)$ values is divided by the variation of perturbed parameter values (Δ) to obtain the elementary effect of each parameter $d_i(X)$. Elementary effects are calculated as follows:

$$d_i(X) = \frac{[y(X_1,X_2,\ldots,X_{i-1},X_i+\Delta, X_{i+1},\ldots,X_k)-y(X)]}{\Delta} \tag{3.4}$$

This calculation process is repeated until the defined number of samples (n) are completed for each parameter. Finally, the mean (μ) and standard deviation (σ) values of d_i for the n samples are used as sensitivity indices, where μ and σ indicate the influence of each parameter on the objective function (Shin et al., 2013). A high μ value indicates an important overall influence of the parameters and a high value of σ (hereafter referred to as Morris interaction) means strong interactions with other parameters or the effect of nonlinearities (Shin et al., 2013). Instead of using μ, this study considers the mean of the absolute values of the n samples of d_i, denoted as μ^* (hereafter referred

to as Morris sensitivity) to overcome the problem of the effects of opposite signs due to a models' non-monotonic characteristics (Campolongo et al., 2011). Further description of Morris method and its implementation for specific purposes can be found in Francos et al. (2003), van Griensven et al. (2006), Shin et al. (2013), and Wainwright et al. (2014).

3.1.2. Sobol method

SoM is a variance decomposition global SA method where all parameters are varied simultaneously. One of its main advantages is that it is a model-free method, i.e., it can compute sensitivity indices regardless of the linearity, monotonicity (or other generic assumptions) on the underlying model (Baroni and Tarantola, 2014). In SoM the variance of the model output is decomposed into fractions that result from either individual parameters or parameter interactions. The sensitivity of each parameter or parameter interaction is then assessed based on its contribution (measured as a percentage) to the total variance computed using a distribution of model responses (Zhang et al., 2013). Sobol sensitivity indices have been shown to be more effective than other approaches in capturing the interactions between a large number of variables for highly nonlinear models (Tang et al., 2007).

As in Eq.3.3, considering that $y(X)$ is the objective function (goodness-of-fit of the model or model output of interest) and $X = (X_1,\ldots, X_k)$ is the parameter set, the total variance of function $y(X)$, $D(y)$, is decomposed into component variances from individual parameters (D_i) and their interactions (D_{ij}, D_{ijk} ,…):

$$D(y) = \sum_i D_i + \sum_{i<l} D_{ij} + \sum_{i<j<l} D_{ijl} + \cdots + D_{12\ldots k} \quad (3.5)$$

where D_i represents the average reduction in variance achieved if the parameter i was known (Ratto et al., 2001) and D_{ij} is the amount of variance due to the interaction between parameter X_i and X_j. The single parameter sensitivity (First-Order Sobol index), S_i, and parameter interaction (Second-Order index), S_{ij}, are then assessed based on their relative contribution to the total variance (D):

$$S_i = \frac{D_i}{D} \quad (3.6)$$

$$S_{ij} = \frac{D_{ij}}{D} \quad (3.7)$$

Also, a third index (Total-Order index), S_{Ti}, that measures the main effect of X_i and its interactions with all the other parameters (Zhang et al., 2013) can be calculated as:

$$S_{Ti} = 1 - \frac{D_{\sim i}}{D} \quad (3.8)$$

where $D_{\sim i}$ is the bottom marginal variance, that accounts for the amount of variance due to all of the parameters except for X_i (Massmann and Holzmann, 2012). Hereafter in this article, S_i is referred to as Sobol sensitivity and S_{Ti} as Sobol interaction. SM main characteristic is the use of two different sets of samples, generated by the same scheme and with the same number of elements. SM uses the first set to calculate the overall output mean and variance (i.e., the combined effects of all parameters) while the second sample is then used to resample each parameter, rather than setting each to a fixed value, for the calculation of total and individual variance contributions (van Werkhoven et al., 2008). D_i and $D_{\sim i}$ can be calculated as described in Massmann and Holzmann (2012) and in Zhang et al. (2013). In the last years SM has been frequently used in different types of hydrological models (Gan et al., 2014; Massmann and Holzmann, 2012; Shin et al., 2013; van Werkhoven et al., 2008; Wainwright et al., 2014).

3.2. CALIBRATION AND VALIDATION PROCEDURE OF TOPLATS MODEL

3.2.1. Optimization algorithm

In this work, a Multi-Start approach of the Powell Method (MSPM) was used to calibrate the TOPLATS model. Powell Method (PM) (Powell, 1964) belongs to the category of local and derivative-free algorithms. PM is a conjugate directions method, which are capable of minimizing quadratic functions in a finite number of steps. Since a general nonlinear function can be approximated reasonably well by a quadratic function near its minimum, this type of conjugate directions method is expected to speed up the convergence of even general nonlinear objective functions (RAO, 2009).

PM can find a global optimum when specifically tuned to a certain objective function, but in cases of sophisticated algorithm optimization (such as complex hydrological models), the selection of appropriate parameter starting points may affect algorithm performance substantially. Inadequate selection of initial parameter values may lead to convergence to inferior local optima or even to numerical dispersion (Paik et al., 2005). All in all, PM has been frequently applied on different hydrological calibration procedures and models (Chen et al., 2005; Geem and Roper, 2010; Yang et al., 2011; Zhang and Lindström, 1997).

In our study, to avoid the algorithm ending at local minima constraint, within each parameter's search range different values were selected as initialization values for the search. Dispersed values covering the full feasible parameter range were selected. The algorithm was free-available and programmed in FORTRAN (Press et al., 1988), the same programming language that was used to develop TOPLATS which facilitated the integration of both tools.

3.2.2. CAL/VAL implementation for TOPLATS

Different studies have previously discussed the advantages of different random period selection techniques (RND) for model calibration and validation (Brath et al., 2004; Kim and Kaluarachchi, 2009; Senarath et al., 2000). Some of them evaluated data length requirements when RND approach is applied, compared to the conventional (CON) approach. For example, Kim and Kaluarachchi (2009) concluded that randomly sampled data required a shorter calibration length (36 months) than continuous data (120 months) to reach good model performance. Similarly, Perrin et al. (2007) tested the random approach with two daily rainfall-runoff models showing that, in general, even just 350 calibration days sampled out of a longer data set including dry and wet conditions could be sufficient to obtain robust estimates of model parameters. On the conventional calibration approach, Yapo et al. (1996) estimated a minimum of 96 months for adequate model calibration and also noted that parameter uncertainty was reduced when wettest data records were used.

In the first of the three studies of this thesis, following referenced studies recommendations on CON and RND period selection, we considered a 12 years period, and included two calibration and validation (CAL/VAL) period selection strategies in order to evaluate the influence of climatic particularities on the CAL/VAL results. First, a "conventional" strategy (CON) was followed, where the first hydrological year was used for warming-up (2000-2001), the next six years for calibration (2001-2007), and the remaining five years for validation (2007-2012). Secondly, a "random" strategy (RND) was proposed and evaluated. On this second approach, each month's data was randomly assigned to either CAL or VAL period according to two conditions: 1) the mean streamflow of CAL and VAL series could not differ more than 10% and, 2) their standard deviations could not differ more than 15%. This second strategy was adopted to circumvent the imbalance between CAL and VAL periods resulting from irregular climatic conditions typical of Mediterranean areas. On this first study, in total, 72 months were randomly assigned to CAL and 60 months to VAL, maintaining the same proportion as in the conventional strategy.

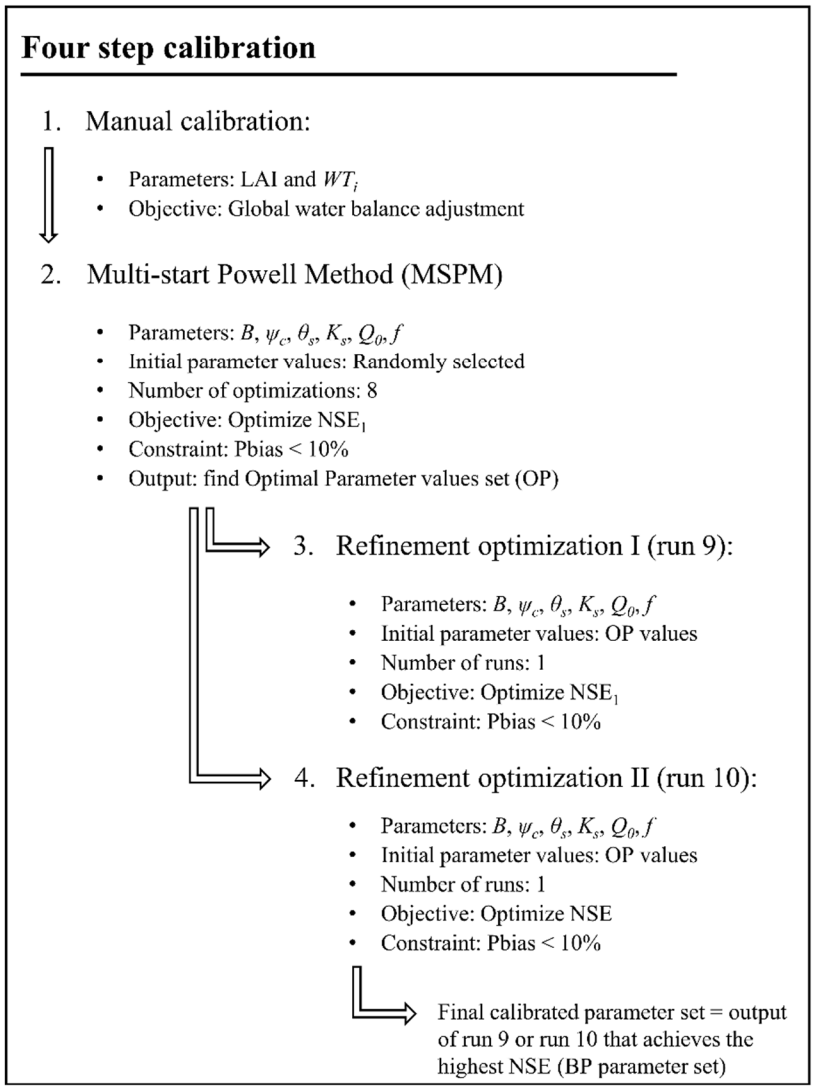

Fig. 3.1. Four Step calibration procedure scheme

A four steps calibration (Fig. 3.1) was then performed exactly in the same way for both approaches (CON and RND): 1) manual calibration of the global water balance by adjusting Leaf Area Index (LAI) and Initial water table depth (WT_i), and 2) MSPM of six parameters (Table 3.1) on 8 different start points. On the latter, the algorithm was setup to maximize NSE_1. Optimization of NSE_1 was assumed to improve model efficiency while maintaining water balance on optimal performance. In a final step, out of the 8 sets of optimal parameter (OP) values obtained, the one offering best results (lower Pbias and higher NSE) was taken and used as a new initial set. Then, a new pair of refinement optimizations (steps 3 and 4) were carried out: run number 9 was set up again with NSE_1 as objective

function (with the objective of finding possible better results with parameter values close to selected OP) and run number 10 using NSE as objective to prioritize high flows simulation improvement. These refinement optimization runs (run 9 and 10) allowed obtaining the Best Performing parameter set (BP).

Table 3.1. TOPLATS parameters included on the calibration and sensitivity analysis with Morris and Sobol methods. Type, symbol, units and parameter value ranges are shown

	Type	Parameter	Symbol	Units	Min limit	Max limit
1.	Soil properties	Brooks-Corey Pore Size distribution Index	B	--	0.1	1.0
2.	Soil properties	Bubbling pressure	ψ_c	m	0.1	1.0
3.	Soil properties	Saturated soil moisture	θ_s	cm^3 / cm^3	0.4	0.6
4.	Soil properties	Surface saturated hydraulic conductivity	K_s	m / s^1	$1e^{-07}$	$1e^{-03}$
5.	Soil properties	First soil resistance parameter	r_{min}	s / m^1	4,000	80,000
6.	TOPMODEL	Subsurface flow at complete saturation	Q_0	mm / day^1	5	175
7.	TOPMODEL	Hydraulic conductivity decay	f	m^{-1}	1	14

3.3. DATA ASSIMILATION

3.3.1. Observed SSM preprocessing: soil water index (SWI) and re-scaling methods

Two data assimilation experiments were performed on this thesis. In the first one, ASCAT data was used for data assimilation into Arga and Nestore catchments, with both MISDc and TOPLATS (statistical mode) models. On this first experiment, ASCAT data was processed through 2 steps: first observed discrete data was transformed into a continuous Soil Water Index (SWI), and secondly, that SWI was re-scaled. On the second DA experiment of this thesis, the SMOS data was treated differently, due to its deeper observation depth (described in section 2.3). In this case, SMOS data was not transformed into a SWI, and was directly re-scaled to be assimilated into a 5 cm depth

model layer. In both cases, satellite observed data were afterwards re-scaled with the three same methods, described later on this section.

Thus, in the first DA experiment, to solve the mismatch between ASCAT observation depth and that of the surface layer considered by models, ASCAT−SSM values were transformed (filtered) in two steps: the soil water index calculation (SWI), followed by an SWI re-scaling procedure (Alvarez-Garreton et al., 2015, 2014; Brocca et al., 2009a; Cho et al., 2015; Matgen et al., 2012a; Paulik et al., 2014). For the SWI calculation, a recursive filter was used (Wagner et al. 1999), which depends on a single parameter, *T*, characterizing the temporal variation of soil moisture within the root-zone profile (Brocca et al., 2012). It functions as a low-pass filter that smoothes the SSM series (Matgen et al., 2012b) and assumes a linear relationship between the SM in the first centimeters of the soil and the SM content in the deeper root zone (Alvarez-Garreton et al., 2014). The recursive filter (Eq. 3.9) at each time step (*k*) is calculated as follows (Albergel et al., 2008):

$$SWI_k = SWI_{k-1} + U_k\,[O_k - SWI_{k-1}] \tag{3.9}$$

where O_k is an available ASCAT observation and U_k is a gain updating term (Eq. 3.10), varying between 0 and 1, calculated as:

$$U_k = \frac{U_{k-1}}{U_{k-1} + e^{\left(\frac{k-(k-1)}{T}\right)}} \tag{3.10}$$

Parameter *T* for ASCAT data was calibrated (considering a variation range between 1 and 200 days) by optimizing the correlation coefficient *R* between SWI and model-simulated SSM time series. This was performed for a 2-year calibration period: Jan 2007 - Jan 2009. Regarding SSM product error, Brocca et al. (2010a) based on in-situ observations, estimated a 10 % error in SWI values obtained from ASCAT data.

In a second step, ASCAT-derived SWI values were re-scaled, comparing different re-scaling techniques (RTs). Three different RTs were selected, and their influence on the DA results was evaluated. On the second DA experiment, those three re-scaling methods were also applied to SMOS data. These RTs were selected to cover a wide range of order-moments rescaling (as in Lievens et al. (2015)):

- 1. Cumulative distribution function matching (CDF). This method was first proposed by Reichle (2004) and has been applied in different assimilation and SSM product evaluation experiments (Alvarez-Garreton et al., 2014; Drusch, 2005; Liu et al., 2012; Massari et al., 2015; Matgen et al., 2012b; Scipal et al., 2008). CDF matching ensures that the statistical distribution of both the satellite data and model time series is the same, so that assimilation only adjusts the model for random variations (Renzullo et al., 2014).
- 2. Linear regression (LR). In this approach, minimization of the mean square difference (*msd*) between modeled and rescaled data is performed (Yilmaz and Crow, 2013) through a least squares linear regression technique (Alvarez-Garreton et al., 2014; Crow et al., 2005a). Details of the numerical solution performed to apply this method are described in Yilmaz and Crow (2013).
- 3. Variance matching (VM). This method involves re-scaling the observed SSM values to match only the first two moments (mean and variance) of the probability distribution of the simulated time series (Lievens et al., 2015; Massari et al., 2015; Sahoo et al., 2013).

Regarding the ASCAT data experiment, the three RTs were first fitted using a 3-year (Jan 2007-Jan 2010) calibration period and then validated using a 2-year and 9-month period (Jan 2010 to Oct 2012). This setup guarantees that re-scaling is always based on previous data; consequently, DA can be performed in real time, similarly to Alvarez-Garreton et al. (2014). On the other hand, re-scaling of SMOS data was only performed for the validation and assimilation period (Oct/2013-Oct/2015). It must be noted that all the three methods guarantee that the rescaling time-series of observed data will have the same mean value of the model-simulated soil moisture. In both ASCAT and SMOS applications for data assimilation, these three RT were tested. They differ on the moments-matching that they offer: 1) LR fits only the first order moment (mean), 2) the second, VM, fits the first and second order moments (mean and variance), while CDF method adjusts all order moments (mean, variance and skewness) of observed data to the simulation, similarly to the research in Lievens et al. (2015).

3.3.2. Ensemble Kalman filter (EnKF)

The EnKF Monte Carlo-based approach (Evensen, 2003) allows model uncertainties to be calculated from the ensemble spread. On this method, to reduce calculation time, it is assumed that the ensemble spread is large enough to represent the true uncertainty of the simulation (Wanders et al., 2014a). The EnKF takes advantage of a statistical approach to evaluate the covariance error matrices of the Kalman filter equations.

In the EnKF, the background state vector becomes an *n* (state variables) x *N* (ensemble members) matrix needed to derive the model error matrix (Thiboult and Anctil, 2015) where: $X^b = \left(X_1^b, \ldots, X_N^b\right)$ with $X_i^b = \left(x_1^b, x_2^b, \ldots, x_n^b\right)_i^T$. As the real true state is unknown, it is approximated by the ensemble mean ($\bar{x}^b$), where *i* refers to the i-*th* member:

$$\bar{x}^b = \frac{1}{N} \sum_{i=1}^{N} X_i^b \tag{3.11}$$

From the ensemble perturbation matrix, defined as $X'^b = X_i^b - \bar{X}^b$, the ensemble background error covariance matrix (*P*) is obtained as in Eq. 3.12:

$$P = \frac{1}{N-1} x'^b x'^{bT} \tag{3.12}$$

On the observation side, uncertainty is considered and evaluated through perturbed observations. An *m* x *N* matrix, where *m* is the number of observations, needs to be calculated to represent perturbed observations ($y_i = y + \varepsilon_i^o$). The perturbations ensemble ($\mathrm{E} = [\varepsilon_1^o, \varepsilon_2^o, \ldots, \varepsilon_N^o]$) is generated with an ensemble mean equal to zero (Trudel et al., 2014), and the ensemble representation of the observation error covariance matrix (*Z*) is then defined as:

$$Z = \frac{1}{N-1} EE^T \tag{3.13}$$

The Kalman gain (G_k) (Eq. 3.14) at each time step *k* (hourly basis in this study) represents the relative importance of the observation error with respect to the prior estimate (i.e., model simulation) and acts as a weighting coefficient. Z_k denotes the covariance of the observational noise (Thiboult and Anctil, 2015) at time step *k*, P_k accounts for model uncertainty, and H_k is the observation operator (SWI vector on the ASCAT DA study). G_k is thus calculated as:

$$G_k = P_k H_k^T \left(Z_k + H_k P_k H_k^T\right)^{-1} \quad (3.14)$$

Different values of ASCAT observation errors were used for the Kalman gain calculation. Thus, the influence of observation error on EnKF DA was evaluated using ten different observation errors (0.01, 0.1, 1, 2, 4, 6, 8, 10, 15 and 20 %). On the SMOS experiment, the observation error was considered fixed at 0.04 cm^3/cm^3, which correspond to the technical reference error of the product.

In the last assimilation step, the new model state matrix (x_k^a) is updated (Eq. 3.15) based on an a priori (forecasted) model state matrix (x_k^b), the Kalman gain (G_k), and the deviation between measured and predicted observations (Abaza et al., 2015):

$$x_k^a = x_k^b + G_k\left(y_k - H_k\left[x_k^b\right]\right) \quad (3.15)$$

The EnKF has been successfully used in different hydrological applications, including streamflow prediction, through assimilation of soil moisture and streamflow data (Abaza et al., 2015; Li et al., 2014; Trudel et al., 2014; Wanders et al., 2014b; Xie and Zhang, 2010).

3.3.3. Ensemble verification criteria

The EnKF requires the generated ensemble to comply with certain spread characteristics, i.e., to generate a meaningful ensemble that represents the uncertainty of each hydrological model's forecasts (Matgen et al., 2012a). The standard deviation must be gradually increased until the ensemble mean differs from the observation by a value that is equal to the time average of the ensemble spread, and the observed trend is statistically indistinguishable from a member of the ensemble (Matgen et al., 2012a; Pauwels and De Lannoy, 2009). For that, in this thesis, the ensemble of model simulations was obtained by perturbing two input variables (rainfall and temperature) and the three most sensitive parameters for each model, previously identified through sensitivity analyses. The parameters perturbed in MISDc were (1) the storage coefficient, (2) hydraulic conductivity (K_s) and (3) the coefficient of potential evapotranspiration (K_c), while in TOPLATS, for both ASCAT and SMOS DA trials, they were (1) the Brooks-Corey pore size distribution index (B), (2) the bubbling pressure (ψ_c) and (3) hydraulic conductivity decay (f).

An ensemble of 50 members was considered sufficiently consistent. Temperature was perturbed with a zero-mean additive Gaussian noise, whereas a log-normal multiplicative noise was added to rainfall in MISDc (Chen et al., 2011), and a Gamma multiplicative noise was added to rainfall in TOPLATS. Both multiplicative functions provide a very similar type of perturbation. On the other hand, model parameters were perturbed by adding a multiplicative random Gaussian noise (Alvarez-Garreton et al., 2015; Brocca et al., 2010b), which was set as a fraction of their values.

To ensure that the created ensemble was meaningful, that is, it adequately represented modeling uncertainty, three ensemble characteristics (Eq. 3.16, 3.17 and 3.18) were calculated: (1) the ensemble spread ($ensp_k$), (2) the ensemble mean square error (mse_k), and (3) the ensemble skill ($ensk_k$):

$$ensp_k = \frac{1}{N_r}\sum_{k=1}^{N_r}(S_k - \bar{S}_k)^2 \quad (3.16)$$

$$mse_k = \frac{1}{N_r}\sum_{i=1}^{N_r}(S_k - O_k)^2 \quad (3.17)$$

$$ensk_k = \left(\overline{S_k} - O_k\right)^2 \quad (3.18)$$

where k indicates the specific time-step, N_r is the number of model runs performed (ensemble size), and an overbar indicates the mean of an ensemble. These features were first computed at each time step (k) and then averaged over the evaluated period. Two conditions must be met by the ensemble (De Lannoy et al., 2006 Alvarez-Garreton et al., 2014; Brocca et al., 2012; Matgen et al., 2012a; Plaza et al., 2012). Firstly, to ensure that the ensemble spread is large enough, the temporal average of the ensemble skill should be similar to the temporal average of the ensemble spread (Alvarez-Garreton et al., 2014) (Eq. 3.19):

$$\frac{\langle ensk \rangle}{\langle ensp \rangle} \approx 1 \quad (3.19)$$

where ‹ › indicates the average over the simulation period. Values larger than 1 indicate spreads that are too small if the model is not biased (De Lannoy et al., 2006). Secondly, Eq. 3.20 must be validated to check that the truth (observed streamflow) is statistically indistinguishable from a member of the ensemble (Matgen et al., 2012a).

$$\frac{\langle\sqrt{ensk}\rangle}{\langle\sqrt{mse}\rangle} \approx \sqrt{\frac{N_p+1}{2N_p}} \quad (3.20)$$

3.4. PERFORMANCE INDICES

Throughout this work, model performance was evaluated through four different measures of agreement, including two efficiency measures, the percentage of volumetric error, and the normalized RMSE.

The first efficiency criteria used was the Nash-Sutcliffe efficiency (NSE) (Nash and Sutcliffe, 1970), which measures the fraction of the observed streamflow variance explained by the model, calculated as the magnitude of the residual variance (noise) relative to the observed variance (information). Its optimal value is 1.0, and values should be larger than 0.0 to indicate a "minimally acceptable" performance. NSE was calculated following Eq. 3.21, being k=2.

$$NSE = 1 - \frac{\sum_{i=1}^{n}(Q_{obs}(i)-Q_{DA}(i))^k}{\sum_{i=1}^{n}(Q_{obs}(i)-\overline{Q_{obs}})^k} \quad (3.21)$$

where n is the length of the discharge time series, Q_{obs} is the observed discharge, Q_{DA} is the discharge simulated after SSM−DA, and $\overline{Q_{obs}}$ is the mean value of the observed discharge. NSE focuses on the simulation performance of high flows.

Two additional efficiency criteria, which are simple modifications of NSE were also used on the calibration and sensitivity analysis of TOPLATS. These two measures used (NSE_1 and $NSE_{0.5}$) are simple modifications of the original NSE equation, designed for the analysis of specific streamflow ranges. In NSE_1, $k = 1$ and in $NSE_{0.5}$, $k = 0.5$ (Eq. 3.21). In NSE, peak flows simulation accuracy is prioritized, whereas NSE_1 focuses on average flows and $NSE_{0.5}$ on low flows.

The second index used was the relative volumetric error (Pbias), which represents the percent volume difference between simulated and observed streamflow fluxes. In this index, negative biases

correspond to model under-estimation and positive biases correspond to over-estimation. The index was calculated using Eq. 3.22.

$$Pbias(\%) = 1 - \frac{\sum_{i=1}^{n}(Q_{DA}(i) - Q_{obs}(i))}{\sum_{i=1}^{n} Q_{obs}(i)} * 100 \quad (3.22)$$

The benefit that can be achieved in streamflow simulation through DA was measured in this study through two specific efficiency measures: Eff_{Val} *and* Eff_{OL}, based on the efficiency criteria defined for DA evaluation in Aubert et al. (2003). Eff_{Val} quantifies the improvement (or worsening) obtained for Q_{DA} compared to the model validation run (Q_{Val}) (Aubert et al., 2003; Brocca et al., 2010b) and is calculated as in Eq. 3.23.

$$Eff_{Val} = \left(1 - \frac{\sum_{k=1}^{Pa}(Q_{DA} - Q_{obs})^2}{\sum_{k=1}^{Pa}(Q_{Val} - Q_{obs})^2}\right) * 100 \quad (3.23)$$

Similarly, Eff_{OL} (Eq. 3.24) measures the positive or negative effect of DA with respect to the open-loop ensemble run (Q_{OL}) (Cenci et al., 2016; Lievens et al., 2015). Q_{OL} is calculated as the mean value of the 50 members of the ensemble at each time step.

$$Eff_{OL} = \left(1 - \frac{\sum_{k=1}^{Pa}(Q_{DA} - Q_{obs})^2}{\sum_{k=1}^{Pa}(Q_{OL} - Q_{obs})^2}\right) * 100 \quad (3.24)$$

In both Eff_{Val} and Eff_{OL}, positive values denote improvements, while negative values indicate worsening (Brocca et al., 2010b). The analysis of these two efficiency criteria allows one to separately account for the added value of the ensemble simulation and SSM information assimilation.

Finally, the normalized RMSE (NRMSE) was calculated for a more detailed evaluation of the influence of DA on streamflow simulation. Similar to Eff_{OL}, this index compares efficiency after DA with that of open-loop simulations, and it is calculated as in Eq. 3.25, where P_a is the period of analysis.

$$NRMSE = \frac{\frac{1}{N}\sum_{i=1}^{N}\sqrt{\frac{1}{P_a}\sum_{k=1}^{Pa}(Q_{DA}^{i} - Q_{obs})^2}}{\frac{1}{N}\sum_{i=1}^{N}\sqrt{\frac{1}{P_a}\sum_{k=1}^{Pa}(Q_{OL}^{i} - Q_{obs})^2}} \quad (3.25)$$

Alvarez-Garreton et al. (2015) recommended NRMSE for DA evaluation as it provides information about both the spread of the ensemble and the performance the ensemble mean, which is considered as the best estimate of the ensemble prediction. Moreover, as it is calculated in linear streamflow space, it gives more weight to high flows. NRMSE values below 1 indicate improvements due to DA.

3.5. EXPERIMENTAL SET-UP

This section details the specific experimental set-ups performed on each of the three experimental studies that form this thesis: 1) TOPLATS sensitivity analysis and calibration for the three studied Spanish catchments, 2) the Data assimilation study with ASCAT SSM product and the statistical TOPLATS mode and MISDc model, on Arga and Nestore catchments, and 3) the data assimilation of the SMOS 1 km resolution product with TOPLATS fully distributed mode for Cidacos catchment.

3.5.1. TOPLATS sensitivity analysis, calibration and validation.

3.5.1.1. Model set-up

TOPLATS requires the following seven climate variables as input: temperature (°C), relative humidity (%), atmospheric pressure (mm), wind speed (m/s), rainfall rate (m/s), longwave downward radiation (W/m^2) and shortwave downward radiation (W/m^2). All of them, except for longwave radiation (LWR), were obtained from direct measurements at catchments' meteo stations; whereas *LR* was estimated from relative humidity (*RH*) and temperature (*T*) (Prata, 1996). Each station data was assigned to its corresponding percentage of catchment area, based on Thisessen polygons distribution. TOPLATS statistical mode was run on both daily and hourly time-scale. For hourly simulations, daily-measuring stations data were hourly distributed according to nearby hourly measurements. On the TOPLATS statistical mode, different land uses can be specified, but soil is considered homogenous. In La Tejeria catchment, five land uses were considered (winter cereals, sunflower, fallow land, riparian vegetation and urban areas). Land use input data for Cidacos and Arga included nine land use types in order to differentiate irrigated from non-irrigated crops, and to distinguish different forest types and their degree of soil coverage. For each type, the parameterization required included root depth, leaf area index, albedo, emissivity, stomatal resistance, etc. Most of those values were adapted from Crow et al. (2005b), Crow and Wood (2002), Houser et al. (1998), Pauwels and Wood (1999), and Peters-Lidard et al. (1997).

Specifically, LAI values for the different forest-types and crops, were obtained from Loaiza-Usuga and Pauwels (2008), Loosvelt et al. (2014a), Lucau-Danila et al. (2005). Vegetation parameters were updated monthly, completing an annual cycle that applied for the whole simulation period (12 years). In La Tejeria, soil parameter information was obtained from available field observations (Casalí et al., 2008). Arga and Cidacos soil parameters were determined based on the soil texture class following (Rawls et al., 1982).

3.5.1.2. Sensitivity analysis implementation

The sensitivity analysis was carried out using SimLab software (EC-JRC, 2008). The SA analysis included three steps: 1) sample generation (DoE), 2) model execution and 3) model's results analysis (referred to as Statistical post processor in SimLab). Seven parameters (i.e. k = 7) (Table 3.1) were selected for the SA based on previous studies (Table 2.1) and manual testing. MM required 80 runs, since n = 10 samples were considered. In contrast, SM required 4096 runs since n = 256 samples were used. As this study aimed to evaluate TOPLATS in all its complexity, model sensitivity was evaluated in terms of nine variables and efficiency measures, grouped in: 1) main hydrological processes (surface runoff, baseflow and evapotranspiration), 2) soil moisture behavior (mean and standard deviation of surface zone) and 3) goodness-of-fit (efficiency) measures.

3.5.2. Data assimilation with lumped and semi-distributed models (TOPLATS statistical mode and MISDc)

This section details the specific location, and the spatial (12.5 km) and temporal coverage of the ASCAT observation points used for the DA study on the Italian Nestore Basin and Spanish Arga river.

For this study, specifically the mean SSM values of four pixels were used (2223595, 2218893, 2218897 and 2214191) for the Nestore catchment, whereas six pixels (2218622, 2218618, 2213916, 2213912, 2209202, and 2209198) were considered for Arga (Fig. 3.2).

In this research, a total study period of 11 years (Oct 2001 - Oct 2012) was considered for both catchments, of which 99 months were used for model calibration (Oct 2001 - Jan 2010), and 33 months were used for validation of and data assimilation (Jan 2010 - Oct 2012) for the two models evaluated. Additionally, regarding SSM observations, ASCAT data were used as follows: 1) Jan 2007 – Jan 2010 data were used for the calibration of re-scaling techniques, and Jan 2010 – Oct 2012 data were used to validate the re-scaling techniques and for the data assimilation.

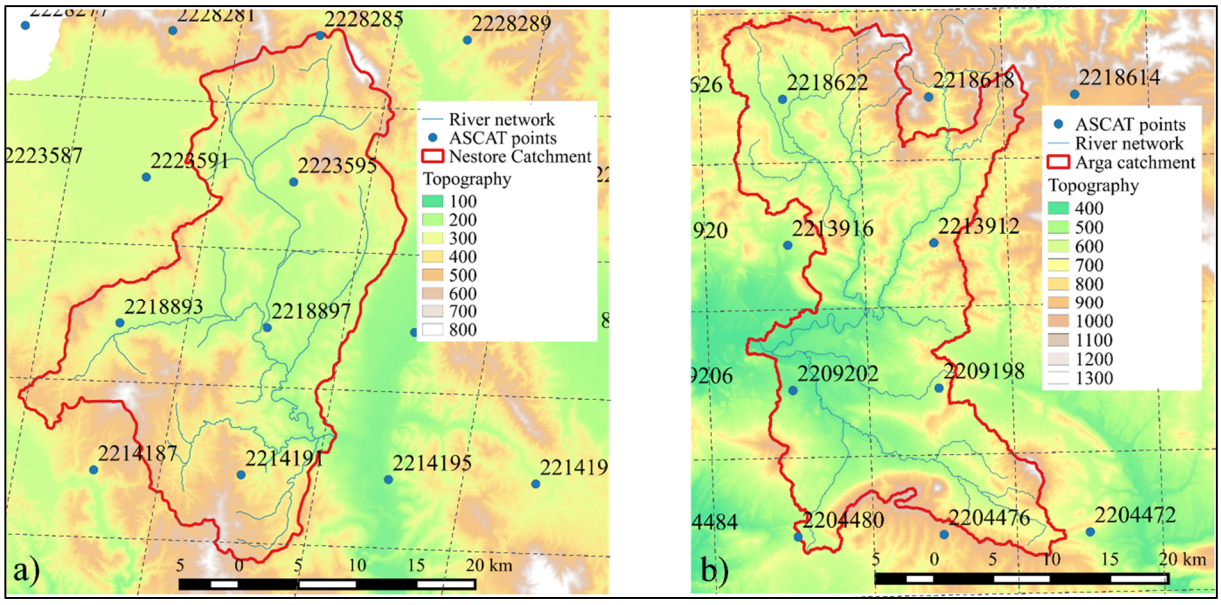

Fig. 3.2. ASCAT grid overlaid on a) the Nestore catchment and b) the Arga catchment.

3.5.3. Data assimilation with TOPLATS fully distributed mode

This section describes the steps to prepare and transform the existing spatial information of Cidacos catchment, into the required distributed data to be used as model input at 1-km resolution.

As mentioned on the introduction and objectives sections of this thesis, the Cidacos catchment, located in the central area of Navarre province, in northern Spain, was the selected study site for a fully distributed mode experimental simulation. Firstly, a simple simulation of Cidacos with the distributed mode of TOPLATS was performed (Validation run). And secondly, SMOS soil moisture information was assimilated into the model through the Ensemble Kalman Filter DA technique. Thus,

in this section all the steps required to transform the existing spatial information into a 1-km resolution input data for TOPLATS model are detailed. Figure 3.3 shows a detailed description of the topography of the catchment. The flat cultivated areas on the western and southern part of the catchment contrast with the mountainous (up to 1,200 m) north-eastern part. The catchment is heavily instrumented with 8 weather stations (4 manual, recording in a daily bases, and 4 automatic recording in a 10-minutes basis). Only 3 automatic stations are shown in this figure, but fully detailed location of all the weather stations is provided in figure 3.7. Location of the main gauging station at Olite is also shown, as well as other intermediate gauging stations. Central observation coordinates of ASCAT and SMOS satellites are also shown, despite only SMOS data was applied for this catchment. Topography of the figure is based on a detailed 25 x 25 m DEM.

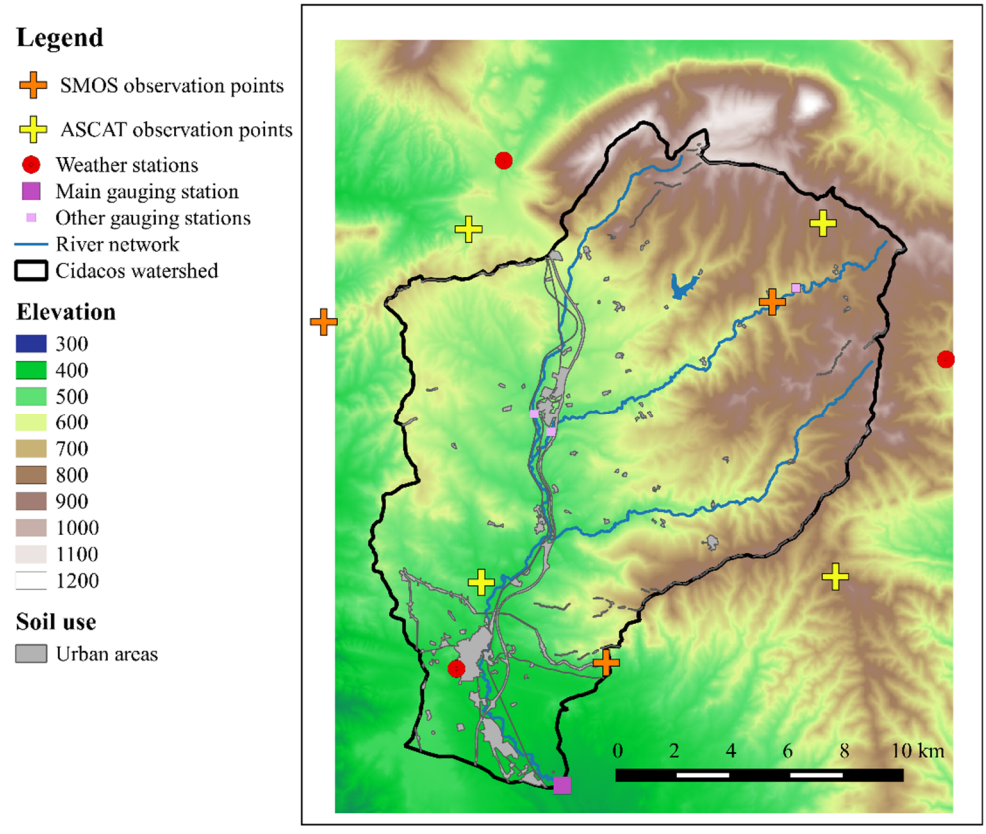

Fig. 3.3. Topography of Cidacos catchment with a 25 m resolution Digital Elevation Model. Main river network, urban areas and gauging stations are also shown.

Detailed Land use and Soil type maps of the catchments were freely obtained from the Government of Navarre (https://idena.navarra.es/portal/Descargar). Original information showed that there were nine soil types within the catchment, being *Typic Calcixerepts*, *Typic Xerorthents* and *Typic Xerofluvents* the predominant ones (Fig 3.4). Regarding Land use, the original data from the Government of Navarre showed the existence of up to 17 land uses in Cidacos catchment, which were reclassified for the sake of simplicity into 9. This number was still sufficient to adequately describe the complexity of the catchment, and to discriminate different irrigated/non irrigated cereal and woody crops. Also, three different forest types remained differentiated (Fig 3.4).

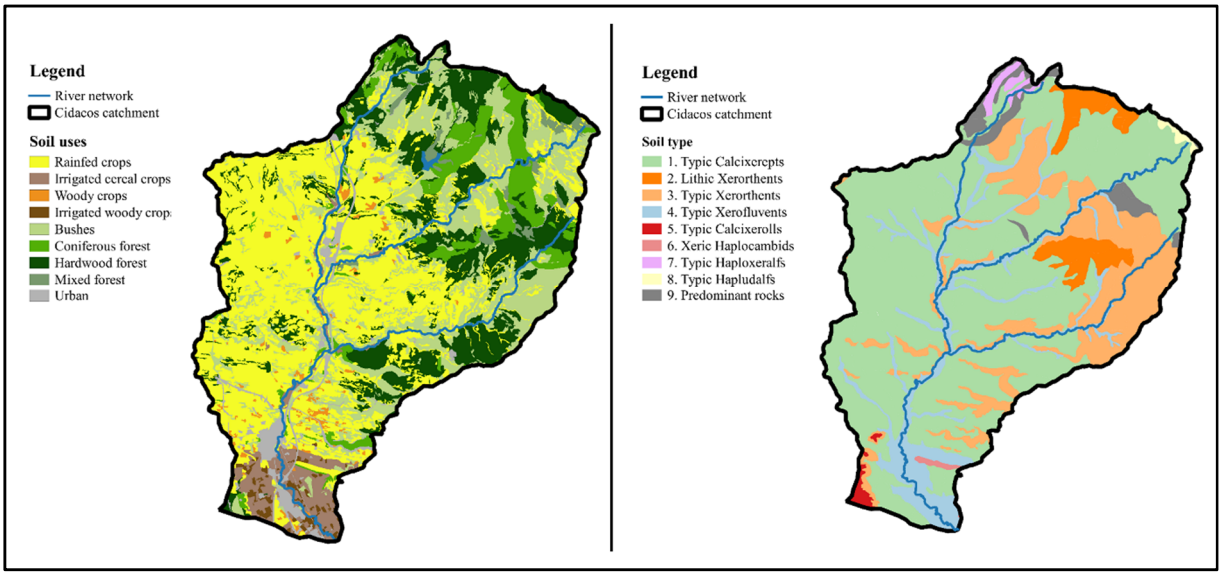

Fig. 3.4. Land use and soil type maps of Cidacos catchment. Main river network is also shown.

As it has been thoughtfully depicted in the TOPLATS description section (2.2.1), the Topographic Index plays a key role on the runoff generation and on the soil moisture distribution within the soil profile. The topographic Index value, calculated from the original 25 x 25 m resolution Digital Elevation Model is shown in figure 3.5. Cells with higher TI values concentrate on the western and southern part of the catchment, as well as in the river network that descend through the steepest north-eastern areas. High TI locations are characterized by low slopes and large upstream areas,

and indicate zones with higher susceptibility to be saturated and thus prone to generate surface runoff.

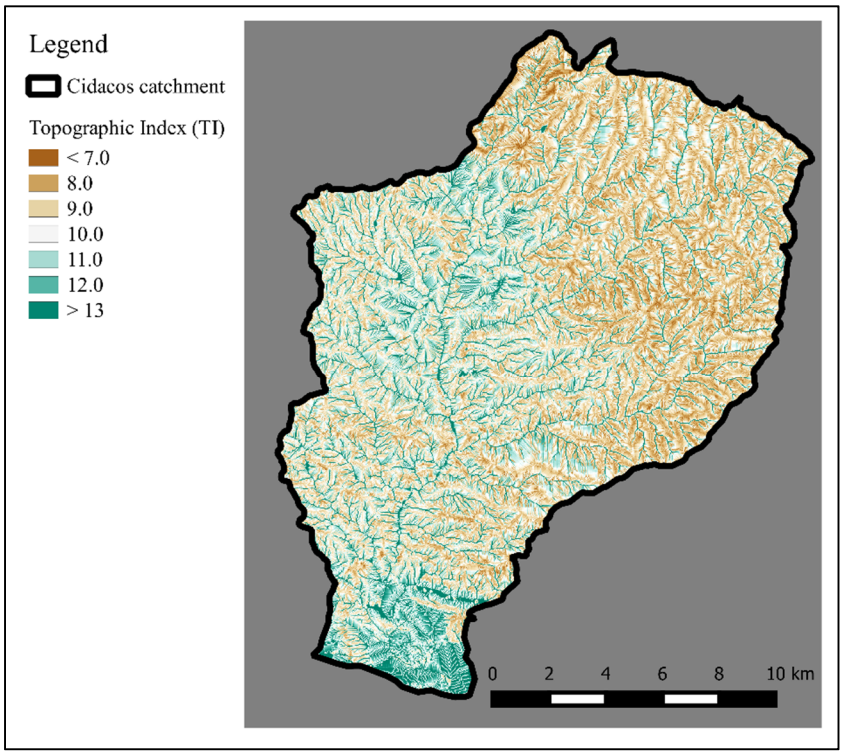

Fig. 3.5. Topographic Index, calculated from a 25 m resolution DEM

Figure 3.6a shows the location (pixel's center and grid) of a 30 x 30 SMOS L4 product covering the Cidacos catchment area (ETRS89 projection). On figure 3.6b the Topographic index calculated for the 1-km resolution grid used as input for TOPLATS distributed mode can be seen. This map can be visually compared to the one obtained from the 25 m resolution. In figure 3.6b brown colors indicate areas with TI below 10, while green areas identify pixels with TI over 10. Cells with TI over 12 locate in flat areas close to the outlet of the catchment. To assign Land use and Soil type to the new 1-km cells, based on the original 25 m cells, the majority method was used, which identifies the land use and soil type that has the largest number of 25 m cells within the new 1 km cell. This was done for land use (Fig. 3.6c) and soil type (Fig. 3.6d). This scale resolution change resulted in a reduction of the soil types and land uses presented in the new grid, as some of them were not majority

in any 1 km-pixel. Thus, only 7 out of nine land used were assigned for distributed modeling. Similarly, only 5 soil types were finally used for the distributed modelling of the catchment. Crops in figure 3.6c are shown in yellow and orange colors. These maps aim to illustrate catchment areas with TI over 10 and to locate cultivated areas, as part of the DA experiment focused on them.

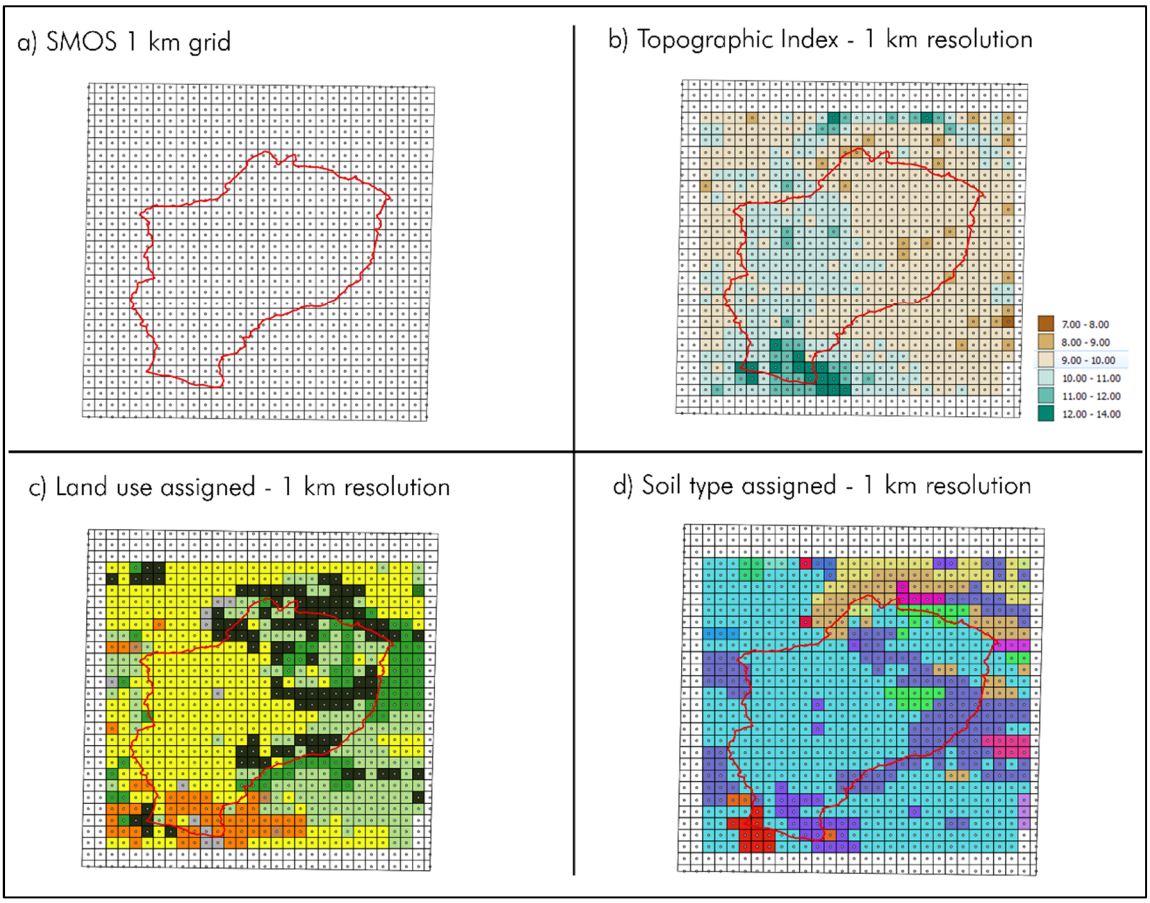

Fig. 3.6. a) Location of SMOS 1-km resolution grid over Cidacos catchment. A cell grid of 30 x 30 km covering the area is shown. b) Topographic Index calculated for the 1 km cells. c) Assignment of Land Use (majority method) to the cells (cultivated cells shown in orange and yellow). d) Assignment of Soil type (majority method to the cells. Maps are shown in ETRS89 coordinate system. Legends not shown in the figure for clarity issues, but more detailed information can be found in figure 3.4.

On this data assimilation study, the weather data was also given as fully distributed input. As shown in figure 3.7a, rainfall data was assigned to each specific cell following the Thiessen method that assigns to each cell, the rainfall from its closest station. For that, 8 weather recording stations,

four manual (orange) and four automatic (red dots) were used. Daily rainfall data measured in the manual stations were distributed to hourly time-steps according to close-by automatic (10 minutes basis) observations. The remaining variables, already described in section 3.5.1.1 were also assigned following Thisessen method (Fig 3.7b). In this case, variable values were obtained from the four automatic weather stations.

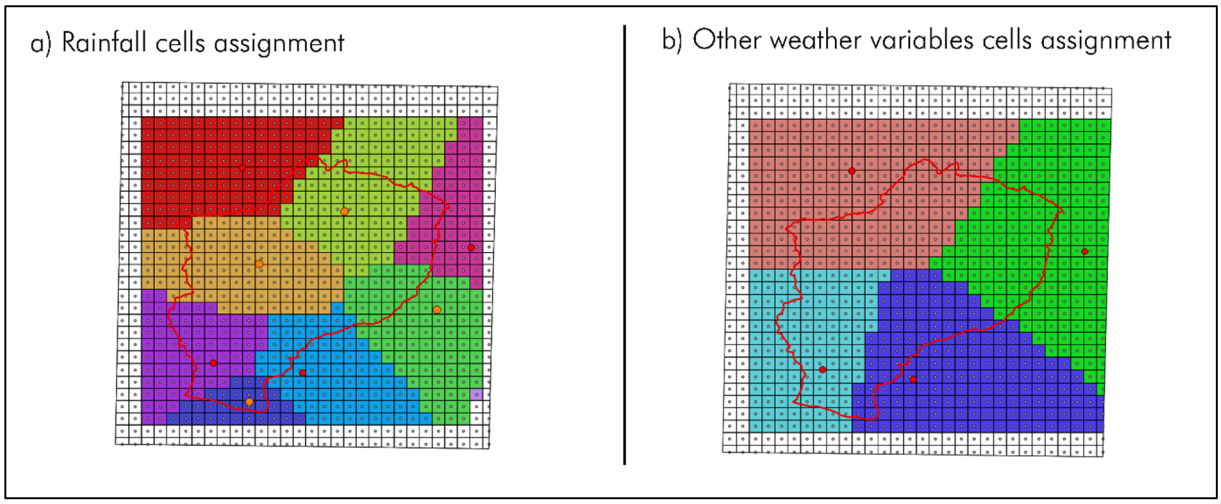

Fig. 3.7. Distributed input of weather data from manual (orange dots) and automatic weather stations (red dots). a) Assignation to the cells of 8 rainfall recording stations. b) The remaining variables were obtained and assigned to the cells also following Thiessen criteria.

CHAPTER 4. RESULTS AND DISCUSSION

This results chapter is divided into 4 sections. The contents of the first and the second section were partly published in Loizu et al., (2016). The first (section 4.1) presents the results of the TOPLATS sensitivity analysis, while the second (section 4.2) includes the model calibration and the evaluation of its performance on three catchments of different size. On the other hand, sections 4.3 and 4.4 show the results of the two data assimilation studies carried out along this PhD thesis. Section 4.3 presents the results of ASCAT assimilation into TOPLATS and MISDc, research under review in (Loizu et al., 2017), and section 4.4 displays the results of a downscaled SMOS assimilation into TOPLATS in distributed mode, research to be submitted (Loizu et al., 2017b).

4.1. SENSITIVITY ANALYSIS

Plots presented in this section (Figs. 4.1 - 4.3) show results from MoM (left) and SoM (right) analysis of daily TOPLATS simulations. Output variables are shown in the y-axis for the three catchments and the evaluated TOPLATS parameters in the x-axis. Circle size represents individual parameter sensitivity (μ^* in MoM and S_i in SoM) while blue color intensity refers to total-order sensitivity (σ in MoM and S_{Ti} in SoM), which includes parameter interaction.

4.1.1. Hydrological processes

SA results indicated that parameter *f* had the overall largest influence on hydrological processes sensitivity. It was the main parameter responsible of hydrological processes in La Tejeria, and shared responsibility with *B* in Cidacos and with ψ_c in Arga.

Both methods, MoM and SoM, identified parameter *f* as the one having the largest influence on surface runoff (*SR* in Fig.4.1) generation in La Tejeria. Parameter *f* was also the most influential in Cidacos, where the second most sensitive was ψ_c. MoM and SoM also agreed in Arga, identifying *f*

and ψ_c as the most influential parameters, but here also Q_0 seemed to have some relevance too according to MoM. Some differences were found among catchments in terms of baseflow sensitivity (*BF* in Fig.4.1), as different parameters appeared as the most influential ones: *f* in La Tejeria, *B* in Cidacos and ψ_c in Arga. Strictly speaking ψ_c shared its relevance with *B* on Arga according to SoM. All in all, these 3 parameters were the most significant ones in all catchments. Results obtained with SoM depicted stronger differences between parameters in terms of baseflow sensitivity, whereas MoM did not show significant differences among most parameters. Evapotranspiration outputs (*ET* in Fig.4.1) were clearly sensitive to *f* in La Tejeria and Arga, while in Cidacos up to four parameters shared a similar influence degree: *B*, ψ_c, *f* and K_s. In terms of parameter interaction for the three processes, ψ_c and *f* had larger interaction levels. This was particularly notorious for ψ_c in Arga, according to MoM, and for *f* in all catchments according to SoM.

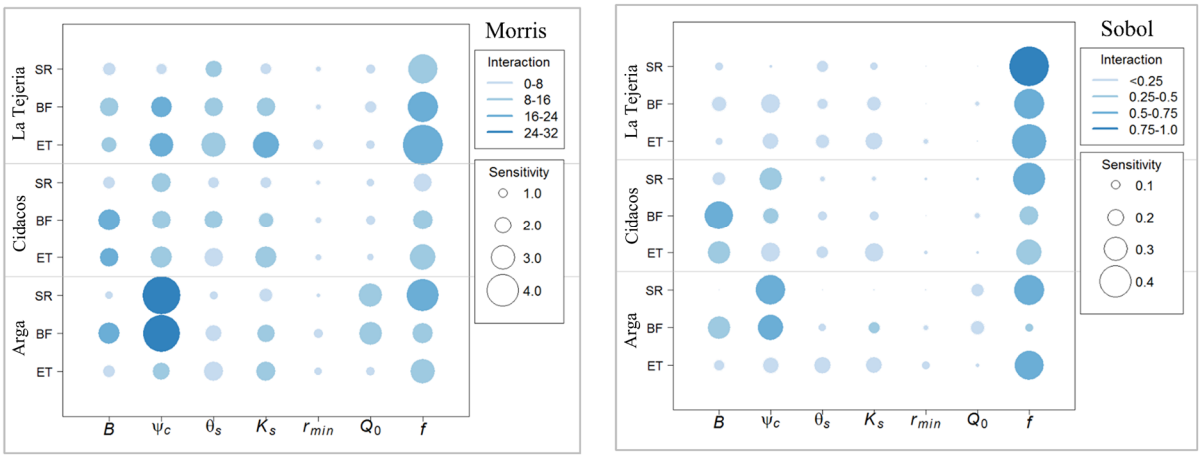

Fig. 4.1. Sensitivity analysis results of main hydrological processes: surface runoff (SR), baseflow (BF) and evapotranspiration (ET) using MoM (left) and SoM (right) methods. Parameter sensitivity (μ^* and S_i) and interaction (σ and S_{Ti}) are shown. MoM results expressed in mm/day and SoM results expressed as a decimal of the total variance.

When comparing the results obtained with MoM and SoM, in most cases both methods came up with the same set of most influential parameters, but some results showed different patterns. Although MoM gave four (out of 7) parameters a similar degree of sensitivity in many cases, SoM was able to

identify more clearly the most influential pair of parameters. This discrepancy on secondary level parameters identification was clearly observed when comparing parameters *B* and ψ_c with parameters θ_s and K_s. Despite having similar individual sensitivities in MoM, there were relevant differences among them on SoM. Thus, SoM was able to differentiate more clearly secondary parameters, especially in *BF* and *ET* sensitivity analysis.

4.1.2. Soil Moisture

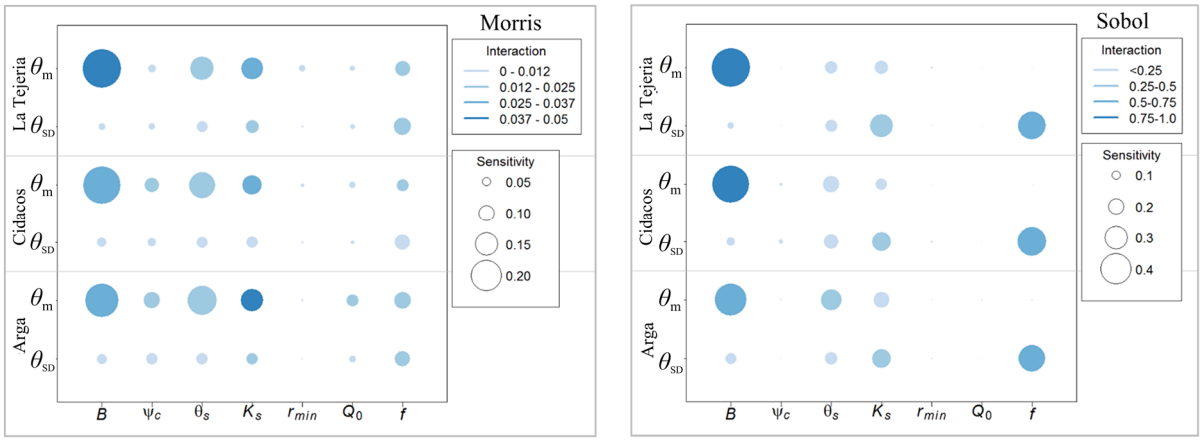

Fig. 4.2. Sensitivity analysis results of Surface Zone (SZ, 5 cm) mean soil moisture (θ_m), and its standard deviation (θ_{SD}) using MoM (left) and SoM (right) methods. Parameter sensitivity (μ^* and S_i) and interaction (σ and S_{Ti}) are shown. MoM results expressed in $mm^3\ mm^{-3}$ and SoM results expressed as a decimal of the total variance.

Soil moisture sensitivity analysis results did not show relevant differences between MoM and SoM despite their different computational requirements (Fig. 4.2). Both were capable of clearly identifying *B* as the main parameter affecting surface zone soil moisture mean value (θ_m) outputs. Regardless of some minor disparities on secondary parameters estimation, both agreed on the estimation of θ_s and K_s as the second and third parameters in terms of individual sensitivity. Despite differences in catchment size, θ_m sensitivity patterns for the three studied catchments were found to be very similar. Pauwels et al. (2009) concluded that K_s, *B* and ψ_c were the three most important soil parameters on the determination of soil moisture content. These results were similar to the ones obtained here, but

differed on the role attributed to ψ_c and θ_s. On a SA following a completely different approach, Loosvelt et al., (2014b) found that TOPLATS soil moisture output was mostly influenced by the residual soil moisture content (θ_r), θ_s, ψ_c, B and K_s. In their study, Loosvelt et al., (2014b) were able to identify areas within the parameter range with different level of sensitivity, related to the shape of the soil moisture retention curve. They found the highest sensitivity for low values of B, ψ_c, θ_s, and for high θ_r values.

Regarding soil moisture dynamics (i.e. surface zone soil moisture standard deviation (θ_{SD}), Fig. 4.2) f was identified as the most influential parameter, followed by K_s and θ_s. These results were clearer with SoM, which seemed to take advantage of its more detailed setup, so primary, secondary and tertiary parameters could be more plainly distinguished from non-influential ones. No significant differences were found among catchments in terms of θ_{SD} sensitivity. As shown in Fig. 4.2, B and K_s presented the highest level of interaction with other parameters on model θ_m output, and f in soil moisture dynamics.

4.1.3. Model efficiency

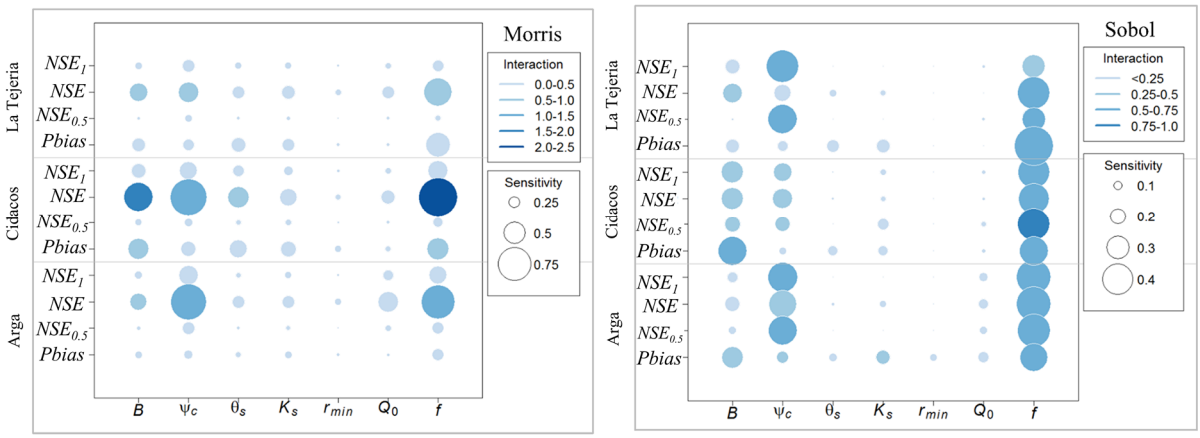

Fig. 4.3. Sensitivity analysis results of model efficiency (NSE_1, NSE, $NSE_{0.5}$ and Pbias) using MoM (left) and SoM (right) methods. Parameter sensitivity (μ^* and S_i) and interaction (σ and S_{Ti}) are shown. MoM results expressed in NSE coefficient value and SoM results expressed as a decimal of the total variance.

In this section, sensitivity results of four efficiency measures are described. These results offered notable differences between catchments, where diverse climate regimes seemed to affect strongly the efficiency results obtained (Fig. 4.3). Furthermore, differences between MoM and SoM were larger than in the previous analyses.

As a general inference of the SA of efficiency measurements, it can be stated that 3 parameters appeared to be responsible for the largest fraction of model sensitivity to medium, high and low flow simulation (Fig. 4.3): Brooks-Corey Pore Size distribution Index (B), Bubbling pressure (ψ_c) and Hydraulic conductivity decay (f). An important remark extracted from this analysis was the similarity of the wettest catchments (i.e. Arga and La Tejeria), where ψ_c was globally more influential than in the dryer Cidacos, where B gained importance. Few discrepancies were found among methods, but for instance although ψ_c was the second most influential parameter in NSE in Cidacos according to MoM, that place was taken by B according to SoM.

NSE_1, (i.e. efficiency for average flows) was mainly controlled by ψ_c and f in La Tejeria and Arga (Fig. 4.3). In Cidacos, in addition to those two parameters, MoM and SoM identified B as an important parameter as well. As in previous analyses, SoM detected more clearly non-influential parameters (e.g. θ_s or r_{min}). Regarding the efficiency of high flows simulation (i.e. NSE, Fig. 4.3) results could be summarized as follows: f was the key factor affecting NSE in La Tejeria, whereas B, ψ_c and f shared similar individual effects in Cidacos and ψ_c and f accounted for most of the sensitivity in Arga. Sensitivity to low flow simulation (i.e. $NSE_{0.5}$, Fig. 4.3) was mostly similar to NSE_1. Lastly, Pbias was primarily affected by f in La Tejeria and by B and f in Cidacos and Arga.

Regarding parameter interactions on the four efficiency measures, f was the parameter that showed the largest interaction with the rest. In general, it could be observed (Fig. 4.3) that B, ψ_c, and f shared the highest levels of interaction. In La Tejeria and Arga those interactions affected mainly ψ_c and f. On the other hand, those interactions were found to be especially intense between B and f in Cidacos.

4.1.4. SA global remarks

Previous studies commented on weakness and advantages of MoM and SoM for hydrological models analysis (Shin et al., 2013). According to Campolongo and Saltelli (1997) there could be a discrepancy between the identification of parameters with both algorithms. However, in this study both methods generally agreed, and identified the same set of most influential parameters on surface runoff (f and ψ_c), baseflow (f, B and ψ_c) and evapotranspiration processes (f and four other secondary parameters, B, ψ_c, θ_s, K_s). They also showed agreement on finding the most sensitive parameter responsible of mean soil moisture (B) and its variations (f). However, some qualitative differences were found on the SA of efficiency.

Parameters identified here as the most influential ones have a clear physical meaning, but some of them, particularly soil parameters, participate on the calculations of several water fluxes, which complicates the understanding of their particular influence on each model output. In any case, parameters Q_0 and f seem to be, together with the varying WTD, the controlling factors of the generated baseflow amount. As observed from the specific formulation detailed in Famiglietti and Wood, (1994), while Q_0 is responsible of the magnitude of the generated baseflow, parameter f defines the shape of the evacuation flow, leading to faster (low f values) or slower (higher f) evacuation of subsurface flow from saturated areas in the catchment. Parameter f controls this way the availability of water in the soil for other processes, such as evapotranspiration, being thus the main responsible of soil moisture patterns in the catchments (including θ_{SD}).

As mentioned above, the interaction of parameters gets more complex when soil parameters are evaluated. In TOPLATS, the soil is modelled through the equations of Brooks and Corey (1964), that numerically calculate the soil moisture content θ_m depending on B, ψ_c, θ_r, θ_s and the matric head (ψ) (Famiglietti and Wood, 1994; Loosvelt et al., 2014b). As it was observed from the SA results, B was the most influential parameter on θ_m. This parameter is the exponent value regulating the θ_m equation in TOPLATS. Higher B values will thus lead to higher mean soil moisture conditions. Also, larger θ_s and ψ_c values will increase soil moisture mean content.

Parameter ψ_c plays an important role on the partitioning between infiltration and runoff generation. This parameter's value defines a discontinuity in TOPLATS when ψ reaches ψ_c. When this point is reached (usually during the wettest winter days), saturation excess runoff is activated and soil moisture and conductivity values are modified accordingly. In any case parameter interactions in TOPLATS are complex, as diffusive flux from SZ to TZ is also controlled by K_s, θ_s, θ_r, and B (Peters-Lidard et al., 1997) and the same parameters take part on the drainage calculations as well (Famiglietti and Wood, 1994).

Globally, differences among methods can be numerically summarized as follows: 1) in most of the cases evaluated in this study (81%) MoM and SoM identified the same parameter as the most influential, being this agreement particularly strong on soil moisture SA, but also on other main hydrological processes and on efficiency and Pbias; 2) in 67% of the cases tested both methods agreed at identifying the same pair of most influential parameters; and 3) in the identification of the three most influential parameters the agreement of both SA techniques was higher on soil moisture (83%), and hydrological processes (78%), but lower on efficiencies and Pbias (50%). This results are in agreement with Wainwright et al. (2014), who presented another comparison of MoM and SoM and concluded that both methods provided consistent parameter importance rankings when used on a reservoir-aquitard-aquifer model. However, as also investigated by Gan et al. (2014), clearer qualitative differences between secondary parameters were provided by SoM.

4.2. CALIBRATION AND PERFORMANCE OF TOPLATS

4.2.1. TOPLATS calibration

4.2.1.1. Multi-Start Powell Method performance

TOPLATS calibration dimensionality was reduced to just 6 parameters thanks to the SA analysis that identified parameter r_{min} as uninfluential to most efficiency and hydrological model outputs, so it was not included on the MSPM calibration. The results of the calibration obtained with the MSPM technique on the different catchments are reported in Table 4.1, showing NSE_1, NSE and Pbias median values (of the 10 optimization runs) at initial (IP) and final optimal points (OP).

Table 4.1. Improvement of efficiencies and Pbias reduction achieved by MSPM on La Tejeria, Cidacos and Arga catchments. Values presented on the table are median values of the 10 (8 MSPM and 2 refinement) optimization runs obtained with the Initial Parameter (IP) values and Optimal Parameter (OP) values.

Catchment	NSE_1		NSE		Pbias (%)	
	IP	OP	IP	OP	IP	OP
1. La Tejeria	0.40	0.68	0.27	0.82	15	3
2. Cidacos	-0.41	0.50	-1.51	0.57	112	4
3. Arga	0.37	0.49	0.38	0.57	5	3

The results obtained clearly identified Cidacos as the catchment where MSPM improved TOPLATS performance the most. IP efficiency values were very low in this catchment, indicating that parameter combinations far from the optimal values had a stronger influence on efficiency results than in the other two catchments. In La Tejeria and Arga, most IP value sets, even the farthest from the final OP values, offered positive NSE values. For Cidacos, extremely large Pbias (112%) values were obtained at IP points. This value dropped to 4% after optimization, showing that using NSE_1 as the optimization criteria also resulted in a well-balanced volume simulation. These strong Pbias reductions in Cidacos contrasted with the more modest Pbias improvements in the other two catchments (12% and 2% in La Tejeria and Arga, respectively), where IP Pbias values were already moderate or even low.

Optimization results showed that TOPLATS offered a more stable behavior on wetter catchments (i.e. Arga), where even before calibration, results were not far from optimal ranges. On the other hand, efficiency results before optimization (IP) showed a large variability in La Tejeria, and extremely large in Cidacos (not shown).

4.2.1.2. Optimal parameter values

Optimal (OP) and Best performing parameter values (BP) found by MSPM are shown in Fig. 4.4. As shown in figure 3.1, BP were the parameter values offering the highest NSE after refinement optimization runs 9 and 10. For simplification and to allow catchment behavior comparison, only CON approach values are shown in this section. Parameter value ranges to be explored by the algorithm were defined according to the literature on TOPLATS calibration (Goegebeur and Pauwels, 2007; Loaiza-Usuga and Pauwels, 2008; Peters-Lidard et al., 1997).

The first parameter evaluated was *B,* whose BP values for La Tejeria and Arga were found at values close to one, while in Cidacos it was substantially lower (0.41). Regarding ψ_c, despite MSPM ended on some local minima in some of the optimization runs, in all cases the BP ψ_c value was within the 0.1 – 0.4 m range. In general, in the three catchments, highest efficiencies were found as a combination of high *B* and low ψ_c values (despite some optimizations ending at the opposite combination, low *B* and high ψ_c). Saturated soil moisture (θ_s) yielded different BP values in La Tejeria, with a low optimal θ_s, and Cidacos and Arga, where optimal θ_s was over 0.55 m^3/m^3.

K_s, had its BP within $1e^{-4}$ and $1e^{-5}$ m/s for La Tejeria and Arga, but in Cidacos these values were higher (between $1e^{-3}$ and $1e^{-4}$ m/s) (Fig. 4.4). Differently from some other parameters (i.e. ψ_c or *f*), optimal K_s values were always located on a small range of the defined parameter search space. Subsurface flow at complete saturation (Q_0) optimal values increased as catchment area increased. Similarly to K_s, optimal Q_0 values (OP) were clearly identified on specific areas (value range). Finally, for the decay parameter (*f*), which is key for event recession flow adjustment, a strong parameter interaction was found, resulting in similar efficiencies with varied *f* values, but BP values were close

to 8.0 in La Tejeria and Arga. In Cidacos lower *f* values were found, which is related to a more rapid decrease of baseflow in this catchment.

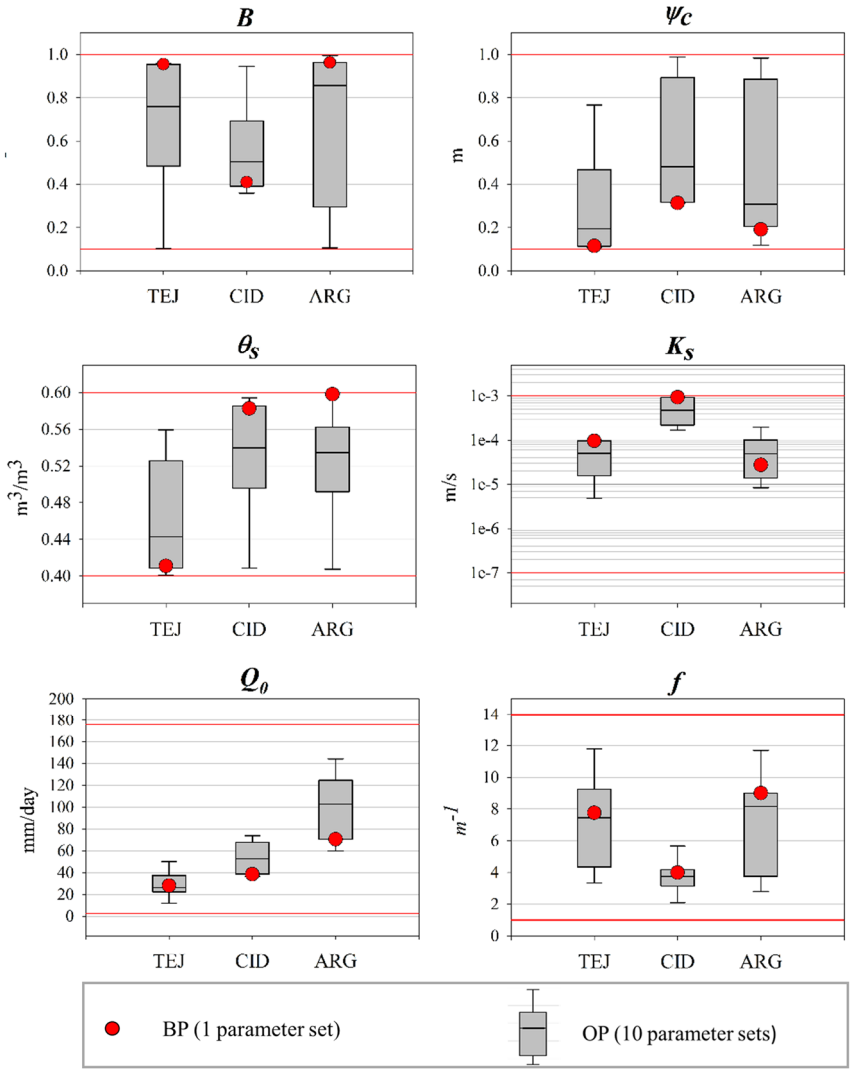

Fig. 4.4. TOPLATS Optimal (OP) and Best Performing (BP) parameter values obtained through MSPM model calibration of daily streamflow simulation with the conventional (CON) approach. Red lines indicate the allowed optimization parameter search range. Results for La Tejeria (TEJ), Cidacos (CID) and Arga (ARG) catchments.

BP values obtained in this study are in general in accordance with parameter values reported in other studies, but significant differences were found on K_s values. Other TOPLATS studies, where parameter values were detailed include Loaiza-Usuga and Pauwels (2008), who calibrated three parameters obtaining the following optimum values: B=0.72; and ψ_c =0.7 m, and K_s=3.8e^{-6} m/s.

They also found an optimal range for other two calibrated parameters at different locations: f (0.01-1.2 m^{-1}) and Q_0 (2.4 – 61 mm/day). Loosvelt et al., (2015) used, after calibration, f = 2.5 m^{-1}, on a 91 km^2 catchment.

On a separate study, Pauwels et al. (2009) reported the following parameter value ranges for different soil types: B (0.47 - 0.65), ψ_c (0.35 - 0.45 m) and K_s ($2.8e^{-6}$ - $3.5e^{-6}$ m/s). Parameter values presented in Loosvelt et al. (2011), for different soil types were in the following ranges: B (0.15 - 0.69), ψ_c (0.2 - 0.94 m) and K_s ($5.8e^{-7}$ – $1.1e^{-5}$ m/s). Altogether, it seems that substantially different parameter values combinations can lead to similar optimal efficiencies, probably due to a significant parameter interaction as depicted on the sensitivity analysis (section 4.1).

4.2.1.3. Comparison of conventional (CON) and random (RND) calibration approach on CAL/VAL results

TOPLATS daily efficiencies and Pbias results after CAL and VAL for both CON and RND strategies are presented in Table 4.2. Simulations of La Tejeria offered similar NSE results when CON and RND strategies were applied, although best efficiency in calibration was obtained with CON (0.82). Similarly, validation NSE results were over 0.7 in this catchment for both strategies and Pbias results were low, below 5% in all cases. Results for Arga were similar, with little differences between CON and RND strategies. In Arga, the conventional approach provided more stable NSE results in CAL (0.63) and VAL (0.60), whereas variation was larger in RND approach (0.71/0.54). Total simulated volumes were close to the observed, with Pbias lower than 5% on calibration and 10% on validation.

Table 4.2. Daily streamflow simulation efficiencies (NSE_1 and NSE) and bias results achieved after optimization

Catchment	Calibration type	NSE_1		NSE		Pbias	
		CAL	VAL	CAL	VAL	CAL	VAL
		--	--	--	--	%	%
1. La Tejeria	CON	0.71	0.65	0.82	0.72	2	2
	RND	0.64	0.69	0.77	0.73	-5	-4
2. Cidacos	CON	0.53	0.35	0.61	0.09	2	-77
	RND	0.54	0.39	0.91	0.25	8	-3
3. Arga	CON	0.50	0.49	0.63	0.60	-3	-9
	RND	0.53	0.46	0.71	0.54	2	-5

In Cidacos, due to the irregularity of its rainfall, extreme events seemed to have a large influence on the NSE. CON calibration achieved a NSE_1 of 0.53 and a corresponding NSE of 0.61 with a low Pbias (2%). But, in this case, validation results were poor, due to an abnormal decrease in simulated water table depth (WTD) that caused a strong streamflow underestimation (77%). The validation period was notably drier than the calibration one, and this affected the results strongly. The RND approach overcame this issue and improved results substantially in Cidacos reaching a NSE_1 of 0.54 and a NSE of 0.91 for the calibration period. Validation yielded then (RND) efficiency values of 0.39 and 0.25 (for NSE_1 and NSE, respectively) and a remarkable reduction in Pbias from 77 to 3%. BP parameter values identified by this second approach helped TOPLATS to perform in a more consistent way. The deficiency of this method was that it was not able to properly simulate extreme flows during validation, but this was principally caused by just 3 single events (later shown in fig. 4.8), where TOPLATS underestimated streamflow notably.

TOPLATS streamflow simulation efficiency values obtained here are similar to those reported by Bormann et al. (2007), on a 693 km^2 wet catchment, with a daily NSE results of 0.66 and 0.61 for CAL and VAL respectively. Two parameters were manually calibrated on that study, reaching a

simulation Pbias below 3%. Bormann et al. (2007) also noted the influence that hydroclimatic conditions had on model's CAL/VAL results. This author signaled that large differences on evapotranspiration, precipitation and discharge among CAL/VAL periods limited the possibility to achieve proper CAL/VAL results. The RND strategy applied here guarantees that enough wet weather data is included on the calibration period, leading to a better and more balanced model performance. This conclusion was also noted by Anctil et al. (2004). Also in accordance with our results in Mediterranean catchments, Kim and Kaluarachchi (2009) found that the number of high-flow months included on the calibration data had a great influence on model efficiency.

One of the points of interests of this study was to evaluate the performance of the model on different climate conditions. Difficulties faced in Cidacos calibration and validation also relate with Perrin et al. (2007) and Li et al. (2010), who concluded that stable parameter values proved more difficult to reach in dry catchments (in Cidacos unstable parameter values were obtained on CON calibration). Also Li et al. (2010) used random selection of CAL/VAL periods of different lengths, and concluded that humid catchments required shorter CAL/VAL periods than dry ones to obtain stable parameter values, in line with our enhanced results with RND approach in dry catchments.

4.2.2. Analysis of model outputs

4.2.2.1. Soil Moisture

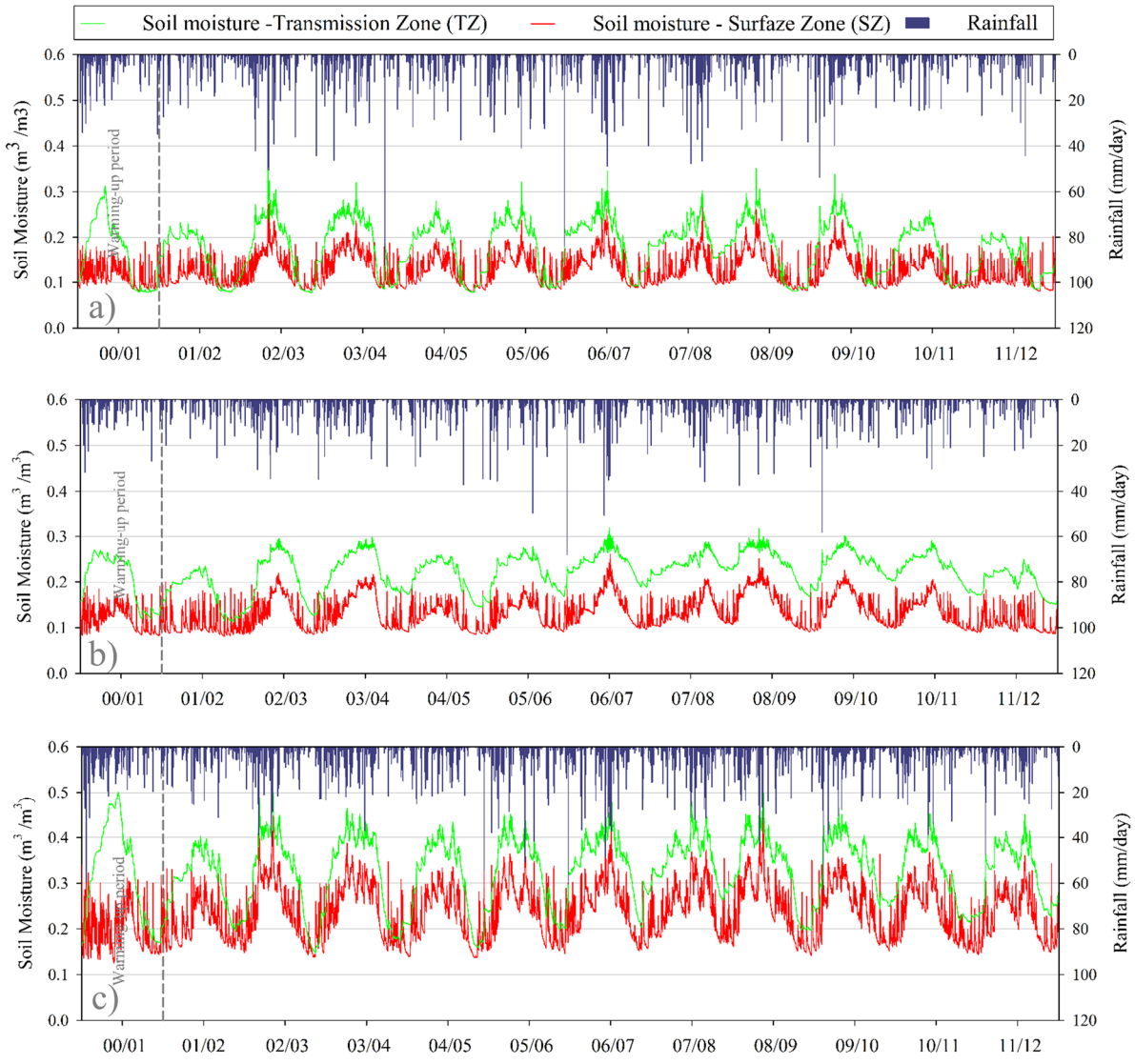

Fig. 4.5. Simulated soil moisture content (θ) (cm3/cm3) in the Surface Zone (SZ) and in the Transmission Zone (TZ) for a) La Tejeria, b) Cidacos and c) Arga catchments.

Figure 4.5 presents daily simulated soil moisture (θ) behavior in relation with recorded rainfall. Following the best results detailed in previous 4.2.1.3 section, for La Tejeria and Arga the results shown in Fig.4.5 and Fig.4.6 are those obtained with CON calibration approach, while Cidacos's ones correspond to RND strategy. The plot represents the whole period studied (i.e. including CAL/VAL and warming-up periods). It can be observed that within each catchment, the deeper TZ

kept higher soil moisture contents than the SZ for most part of the year. This difference was higher during winter periods and lower during summer when θ dropped in both layers.

Simulated mean soil moisture (θ_m) values in the SZ were 0.13 cm^3 cm^{-3} in La Tejeria, 0.13 cm^3 cm^{-3} in Cidacos and 0.24 cm^3 cm^{-3} in Arga. La Tejeria presented the smallest mean value difference between layers (5%), whereas that difference reached 9% in Cidacos and Arga. For the TZ θ_m values were 0.18 cm^3 cm^{-3} in La Tejeria, 0.22 cm^3 cm^{-3} in Cidacos and 0.33 cm^3 cm^{-3} in Arga. During summer periods, larger differences among layers were found in Cidacos. Differences between Arga (with the highest θ_m in both layers) and the other two catchments were especially remarkable on the SZ. In our study, obtained soil moisture values were, globally, low in comparison with other studies (Goegebeur and Pauwels, 2007; Loosvelt et al., 2011). Soil moisture fluctuation (θ_{SD}) was in all the catchments larger in TZ than in SZ. In both layers, largest fluctuations were found in Arga catchment. θ_{SD} values in La Tejeria were 0.03 cm^3 cm^{-3} (SZ) and 0.06 cm^3 cm^{-3} (TZ); in Cidacos 0.03 cm^3 cm^{-3} and 0.04 cm^3 cm^{-3}; and in Arga 0.06 cm^3 cm^{-3} and 0.07 cm^3 cm^{-3}.

Regarding the proportion of saturated catchment area (Fig. 4.6), it can be observed that intense and persistent rainfall events resulted in similar maximum percentages of saturated catchment in La Tejeria (43.9%), Cidacos (37.3%) and Arga (37.4%). However, mean and percentile analysis of saturation degrees showed large variation among catchments (not shown). In Arga, up to 24% of the simulation days presented more than 10% of its area as fully saturated. In La Tejeria, that saturation level (10%) was reached only during 6% of the days and in Cidacos in 3%. Mean value of saturated area (%) in La Tejeria, Cidacos and Arga were 1.5 %, 1.7 % and 6.7 % respectively. The largest proportion of saturated areas was found in Arga, about four times the values obtained for the other 2 catchments. Highest saturation variability rates were also found in Arga, with a standard deviation of 6%, while variation was 4.3 % in La Tejeria and 3.3 % in Cidacos.

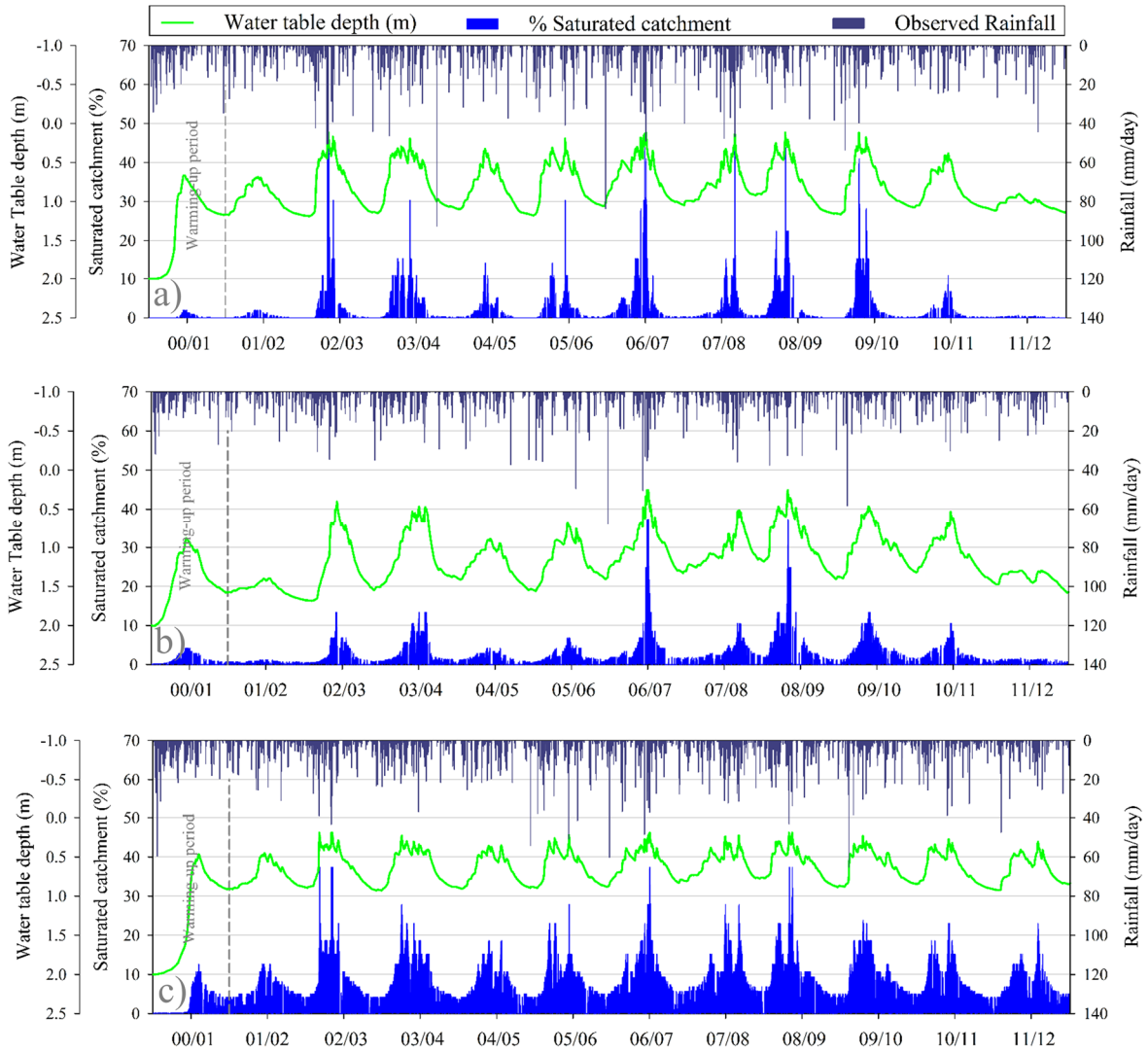

Fig. 4.6. TOPLATS daily simulated plot: 1) water table depth (m), and 2) Percentage of catchment area with fully saturated soil profile (%) for a) La Tejeria, b) Cidacos and c) Arga catchments.

Figure 4.6 also depicts the water table depth, whose principal statistical measures (mean, WTD_m, and standard deviation, WTD_{SD}) are detailed as follows: WTD_m in La Tejeria was 0.71 m, in Cidacos 1.14 m and in Arga 0.63 m. Regarding water table variation, WTD_{SD} in La Tejeria was 0.27 m, in Cidacos 0.31 m and in Arga 0.19 m. As in Fig.4.5, in Fig.4.6 La Tejeria and Arga results are those obtained with CON calibration approach, while Cidacos's ones correspond to RND strategy. As it was commented for Table 4.2, and can be observed in Fig.4.6, RND approach was able to maintain a stable behavior of WTD in Cidacos. Water table depth, especially its minimum values (i.e. closer to surface, mainly during persistent winter events) is a key factor in TOPLATS runoff generation. When

WTD reaches the value of ψ_c (m), simulated runoff increases non-linearly, affecting remarkably simulation efficiency results and model performance. Cidacos, the driest catchment had the deepest WTD_m (1.14 m) and also the highest WTD_{SD}. Arga had the most stable WTD with a standard deviation of just 0.19 m.

4.2.2.2. Daily streamflow

Results presented hereafter (Figs 4.7, 4.8 and 4.9) for La Tejeria and Arga also correspond to the conventional CAL/VAL strategy, while Cidacos results are the ones obtained with RND. Streamflow results are presented in three types of plots: time series (Fig. 4.7), simulated vs observed scatter plots (Fig. 4.8) and streamflow duration curves (Fig. 4.9) to allow for a detailed TOPLATS performance analysis. On the time-series plot (Fig.4.7) it can be observed that almost no runoff was simulated during the warming-up one-year period in all three catchments. This was due to the initial value defined for the water table depth (2 m). Shallower initial WTD values resulted in a more rapid model response but worse overall results for the remaining period. Large inter-annual variability (Fig.4.7) was observed in terms of streamflow in la Tejeria and Cidacos. Despite this large variability, TOPLATS was able to respond adequately, particularly in La Tejeria. Streamflow behavior was much more stable in Arga, allowing better model response, but TOPLATS faced difficulties on Cidacos extreme storm events simulation.

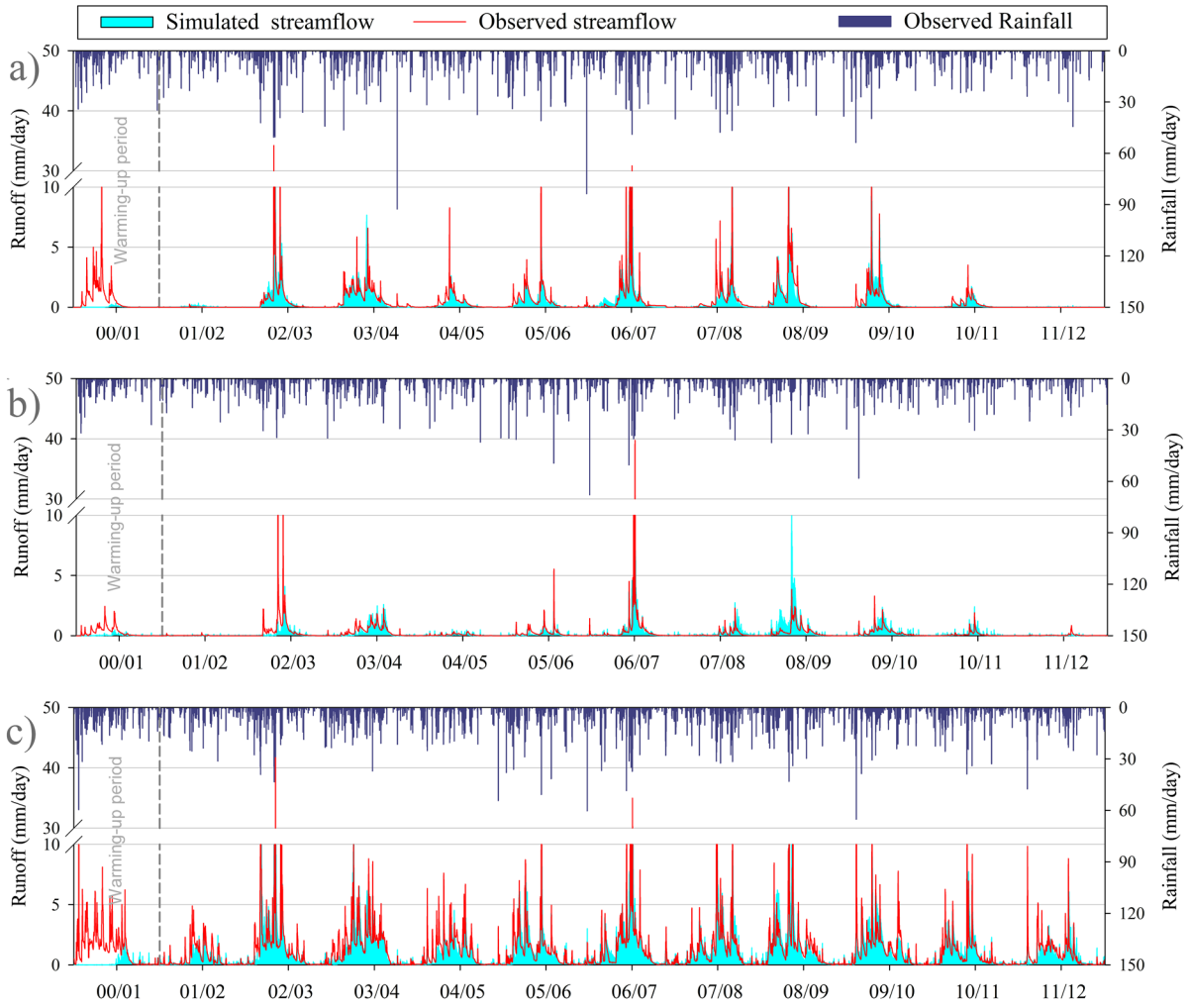

Fig. 4.7. Daily rainfall, observed streamflow and simulated streamflow in: a) La Tejeria, b) Cidacos and c) Arga.

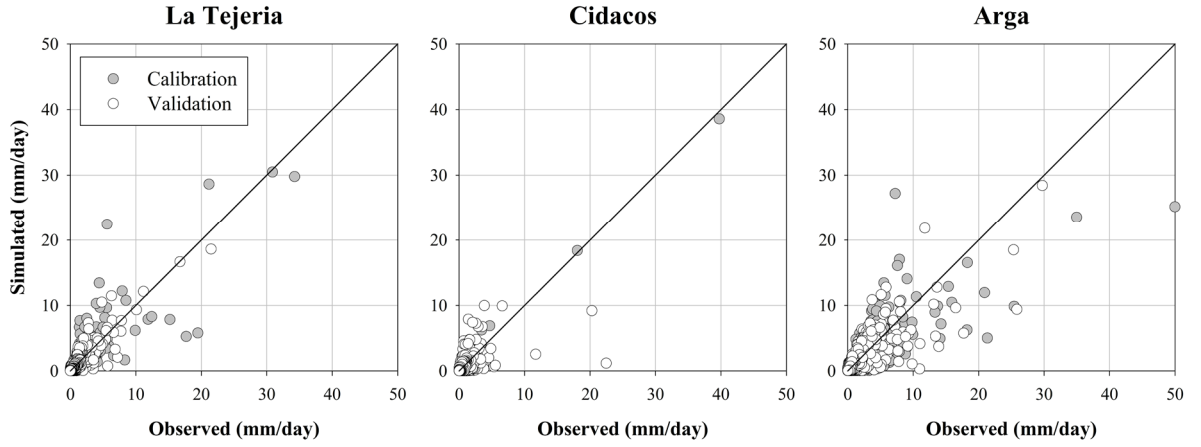

Fig. 4.8. Scatter plot of daily observed and simulated streamflow (mm/day) in: a) La Tejeria, b) Cidacos and c) Arga.

Scatter plots (Fig.4.8) illustrate very clearly how few streamflow peaks affected NSE results. In Cidacos, two high peak flows were very accurately simulated during the calibration period, and account large responsibility for the NSE = 0.91 efficiency obtained (Table 4.2). But on the other hand, main peak events during validation were poorly simulated (Cidacos validation: NSE = 0.25). NSE validation efficiency results were extremely affected by just 7 days data with large simulation miscalculations (out of a 4,383 days simulation), while validation Pbias remained very low (3%). In La Tejeria and Arga there were no such differences in CAL and VAL events and NSE results were more balanced (Table 4.2).

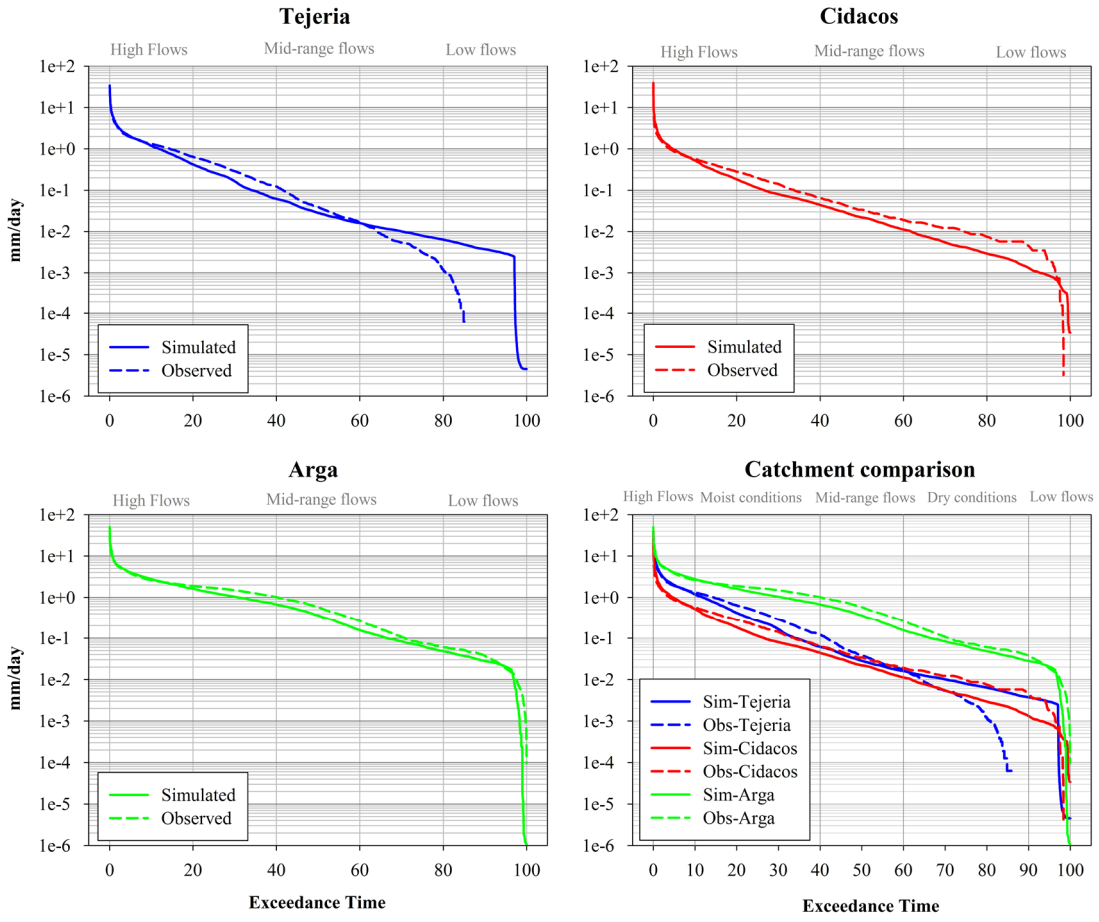

Fig. 4.9. Daily streamflow duration curves (observed vs simulated) in a) La Tejeria, b) Cidacos, c) Arga and d) catchments comparison.

Daily simulated streamflow was also evaluated according to detailed specific flow ranges (high flows, mid-range flows and low flows) in flow duration curves comparing simulated and observed flows (Fig. 4.9). Main divergences were found in low rate flows in La Tejeria, where TOPLATS clearly over-estimated observed streamflows. This was apparent, since up to 14% of the studied days (mostly summer periods) no streamflow was recorded at all, but TOPLATS kept simulating small streamflow amounts. In any case, this overestimation of low flows, has a very limited impact on the total volume and efficiency results. In La Tejeria, also a slight underestimation of modeled flows was found during catchment's moist conditions (10 to 50%). In Cidacos, largest discrepancies (underestimation) between simulated and observed values were found on the 40% of lower-flow days. The same pattern applied for most of the days, where TOPLATS underestimated most of the flow ranges, yet the difference decreased towards high flows. During the driest 1.5% of the days, no streamflow was observed in Cidacos, so the model showed overestimation on that range (right tale of the curve, 97%-100%). Arga presented the best agreement between simulated and observed flows in all streamflow level ranges but TOPLATS tended to underestimate mid-range flows. When all catchment results are plotted together, it is observed that Arga (wettest catchment) patterns clearly differentiate from the other two due to its highest rainfall conditions. On the highest streamflow data range, it could be observed that Arga had the most intense (mm/day) runoff events and Cidacos the least. High flow rate range, as presented in the catchments' comparative plot of Fig. 4.9, include the 10% of the days with the highest streamflow values (438 days).

4.2.2.3. Monthly streamflow

Daily observed and simulated streamflow values were aggregated on a monthly basis to enable a seasonal analysis. These monthly results are useful to understand and evaluate model performance at a seasonal time-scale, but also for different modeling purposes (e.g. for hydrological resource management). Three types of monthly streamflow simulation results are shown in Figure 4.10: 1) monthly NSE, 2) monthly Pbias (%) and 3) Volume bias (mm/month).

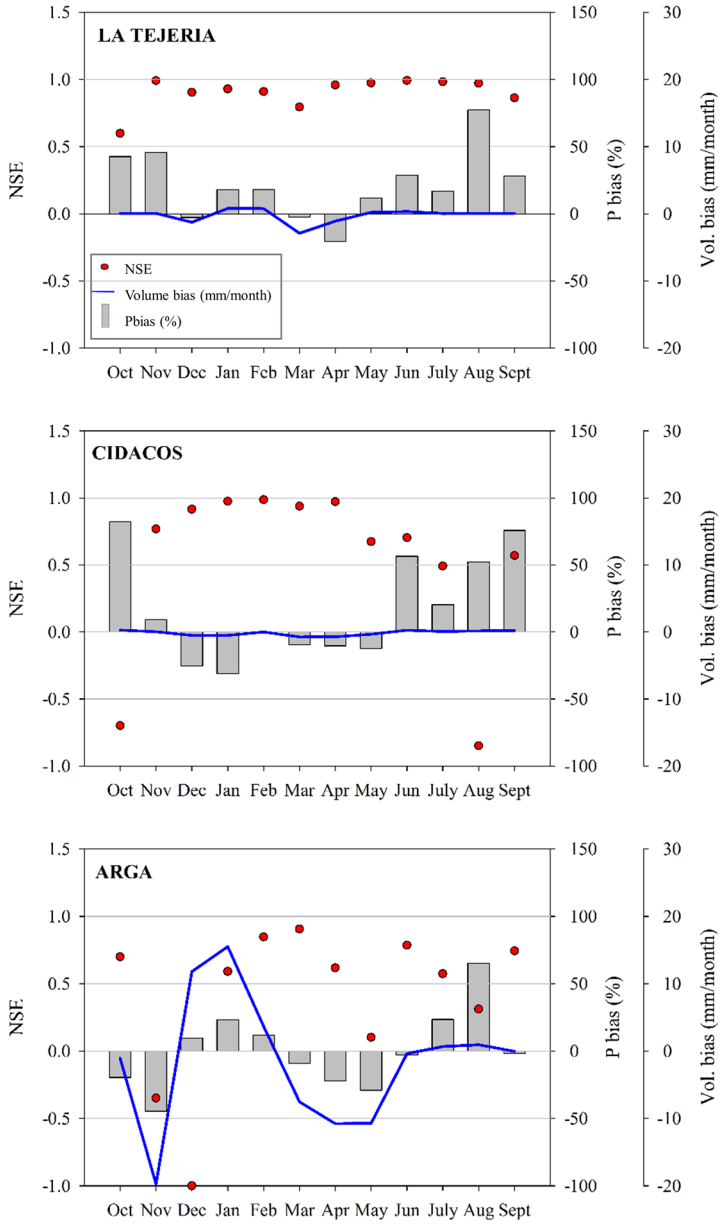

Fig. 4.10. Comparison of monthly observed and simulated streamflow results: 1) NSE (dots), 2) Pbias (%) (bar plot), and 3) volume bias (mm) (line plot) results in La Tejeria, Cidacos and Arga.

Results obtained in La Tejeria showed a high 0.94 overall NSE value. In nine out of twelve months, results were over 0.9 in terms of NSE. The lowest efficiency was found in October (0.6), at the beginning of the hydrological year. The largest Pbias was found during the simulation of summer and autumn months, when intense rainfall events occurred while TOPLATS simulated water table was at its deeper values, and saturated catchment area values were low. Since Pbias is expressed as percentage, its largest values were obtained in august, when streamflow was largely overestimated

(77%). However, this high Pbias value corresponded with very minor errors in volume units (mm/month), as commented for daily results (Fig. 4.9). Largest Volume bias in La Tejeria were obtained in the March-April (spring) period, where TOPLATS underestimated monthly streamflow. That streamflow underestimation in March months caused a lower (0.80) NSE.

NSE monthly median was 0.74 in Cidacos. In this catchment, two different periods could be distinguished in terms of monthly efficiency results. First, from December to April, TOPLATS offered a very accurate performance, reaching NSE values over 0.9 for each month of that winter-spring five months period. On the contrary, the model was unable to properly simulate low flows typical in August, September and October. In Cidacos, the model clearly tended to overestimate streamflow for dry periods. Mean monthly overestimation from June to October was 57%. In terms of streamflow volumetric error, largest discrepancies, but still rather low, were found in March and April, when the model underestimated flow volumes. That systematic underestimation was similarly observed for the whole winter-spring period.

Out of the three evaluated catchments, TOPLATS performed worst in Arga, in terms of monthly efficiency results. Monthly median NSE in Arga was 0.60. This catchment showed the largest NSE variability between months, offering its best NSE results in February (0.85) and March (0.9). Results indicated a clear pattern of modeled overestimation during winter months (December – January - February) and underestimation in autumn (October-November) and spring (March-April-May).

When daily and monthly NSE were compared, it was observed that best results in both cases were obtained in La Tejeria. In Cidacos, monthly results outperformed clearly daily NSE, while the opposite occurred in Arga, where very low efficiencies, mainly in November and December caused low monthly NSE. Bormann (2006b) also performed TOPLATS applications in several catchments in Germany, ranging from 63 to 134 km^2. Daily NSE results presented, varied from 0.59 to 0.73 on the calibration period and from 0.52 to 0.69 on validation years. Efficiency results were found to increase on that study, reaching 0.76-0.85 on weekly analysis and 0.82-0.90 on monthly evaluation.

4.2.2.4. Hourly streamflow simulation

Hourly simulation of the catchments was also similarly performed for the same 12 years (2000-2012) period, with a total of 96,432 hours simulation. At this time-scale, only the CON calibration period method was applied, as no abnormal behavior of the model was found in any of the catchments. Similarly to the daily analysis, the first year was considered as warming-up. Hourly streamflow simulated values (mm/h) versus observed data (mm/h) are first presented (Fig. 4.11) in a scatter plot. While in La Tejeria no clear pattern of over or under-estimation could be identified, in Cidacos and Arga extreme events were significantly underestimated (Fig. 4.11). As observed in figure 4.11, for most of the time-series, Cidacos had the lowest streamflow values (most points below 0.5 mm/h), but also the highest intensity events were observed in that catchment.

Table 4.3. Hourly streamflow simulation efficiency (NSE1 and NSE) and bias results achieved after optimization with the conventional (CON) calibration approach

Catchment	NSE_1		NSE		Pbias	
	CAL	VAL	CAL	VAL	CAL	VAL
	--	--	--	--	%	%
1. La Tejeria	0.56	0.58	0.55	0.66	8	5
2. Cidacos	0.48	0.51	0.41	0.77	-6	8
3. Arga	0.51	0.52	0.64	0.66	1	4

Best NSE_1 results obtained for hourly calibration period (Table 4.3) were similar to their corresponding daily results (Table 4.2) in Cidacos (0.48 vs 0.53) and Arga (0.51 vs 0.50). On the contrary, in La Tejeria, NSE_1 was significantly lower for hourly calibration (0.56 vs 0.71). For the validation period, NSE_1 hourly results were notably better in Cidacos (0.51 vs 0.35) and slightly better Arga (0.52 vs 0.49), but hourly results performed worse in La Tejeria (0.58 vs 0.65).

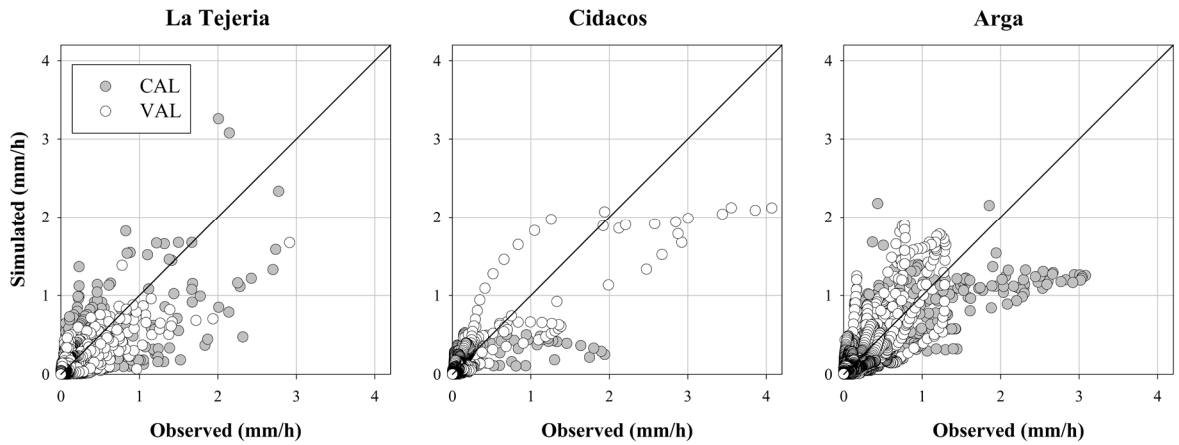

Fig. 4.11. Scatter plot of hourly observed and simulated streamflow (mm/h) in: a) La Tejeria, b) Cidacos and c) Arga.

Analysis of NSE performance concluded that in La Tejeria daily simulations outperformed substantially hourly simulations. This results can be explained by the small size of La Tejeria, with very short runoff evacuation times (hours), which may not be properly captured by the model when run at hourly time step, even though the model was added a specific routing capability. In Cidacos, the NSE value of 0.77 obtained in validation when run hourly contrasted with the poor value obtained with daily time-step (0.09). NSE results in Arga were quite stable from calibration to validation periods at both running time-scales: the difference in daily simulation was -0.03 (calibration NSE was 0.63 and validation 0.60) and +0.02 in hourly results (Table 4.3). Total simulation NSE (CAL + VAL) in Arga was 0.62 for daily data and 0.65 for hourly. Hourly simulation with TOPLATS was also performed by Loosvelt et al., (2015) on a 91 km^2 catchment in Belgium, reporting NSE = 0.33 for CAL and 0.44 for VAL.

Application of MSPM in combination with NSE_1 as objective function proved to achieve excellent Pbias reduction (all volume errors lower than 8%, Table 4.3) allowing TOPLATS to be used as a consistent water resources management tool for continuous simulation both at the daily and hourly scale.

4.3. ASSIMILATION OF ASCAT DATA WITH LUMPED AND SEMI-DISTRIBUTED MODELS

4.3.1. Model calibration and validation

On a first evaluation of TOPLATS and MISDc performance (Fig. 4.12), it was observed that although both models adequately predicted the highest streamflow peaks recorded in Nestore, a systematic underestimation was found for Arga. Streamflow variability in both calibration and validation periods in Nestore was similar, whereas in Arga, variability was significantly higher in the calibration than in the validation period (Fig. 4.12b), with most streamflow peaks below 100 $m^3 s^{-1}$ in the validation and up to 600 $m^3 s^{-1}$ in the calibration period. Almost no large flood events occurred in Arga during the validation period, except for one recorded at the very beginning of this period (Jan 2010).

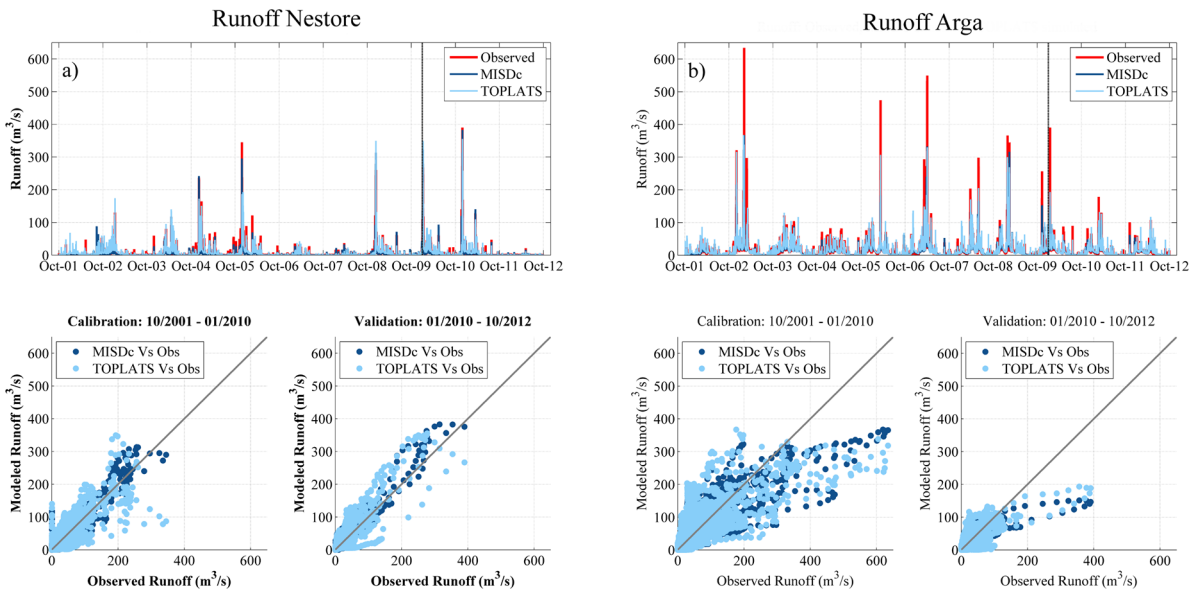

Fig. 4.12. Model calibration and validation results: a) Nestore catchment and b) Arga catchment. Time series and scatter plots of calibration and validation periods (separated with a dotted vertical line in the upper plots).

Overall, MISDc outperformed TOPLATS in both catchments (Table 4.4), both in terms of NSE and Pbias. Additionally, better results were obtained in Nestore than in Arga for both models, in terms of NSE. On the contrary, Pbias errors were very low in Arga compared with Nestore (Table 4.4). The

overall NSE obtained for the whole period studied (including both calibration and validation) was 0.88 and 0.70 for Nestore and 0.75 and 0.64 for Arga using MISDc and TOPLATS, respectively.

Table 4.4. The NSE and Pbias results for the calibration and validation periods obtained using the MISDc and TOPLATS models in the Nestore and Arga catchments.

Model	Nestore				Arga			
	CAL		VAL		CAL		VAL	
	NSE	Pbias	NSE	Pbias	NSE	Pbias	NSE	Pbias
MISDc	0.87	-27%	0.90	-6%	0.76	-2%	0.72	0%
TOPLATS	0.70	5%	0.71	38%	0.64	6%	0.58	4%

4.3.2. ASCAT–SSM preprocessing

- Soil water index (SWI)

The optimal *T* values obtained varied from case to case and were higher for Nestore than for Arga, as well as for MISDc than for TOPLATS. For Nestore catchment, calibrated values were $T = 114$ using MISDc and $T = 45$ when TOPLATS was used (Fig. 4.13). For Arga catchment, an optimal value of $T = 64$ days was obtained using MISDc and a lower one, $T = 24$ days, when TOPLATS was applied (Fig. 4.13). Optimal *T* values were obtained by searching on a range of $T=1$ to $T=200$ for the optimum value. Thus, *T* values providing the higher correlation of simulated and observed values were selected.

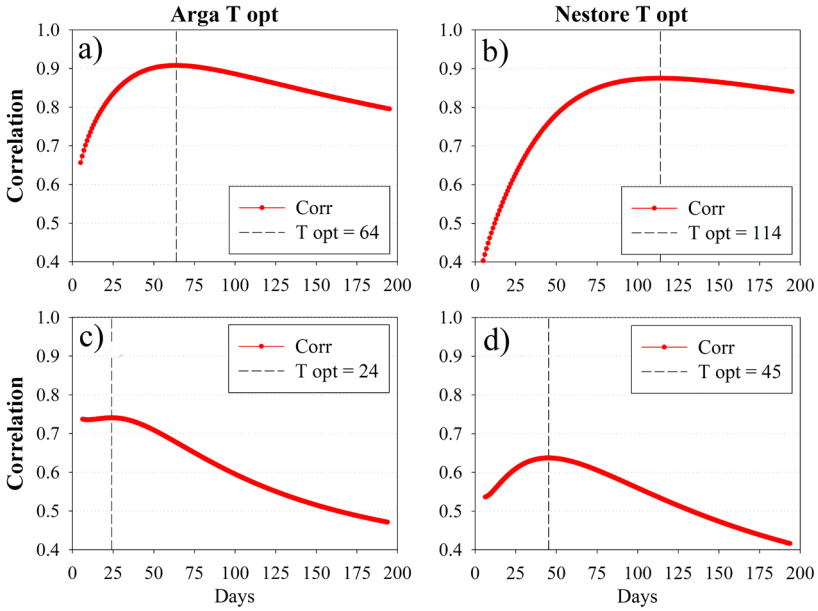

Fig. 4.13. Parameter *T* calibration. A range from 0 to 200 days was explored. The selected optimal *T* values are shown on the plots.

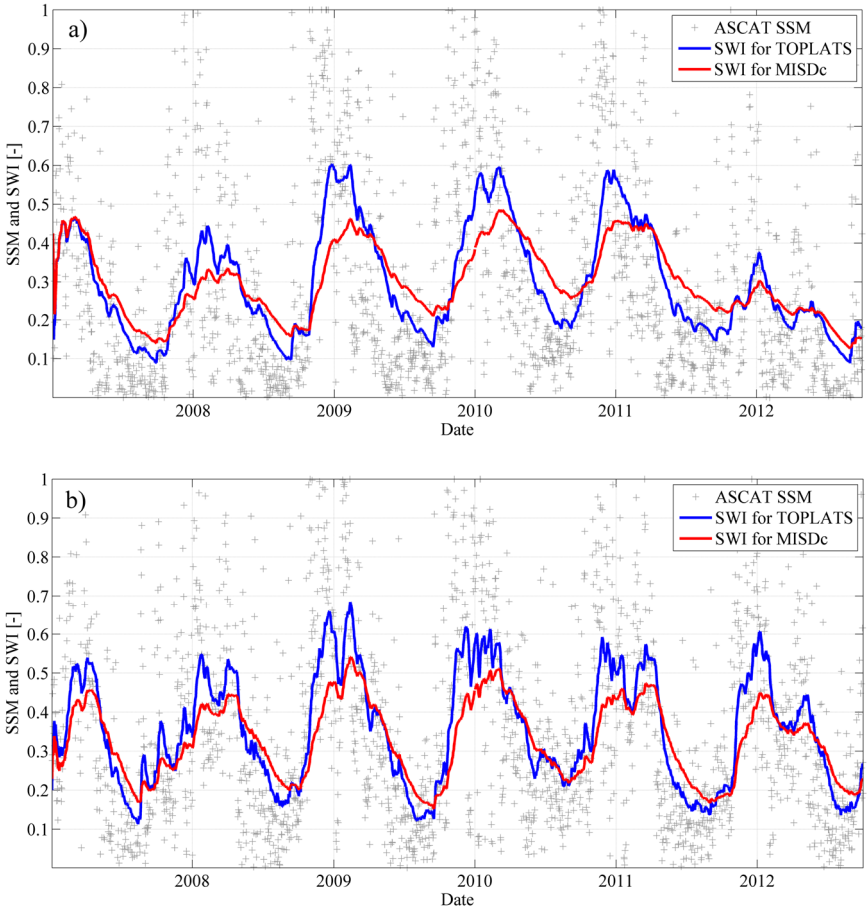

Fig. 4.14. Soil Water Index (SWI) obtained from ASCAT SSM data using the optimal *T* values in Nestore (a) and Arga (b)

SWI calculated for TOPLATS exhibited a larger variability in both Nestore and Arga (Fig 4.14). This is related to the shallower soil surface layer considered in this model, which was set to 5 cm. In MISDc the root layer was deeper in both catchments (larger capacity as deposit for SWB), which resulted in a lower temporal variability of SWI.

- SWI re-scaling

Fig. 4.15 shows the transformation of the SWI series after applying the three different re-scaling techniques to the MISDc model in the two catchments. Fig. 4.16 shows the same information for TOPLATS model.

Note that MISDc and TOPLATS use different units to model soil water content, i.e., relative units [0-1] and volumetric units (m^3 m^{-3}) for MISDc and TOPLATS, respectively. Different re-scaling techniques (CDF, LR and VM) lead to different amounts of variability in the resulting time series (Fig. 4.15 and 4.16). While the LR and VM methods showed a close behavior, CDF reached higher peak values, especially when fitted to TOPLATS (mainly during the calibration period) (Fig. 4.16). Minimum variability between dry and wet periods was obtained using the LR method. Again, TOPLATS simulations had a higher short-term variability than those of MISDc because of its shallower surface zone soil layer (SZ) (Fig.4.16).

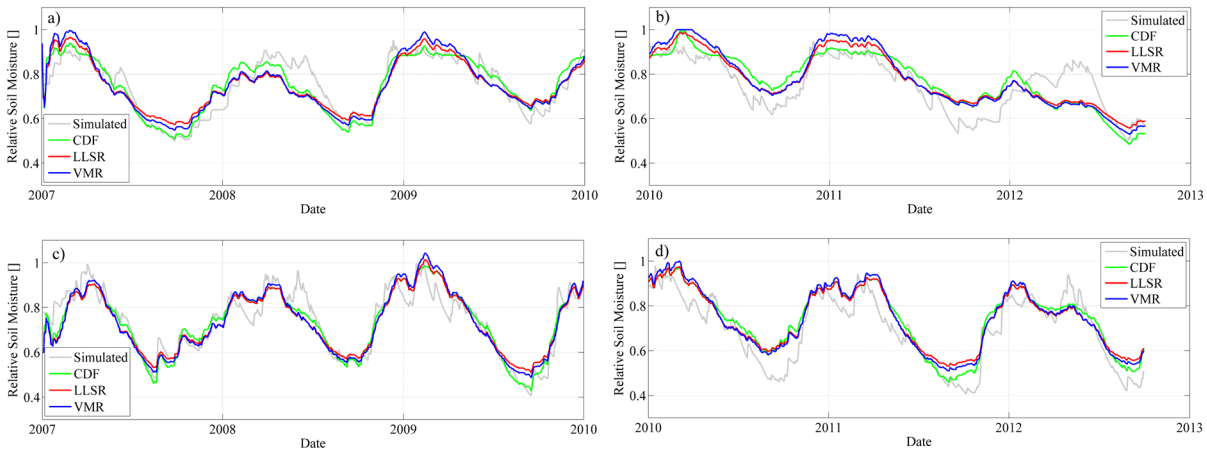

Fig. 4.15. Results of SWI re-scaling for the different techniques evaluated (CDF, LR and VM) for MISDc. Plot (a) shows the calibration period for Nestore, while plot (b) shows validation in Nestore. Plot (c) shows calibration in Arga and (d) validation in the same catchment.

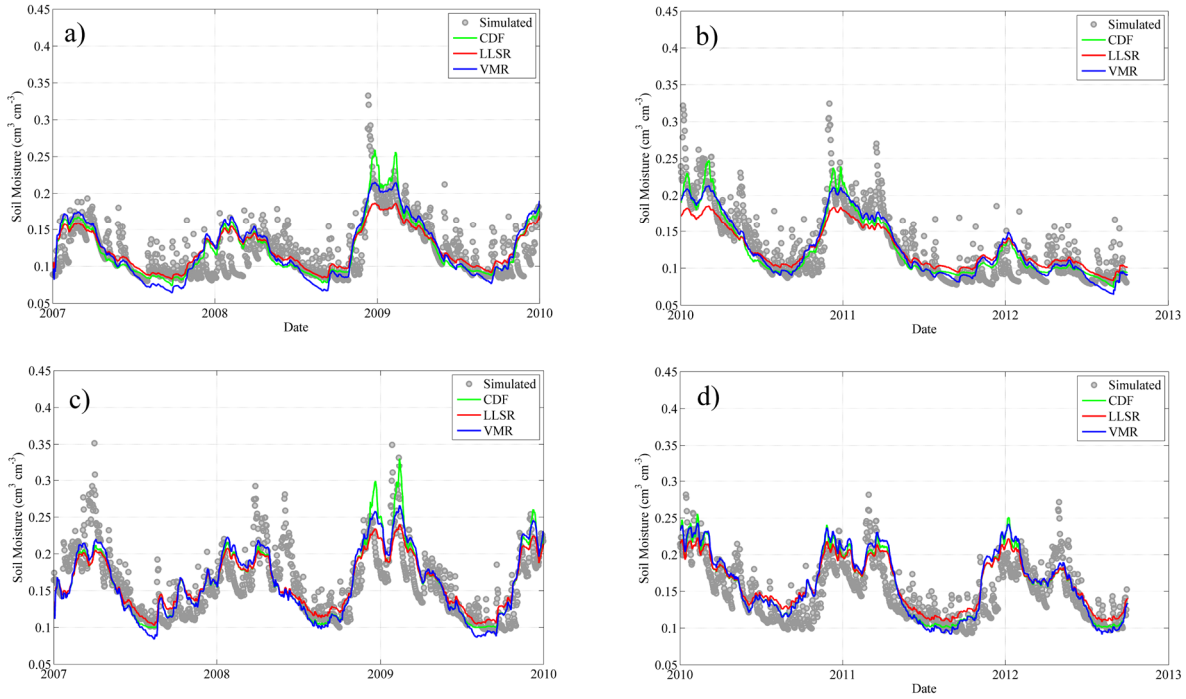

Fig. 4.16. Results of SWI re-scaling for the different techniques evaluated (CDF, LR and VM) for TOPLATS. Plot (a) shows the calibration period for Nestore, while plot (b) shows validation in Nestore. Plot (c) shows calibration in Arga and (d) validation in the same catchment. The TOPLATS simulated values shown are daily mean values.

.

4.3.3. Ensemble validation

Fig. 4.17 shows the streamflow and SSM ensembles generated using MISDc model, while Fig. 4.18 shows the ensembles generated with TOPLATS. It is observed that the SSM ensemble has a larger spread (Fig. 4.17) in Nestore than in Arga for the MISDc simulations. On the contrary, the ensemble spread appears to be mostly controlled by rainfall perturbation in the TOPLATS ensembles (Fig. 4.18).

The streamflow ensembles obtained successfully met the two criteria presented in Eq. 3.19 and 3.20. Specifically, the ensemble results obtained using MISDc were 1.15 for Nestore and 1.1 for Arga (using Eq. 3.19) and 0.73 for Nestore and 0.72 for Arga (using Eq. 3.20); these latter values were sufficiently close to the criteria reference value ($\approx$ 0.714). TOPLATS also met the required values for the first criteria (Eq. 3.19): 0.98 for Nestore and 1.01 for Arga. For the second criteria (Eq. 3.20), the TOPLATS ensemble was also good for Nestore (0.71), but a lower value was obtained for Arga (0.61), which could be explained by the larger simulation error for this catchment (Table 4.4). To generate the ensemble in Nestore, parameters were perturbed in MISDc with a multiplicative noise with a STD = 0.3-0.8 and 0.15 in TOPLATS. For that catchment the rainfall noise was perturbed with also a multiplicative noise of STD = 0.25 in MISDc and 0.9 in TOPLATS. For Arga catchment the added noise was of STD = 0.1-0.8 for MISDc parameters and 0.25 for parameters in TOPLATS. Rainfall added noise was STD = 1.2 in MISDc and 2.8 in TOPLATS. Temperature was modified through an additive noise of STD = 3.0 in MISDc and 2.0 in TOPLATS.

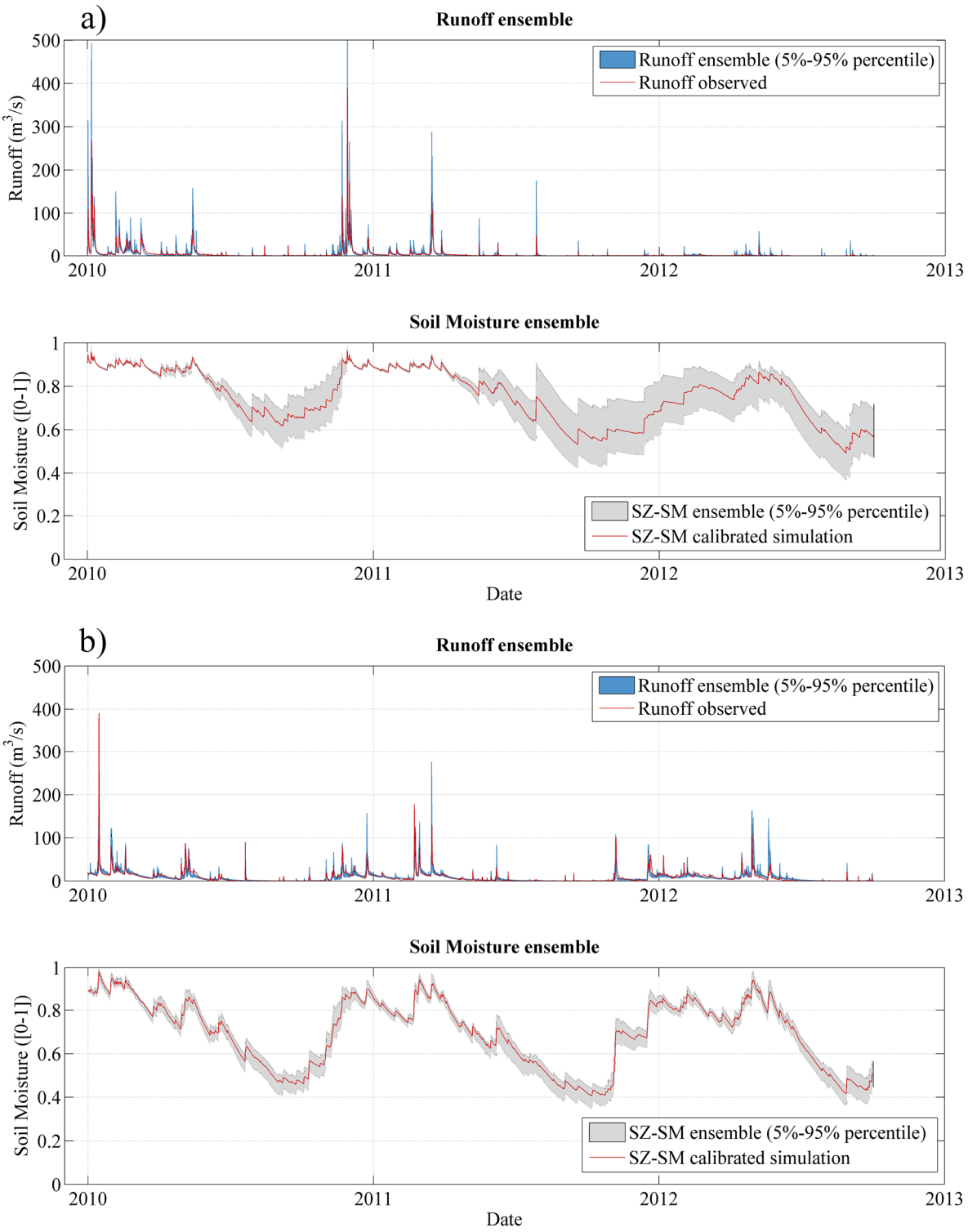

Fig. 4.17. MISDc model streamflow and surface soil moisture (SSM) ensembles: a) Nestore catchment, and b) Arga catchment. The ensembles are represented by their 5-95 percentile range. Soil moisture in MISDc is expressed as saturation degree [0-1].

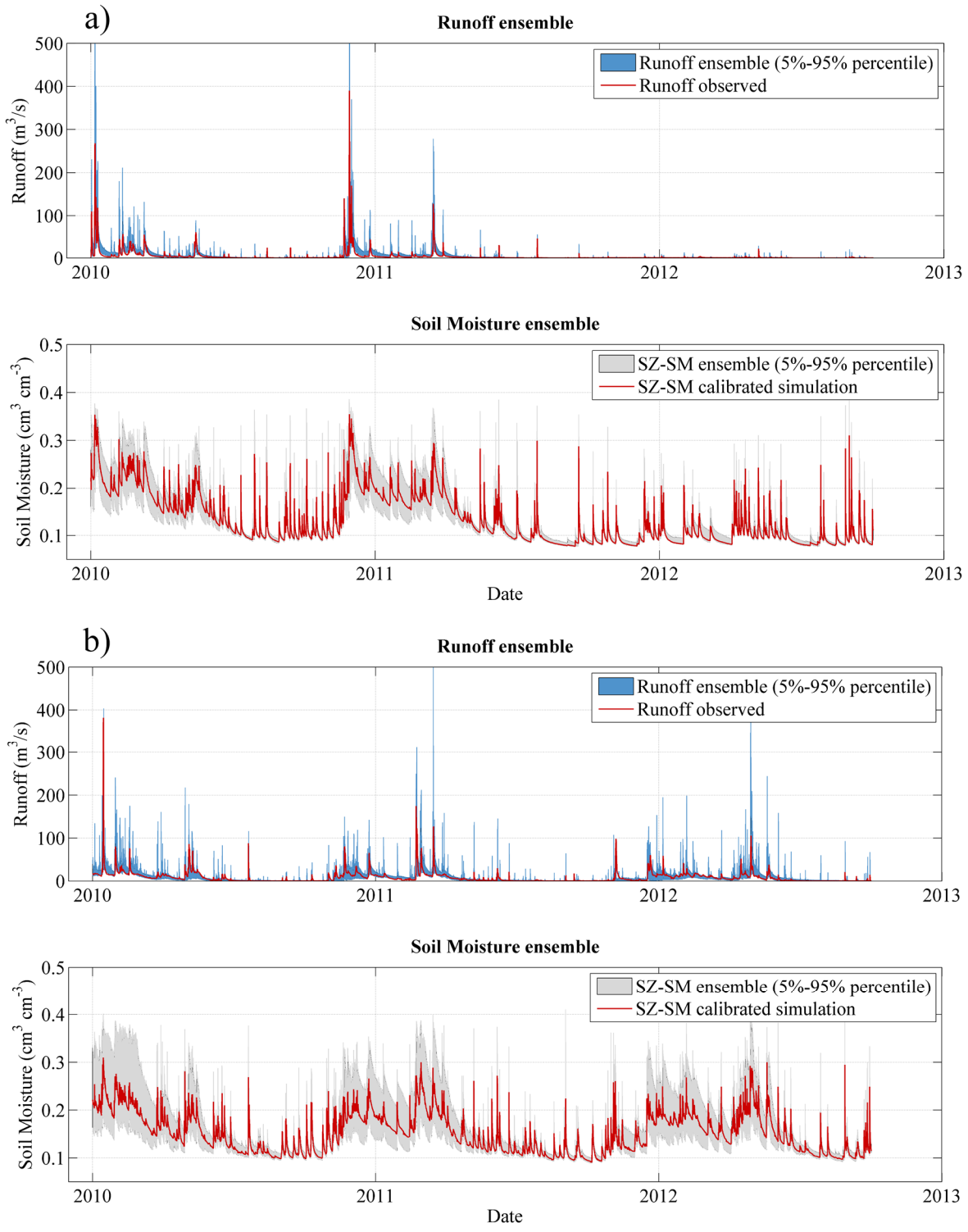

Fig. 4.18. TOPLATS model streamflow and surface soil moisture (SSM) ensembles: a) Nestore catchment, and b) Arga catchment. The ensembles are represented by their 5-95 percentile range. Soil moisture in TOPLATS is expressed in volumetric units ($cm^3\ cm^{-3}$).

4.3.4. DA with MISDc

In Nestore, the NSE achieved using MISDc in the open-loop run (0.91) (Table 4.5) was slightly higher than in the validation run (0.90) (Fig. 4.19a). Similarly, in Arga, NSE increased from 0.72 in the validation run to 0.73 in the OL run (Fig. 4.19b). These results indicate that using an ensemble generated by including random noise in model parameterization and input forcings only marginally improved NSE in MISDc. The NSE value of 0.91, achieved in the OL run in Nestore, was not further improved after DA (Fig. 4.19a), regardless of the different observation error values assumed for the ASCAT data. Furthermore, when low observation errors were considered, NSE decreased sharply, and the other criteria also worsened (Fig. 4.19c, e and g), especially with observation errors below 2 %. Regarding re-scaling methods, CDF produced the worst results, while LR and VM yielded very similar results.

On the other hand, in Arga, DA provided a slightly larger improvement (Fig. 4.19b) compared with the NSE value (0.73) (Table 4.5) obtained in the OL run. In this catchment, the best NSE improvement was always reached when a 4 % observation error was considered (Table 4.5), regardless of the applied RT. In this case (catchment and model combination) the influence of the RTs was only marginal. An increase of 10 % in Eff_{OL} was obtained for Arga after DA (Fig. 4.19f). It must be noted that assuming satellite observation errors below 1 % leads to a significant deterioration in streamflow simulations, as shown by the NRMSE criteria in Fig. 4.19h.

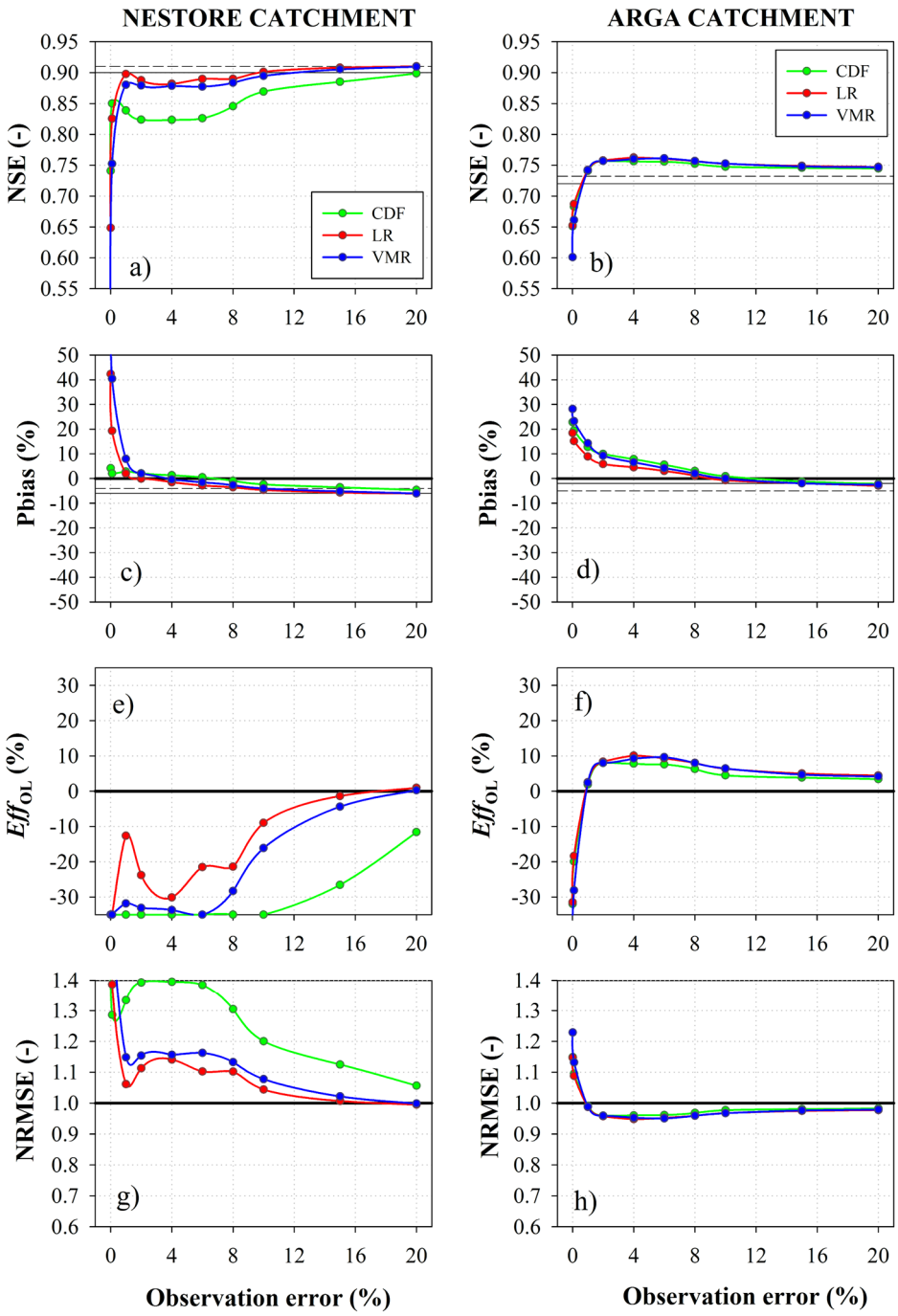

Fig. 4.19. Streamflow simulation efficiency after DA using MISDc for the Nestore (a, c, e, and g plots) and Arga (b, d, f, and h plots) catchments. Four efficiency evaluation criteria results are shown: NSE (plots a and b), Pbias (c, and d), Eff_{OL} (e, and f) and NRMSE (g, and h). Horizontal axes correspond to the assumed ASCAT observation error values. Colors correspond to different SWI re-scaling techniques. In NSE and Pbias plots (a, b, c, and d) the solid horizontal line indicates the Val results, and the dashed line indicates the OL results (Table 4.5).

Fig. 4.20 shows the MISDc-DA results obtained with the best combination of re-scaling technique and ASCAT observation error for Nestore (Fig. 4.20a) and Arga (Fig. 4.20b), as detailed in Table 4.5. Although no improvement was achieved through DA for Nestore, the best combination was considered to be a 4 % observation error and LR re-scaling (Fig. 4.20a) (Table 4.5). In Arga (Fig. 4.20b), the best combination was also obtained by using LR re-scaling and a 4 % observation error. DA offered an increase in NSE from 0.72 to 0.76 in this case (Fig 4.19b). It can be observed that the largest and more systematic improvements were obtained during the spring months of 2010 and 2012 (Fig. 4.20b, error reduction plot (iii)). On the contrary, DA could not reduce sufficiently the large simulation error (>100 $m^3 s^{-1}$) (Fig 4.20b, plot ii) that MISDc offered on a large event that occurred at the beginning of the validation period (Jan 2010).

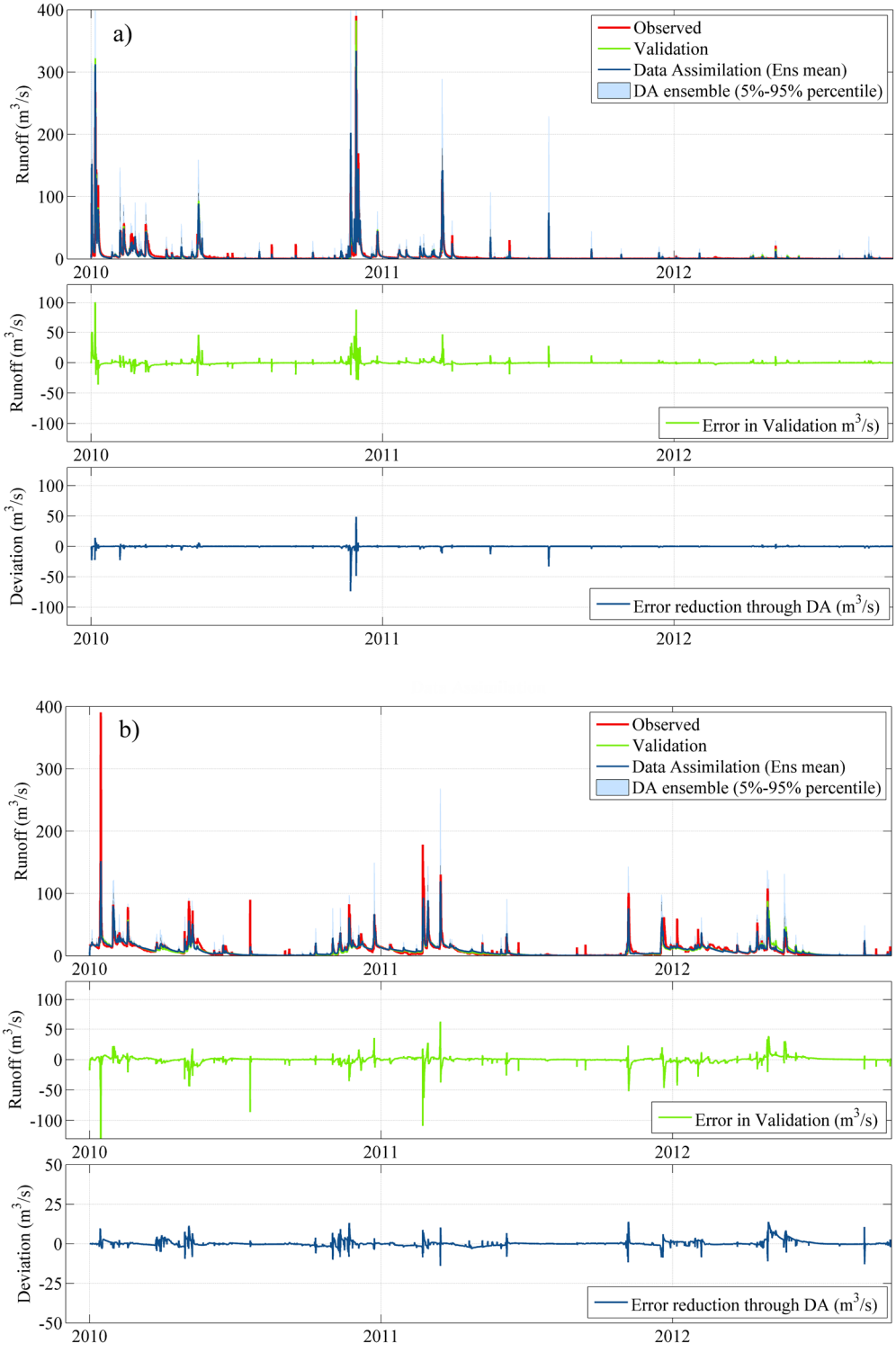

Fig. 4.20. MISDc data assimilation results for the Nestore (a) and Arga (b) catchments. Three plots are presented per catchment: (i) observed, validation and DA time series, (ii) error between observed and validation series and (iii) error reduction achieved after DA, where positive values indicate error reduction. Results shown in this figure are those obtained with the best DA set-up, as detailed in Table 4.5 for each model and catchment combination.

4.3.5. DA with TOPLATS

A high NSE result (0.71) was already obtained in the validation time series for Nestore using TOPLATS, but after generating the ensemble, a significant improvement was obtained in the OL run, increasing NSE to 0.77 (Fig. 4.21a) (Table 4.5). This value further increased after SSM–DA to a value of 0.85 (Fig. 4.21a). DA also reduced the large Pbias value obtained for Nestore during validation to a value of approximately 20 % when LR re-scaling was used (Fig. 4.21c) and led to improved Eff_{OL} values of 34 % (Fig. 4.21e).

The improvements for Arga were not that remarkable, with a total NSE increase from 0.58 during validation (and 0.60 for OL) to 0.62 after SSM–DA when a 6 % observation error was considered (Fig. 4.21b) (Table 4.5). Using this error value, there was a slight reduction in the Pbias value to 9 % (Fig. 4.21d), and the efficiency increase (Eff_{OL}) was 6 % (Fig. 4.21f).

Clear differences in terms of NSE variation were found depending on the re-scaling technique applied (Fig. 4.21a and 4.21b), with LR providing the best results, followed by VM for Nestore and CDF for Arga. For Nestore, any combination of re-scaling technique and observation error increased Eff_{OL} by at least 8 % (Fig. 4.21e). In fact, this was the case where DA provided the highest improvements out of the four combinations of models and catchments evaluated. On the other hand, the DA results for Arga depended strongly on the observation error considered. When observation errors below 4 % were used and CDF or VM re-scaling was applied, efficiency was lower than in the open-loop run (Fig. 4.21b). The highest efficiencies, regardless of the re-scaling technique applied, were obtained for Arga with observation errors within the 4-8 % range, while the best improvements for Nestore were obtained by considering low (<2 %) observation errors.

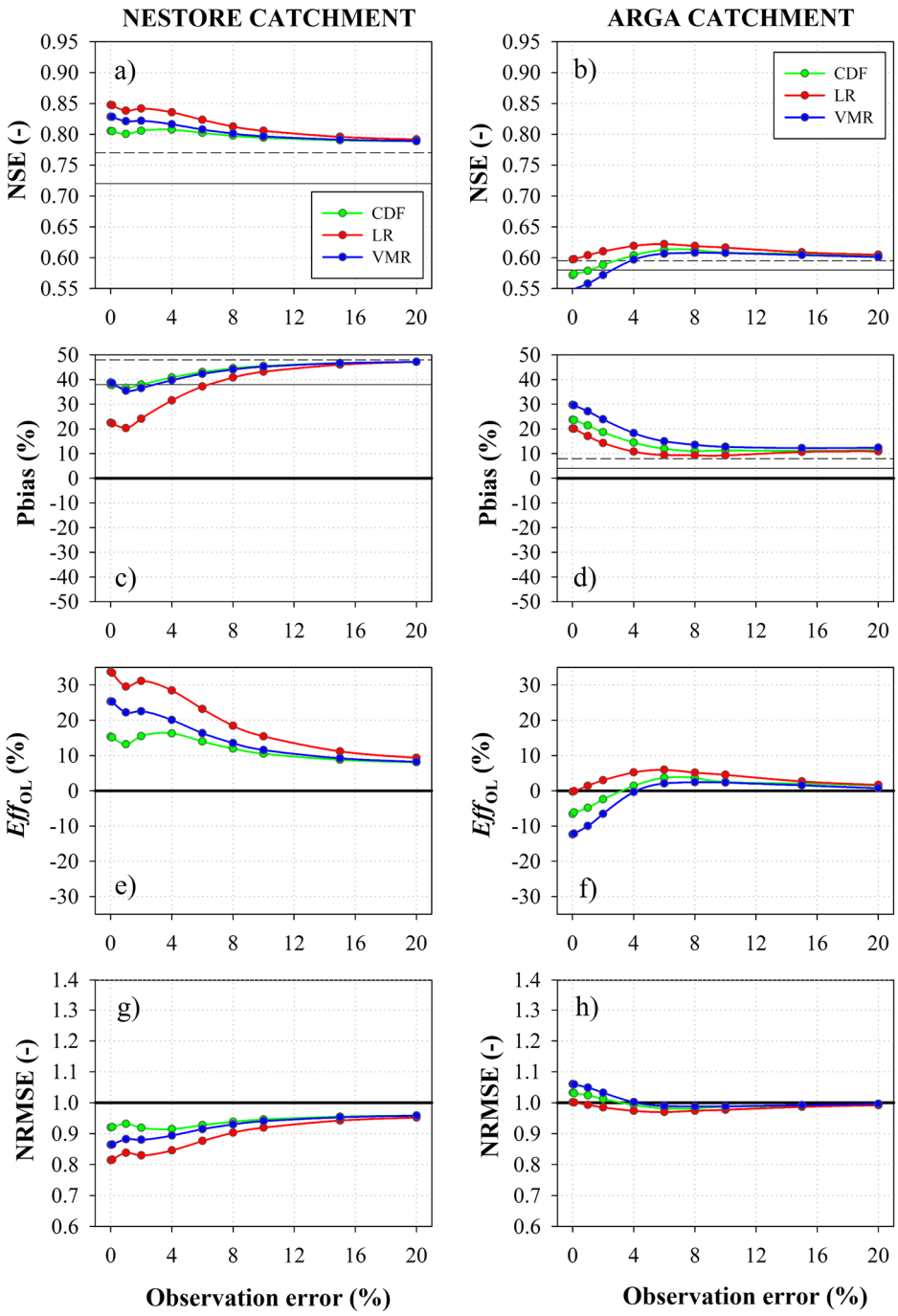

Fig. 4.21. Streamflow simulation efficiency after DA using TOPLATS for the Nestore (a, c, e, and g plots) and Arga (b, d, f, and h plots) catchments. Four efficiency evaluation criteria results are shown: NSE (plots a and b), Pbias (c, and d), Eff_{OL} (e, and f) and NRMSE (g, and h). Horizontal axes correspond to the assumed ASCAT observation error values. Colors correspond to different SWI re-scaling techniques. In NSE and Pbias plots (a, b, c, and d) the solid horizontal line indicates the Val results, and the dashed line indicates the OL results (Table 4.5).

In Nestore, the largest simulation errors occurred during two important events (within a 200-400 m^3/s observed streamflow peak), one in Jan 2010 and the other (the highest) in Nov 2010 (Fig. 4.22a, plot i); these were not accurately simulated, with errors over 100 m^3/s (Fig. 4.22a, plot ii). These large errors were substantially reduced after DA (using LR-RT and a 0.01 % observation error (Table 4.5)), with a correction of up to 100 m^3/s for the first event and over 50 m^3/s for the second (Fig. 4.22a, plot iii). In Arga (Fig. 4.22b), the largest error was also found for a storm event that occurred at the beginning of the validation period (Jan 2010). However, DA performed poorly in reducing this error (it was even increased during certain times of the event). The more continuous improvements were obtained in 2011 and 2012 spring months (Fig 4.22b, plot iii).

Table 4.5. Summary of results and efficiency variations after best set-up DA application. Optimal rescaling method (Opt. RT) and ASCAT observation error (Opt. ASCAT) are also shown. Nestore results using MISDc model are not shown as no improvement was obtained through DA.

Model	Catch-ment	Cal/val	Cal/Val	OL	Opt. ASCAT observation Error	Opt. RT	DA			
		Cal	Val	Val			Val			
		NSE	NSE	NSE			NSE	Eff_{Val}	Eff_{OL}	NRMSE
MISDc	Nestore	0.87	0.90	0.91	--	--	--	--	--	--
	Arga	0.76	0.72	0.73	4%	LR	0.76	10 %	10 %	0.95
TOPLATS	Nestore	0.70	0.71	0.77	<1%	LR	0.85	48 %	34 %	0.81
	Arga	0.64	0.58	0.60	6%	LR	0.62	10 %	6%	0.97

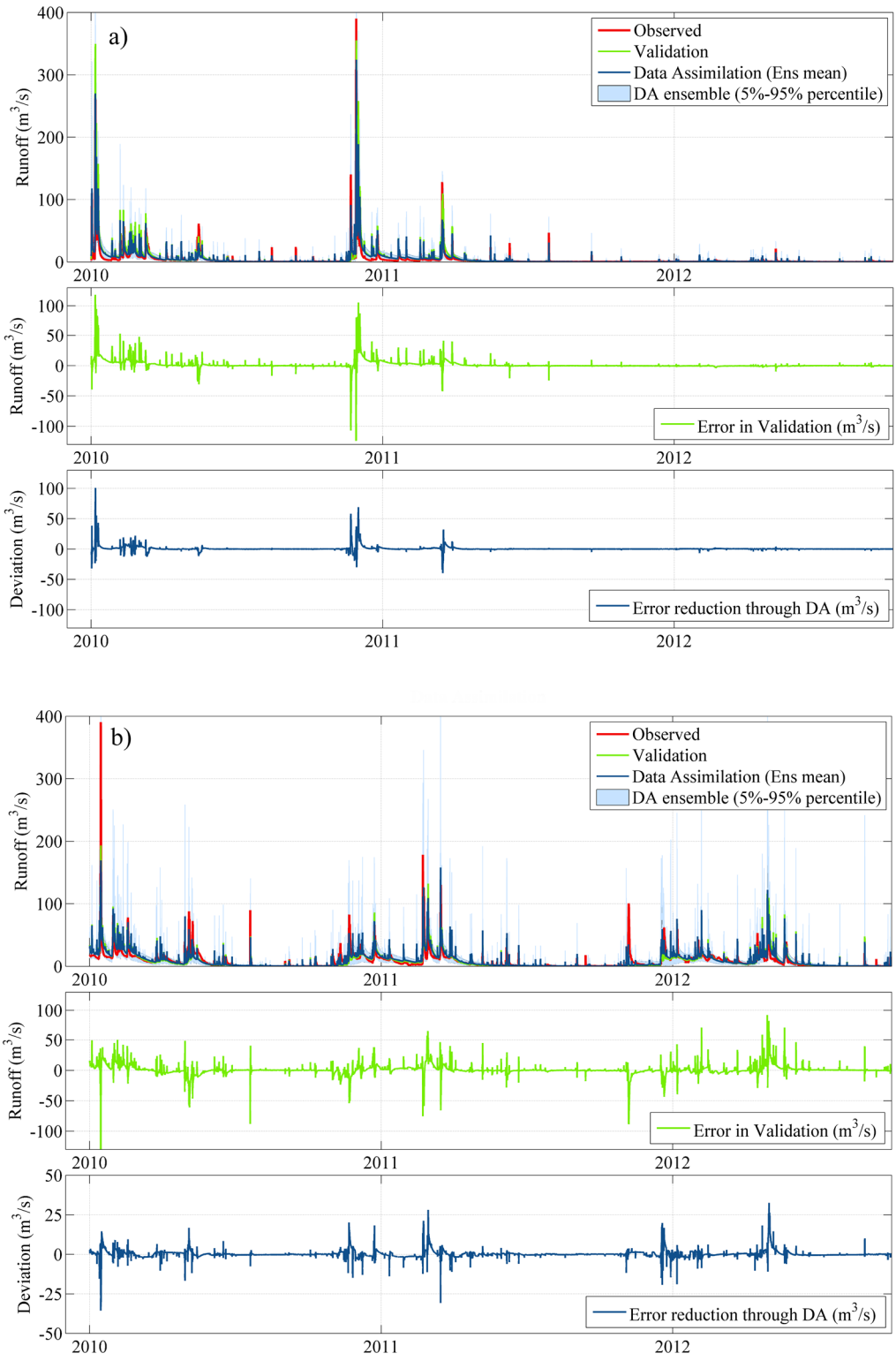

Fig. 4.22. TOPLATS model assimilation results for the Nestore (a) and Arga (b) catchments. Three plots are presented per catchment: (i) observed, validation and DA time series, (ii) error between observed and validation series and (iii) error reduction achieved after DA, where positive values indicate error reduction. Results shown in this figure are those obtained with the best DA set-up, as detailed in Table 4.5 for each model and catchment combination.

4.3.6. Comparison of DA results for the MISDc and TOPLATS models

As a summary of results and to provide a numerical and visual comparison of DA performance for both models, the Eff_{Val} index was used. Best Eff_{Val} results and DA set-up for obtaining them are also shown in Table 4.5.

In the first case, i.e., using MISDc for Nestore, SSM–DA did not provide any streamflow simulation improvement, regardless of the RT used and the SSM observation error assumed (Fig. 4.23a). On the contrary, large Eff_{Val} improvements (>30 %) were obtained for this catchment using TOPLATS (Fig. 4.23c), irrespective of the observation error or the RT. Both models yielded the best results when LR re-scaling was used. With respect to Arga, the DA improvements were similar for both models (Fig. 4.23b and d). DA improved Eff_{Val} by a 10 %, especially when observation errors between 4 % and 8 % were considered. Lower observation errors resulted in a worsening of model forecasts. Differences among re-scaling techniques were smaller for Arga than for Nestore, but in all cases, LR was the best method.

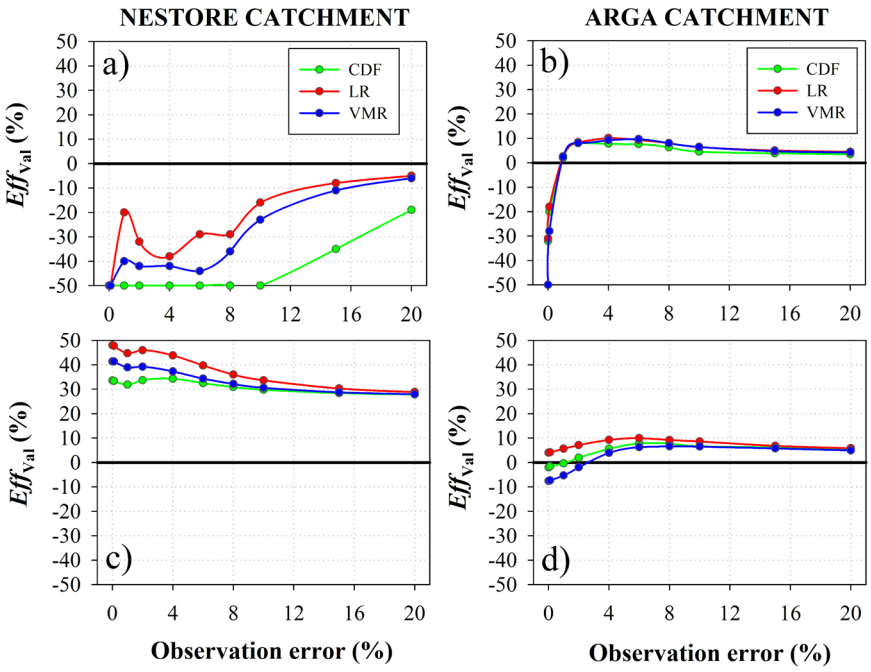

Fig. 4.23. Efficiency variation (Eff_{Val}) compared to validation time series for the Nestore (a and c) and Arga catchments (b and d). The MISDc model results are shown in plots a and b, while the TOPLATS results are presented in plots c and d.

4.3.7. Monthly evaluation

With respect to Nestore, DA generally decreased MISDc model accuracy in terms of monthly simulation (Fig. 4.24a). On the contrary, the error reduction thanks to DA was high for this catchment when TOPLATS was used (Fig. 4.24c), especially in the winter months (from November until March). This seasonal trend contrasted with that obtained for Arga using TOPLATS (Fig. 4.24d), where the largest corrections were observed in November and later in spring (April and May). On the contrary, no clear seasonal pattern was found for the MISDc DA results for Arga (Fig. 4.24b), but most of the improvement occurred in May and June. Therefore, for Arga, highest correction rates after DA were achieved in May for both models.

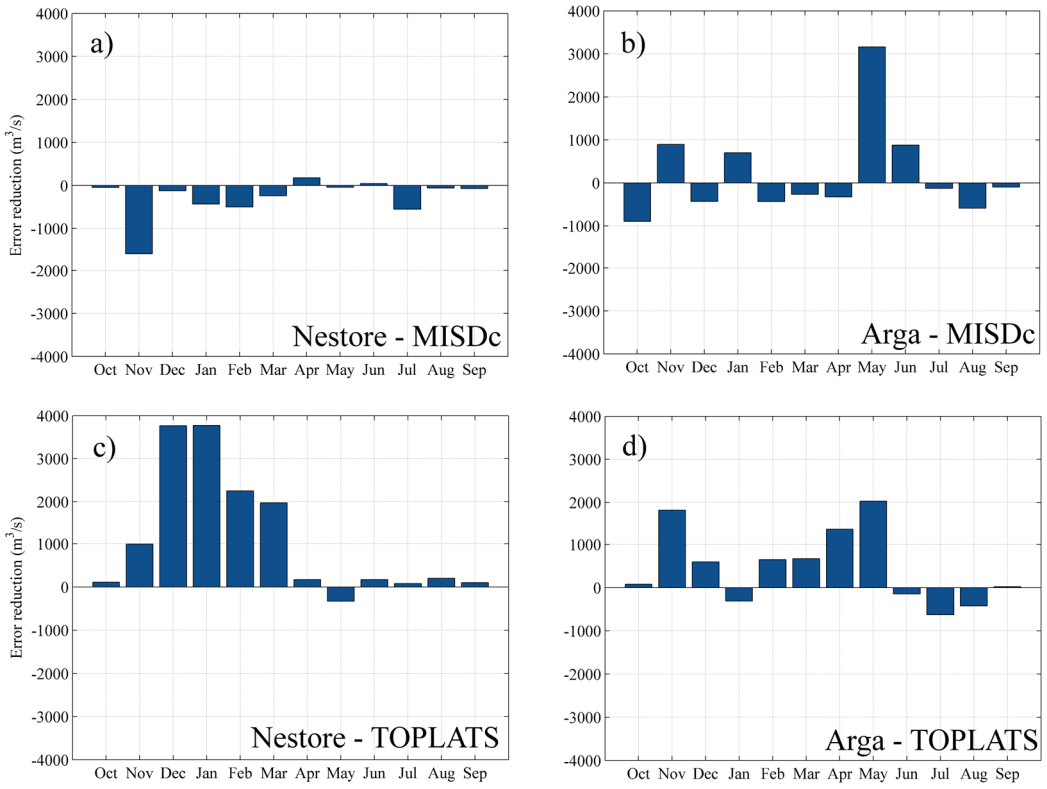

Fig. 4.24. Monthly variation (expressed as monthly m^3/s) in simulation accuracy after DA in the validation period for a) Nestore using MISDc, b) Arga using MISDc, c) Nestore using TOPLATS and d) Arga using TOPLATS. Positive values indicate that simulation after DA increased the accuracy of the total monthly simulated streamflow volume. Negative values indicate a reduction in the simulation accuracy. Monthly results also correspond to best set-up conditions, as detailed in Table 4.5 (For Nestore using MISDc, LR and 4% observation errors were used).

4.3.8. Discussion

Despite significant efforts in DA research, there is still no consensus in the community regarding the improvement in streamflow prediction skill based on the assimilation of satellite soil moisture observations because many factors affect the DA performance. These factors include: the DA algorithm, the particular model structure, the choice of bias correction technique, the appropriate quantification of observation and model forecast errors, the spatial mismatching between modelled and satellite soil moisture, and the watershed topography and climatology (Yan and Moradkhani, 2016). Through the use of different models, RTs, observation errors and catchments, this research aimed to develop a study that could provide valuable results regarding some of these main factors. The results are discussed based on the following research questions:

4.3.8.1. Did EnKF data assimilation of ASCAT data improve hourly streamflow prediction?

This study demonstrated that ASCAT-derived SWI can improve hourly streamflow simulation of medium-sized (750 km^2) Mediterranean catchments using physically based and conceptual models. Moreover, a significant specific merit of this study is that the improvements were achieved in a fully independent validation period, different of the periods used for model calibration and SWI RTs calibration. As shown in Figures. 4.23 and 4.24, one of the models (TOPLATS) improved streamflow prediction for Nestore, while both models improved the Arga simulations. The results obtained for the Arga catchment using MISDc are of similar magnitude as those reported in the literature, such as Brocca et al. (2010b), who reported increases in NSE from 0.75 to 0.84 and from 0.62 to 0.76 in catchments in central Italy after ASCAT−SSM assimilation. With respect to MISDc model application, similar results were obtained by Brocca et al. (2012), where ASCAT−SSM assimilation was also found to improve NSE from 0.76 to 0.79 and to increase $Eff_{Val} \approx 10$ %, but in smaller Mediterranean catchments. Regarding TOPLATS DA results, efficiency improvements obtained here after ASCAT−SSM assimilation outperform those of previous TOPLATS-DA studies (Pauwels et al., 2002, 2001), which in any case already indicated that this model was suitable for improvements in

simulation capability through DA. Similarly, different SSM-DA methods were tested using TOPLATS by Houser et al. (1998) whose final recommendations included the use of DA methods of moderate complexity that are sound and computationally efficient, and also the use of long data series, as it has been done on this study. Although the DA method used might have a significant effect on the assimilation results (Yan and Moradkhani, 2016), this was not the focus of this research.

The variability of the results in our study is not exceptional in the SSM−DA literature. Studies of this type have reported a variety of results, ranging from successful improvements (Francois et al., 2003; Lievens et al., 2015; López López et al., 2016), to slight improvements (Pauwels et al., 2002), no significant differences (Lü et al., 2016) or even significant decreases in model performance (Chen et al., 2011; Matgen et al., 2012a). Studies on the topic cover a wide range of catchment sizes, climate conditions, remote sensing sources, model conceptualizations and assimilation methods. Among the studies where SSM−DA proved ineffective in improving streamflow forecasts (e.g., Chen et al. (2011), Draper et al. (2011), Han et al. (2012)), some authors noted that the limited efficiency of DA might be due to the low accuracy of precipitation forcing data and the inaccuracy of the rainfall-runoff simulation mechanism in the model (Han et al., 2012). Other studies reported that while dual assimilation of streamflow and ASCAT−SSM improved streamflow simulation, SSM assimilation alone did not result in any improvements (Yan and Moradkhani, 2016).

On the other hand, other studies obtained more positive results and confirmed the possibility of enhancing model streamflow prediction through remotely sensed SSM−DA (Alvarez-Garreton et al., 2014; Massari et al., 2015). Improvements were reported using different metrics; however, efficiency increases between ~15 % (Francois et al., 2003) and ~30 % (Massari et al., 2015) and NRMSE reductions of ~25 % (Alvarez-Garreton et al., 2014) were obtained. In a study conducted by Laiolo et al. (2015), where ASCAT−SSM assimilation based on the EnKF was applied over two catchments with a similar size to those studied here, Eff_{OL} values ranging from 26 to 33 % were obtained. ASCAT−SSM assimilation based on the EnKF also improved streamflow forecasts for larger

catchments (Wanders et al., 2014b), although limitations on high peaks accurate simulation were also found.

4.3.8.2. Was monthly simulation improved through EnKF data assimilation?

As shown in Fig. 4.24, the DA results differed depending on the season and the particular month of the year. This seasonal trend also varied depending on the particular model and catchment combination, with no clear or consistent patterns. With respect to Arga (Fig. 4.24b and 4.24d), ASCAT−SSM assimilation improved both models, especially in the autumn and spring months (mainly in Nov and May). These results are in line with those of Cenci et al. (2016) and Matgen et al. (2012a), who showed that ASCAT−SSM assimilation was more efficient during hydro-meteorological transition periods (e.g., from dry to wet seasons or vice versa). In these periods, the temporal variability of SSM is expected to be higher, and its correction might have a stronger impact on model performance (Massari et al., 2015). On the contrary, the largest positive results were obtained during winter months in Nestore, for the TOPLATS model (Fig. 4.24c). This result might be in line with other study performed in a Mediterranean area by Laiolo et al. (2015). On that study, different ASCAT-derived products were assimilated to a distributed, physically based model (similar to TOPLATS conceptualization) in three Italian catchments (two of which were ≈ 800 km^2), and their efficiency was evaluated in seasonal terms. The results showed that improvements in the one catchment occurred mainly in winter and summer.

4.3.8.3. Did re-scaling techniques have a significant influence on the DA results?

The results obtained here do not fully agree with those reported by Massari et al. (2015), who observed a small effect of re-scaling on assimilation results. Although all three RTs behaved similarly in some cases (MISDc used in Arga) (Fig. 4.19f), large differences were found in other cases (e.g., TOPLATS used in Nestore (Fig. 4.21e). In any case, LR consistently produced the best results and CDF the poorest. LR is probably the most popular RT used in DA studies (Alvarez-Garreton et al., 2015; Chen et al., 2011; Crow et al., 2005a; Crow and Zhan, 2007; López López et al., 2016;

Wanders et al., 2014a, 2014b). CDF has also been frequently used (Alvarez-Garreton et al., 2014; Lievens et al., 2016; Renzullo et al., 2014), while VM and triple collocation (TC) have been applied less frequently (Yilmaz and Crow, 2013). Lievens et al. (2015) found that a first-order matching (similar to the LR-RT applied here) provided better results than higher-order CDF matching techniques. Yilmaz and Crow (2013) also discussed the risks associated with applications of RT methods that match the total variance of observations with the model (VM and CDF), as they may partly neglect the noise contributions of the datasets.

Some authors have noted the limitations of the RTs used in this study (Alvarez-Garreton et al., 2014). For instance, since a data assimilation scheme explicitly updates the model prediction based on the relative weights of the model and the observation errors, assuming a constant observation error may lead to overcorrection of the model state if the actual error is higher, and vice versa. Thus, application of TC techniques should be considered in further research (Alvarez-Garreton et al., 2014; Yilmaz and Crow, 2013). Moreover, selecting an inadequate RT can compromise the DA results, as shown in Lievens et al. (2016), where limited improvements in SMOS DA results were attributed to the RT used (CDF). That study also concluded recommending further research on this topic.

4.3.8.4. Did the SSM observation error assumed have a significant influence on the DA results?

The estimation of an appropriate observation error for DA techniques is a key question that remains open and requires further research (Massari et al., 2015; Trudel et al., 2014). Different studies have attempted to characterize the satellite SSM error either by comparing satellite SSM data with ground observations (Albergel et al., 2009; Brocca et al., 2010a; Matgen et al., 2012b) or by providing an independent error estimate. Furthermore, data providers may also supply a retrieval error value as ancillary data (Massari et al., 2015). However, these gross error estimates can be highly variable depending on different factors, and given its influence on the outcome of DA

techniques, optimization of the observation error for each particular site and dataset is an appealing alternative.

Ten different observation error values, ranging from 0.01 % to 20 %, were tested here. The best NSE results using TOPLATS in the Arga catchment corresponded to an observation error of ~6 % (Fig. 4.21f), while in Nestore, even lower observation errors (0.01 %) yielded the best NSE results (Fig. 4.21a). These values contrast with the 10 % error value reported in the literature for ASCAT (Albergel et al., 2009; Brocca et al., 2010a; Matgen et al., 2012b) and can be interpreted as ASCAT providing more useful information than initially expected. On the other hand, using MISDc similar optimum efficiency values were obtained for Arga when error was within a 2 to 6 % range (also lower than the 10 % referred to in the literature) (Fig. 4.19b), but no improvement was obtained for Nestore despite the error value assumed (Fig. 4.19a). This reveals that the characteristics of the site appear to influence the optimum error value to be used for EnKF DA, but in any case, it was always found on the range below 6 %.

4.3.8.5. Did the model choice influence the results?

The added value of SSM–DA varied strongly in the four different model-catchment settings evaluated here. For Arga catchment, regardless of the model applied (MISDc or TOPLATS), similar simulation improvements of ~10 % were obtained (Fig 4.23b and 4.23d). On the other hand, the results obtained for Nestore varied dramatically depending on the model used, with improvements of ~50 % using TOPLATS but a worsening effect of >50 % for Nestore (Fig 4.23a and 4.23c). Therefore, it cannot be concluded that model type and complexity influences DA results in a specific improving or worsening direction. Also different models did not condition the magnitude of DA influence. This study found that assimilation of SSM data into a thin surface layer of a model (TOPLATS) does not limit the capabilities of DA to substantially vary streamflow results. This finding contrasts with results in (Brocca et al., 2012) where assimilation on the surface layer had a very

limited impact. Moreover, differences on the results might not be explained by the type of model but rather by the accuracy of model predictions before SSM-DA (i.e., after calibration).

Several studies demonstrated the ability of SSM–DA to improve streamflow prediction using models with different types of conceptualizations, ranging from conceptual RR models (Alvarez-Garreton et al., 2015; Brocca et al., 2012; Lü et al., 2016) to complex, physically based models (Houser et al., 1998; Lievens et al., 2015; Pauwels et al., 2002). The enhancements obtained in these studies varied from case to case, but the type of model could not be identified as the main factor influencing them. However, different studies related the performance of SSM–DA to the quality of simulation achieved after model calibration (Alvarez-Garreton et al., 2015, Matgen et al., 2012a); this effect is clearly visible in the results obtained using MISDc in Nestore, where an NSE of 0.90 after calibration offered few possibilities for further improvements after SSM–DA. The improvements in streamflow simulation accuracy achieved after a successful calibration of the model might be even larger than those achieved after SSM (or even streamflow) assimilation (López López et al., 2016; Wanders et al., 2014a). Thus, some studies have used SSM–DA as a tool for improving model parameter calibration instead of directly enhancing streamflow simulation (Bach and Mauser, 2003; Moradkhani et al., 2005b; Wanders et al., 2014a).

4.3.8.6. Was DA performance influenced by catchment characteristics, i.e., climate and topography?

Soil type and catchment characteristics, unlike catchment area, might play a role in the performance of SSM-DA (Massari et al., 2015). The significant improvement in NSE obtained for Nestore using TOPLATS can be explained by the climate conditions of the area. Since central Italy is not characterized by a proper rainy season, soil hardly remains constantly saturated. Under such conditions, when a significant meteorological event occurs, SM conditions change rapidly. Therefore, SSM−DA might be useful for correcting the antecedent wetness conditions, thus contributing to an enhanced prediction of high flows (Cenci et al., 2016). SSM−DA might be more efficient when SSM temporal variability is higher (Cenci et al., 2016) and direct runoff processes are predominant

(instead of baseflow contribution) (López López et al., 2016)). In any case, as pointed out on the monthly results analysis section, it must be noted that most of the improvement concentrated on winter months events. Longer and more stable dry and wet climatic patterns, characteristic of the Arga catchment, somehow limited the effectivity of DA in this catchment to certain particular transition periods (e.g., November and May) where model inertia did not enable a rapid response. Rainfall large spatial variability characteristic of the area may have also limited the potential for improvements trough DA in Arga.

4.3.8.7. Which topics within SSM-DA require further research and better understanding for improved streamflow prediction?

Three different issues that require further research can be identified. (1) A thorough evaluation of the added value of SSM−DA compared to the enhancements achieved when other variables (e.g., streamflow or LAI) are assimilated. (2) The identification of the causes of model bias as a means of enhancing simulations depending on the particular cause (i.e., poor model calibration, errors in forcing data, model structure, etc.), rather than relying on DA as a tool for fixing everything. (3) The development of models that better reflect the vertical coupling between surface and subsurface soil moisture states. As shown in this work, there is potential to improve catchment model streamflow simulations through data assimilation of remotely sensed soil moisture products. However, systematic model bias should first be reduced to a minimum, through calibration, so the model performance is close to its optimal behavior before data assimilation.

4.4. ASSIMILATION OF SMOS DOWNSCALED L4 PRODUCT WITH A DISTRIBUTED MODEL

This section shows the results obtained on the third, and last research work included on this thesis (Loizu, 2017). Results are organized in 5 parts, which are: 1) Streamflow simulation efficiency results obtained with TOPLATS distributed (TOPLATS-dis) mode during the validation period (Oct/2013-Oct/2015). 2) Details and validation of the ensemble generated. 3) Description, through their mean and standard deviation values, of the distributed SSM time-series observed by SMOS (BEC L4 product) and simulated by TOPLATS. 4) Re-scaling SMOS/MODIS data through different re-scaling techniques. 5) Data assimilation results, including three different experiments: in a first one, data assimilation was performed over each of the 266 1-km cells within the catchment (Cidacos river), in a second one EnKF was applied only on cells with agricultural use (Figs. 3.4 and 3.6c), and in the third, DA was performed only in flat areas (cells with TI>10) (Fig 3.6b).

4.4.1. Calibration and validation

For this study, it was assumed that optimal parameter values obtained after calibration in the statistical mode of TOPLATS (section 4.2.2.4) corresponded with the average optimal parameter values for the distributed mode. Specifically, as detailed in section 4.2.2.4, optimal parameter values were obtained for the 2001-2007 period and were used for validation during the 2007-2012 period. In that case NSE achieved in Cidacos for the calibration period was 0.41, with a Pbias of 6%, while results for the validation period were 0.77 and Pbias 8%. Soil parameters were then adapted to the different soils present in the catchment (Fig. 3.4), always maintaining a catchment average value equal to the optimal value found in the statistical mode.

Table 4.6. TOPLATS calibrated parameters for Cidacos catchment. Type, symbol, units and mean parameter values of the catchment are given

	Symbol	Parameter	Type	Calibrated optimal value	Units
1.	B	Brooks-Corey Pore Size distribution Index	Soil properties	0.32	--
2.	ψ_c	Bubbling pressure	Soil properties	0.83	m
3.	ϑ_s	Saturated soil moisture	Soil properties	0.50	cm^3 / cm^3
4.	K_s	Surface saturated hydraulic conductivity	Soil properties	$2e^{-07}$	m / s^1
5.	r_{min}	First soil resistance parameter	Soil properties	40,013	s / m^1
6.	Q_0	Subsurface flow at complete saturation	TOPMODEL	399	mm / day^1
7.	f	Hydraulic conductivity decay	TOPMODEL	5.00	m^{-1}

Using these parameter values a NSE of 0.68 was obtained with TOPLATS distributed mode for the 2 years studied period (Oct/2013-Oct/2015). The statistical mode of TOPLATS was also run for the same period and parameter values, obtaining a 0.71 efficiency. Distributed mode simulation obtained a remarkable low Pbias value (2%), significantly lower than in statistical model (13%). Figure 4.25 shows different plots to visually compare TOPLATS distributed mode simulated and observed streamflow in Cidacos for the two years study period. As observed in plot 4.25a, catchment streamflow remained below 100 m^3/s during the evaluated period, with most of the streamflow concentrating during winter and spring, mainly of the second year. Also, some large storm events occurred in summer (July 2015) and autumn (October 2013), this is typical on Mediterranean areas. As observed on the scatterplot (Fig 4.25b) and Flow duration curves plot (4.25c) the model performed better on the 20% of largest streamflow values, but clearly tended to underestimate during the low 60% streamflow values (Fig. 4.25c). In any case, it must be noted that those 60% of simulated hours correspond to streamflow values below 0.5 m^3/s (Fig. 4.25b and c). Simulation performance improved as we move to the left (high flows) on the flow duration curves. Some overestimation was found during the highest event (spring 2015) of the period, but simulated and observed peak values

remain quite close to each other (Fig4.25b). This overestimation effect appeared as the timing of the simulation was not correctly captured by the model.

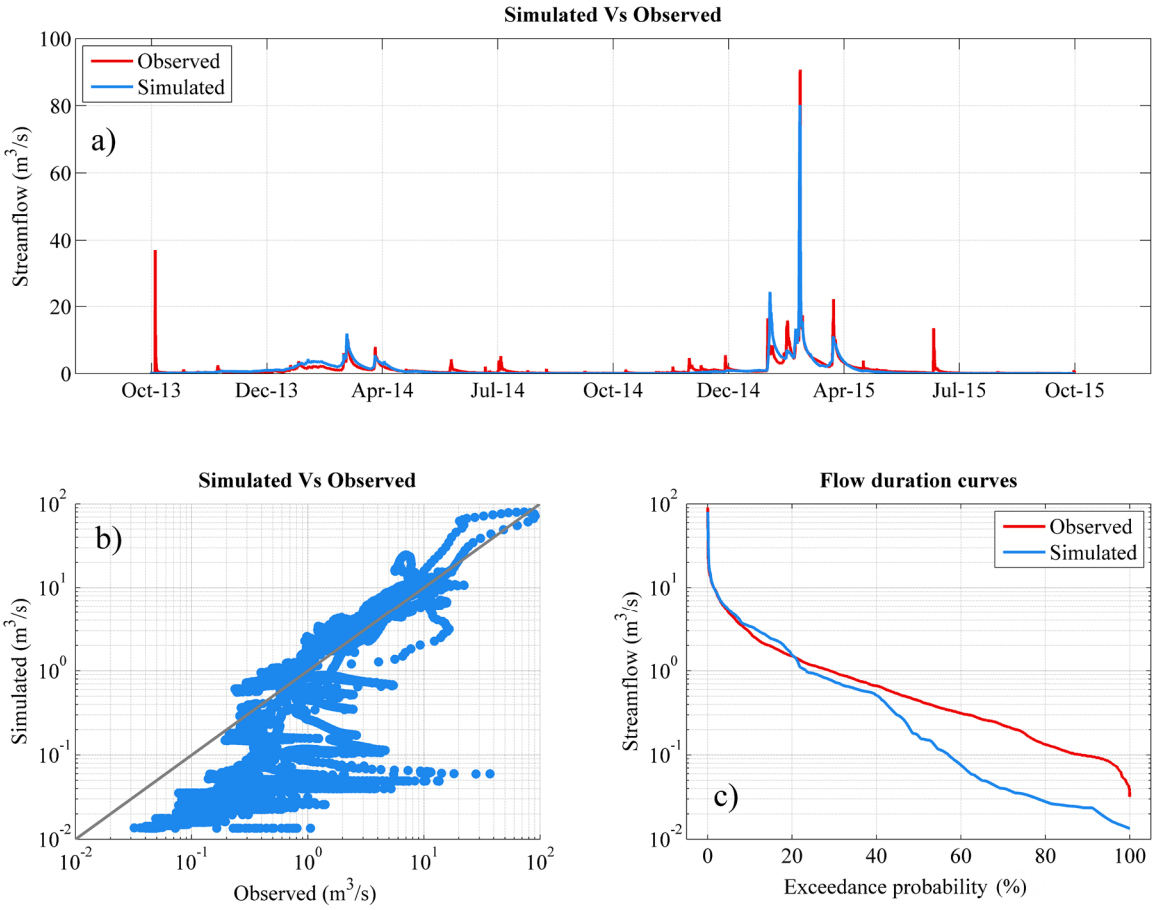

Fig. 4.25. Validation streamflow results. Comparison of simulated and observed time series. Three plots are shown: a) time series, b) logarithmic scatterplot of simulated versus observed streamflow and c) flow duration curves.

The mean value of the SSM for this validation run simulation is shown in figure 4.26 (red line). Also in this figure, the grey lines indicate the behavior SSM in each of the 266 simulated cells within Cidacos. This plot shows the large variability that can be found among the different cells in the same time-step, which is especially large in summer, where a number of cells appeared very dry and close to the minimum (residual) moisture value. It can also be observed that during winter and spring periods a number of cells remained constantly saturated. Altogether, SSM variability was larger in

summer than in winter (the latter showing values over 0.3 cm^3/cm^3 for the whole catchment during several months). Summer rainfall events caused substantial increases on SSM (e.g., summer 2014), but these were characterized by a quick return to an equilibrium value, and the water transfer to the transmission zone of the soil.

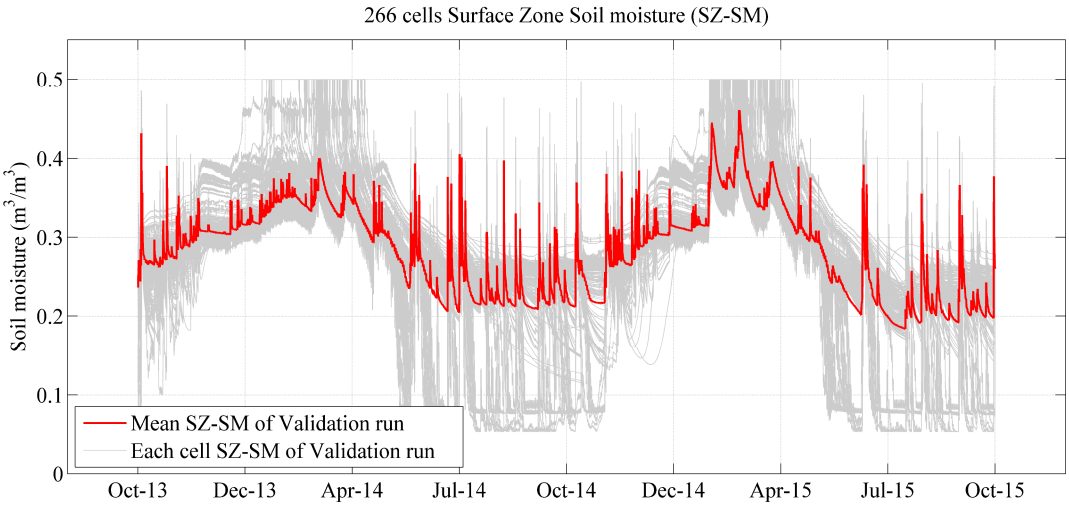

Fig. 4.26. Surface soil moisture (SSM) simulations for each of the 266 catchment cells. Mean catchment SSM value is also shown (in red).

4.4.2. Ensemble generation and validation

Similarly to the procedure used in section 4.3, this study performed SSM data assimilation with the Ensemble Kalman Filter (EnKF), which has been already described in section 3.3.2. This method requires the estimation of the uncertainty of the model. For this, a 50-member ensemble was generated by adding random noise to three TOPLATS parameters and to two climatic forcings. Similarly to section 4.3, three TOPLATS parameter were perturbed by adding a zero mean multiplicative noise. Selected parameters were chosen from the sensitivity analysis performed in section 4.1. The three most sensitive parameters were thus selected: (1) the Brooks-Corey pore size distribution index (B), (2) the bubbling pressure (ψ_c) and (3) hydraulic conductivity decay (f) (already mentioned in section 3.3.3). Perturbed climatic forcings were rainfall and temperature. The first was

perturbed with a zero mean Gamma distribution multiplicative error, and the latter was added an additive noise. Ten different combinations of noise amplitude (standard deviation) were tested for the multiplicative and additive noises, in order to find the best combination to comply with the two validation criteria introduced in section 3.3.3, specifically in equations 3.19 and 3.20. In this experiment, the selected noise achieved a value of 1.24 (≈1.0) for the first validation criteria and 0.68 (≈0.71) for the second. Despite these values are not as good as the ones obtained on section 4.3, they were considered acceptable. The difficulty of achieving better ensemble validation criteria values relies on the NSE of the validation run. Validations with low NSE values result in ensembles with first validation criteria values higher than 1.

Figure 4.27 shows the streamflow and SSM ensembles of 50 members generated by adding the described random noise. As it can be observed in both cases, variability due to the added noise increases during winter months, indicating higher uncertainty on model's prediction during those seasons. To generate the ensemble, TOPLATS parameters were added a multiplicative noise of STD = 0.2 and the rainfall was perturbed with a noise of STD = 2.0. Temperature was modified through an additive noise of STD = 2.0.

Figure 4.28 shows the Kalman Gain (G_k) calculated for each cell of the catchment assuming an uncertainty of 0.04 cm^3 cm^{-3} for the SMOS L4 product (Piles et al., 2010). As it can be observed, the mean G_k value for the 2013-2015 data assimilation period ranges between 0.7 and 0.3, indicating that the uncertainty of the model and the observation are similar (i.e., G_k = 0.5). The model was run 50 times, and the specific uncertainty of each cell, at each time step was calculated, and afterward used for EnKF data assimilation. This means that for each cell, and time step, one G_k value was calculated and used to weight the reliance attributed to the model and the satellite observation. G_k values close to 1 indicate that the model will be updated to the observed satellite value, while values close to zero indicate that the model has no uncertainty and should not be corrected at all.

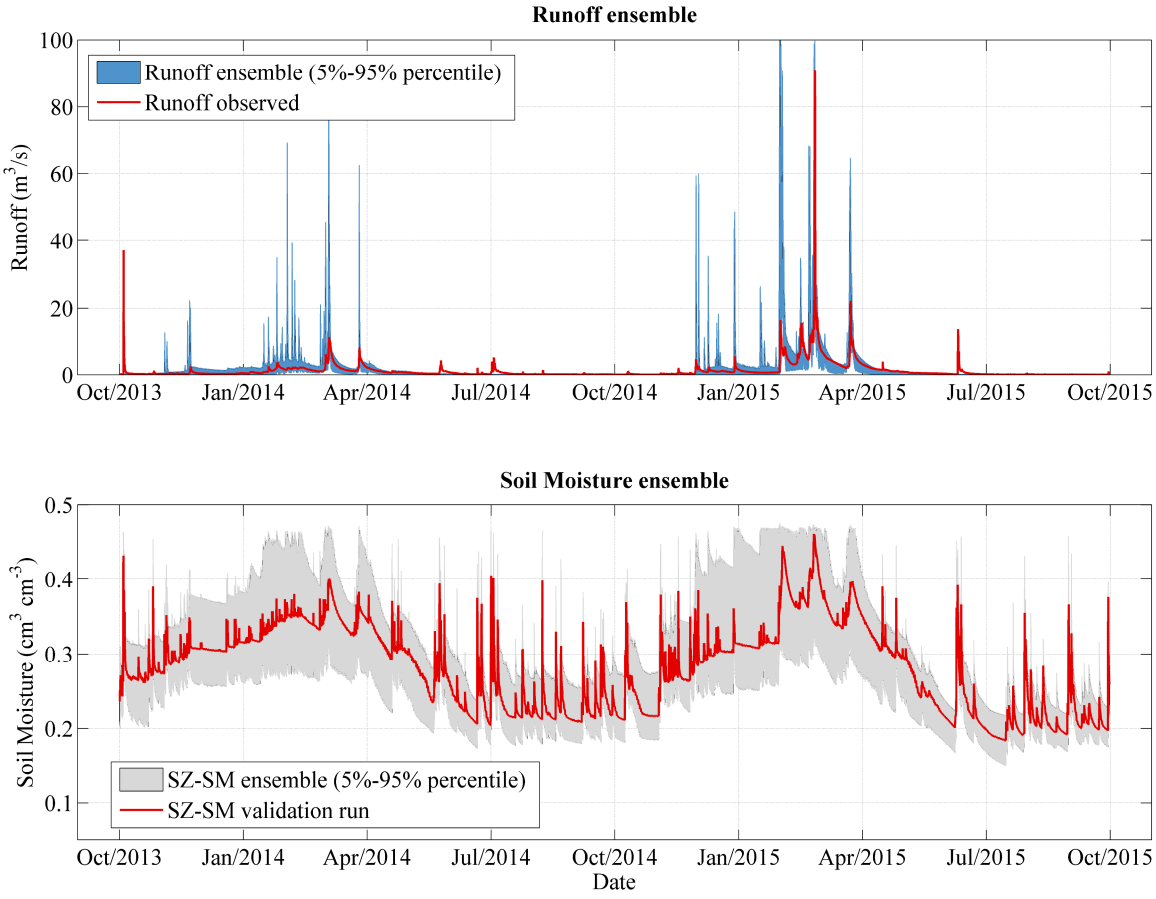

Fig. 4.27. Streamflow and surface zone soil moisture ensembles with TOPLATS distributed mode. The red line in the streamflow ensemble plot indicates the observed streamflow values, while the red line in the soil moisture ensemble plot shows the soil moisture mean content in the catchment for the validation run.

Figure 4.27 shows that SSM simulation uncertainty increased during winter and spring seasons, thus increasing the G_k values (Fig 4.28) and giving more trust to the observation values during those time-steps. On the other hand, mean catchment G_k, and specially some of the cells show very low G_k values during the dry summer in 2015 (Fig 4.28).

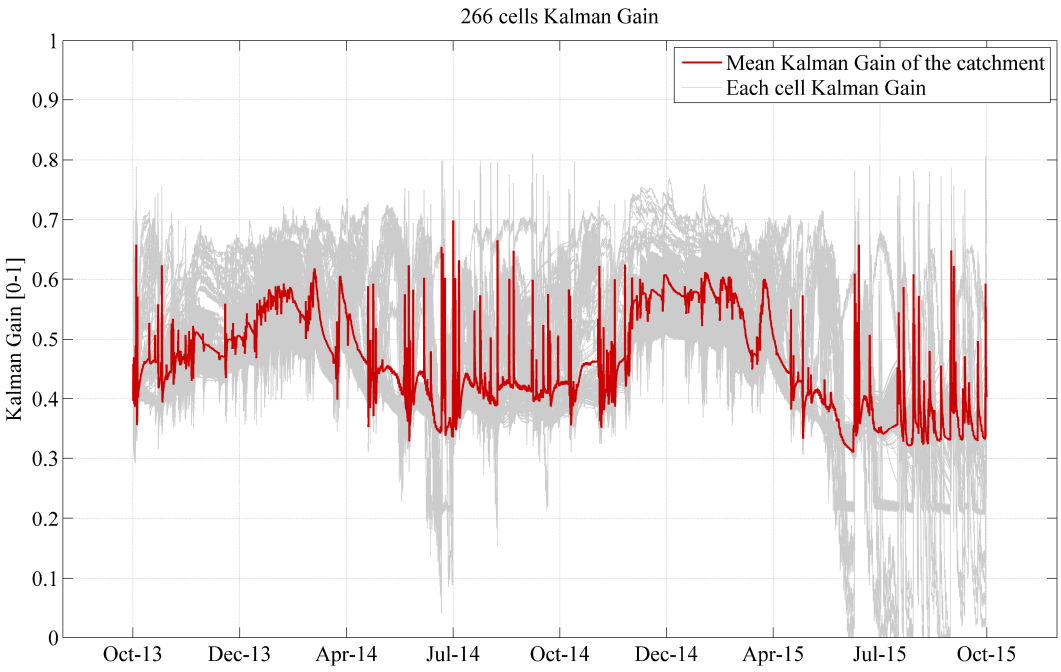

Fig. 4.28. Kalman Gain used for Ensemble Kalman Filter data assimilation. Specific time series of Kalman Gain were calculated for each cell. The red line indicates the mean value of the Kalman Gain for Cidacos catchment.

4.4.3. Observed and simulated SSM

This section aims to give some general insight of the observed and simulated SSM content at 1-km resolution. Figure 4.29 illustrate two relevant statistical measures of the Oct 2013-Oct 2015 period. Plots in the upper part show the mean values (for the whole period) of the SMOS L4 product (left), the TOPLATS simulation (center) and the difference between simulated and observed (right). Plots in the lower part show standard deviation values of observed (left), simulated (center) and the difference between them (right). These two statistical measures are representative of the mean soil moisture content and its fluctuation during the studied period.

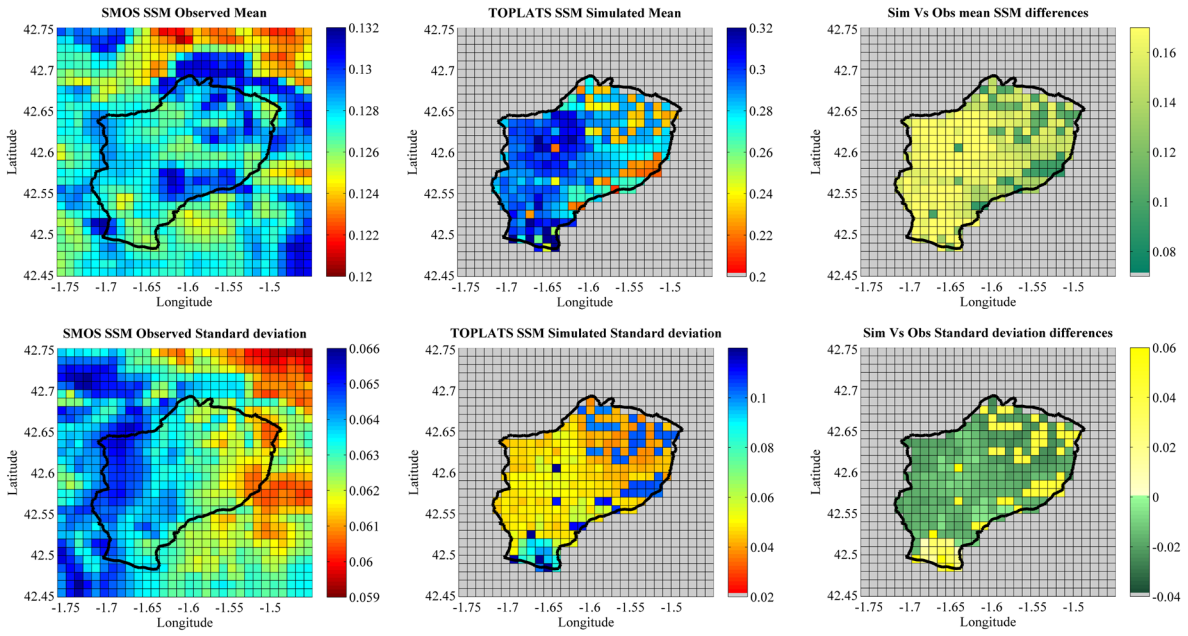

Fig. 4.29. Mean and Standard deviation value of SMOS L4 (left) and TOPLATS simulated SSM (center) for the whole study period (2013-2015) and their difference (right).

It can be clearly observed that different patterns appeared, in terms of mean value, between the simulated and observed SSM. Observation plots show the results within a 30 x 30 matrix of 1-km cells (900 cells), while simulated values are only shown for the cells within the catchment (266 cells). It must also be noted that the SSM observations ranged only between 0.12 and 0.132 (0.012 range) while simulated values ranged between 0.2 and 0.32 cm^3/cm^3 (0.12 range, 10 times larger). SMOS observations appeared to be clearly related to the topography, identifying the north face of the mountainous areas as the most humid ones. That effect is clearly observed in the northern boundary of the catchment (mountain range of Alaitz, as observed in Fig. 3.3). Also, the north face of several valleys within the catchment, in the eastern part, appeared wetter on the SMOS L4 observations. On the other hand, the driest cells, in terms of observed mean values were found outside the limits of the catchment, in the flat and cultivated areas to the north (Elorz river valley). Within the catchment the driest cells were all close to the outlet, in the south-most part of the catchment.

A quite different spatial pattern was obtained in TOPLATS simulations. In this case, the mountainous eastern part appeared the driest, and wetter areas were located in the flatter agricultural areas in the west (Fig 4.29). TOPLATS updates the soil moisture content of the layers depending on the Topographic Index (TI), therefore cells with higher slopes dry out more quickly than valley bottoms and flat areas. On the other hand, these lower slope areas tend to keep the soil moisture content after a rainfall event for longer time in TOPLATS simulations. This effect was especially remarkable in some cells situated close to the outlet of the catchment, with very low slope. There is thus a clear relation between the TI (Fig. 3.6b) and the simulated SSM values, clearly apparent in the drier areas simulated on some steep relief locations of the catchments eastern boundary. Finally, the upper-right plot in Fig. 4.29 shows the difference between simulated and observed mean values, depicting larger differences for the flat cultivated western part of the catchment (differences up to 0.18 cm^3 cm^{-3}) while in the mountainous areas differences were significantly lower (0.07 cm^3 cm^{-3}).

In terms of standard deviation (STD), also quite some different patterns were found between the observation and simulation (Fig. 4.29 lower panel). Although SMOS L4 data identified the western part of the catchment as the area with higher SSM oscillation, a different behavior was obtained from TOPLATS simulation. The latter showed a higher SSM variability on cells located in the mountainous north-eastern part of the catchment. In any case, it must be noted that also some cells with low STD values were found on this area. Variability was also large in some cells close to the outlet. The difference between simulated and observed STD values (Fig. 4.29 lower right) showed a different pattern to the mean difference (Fig. 4.29 upper right). In particular, it was found that only in some few areas (yellow ones) the STD of the simulated time series were higher than the observed ones. In general, the variability during the 2013-2015 period was higher in the observed records than in the simulations (green areas).

4.4.4. Observed SSM re-scaling

SMOS L4 product was re-scaled to fit the TOPLATS simulated time-series. Three different re-scaling methods, of different intensity, described in section 3.3.1 were applied. Those were: 1) Linear regression (LR), 2) Variance matching (VM) and Cumulative Distribution Function matching (CDF). Similarly to previous figure 4.29, in figure 4.30 upper plots indicate mean values and lower plots present standard deviation values. Plots in the left were obtained with LR, plots in the center with VM and plots in the right with CDF. The re-scaling techniques were separately applied to each pixel, so the different methods (LR, VM and CDF) fitted the observed SMOS L4 data of each cell to the simulated SSM values of the same cell.

As explained in section 3.3.1, all the three methods fitted at least the mean value of the simulated time series. This can be corroborated by the three figures on the upper pane (Fig. 4.30), which showed the same mean values after applying the three different re-scaling techniques, also equal to the mean simulated values presented in figure 4.29 (upper central plot). Thus, all the three methods guaranteed that the first moment (mean) was corrected to fit the simulated mean. On the other hand, only VM and CDF matching methods fit the second order moment (standard deviation), as it was observed in the lower plots in figure 4.30. In this case, standard deviation was clearly modified differently with the LR method, when compared to VM and CDF techniques, which performed very similar affection in terms of STD. VM and CDF techniques modified the observed time-series to fit the new data to the STD of the simulated data (shown in figure 4.29, lower central plot). As observed in figure 4.30 data assimilation of LR re-scaled SMOS L4 data will be perform with a lower STD correction.

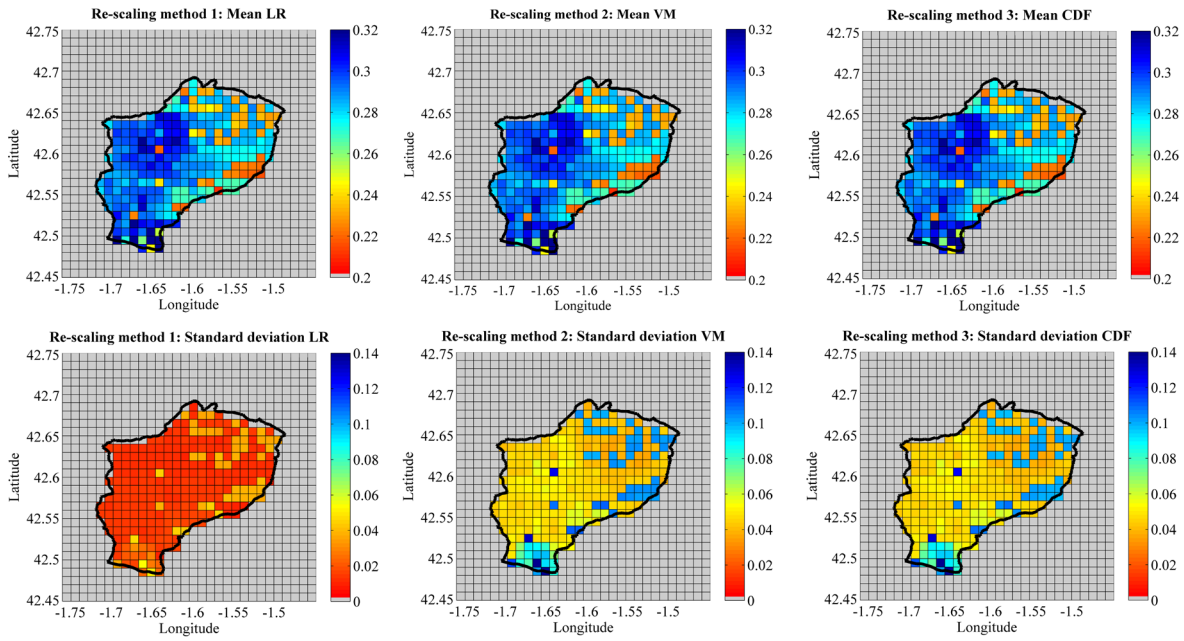

Fig. 4.30. Mean and standard deviation distributed values after LR, VM and CDF re-scaling of the SMOS observed data. Mean values in the upper row and standard deviation in the lower one. From left to right, re-scaling methods as follows: LR, VM and CDF.

4.4.5. Data assimilation

This third study consists of three data assimilation experiments. First, re-scaled SMOS L4 data was assimilated over each of the 266 cells of the catchment. On the second trial, DA assimilation was performed only on cultivated areas (indicated in Figure 3.6c). On the third experiment, DA was performed only on flat areas with a topographic index > 10 (Figure 3.6b). As detailed in section 4.4.1, the model calibrated parameters were obtained from the 2000-2007 period, and the validation and data assimilation period used in this third study were the two years period covering from Oct 2013 to Oct 2015. NSE performance of TOPLATS model without assimilation was 0.68 and Pbias 2% in 2013-2015 validation (Table 4.7).

Table 4.7. Distributed data assimilation results. Validation, data assimilation over the whole catchment, data assimilation results over cultivated areas and data assimilation results over high TI cells.

	VAL	DA – Whole catchment			DA – cultivated land			DA - flat areas		
Re-scaling Method	--	LR	VM	CDF	LR	VM	CDF	LR	VM	CDF
NSE	**0.68**	0.65	0.64	0.65	0.76	0.72	0.72	0.77	0.72	0.72
Pbias	**2%**	-48%	-31%	-31%	-26%	-15%	-15%	-23%	-12%	-12%

Table 4.7 shows the impact, in terms of NSE and Pbias, caused by the three data assimilation experiments performed. Assimilation of SMOS-BEC L4 product into all the cells of the catchment, resulted, despite the re-scaling method applied, in a reduction of NSE. LR, VM and CDF matching offered very similar results in this sense, decreasing NSE from 0.68 to ≈0.65. Assimilation over the whole catchment resulted also on a deterioration of the total simulated streamflow volume, expressed as Pbias, resulting in a large underestimation of volumes (≈30-50%). In this case, LR offered substantially worse Pbias results as compared with the other two methods.

In contrast with this first experiment results, performing EnKF data assimilation only over cultivated areas, or over flat, resulted in a clear improvement in terms of NSE, while Pbias slightly deteriorated but still remained at acceptable values. In both trials (cultivated and flat areas), results obtained with VM and CDF matching methods offered very similar results, being LR the one that provided the higher efficiency increases (from 0.68 to 0.76 and 0.77), but at the expense of generating the largest Pbias error (23 -26%).

As it can be clearly observed in figure 3.6c and 3.6b, cultivated areas corresponded to a great extent with flat areas, which explains why in both experiments results were quite similar. In any case, it has to be pointed out that lowest errors in terms of Pbias were achieved on DA over flat areas (≈3% lower than DA in cultivated areas). A detailed description of the spatial behavior of distributed data assimilation on each experiment is given in the following sections. Also, the effect of DA on soil

moisture content in both surface and transmission zone layers is shown. DA impact on streamflow simulation is also shown graphically.

4.4.5.1. Data assimilation experiment 1: Over the whole catchment

As it can be observed in figure 4.31, data assimilation of SMOS L4 product over the whole catchment resulted in a decrease in terms of mean SSM values on the western part of the catchment, while mean SSM content was increased after DA in most of the cells located in the more mountainous eastern part of Cidacos. This impact pattern seems to be similar regardless the RT employed, but the effect was more intense when LR was used, compared to the other two methods. Variations in the mean simulated value are shown in the upper panel (LR in the left, VM in the center and CDF in the right). Soil moisture variability was differently affected depending on the RT when standard deviation correction after DA was evaluated. As shown in the lower figures, LR caused a larger reduction of SSM standard deviation. This effect spread systematically all over the catchment (low figures, left plot). All the three methods caused a general reduction of the STD all over the catchment, but when VM and CDF were applied, that reductive effect had a smaller impact over the cells in the north-eastern part.

Impact of DA when DA was performed over the whole catchment is shown in Table 4.7. As mentioned above, this experimental set-up caused NSE worsening with all the RTs. As LR also caused a significant worsening of the Pbias values, we discarded this option and results in figure 4.32 are those obtained with CDF re-scaling method (VM results are not shown, as the plots would look like very similar to the CDF ones). Results shown in figure 4.32 illustrate the impact of DA on the soil moisture content of the surface layer (Fig. 32a), on the transmission zone layer (Fig 32b) and on the simulated streamflow (Fig 32c and d). In the soil moisture plots, the red line indicates the soil moisture content of the layers prior to assimilation (validation run), while the blue line presents the SM content, once the data assimilation correction was performed through the EnKF. Correction caused on SM by DA is indicated by the green line. In this example with CDF method, satellite data caused quick

both positive and negative modifications on the SM content of the upper layer, which shows no clear patter during some periods of the studied years. But there are 3 periods were systematic modifications of the SM can be identified: 1) decreasing SM in spring 2014, 2) increasing SM in autumn 2014 and the highest impacted period which was again spring, in 2015, where the largest decrease of SM occurred due to DA. These periods when the assimilation worked constantly in the same direction (increasing or reducing SM), also updated the SM in the Transmission Zone (Fig 32.b).

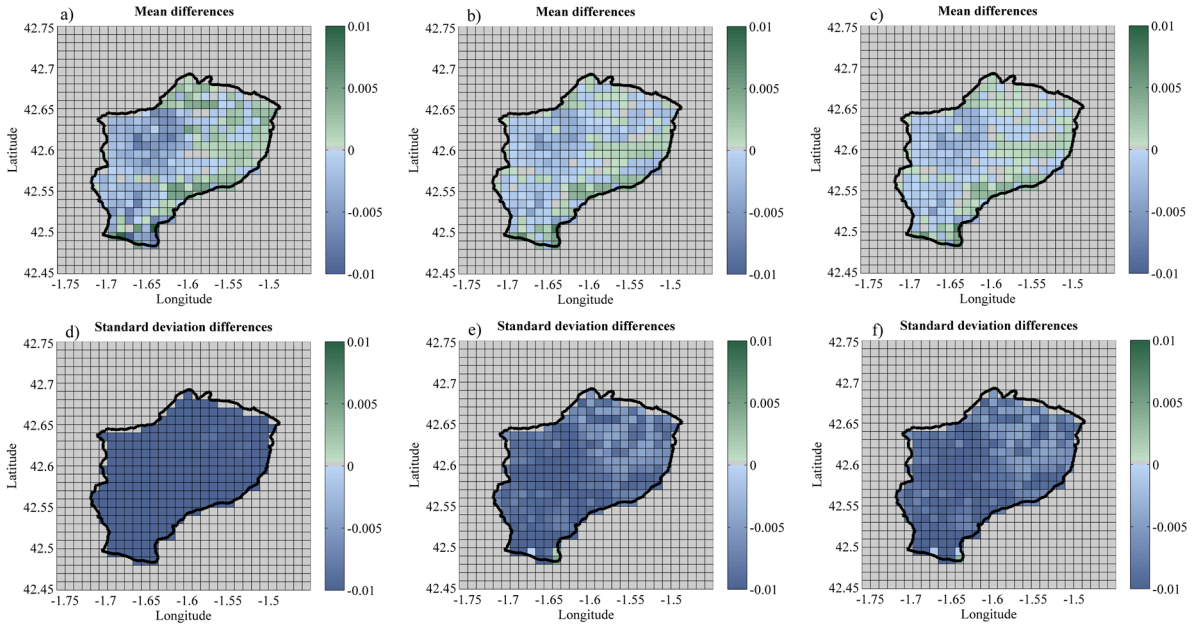

Fig. 4.31. Corrections on the mean (upper row maps) and standard deviation (lower row) SSM after data assimilation over the whole catchment. Plots a) and d) correspond to DA after LR. Plots b) and e) correspond to DA after VM. Plots c) and f) correspond to DA after CDF.

Figure 32.d shows that data assimilation impacted substantially the streamflow generation, which was particularly affected through a reduction of streamflow in February and March, 2015. Reduction in streamflow generation in this period was proportionally much larger than the increases generated in spring 2014 or the decreases in autumn 2014. Despite the magnitude of SM correction were not that different on those three periods, it affected differently the streamflow generation. Assimilation

over all the catchment with CDF re-scaling method resulted on a reduction in NSE (-3%) and on an increase in Pbias error (+29%) (Table 4.7).

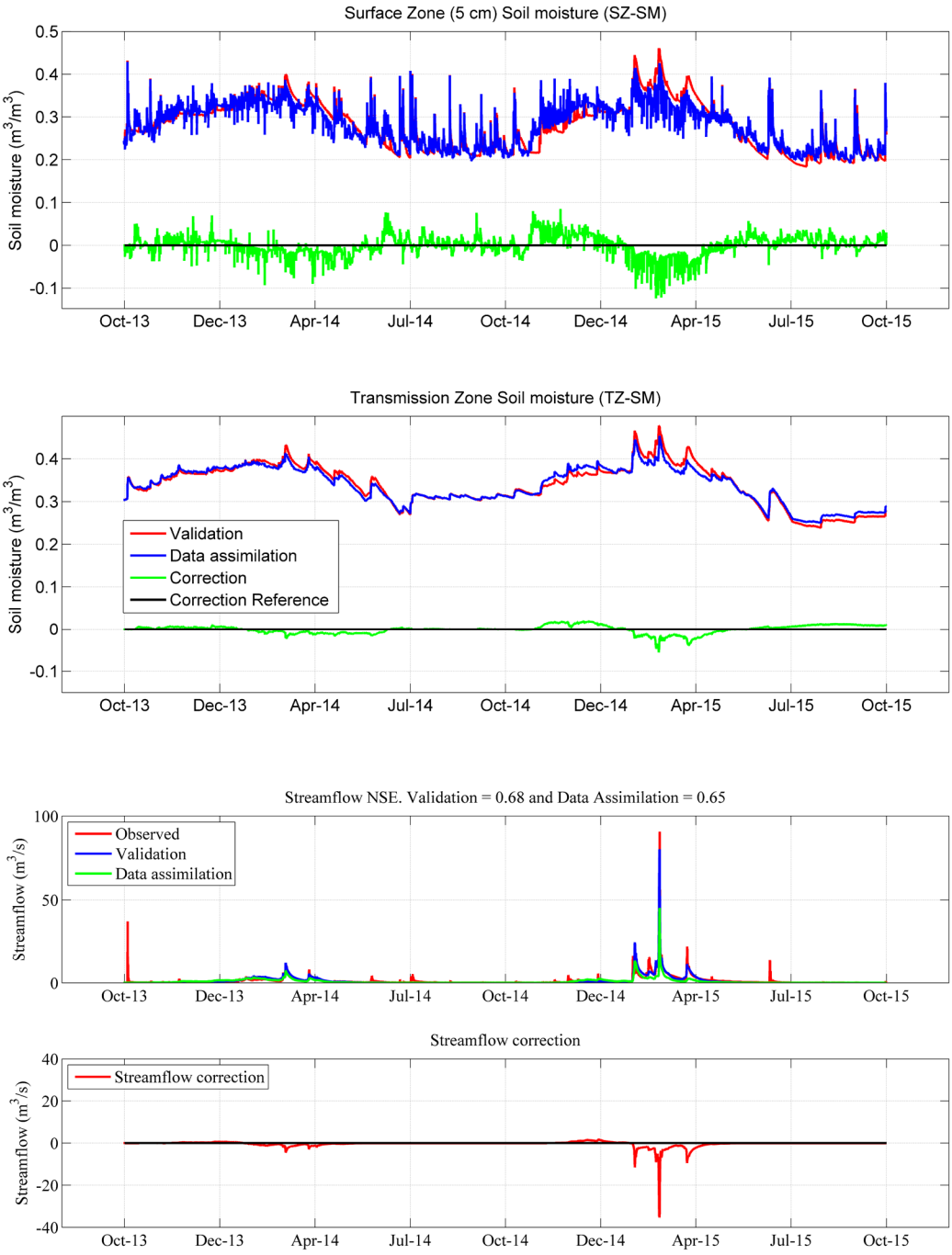

Fig. 4.32. Impact of DA over the whole catchment on catchment average TOPLATS outputs: a) Surface soil moisture content, b) Transmission zone soil moisture content, c) streamflow and d) streamflow correction. These results correspond to CDF re-scaling.

4.4.5.2. Data assimilation experiment 2: Only over agricultural areas

As satellites observing SM are expected to provide lower quality data over forested areas (Escorihuela and Quintana-Seguí, 2016; Grant et al., 2007; Kurum et al., 2012; Rahmoune et al., 2013), we decided to test the impact of DA when performed only over cultivated areas. Specifically, Cidacos catchment is manly covered by rainfed cereals (Fig 3.4), except for the north-eastern part where shrubs and forests exist. Unlike it happened when assimilation was performed in the whole catchment (Fig 4.31), assimilating only over cultivated areas caused the mean SSM value to increase on the cells located in the western part of the catchment (Fig 4.33, upper plots). The particular cells where DA was performed in this test can be clearly identified on the LR STD correction plot (Fig 4.33 lower left plot). While some isolated cells correspond to cultivated areas on the eastern part, most of them concentrated on the western half. The mean value correction effect was similar with all RT, but somehow more intense with LR. In terms of STD correction, LR clearly performed more intensely than the other two methods.

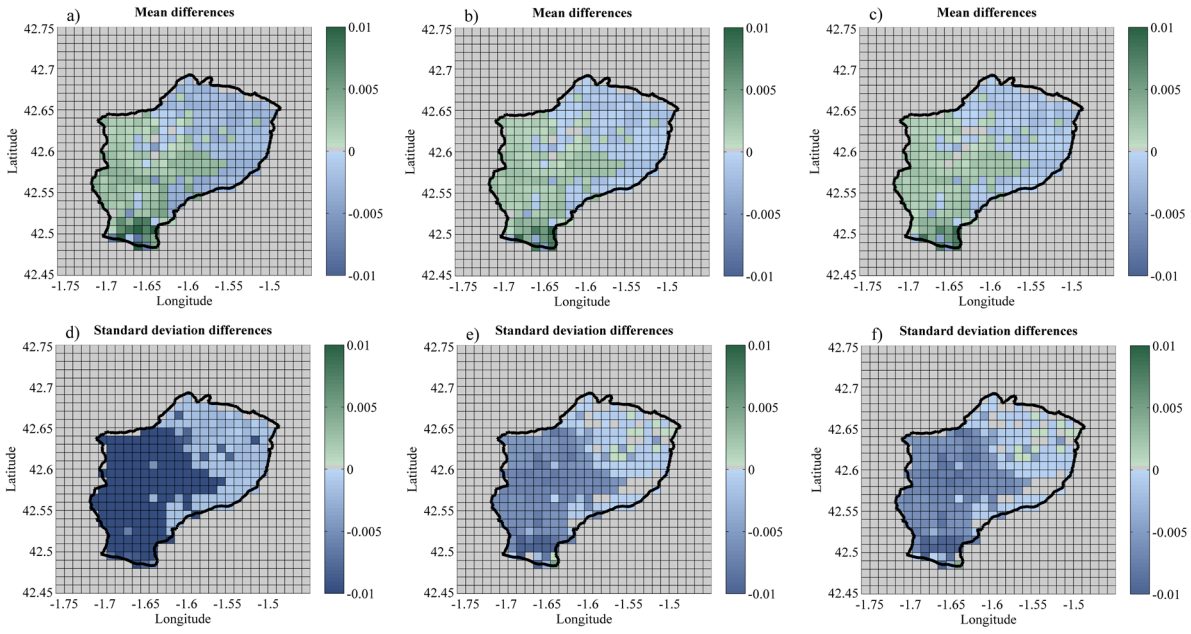

Fig. 4.33. Corrections on the mean (upper row maps) and standard deviation (lower row) after data assimilation only over agricultural cultivated areas. Plots a) and d) correspond to DA after LR. Plots b) and e) correspond to DA after VM. Plots c) and f) correspond to DA after CDF.

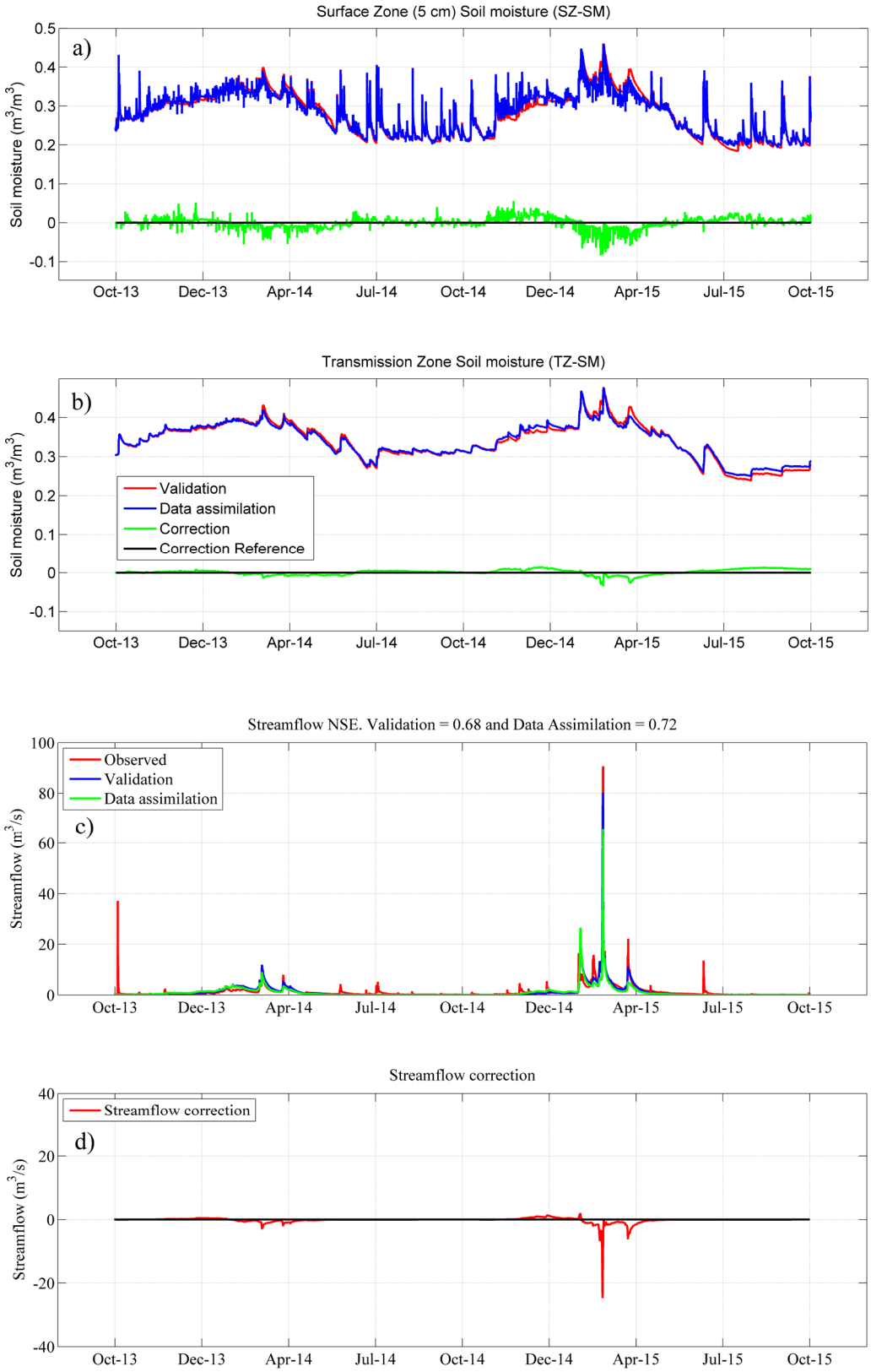

Fig. 4.34. Impact of DA over cultivated areas on catchment average TOPLATS outputs: a) Surface soil moisture content, b) Transmission zone soil moisture content, c) streamflow and d) streamflow correction. These results correspond to CDF re-scaling.

As illustrated in figure 4.34a and 4.34b, the effect of DA over cultivated areas on SM, when CDF method was used, offered similar corrections to the whole catchment assimilation. But in this case, the Pbias did not worsen up to 30% as in the previous trials and remained in a more moderate 15% error. Assimilating SMOS L4 data only over cultivated lands enhanced TOPLATS distributed streamflow prediction 4%, in terms of NSE, when VM and CDF methods were used. Efficiency increased 8% when LR was applied (Table 4.7), but substantial worsening in Pbias was generated in that case (+24%). Assimilating over cultivated areas also caused an important reduction (≈20 m^3/s) on the highest event peak flow (February 2015) of the assimilation period (Fig 4.34d). Despite the peak flow of that large event was reduced due to assimilation, and thus difference to the observed value increased, data assimilation helped improving the simulation in terms of timing, better adjusting the time (simulation was performed with hourly time-step) at which the runoff peak occurred. This resulted on an efficiency rising (Table 4.7).

4.4.5.3. Data assimilation experiment 3: Only over flat areas

This section presents the results obtained by assimilating re-scaled SMOS L4 data only on cells with TI higher than 10 (Fig 3.6b). Similarly to the previous experiment, this one was based on the limitations referred to SMOS observation over complex topographic areas (Pellarin et al., 2015; Utku and Le Vine, 2011). The hypothesis here is that SMOS observations over steep areas are affected by errors, so excluding those areas from the observations might improve the assimilation results. As already shown in Table 4.7, this experiment had a very similar impact on model efficiency to the previous one. LR was again the method offering the largest improvements in terms of NSE (+9%), whereas the other two methods offered a more modest 4% NSE improvement. The main difference between the previous analysis and this one was found in terms of Pbias, as assimilating flat areas only offered lower Pbias values compared to assimilating only agricultural areas. This difference of 3% was observed consistently, regardless of the RTs method applied (Table 4.7). Cells affected by this experiment can be also clearly identified on the STD correction plots of figure 4.35

(lower panels). Similarly to the previous testing, DA increased the mean SSM on the affected cells (western area), and caused a moderate SSM decrease on the other parts of the catchment (Fig 4.35, upper plots). Similarly to the other two tests, the obtained SSM correction was stronger when LR was used, with the other two methods affecting SSM more weakly and in a very similar way. LR caused a decrease in STD all over the catchment, while on the contrary VM and CDF methods caused some minor STD increments on some particular cells on mountainous areas (Fig. 4.35, lower panel, green cells in the eastern part).

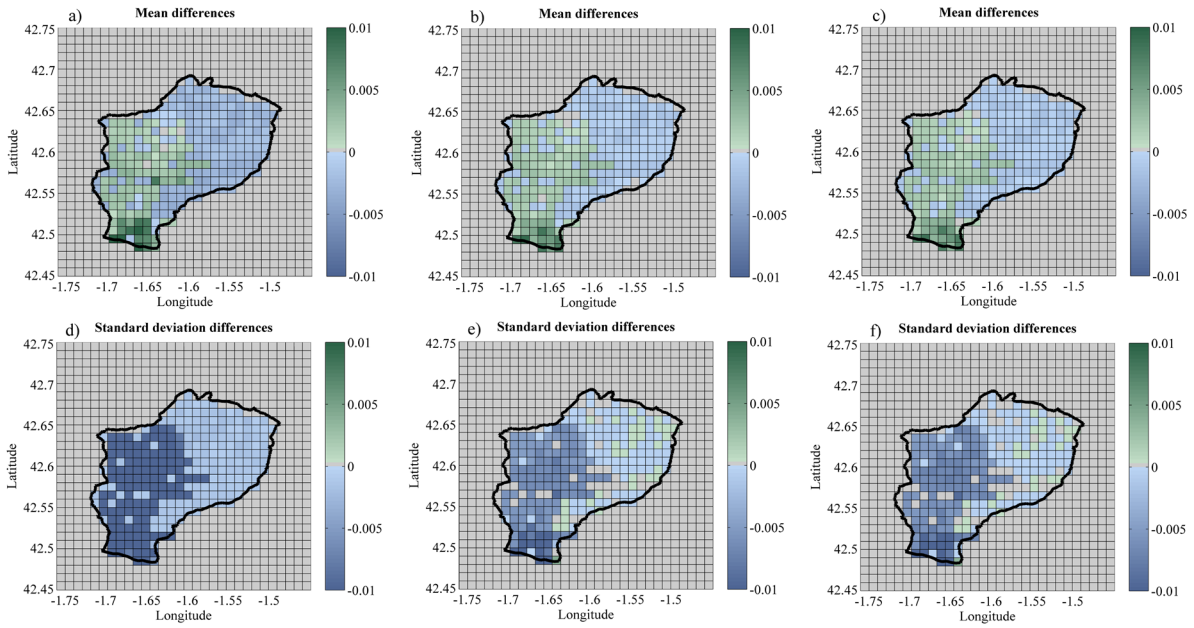

Fig. 4.35. Corrections on the mean SSM (upper panel) and its standard deviation (lower panel) after data assimilation on flat areas. Plots a) and d) correspond to LR re-scaling. Plots b) and e) correspond to VM. Plots c) and f) correspond to CDF.

The effect of DA was here also similar to the test over cultivated areas, but in this case Pbias worsening was slightly lower (Table 4.7). Compared to the 2% Pbias value obtained in the validation run, after this experiment Pbias raised to 12% with both VM and CDF methods, which can still be considered acceptable. Thus, despite LR achieved the highest efficiency improvements with a remarkable 0.77 NSE, this RT should not be recommended when DA is applied for water resources management purposes, as the Pbias obtained by this method was much larger than the rest (23%).

In any case, on DA assimilation studies focused on flood prediction this RT should be explored as has been demonstrated here, it was capable of enhancing high flow simulation up to 9%.

Some differences can be found between impact on streamflow in figures 4.34d and 4.36d. On the latter, the reduction on the peak flow of the largest event of the period, appears to be lower than on the previous experiments, which probably explains to some extent the slightly lower Pbias results (12% compared to 15%) obtained here.

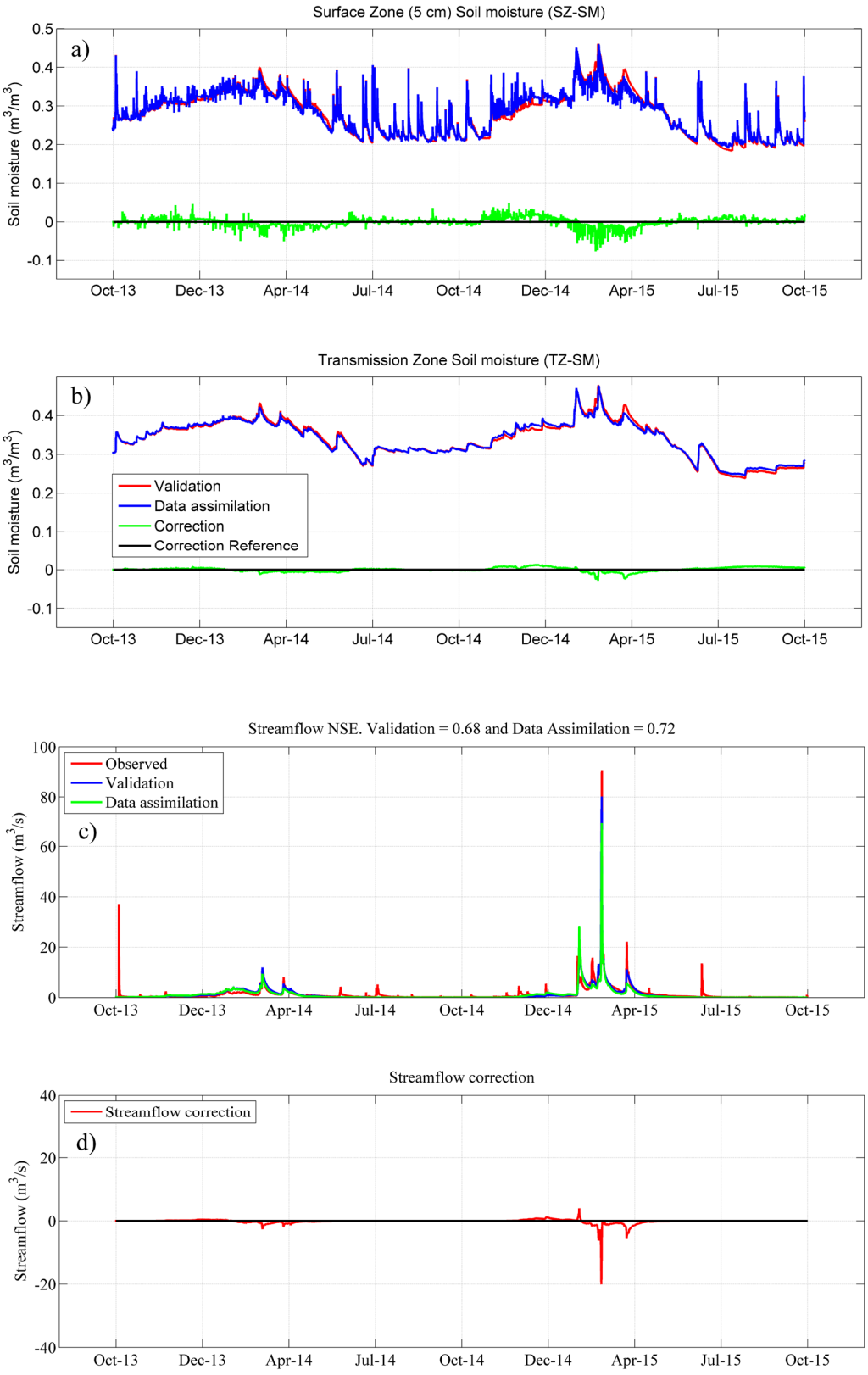

Fig. 4.36. Impact of DA over flat areas on catchment average TOPLATS outputs: a) Surface soil moisture content, b) Transmission zone soil moisture content, c) streamflow and d) streamflow correction. These results correspond to CDF re-scaling.

4.5.6. Discussion

In recent years, different approaches have been followed to propose SSM downscaling or disaggregation methods, which vary with respect to the input ancillary data required (e.g., optical data, topography, soil depth, field capacity), the nature of the scale linking model (physical, semiempirical, empirical), and the underlying physical assumptions (i.e., how SSM is related to the available fine-scale modeled or observational information) (Piles and Sánchez, 2016). In order to account for the input ancillary data, this study considered different experiments, applying assimilation differently depending on land use and topography of the Cidacos catchment.

A wide effort has been put into the development and validation of different down-scaled SMOS products, leading to a number of different techniques. As an example, the Disaggregation based on Physical And Theoretical scale Change (DisPATCh) 1-km resolution product proposed by Merlin et al. (2015) and Molero et al. (2015), which has also been recently improved by (Djamai et al., 2016). Down-scaled products with this resolution can bring SSM-DA to applications requiring higher spatial detail, e.g. the quantification of drought impacts on cultivated areas (Chakrabarti et al., 2014), or improved streamflow prediction (Lievens et al., 2016). Some of these products have already been validated in specific areas, i.e. SMOScat product (Escorihuela et al., 2012). Additionally, other investigations are recently focusing on the development of new down-scaled products based on the synergistic use of C-band SAR and L-band radiometer data (SMAP, SMOS) (Rudiger et al., 2016).

In this study, a first visual comparison of the mean observed and simulated surface soil moisture values, already showed very different spatial patterns. This suggested that assimilation would affect very differently the different areas of the catchment. In both cases, soil moisture seemed to be controlled by topography, but different patterns were found. In the observed time-series, wetter areas were located in the northern faces of the mountainous areas of the catchment, whereas those were mainly found on the flat cultivated areas in the model results.

Some studies, similar to the one presented here, that focused on the improvement of streamflow prediction after SSM assimilation into distributed models have already achieved positive results.

Cenci et al. (2016) assimilated ASCAT data and achieved very positive results in terms of high peak flows simulation on Mediterranean catchments. Moreover, Laiolo et al. (2016) reported an increase of NSE from 0.6 to 0.7 after ASCAT assimilation in northern Italian catchments. They also achieved a Pbias reduction of 10% after data assimilation. That study also assimilated SMOS, but no improvements were achieved in this case, probably due to the few observations available over the catchment (Laiolo et al., 2016).

Despite some studies reported positive impacts on streamflow simulation thanks to SMOS assimilation into distributed models (Lievens et al., 2015; Wanders et al., 2014b), in some others no significant improvements were achieved. For instance, Lievens et al. (2016) reported remarkable improvements in SM simulation due to SMOS DA, but also found that only minor impacts were observed for the streamflow simulation analysis. Similarly, Tian et al. (2017) reported only slight/moderate improvements.

Different aspects have been identified as potential limitations for a successful improvement of streamflow prediction by means of SMOS data assimilation. Those possible limitations include: the selected re-scaling technique (Lievens et al., 2016), the catchment size (Wanders et al., 2014a) or the prevalent type of runoff, especially in arid areas (Alvarez-Garreton et al., 2014). Lievens et al. (2016) attributed the limited effect of DA on streamflow simulation found on their study to the selected RT, which was CDF. They pointed out that this RT method adequately restricts the impact of the assimilation to the correction of random errors in the soil moisture simulations, but the impacts of these random corrections on the simulated streamflow volume may be very limited, particularly when the threshold soil moisture level to start runoff generation is either not reached or sufficiently exceeded. Therefore, the streamflow simulations may generally show a larger sensitivity to precipitation than to antecedent soil moisture conditions (Lievens et al., 2016). Wanders et al. (2014a) proposed the existence of an inverse relation between catchment size and DA impact, and considered that DA influence might be limited for large catchments.

Our study was able to improve NSE by a 9%, obtaining a NSE up to 0.77 (0.68 on the validation run) (Table 4.7). This best-efficiency result was obtained when the SMOS 1-km resolution product

was assimilated only over flat areas. Similarly, an 8% improvement was achieved when assimilation was performed only over cultivated areas. Although our study was able to improve the efficiency of high flows simulation over a period of 2 years, some error was added to the total simulated volume (Pbias in Table 4.7). This contrasts with the results reported in Wanders et al. (2014b) who obtained a reduction of 10% in terms of Mean Absolute Error (MAE) of total simulated discharge, and attributed this to SSM-DA. In that study, Wanders et al. (2014b) concluded that SSM-DA improved the quality of the flood alerts, both in terms of timing and in the exact height of the flood peak, which is something that we also partially observed in our study, as data simulation was capable of improving the timing-prediction of the highest event of the simulation period (see figure 4.36, in section 4.4.5.3). As a finding from our study, we observed that despite worsening the simulated peak flow, data assimilation can improve the timing of an event, increasing the simulation efficiency.

Lievens et al. (2015) obtained improvements in both SM (compared to observed values) and streamflow simulation, showing that improvements in antecedent SM conditions (due to SMOS assimilation) can propagate to improvements in streamflow prediction. This study (Lievens et al., 2015), similarly to ours, evaluated three RT, i.e., fitting first, first and second, and all order moments. They found out that the better performance was offered by a first moment fitting method (named DA-MEAN in their study, LR in our study) for improved streamflow simulation. They discussed that this finding might be explained by the fact that rescaling second and higher order moments reduced the variability and extremes of the soil moisture retrievals, and consequently confined runoff peaks. This study reported a 4% efficiency improvement with a LR method, and 2% efficiency improvements with VM and CDF methods for a two years period. Our results improved NSE by 8-9% with LR, and 4% with the other two re-scaling methods (VM and CDF). Lievens et al. (2015) also found that efficiency enhancements were mainly achieved during the 10 % of highest peak flows. Results in Lievens et al. (2015) are thus in line with our results in terms of RT efficiency, with first-moment fitting method as the one providing highest efficiency improvements.

To our knowledge, few assimilation studies have been performed with 1-km resolution downscaled SMOS products. Ridler et al. (2014) performed SM-DA over a 1,000 km^2 catchment in Denmark and used a land cover classification for SMOS disaggregation to correct observation bias. They were able to improve peak flows simulation with a coupling approach of a hydrological model and a SVAT model. Despite peak flows were better simulated after DA, some over-correction was found as well. Lievens et al. (2016) compared the performance of different SMOS-derived products of different spatial resolution, including the DisPATCh 1-km product. The assimilation of this down-scaled product did not provide any efficiency increase on streamflow simulation, probably not attributable to the quality of the product, but to the sparser observations available during cloudy conditions (Lievens et al., 2016). They also concluded that there was no clear spatial clustering of the results, indicating that assimilation impacts were not clearly related to regional conditions, such as land cover or basin characteristics (Lievens et al., 2016).

Regarding the different experiments performed in our study, obtaining better results when assimilating SMOS data over flat areas, there is some agreement with Wanders et al., (2014a) who found out that assimilation of SMOS data provided its best results on SM estimation when observation of flat areas was applied (Wanders et al., 2014a).

CHAPTER 5. CONCLUSIONS

5.1. Conclusions on the Sensitivity analysis of TOPLATS model

The evaluation of TOPLATS performed in this research provides model users with useful guidelines to: 1) identify the model parameters having the largest influence on main hydrological processes and on streamflow simulation efficiency; 2) perform an efficient calibration of the model through an automatic calibration algorithm applied with a multi-start approach; 3) gain insight on the performance, advantages and limitations of the model when applied at daily and hourly time-scales and 4) be aware of the importance of climatological variability to be contained on the calibration period in Mediterranean catchments.

Sensitivity analyses performed with Morris and Sobol methods yielded very similar results and concluded that 3 parameters: Brooks-Corey Pore Size distribution Index (B), Bubbling pressure (ψ_c) and Hydraulic conductivity decay (f) had the overall largest influence on the hydrological processes (surface runoff, baseflow, evapotranspiration and surface zone soil moisture dynamics) and streamflow simulation efficiency. Thus, their inclusion in any TOPLATS calibration is recommended. Morris method gave similar results to Sobol, with lower computational requirements, which makes it a reliable and suitable method to be applied on complex and largely parameterized physically based models similar to TOPLATS.

Regardless of catchment size or climate influence, mean surface soil moisture was found to be controlled by B, and its dynamics by f. Streamflow generation on wet catchments (Arga and La Tejeria) seemed to be mainly influenced by ψ_c, whereas the drier catchment (Cidacos) was largely affected by B.

5.2. Conclusions on TOPLATS model calibration

Model calibration achieved a substantial efficiency improvement in the three evaluated catchments, and reduced Pbias to values below 10% (in most cases below 5%). Calibration improved both average flows simulation accuracy and high peaks simulation results, in both calibration and validation periods.

Climatic variations between calibration and validation periods compromise model performance and parameter stability, particularly in arid zones. A random and discontinuous period selection strategy was applied in this study to overcome this issue, which outperformed model calibration with the conventional calibration and validation period selection strategy. This random approach is thus recommended when large climate variability is found between calibration and validation periods, and particularly when run on daily basis.

In terms of streamflow simulation efficiency, when TOPLATS was run in hourly and daily basis, catchment size had an influence on the results. Mean NSE of calibration and validation periods on the experimental micro-catchment studied (La Tejeria) was higher in hourly basis (NSE 0.77) than in daily basis (NSE 0.60). The opposite occurred on the largest catchment (Arga) where hourly efficiency (0.65) outperformed daily results (NSE 0.62). On the intermediate size catchment (Cidacos), efficiency results were very similar (NSE 0.58 and 0.59). Surface soil moisture behavior (characterized by rapid variations) seemed not to be properly simulated at longer time scales, affecting model behavior.

Monthly efficiency results showed that TOPLATS performed optimally in the two smallest catchments, but some systematic deviation was found on the largest, uncovering a clear overestimation pattern during winter and underestimation in autumn and spring. This seasonal deviations could be compensated by implementing data assimilation techniques and using observed streamflow, remote sensing or in-situ soil moisture data, to update model variables (i.e. soil moisture, water balances) in order to correct that systematic deviated pattern).

5.3. Conclusions on Data assimilation with statistical and semi-distributed models and ASCAT SSM data

This study has demonstrated that ASCAT SSM assimilation into models with different conceptualization approaches can improve hourly streamflow simulation in medium-size catchments located in Mediterranean climate areas when an adequate DA configuration, in terms of SSM observation re-scaling and observation error, is set-up. The main findings are summarized in the following paragraphs.

After model calibration, streamflow forecasts for the Mediterranean catchments investigated were more accurate using a conceptual and less parameterized model (i.e., MISDc) than with a physically based complex model (TOPLATS). In any case, both models offered overall NSE $>$ 0.65 for the 11 years studied period.

ASCAT data assimilation increased the NSE in three out of the four catchment/hydrological model combinations evaluated. For the remaining case, DA could not increase model performance due to the already high NSE efficiency obtained through an extremely accurate calibration.

The open-loop ensemble streamflow simulation (Q_{OL}) outperformed the deterministic simple model validation (VAL) run. This indicates that improvements in streamflow simulation efficiencies could be achieved by considering forcing and parameter uncertainties in modelization.

The re-scaling technique used strongly conditioned the results obtained in one of the catchments (Nestore), but showed a much more limited impact on the other one (Arga). This effect was similar with both models. In general, linear re-scaling (LR) offered better results than variance matching (VM) and cumulative distribution function matching (CDF).

The ASCAT surface soil moisture observation error largely influenced the assimilation results obtained. The best DA performance was achieved when low observation error values (4-6 %, or even $<$1 %) were considered.

The magnitude of the DA impact seemed to be closely related to the specific catchment conditions rather than to a specific model characteristic (i.e. conceptualization and parameterization complexity or soil layer configuration). In addition, the success achieved in model calibration for a specific catchment had a great influence on the ability of DA to improve its predictions.

EnKF based SSM-DA provided efficiency increases that reached 45 %, but the variation obtained depended largely on the catchment, model and DA set-up combination.

5.4. Conclusions on data assimilation with a fully distributed model and a SMOS/MODIS 1-km resolution SSM product

The TOPLATS model in distributed mode, provided a very valuable result in both efficiency (NSE = 0.68) and total simulated volume (Pbias = 2%) after validation. TOPLATS was thus validated as useful tool to simulate streamflow in Mediterranean catchments of medium size.

This study tested the assimilation of a SMOS downscaled product only over cultivated or flat areas, and it was found out that these experiments outperformed the results obtained on the experiment when assimilation was performed over all the catchment. This suggests that SMOS downscaled observations over forested areas or observations of steep relief areas might not be as accurate as the observation of flat cultivated areas. Thus, results from this study recommend the assimilation of observations over flat and cultivated areas to achieve improved streamflow simulations. Assimilation over the whole catchment resulted in a slight deterioration of the efficiency, and in a large underestimation of total simulated streamflow. The other two experiments, assimilation only over cultivated or flat areas offered increments on the efficiency, up to 9% and NSE = 0.77 in some cases. Underestimation was found in these cases as well, but more limited (12%).

There is still the need for further research, to fully understand the modeling processes that generated those large errors in terms of total simulated volumes, especially when it is taken into account that all the three re-scaling methods applied guarantee that the integrated data has the

same mean value of the simulated time-series. This effect might be related to the uncertainty of the model varying with time. Models uncertainty was larger during winter, which might be a period when the observations were below simulated values, thus reducing a significant portion of the water in the soil, and hence causing the commented error. Different transmission rates between the two soil layers (upwards and downwards) also seem to influence this balance.

The downscaled product used in this study seems to be a very valuable information source to improve streamflow prediction in dry catchments, and it allows to easily exclude assimilation of areas where dense vegetation or high slopes may limit satellite observation accuracy.

Linear Re-scaling method offered the best results in terms of improving efficiency, but at the expense of large volume errors. Variance Matching and Cumulative Distribution Function offered very similar results. Both were able to provide efficiency increments, while maintaining lower errors in terms of total simulated volumes.

It was observed that distributed assimilation of SSM only over certain areas of the catchment, also affected the remaining zones, due to the soil moisture content redistribution performed by the TOPLATS model. When the assimilation was performed over the whole catchment or over specific areas, the model reacted differently in terms of the spatial redistribution of moisture across the catchment. In TOPLATS, this redistribution of SM content is done based on catchment's mean water table depth and on each cell's specific Topographic Index (TI). This type of singular effects needs to be taken into account when data assimilation is performed with different models, as each model has its specificities that can influence assimilation performance.

Data assimilation of SSM observations was able to improve simulation efficiency, and it was found that simulation improved not only in terms of magnitude, but also in terms of better simulation timing of some of the highest events.

Results in this study, clearly showed that correcting SSM of the upper 5 cm layer, through data assimilation of remotely sensed observations, also has a significant impact on the deeper transmission layer. Furthermore, it was observed that similar corrections of soil moisture content, in terms of magnitude, have very different impacts in terms of streamflow correction. This seemed to be

related to the continuity of the type of correction, specifically on its direction, whether it is upwards or downwards. When the assimilation modifies the simulated value, over a large period of time in the same direction, it finally turns out in larger streamflow modifications. In any case, some type of discontinuities seem to affect streamflow correction magnitude, and need to be further investigated.

5.5. General conclusions

This study showed that applying widely validated Sensitivity Analysis techniques can substantially reduce the calibration effort to be done on complex models such as TOPLATS, and that they can provide relevant information on the parameters principally responsible of controlling the simulated hydrological processes. Moreover, nowadays, optimization algorithms can be very useful tools to perform efficient hydrological model calibration. These two tools are especially convenient in largely parameterized models, and when models are applied in complex catchments, such as the ones located in Mediterranean climate areas that are affected by large inter-event and inter-annual rainfall variability.

In this thesis, two widely applied sensitivity methods, Morris and Sobol were used to analyze TOPLATS model. It was found, that Morris, despite having a much lower computational cost, was able to identify correctly most of the sensitive parameters to the main hydrological processes and the goodness of fit measures evaluated. It was also capable of identifying non-influential parameters. Thus, it can be considered a very valuable option to develop sensitivity analysis of a large number of parameters, or in models with high computational requirements.

This thesis evaluated the performance of TOPLATS as a suitable model to simulate streamflow in Mediterranean catchments, at both hourly and daily time-step. It was found that the model can provide optimal results, both in terms of high flows simulation, and in terms of total simulated volumes. But, it must be noted that significant efforts have to be done to achieve these positive results.

These efforts must include the application of a thorough calibration strategy capable of avoiding local minima issues, as the one proposed in this work.

In order to identify stable calibrated parameter values, this study found out that it is important to select calibration periods that contain enough weather variability, especially in terms of containing enough wet periods. More stable parameter values will be obtained when there is an equilibrium of weather states in the calibration and validation periods. For that, when the available calibration periods do not contain enough weather variability, or when only short time-series are only available for calibration, a random selection of data is recommended for calibration. This random selection should be conditionally performed, so that enough wet periods are included. This will help finding parameter values that will also offer optimal results on validation periods.

The assimilation of ASCAT data into models of different complexity in terms of spatial representation and level of parameterization, was able to provide in most cases, an improvement on the streamflow simulation accuracy, but the adequate combination of re-scaling technique and observation error estimation needs to be found. Thus, there is no simple and general rule to follow that could be made extensive to any combination of catchments and models. Altogether, this study provides significant information on the observation error range that may provide the best assimilation results in similar catchments. Moreover, this study also provides information regarding the performance of the different re-scaling techniques. Additionally, in very well calibrated models, it can be found that further improvements are no longer possible to achieve, as the model already represents accurately most of the hydrological processes. It was also found that assimilation performance may be related to specific catchments characteristics, mainly rainfall regime, size and topography.

This PhD thesis also found out that there is a potential to improve fully-distributed hydrological models with down-scaled surface soil moisture remotely sensed products, such as the L4 product based on SMOS and MODIS, and produced at the Barcelona Expert Center. Three different re-scaling techniques were tested to fit observed SSM values to simulated SSM. These techniques provided different results that impacted peak flow and total volume simulation in different ways. It

was found that the assimilation of this product, through the Ensemble Kalman Filter over a catchment, produced a slight reduction of the efficiency, and even worst, generated large errors in the simulated volume. Nevertheless, this analysis also found that those errors might come from specific areas of the catchment. Specifically, densely vegetated areas and areas with rough topography were the ones where satellite observation may perform worst. When these areas were exclude, significant efficiency improvements were achieved through data assimilation. This finding suggests that new research efforts are needed within the distributed modeling and data assimilation community on removing or filtering out areas where large observation errors might turn out into streamflow simulation worsening.

The overall view of this PhD thesis shows that TOPLATS can be used to simulate streamflow in complex catchments, such as Mediterranean ones. For that, proper analysis of the sensitivity to different parameters is required. Once the most sensitive parameters are identified, optimization algorithms can reduce substantially the efforts to calibrate the model, and are helpful to obtain stable parameter values that also offer optimal simulations during validation periods. Selecting calibration periods with enough weather variability will assure obtaining such stable values. Furthermore, this study tested different combinations of satellite estimated error value (of ASCAT) and re-scaling methods to improve a lumped and a semi-distributed catchment model streamflow simulation. Improvements on streamflow simulation were achieved for most of the model/catchment combinations. Lastly, this work also improved the streamflow simulation of a distributed model through the assimilation a downscaled SSM product, derived from SMOS and MODIS satellites. While this improvement was not achieved on a first attempt, assimilating SSM data over the whole catchment, assimilating SSM only over cultivated or flat areas resulted in substantial efficiency improvements.

REFERENCES

Abaza, M., Anctil, F., Fortin, V., Turcotte, R., 2015. Exploration of sequential streamflow assimilation in snow dominated watersheds. Adv. Water Resour. 86, 414–424. doi:10.1016/j.advwatres.2015.10.008

Albergel, C., de Rosnay, P., Gruhier, C., Muñoz-Sabater, J., Hasenauer, S., Isaksen, L., Kerr, Y., Wagner, W., 2012. Evaluation of remotely sensed and modelled soil moisture products using global ground-based in situ observations. Remote Sens. Environ. 118, 215–226. doi:10.1016/j.rse.2011.11.017

Albergel, C., Rüdiger, C., Carrer, D., Calvet, J.C., Fritz, N., Naeimi, V., Bartalis, Z., Hasenauer, S., 2009. An evaluation of ASCAT surface soil moisture products with in-situ observations in Southwestern France. Hydrol. Earth Syst. Sci. 13, 115–124.

Albergel, C., Rüdiger, C., Pellarin, T., Calvet, J.C., Fritz, N., Froissard, F., Suquia, D., Petitpa, A., Piguet, B., Martin, E., 2008. From near-surface to root-zone soil moisture using an exponential filter: An assessment of the method based on in-situ observations and model simulations. Hydrol. Earth Syst. Sci. 12, 1323–1337.

Alvarez-Garreton, C., Ryu, D., Western, A.W., 2013. Impact of observation error structure on satellite soil moisture assimilation into a rainfall-runoff model. 20th Int. Congr. Model. Simul.

Alvarez-Garreton, C., Ryu, D., Western, A.W., Crow, W.T., Robertson, D.E., 2014. The impacts of assimilating satellite soil moisture into a rainfall-runoff model in a semi-arid catchment. J. Hydrol.

Alvarez-Garreton, C., Ryu, D., Western, A.W., Su, C.-H., Crow, W.T., Robertson, D.E., Leahy, C., 2015. Improving operational flood ensemble prediction by the assimilation of satellite soil moisture: comparison between lumped and semi-distributed schemes. Hydrol. Earth Syst. Sci. 19, 1659–1676. doi:10.5194/hess-19-1659-2015

Alvarez-Mozos, J., Casali, J., Gonzalez-Audicana, M., Verhoest, N.E.C., 2006. Assessment of the operational applicability of RADARSAT-1 data for surface soil moisture estimation. IEEE Trans. Geosci. Remote Sens. 44, 913–924. doi:10.1109/TGRS.2005.862248

Anctil, F., Perrin, C., Andréassian, V., 2004. Impact of the length of observed records on the performance of ANN and of conceptual parsimonious rainfall-runoff forecasting models. Environ. Model. Softw. 19, 357–368.

Array Systems Computing Inc, 2014. Algorithm Theoretical Basis Document (ATBD) for the SMOS Level 2 Soil Moisture Processor Development Continuation Project.

Attema, E.P.W., Ulaby, F.T., 1978. Vegetation modeled as a water cloud. Radio Sci. 13. doi:10.1029/RS013i002p00357

Aubert, D., Loumagne, C., Oudin, L., 2003. Sequential assimilation of soil moisture and streamflow data in a conceptual rainfall - Runoff model. J. Hydrol. 280, 145–161.

Bach, H., Mauser, W., 2003. Methods and examples for remote sensing data assimilation in land surface process modeling. IEEE Trans. Geosci. Remote Sens. 41, 1629–1637. doi:10.1109/TGRS.2003.813270

Balenzano, A., Mattia, F., Satalino, G., Davidson, M.W.J., 2011. Dense Temporal Series of C- and L-band SAR Data for Soil Moisture Retrieval Over Agricultural Crops. IEEE J. Sel. Top. Appl. Earth Obs. Remote Sens. 4. doi:10.1109/JSTARS.2010.2052916

Baroni, G., Tarantola, S., 2014. A General Probabilistic Framework for uncertainty and global sensitivity analysis of deterministic models: A hydrological case study. Environ. Model. Softw. 51, 26–34.

Bartalis, Z., Wagner, W., Naeimi, V., Hasenauer, S., Scipal, K., Bonekamp, H., Figa, J., Anderson, C., 2007. Initial soil moisture retrievals from the METOP-A Advanced Scatterometer (ASCAT). Geophys. Res. Lett. 34.

Berg, A.A., Mulroy, K.A., 2006. Streamflow predictability in the Saskatchewan/Nelson River basin given macroscale estimates of the initial soil moisture status. Hydrol. Sci. J. 51. doi:10.1623/hysj.51.4.642

Beven, K., 2006. A manifesto for the equifinality thesis. J. Hydrol. 320. doi:10.1016/j.jhydrol.2005.07.007

Beven, K., 1989. Changing ideas in hydrology - The case of physically-based models. J. Hydrol. 105, 157–172.

Beven, K., Binley, A., 1992. The future of distributed models: Model calibration and uncertainty prediction. Hydrol. Process. 6. doi:10.1002/hyp.3360060305

Beven, K.J., Kirkby, M.J., 1979. Physically based, variable contributing area model of basin hydrology. Hydrol Sci Bull Sci Hydrol 24, 43–69.

Bhimala, K.R., Goswami, P., 2015. A Comparison of ASCAT Soil Moisture Data With In Situ Observations Over the Indian Region: A Multiscale Analysis. IEEE Trans. Geosci. Remote Sens. 53. doi:10.1109/TGRS.2015.2422377

Blankenship, C.B., Case, J.L., Zavodsky, B.T., Crosson, W.L., 2016. Assimilation of SMOS Retrievals in the Land Information System. IEEE Trans. Geosci. Remote Sens. 54. doi:10.1109/TGRS.2016.2579604

Bogena, H.R., Huisman, J.A., Schilling, B., Weuthen, A., Vereecken, H., 2017. Effective calibration of low-cost soil water content sensors. Sensors (Switzerland) 17. doi:10.3390/s17010208

Borken, W., Matzner, E., 2009. Reappraisal of drying and wetting effects on C and N mineralization and fluxes in soils. Glob. Chang. Biol. 15. doi:10.1111/j.1365-2486.2008.01681.x

Bormann, H., 2006a. Effects of grid size and aggregation on regional scale landuse scenario calculations using SVAT schemes. Adv. Geosci. 9, 45–52.

Bormann, H., 2006b. Impact of spatial data resolution on simulated catchment water balances and model performance of the multi-scale TOPLATS model. Hydrol. Earth Syst. Sci. 10, 165–179.

Bormann, H., Breuer, L., Gräff, T., Huisman, J.A., 2007. Analysing the effects of soil properties changes associated with land use changes on the simulated water balance: A comparison of three hydrological catchment models for scenario analysis. Ecol. Modell. 209, 29–40.

Brath, A., Montanari, A., Toth, E., 2004. Analysis of the effects of different scenarios of historical data availability on the calibration of a spatially-distributed hydrological model. J. Hydrol. 291, 232–253. doi:http://dx.doi.org/10.1016/j.jhydrol.2003.12.044

Breuer, L., Bormann, H., Bronstert, a, Frede, H., Hubrechts, L., Huisman, J. a, Jakeman, a J., Kite, G.W., Lanini, J., Leavesley, G., Lettenmaier, D.P., Seibert, J., Sivapalan, M., Willems, P., 2005. Ensemble modelling of the hydrological impacts of land use change, in: MODSIM05 -International Congress on Modelling and Simulation (2005□: Melbourne, Vic.). pp. 2967–2973.

Brocca, L., Ciabatta, L., Massari, C., Camici, S., Tarpanelli, A., 2017. Soil moisture for hydrological applications: Open questions and new opportunities. Water (Switzerland) 9. doi:10.3390/w9020140

Brocca, L., Liersch, S., Melone, F., Moramarco, T., Volk, M., 2013. Application of a model-based rainfall-runoff database as efficient tool for flood risk management. Hydrol. Earth Syst. Sci. 17, 3159–3169.

Brocca, L., Melone, F., Moramarco, T., 2011a. Distributed rainfall-runoff modelling for flood frequency estimation and flood forecasting. Hydrol. Process. 25, 2801–2813.

Brocca, L., Melone, F., Moramarco, T., 2008. On the estimation of antecedent wetness conditions in rainfall–runoff modelling. Hydrol. Process. 22, 629–642. doi:10.1002/hyp.6629

Brocca, L., Melone, F., Moramarco, T., Morbidelli, R., 2009a. Soil moisture temporal stability over experimental areas in Central Italy. Geoderma 148, 364–374. doi:10.1016/j.geoderma.2008.11.004

Brocca, L., Melone, F., Moramarco, T., Morbidelli, R., 2009a. Antecedent wetness conditions based on ERS scatterometer data. J. Hydrol. 364, 73–87.

Brocca, L., Melone, F., Moramarco, T., Penna, D., Borga, M., Matgen, P., Heitz, S., 2011b. Investigation of the hydrologic response of three experimental basins across Europe. Bodenkultur 62, 31–37.

Brocca, L., Melone, F., Moramarco, T., Singh, V.P., 2009b. Assimilation of observed soil moisture data in storm rainfall-runoff modeling. J. Hydrol. Eng. 14, 153–165.

Brocca, L., Melone, F., Moramarco, T., Wagner, W., Hasenauer, S., 2010a. ASCAT soil wetness index validation through in situ and modeled soil moisture data in central Italy. Remote Sens. Environ. 114, 2745–2755. doi:10.1016/j.rse.2010.06.009

Brocca, L., Melone, F., Moramarco, T., Wagner, W., Naeimi, V., Bartalis, Z., Hasenauer, S., 2010b. Improving

runoff prediction through the assimilation of the ASCAT soil moisture product. Hydrol. Earth Syst. Sci. 14, 1881–1893.

Brocca, L., Moramarco, T., Melone, F., Wagner, W., Hasenauer, S., Hahn, S., 2012. Assimilation of surface- and root-zone ASCAT soil moisture products into rainfall-runoff modeling. IEEE Trans. Geosci. Remote Sens. 50, 2542–2555.

Brooks, R.H., Corey, A.T., 1964. Hydraulic properties of porous media and their relation to drainage design. Trans. ASABE 7, 26–0028.

Burnash, R.J.C., Ferral, R.L., McGuire, R.A., 1973. A generalized streamflow simulation system – Conceptual modelling for digital computers.

Camici, S., Tarpanelli, A., Brocca, L., Melone, F., Moramarco, T., 2011. Design soil moisture estimation by comparing continuous and storm-based rainfall-runoff modeling. Water Resour. Res. 47, W05527. doi:10.1029/2010WR009298

Campolongo, F., Saltelli, A., 1997. Sensitivity analysis of an environmental model: An application of different analysis methods. Reliab. Eng. Syst. Saf. 57, 49–69.

Campolongo, F., Saltelli, A., Cariboni, J., 2011. From screening to quantitative sensitivity analysis. A unified approach. Comput. Phys. Commun. 182, 978–988.

Carlson, T., 2007. An overview of the "triangle method" for estimating surface evapotranspiration and soil moisture from satellite imagery. Sensors 7.

Casalí, J., Gastesi, R., Álvarez-Mozos, J., De Santisteban, L.M., Lersundi, J.D.V. de, Giménez, R., Larrañaga, A., Goñi, M., Agirre, U., Campo, M.A., López, J.J., Donézar, M., 2008. Runoff, erosion, and water quality of agricultural watersheds in central Navarre (Spain). Agric. Water Manag. 95, 1111–1128. doi:10.1016/j.agwat.2008.06.013

Cassardo, C., Balsamo, G.P., Cacciamani, C., Cesari, D., Paccagnella, T., Pelosini, R., 2002. Impact of soil surface moisture initialization on rainfall in a limited area model: A case study of the 1995 South Ticino flash flood. Hydrol. Process. 16. doi:10.1002/hyp.1063

Cenci, L., Laiolo, P., Gabellani, S., Campo, L., Silvestro, F., Delogu, F., Boni, G., Rudari, R., 2016. Assimilation of H-SAF Soil Moisture Products for Flash Flood Early Warning Systems . Case Study: Mediterranean Catchments. Accept. Publ. IEEE J. Sel. Top. Appl. Earth Obs. Remote Sens. July 2016. doi:10.1109/JSTARS.2016.2598475

Chakrabarti, S., Bongiovanni, T., Judge, J., Zotarelli, L., Bayer, C., 2014. Assimilation of SMOS soil moisture for quantifying drought impacts on crop yield in agricultural regions. IEEE J. Sel. Top. Appl. Earth Obs. Remote Sens. 7. doi:10.1109/JSTARS.2014.2315999

Chaney, N.W., Roundy, J.K., Herrera-Estrada, J.E., Wood, E.F., 2015. High-resolution modeling of the spatial heterogeneity of soil moisture: Applications in network design. Water Resour. Res. doi:10.1002/2013WR014964

Chen, F., Crow, W.T., Ryu, D., 2014. Dual Forcing and State Correction via Soil Moisture Assimilation for Improved Rainfall–Runoff Modeling. J. Hydrometeorol. 15, 1832–1848. doi:10.1175/JHM-D-14-0002.1

Chen, F., Crow, W.T., Starks, P.J., Moriasi, D.N., 2011. Improving hydrologic predictions of a catchment model via assimilation of surface soil moisture. Adv. Water Resour. 34, 526–536.

Chen, R.S., Pi, L.C., Hsieh, C.C., 2005. Application of parameter optimization method for calibrating tank model. J. Am. Water Resour. Assoc. 41, 389–402.

Chiew, F.H.S., McMahon, T.A., 2002. Modelling the impacts of climate change on Australian streamflow. Hydrol. Process. 16, 1235–1245. doi:10.1002/hyp.1059

Cho, E., Choi, M., Wagner, W., 2015. An assessment of remotely sensed surface and root zone soil moisture through active and passive sensors in northeast Asia. Remote Sens. Environ. 160, 166–179. doi:10.1016/j.rse.2015.01.013

Christensen, N.S., Wood, A.W., Voisin, N., Lettenmaier, D.P., Palmer, R.N., 2004. The effects of climate change on the hydrology and water resources of the Colorado River basin. Clim. Change 62. doi:10.1023/B:CLIM.0000013684.13621.1f

Crow, W.T., Bindlish, R., Jackson, T.J., 2005a. The added value of spaceborne passive microwave soil moisture retrievals for forecasting rainfall-runoff partitioning. Geophys. Res. Lett. 32, 1–5.

Crow, W.T., Drusch, M., Wood, E.F., 2001. An observation system simulation experiment for the impact of land surface heterogeneity on AMSR-E soil moisture retrieval. IEEE Trans. Geosci. Remote Sens. 39, 1622–1631.

Crow, W.T., Kustas, W.P., Prueger, J.H., 2008. Monitoring root-zone soil moisture through the assimilation of a thermal remote sensing-based soil moisture proxy into a water balance model. Remote Sens. Environ. 112. doi:10.1016/j.rse.2006.11.033

Crow, W.T., Reichle, R.H., 2008. Comparison of adaptive filtering techniques for land surface data assimilation. Water Resour. Res. 44, n/a-n/a. doi:10.1029/2008WR006883

Crow, W.T., Ryu, D., 2009. A new data assimilation approach for improving runoff prediction using remotely-sensed soil moisture retrievals. Hydrol. Earth Syst. Sci. 13, 1–16.

Crow, W.T., Ryu, D., Famiglietti, J.S., 2005b. Upscaling of field-scale soil moisture measurements using distributed land surface modeling. Adv. Water Resour. 28, 1–14.

Crow, W.T., Van Loon, E., 2006. Impact of incorrect model error assumptions on the sequential assimilation of remotely sensed surface soil moisture. J. Hydrometeorol. 7. doi:10.1175/JHM499.1

Crow, W.T., Wood, E.F., 2003. The assimilation of remotely sensed soil brightness temperature imagery into a land surface model using Ensemble Kalman filtering: A case study based on ESTAR measurements during SGP97. Adv. Water Resour. 26, 137–149.

Crow, W.T., Wood, E.F., 2002. The value of coarse-scale soil moisture observations for regional surface energy balance modeling. J. Hydrometeorol. 3, 467–482.

Crow, W.T., Zhan, X., 2007. Continental-scale evaluation of remotely sensed soil moisture products. IEEE Geosci. Remote Sens. Lett. 4. doi:10.1109/LGRS.2007.896533

De Lannoy, G.J.M., Houser, P.R., Pauwels, V.R.N., Verhoest, N.E.C., 2006. Assessment of model uncertainty for soil moisture through ensemble verification. J. Geophys. Res. Atmos. 111.

Demaria, E.M., Nijssen, B., Wagener, T., 2007. Monte Carlo sensitivity analysis of land surface parameters using the Variable Infiltration Capacity model. J. Geophys. Res. 112, D11113. doi:10.1029/2006JD007534

Djamai, N., Magagi, R., Goïta, K., Merlin, O., Kerr, Y., Roy, A., 2016. A combination of DISPATCH downscaling algorithm with CLASS land surface scheme for soil moisture estimation at fine scale during cloudy days. Remote Sens. Environ. 184. doi:10.1016/j.rse.2016.06.010

Dobriyal, P., Qureshi, A., Badola, R., Hussain, S.A., 2012. A review of the methods available for estimating soil moisture and its implications for water resource management. J. Hydrol. 458–459. doi:10.1016/j.jhydrol.2012.06.021

Dorigo, W.A., Wagner, W., Hohensinn, R., Hahn, S., Paulik, C., Xaver, A., Gruber, A., Drusch, M., Mecklenburg, S., Van Oevelen, P., Robock, A., Jackson, T., 2011. The International Soil Moisture Network: A data hosting facility for global in situ soil moisture measurements. Hydrol. Earth Syst. Sci. 15. doi:10.5194/hess-15-1675-2011

Draper, C., Mahfouf, J.F., Calvet, J.C., Martin, E., Wagner, W., 2011. Assimilation of ASCAT near-surface soil moisture into the SIM hydrological model over France. Hydrol. Earth Syst. Sci. 15, 3829–3841. doi:10.5194/hess-15-3829-2011

Draper, C.S., Reichle, R.H., De Lannoy, G.J.M., Liu, Q., 2012. Assimilation of passive and active microwave soil moisture retrievals. Geophys. Res. Lett. 39. doi:10.1029/2011GL050655

Drusch, M., 2005. Observation operators for the direct assimilation of TRMM microwave imager retrieved soil moisture. Geophys. Res. Lett. 32, L15403. doi:10.1029/2005GL023623

Duan, Q., Sorooshian, S., Gupta, V., 1992. Effective and efficient global optimization for conceptual rainfall-runoff models. Water Resour. Res. 28, 1015–1031. doi:10.1029/91WR02985

Duan, Q.Y., Gupta, V.K., Sorooshian, S., 1993. Shuffled complex evolution approach for effective and efficient global minimization. J. Optim. Theory Appl. 76, 501–521. doi:10.1007/BF00939380

Dumedah, G., Walker, J.P., Merlin, O., 2015. Root-zone soil moisture estimation from assimilation of downscaled Soil Moisture and Ocean Salinity data. Adv. Water Resour. 84. doi:10.1016/j.advwatres.2015.07.021

EC-JRC, 2008. SimLab 2.2 Reference Manual Rep.

Elsanabary, M.H., Gan, T.Y., 2015. Evaluation of climate anomalies impacts on the Upper Blue Nile Basin in Ethiopia using a distributed and a lumped hydrologic model. J. Hydrol. doi:10.1016/j.jhydrol.2015.09.052

Endreny, T.A., Wood, E.F., Lettenmaier, D.P., 2000. Satellite-derived digital elevation model accuracy: Hydrological modelling requirements. Hydrol. Process. 14, 177–194.

Entekhabi, D., Njoku, E.G., O'Neill, P.E., Kellogg, K.H., Crow, W.T., Edelstein, W.N., Entin, J.K., Goodman, S.D., Jackson, T.J., Johnson, J., Kimball, J., Piepmeier, J.R., Koster, R.D., Martin, N., McDonald, K.C., Moghaddam, M., Moran, S., Reichle, R., Shi, J.C., Spencer, M.W., Thurman, S.W., Tsang, L., Van Zyl, J., 2010. The soil moisture active passive (SMAP) mission. Proc. IEEE 98. doi:10.1109/JPROC.2010.2043918

Escorihuela, M.J., Merlin, O., Escorihuela, A., Quintana, P., Martinez, D., 2012. SMOSCAT: Towards operational high resolution Soil Moisture with SMOS, in: International Geoscience and Remote Sensing Symposium (IGARSS). doi:10.1109/IGARSS.2012.6350493

Escorihuela, M.J., Quintana-Seguí, P., 2016. Comparison of remote sensing and simulated soil moisture datasets in Mediterranean landscapes. Remote Sens. Environ. 180, 99–114. doi:10.1016/j.rse.2016.02.046

Evensen, G., 2003. The Ensemble Kalman Filter: theoretical formulation and practical implementation. Ocean Dyn. 53, 343–367. doi:10.1007/s10236-003-0036-9

Evensen, G., 1994. Sequential data assimilation with a nonlinear quasi-geostrophic model using Monte Carlo methods to forecast error statistics. J. Geophys. Res. 99, 10,110-143,162.

Evett, S.R., Schwartz, R.C., Casanova, J.J., Heng, L.K., 2012. Soil water sensing for water balance, ET and WUE. Agric. Water Manag. 104. doi:10.1016/j.agwat.2011.12.002

Famiglietti, J.S., Wood, E.F., 1994. Multiscale modeling of spatially variable water and energy balance processes. Water Resour. Res. 30, 3061–3078.

Fang, B., Lakshmi, V., 2014. Soil moisture at watershed scale: Remote sensing techniques. J. Hydrol. 516. doi:10.1016/j.jhydrol.2013.12.008

Francois, C., Quesney, A., Ottle, C., 2003. Sequential assimilation of ERS-1 SAR data into a coupled land surface-hydrological model using an extended Kalman filter. J. Hydrometeorol. 4, 473–487. doi:10.1175/1525-7541(2003)4<473:SAOESD>2.0.CO;2

Francos, A., Elorza, F.J., Bouraoui, F., Bidoglio, G., Galbiati, L., 2003. Sensitivity analysis of distributed environmental simulation models: understanding the model behaviour in hydrological studies at the catchment scale. Reliab. Eng. Syst. Saf. 79, 205–218. doi:http://dx.doi.org/10.1016/S0951-8320(02)00231-4

Gan, T.Y., Biftu, G.F., 1996. Automatic calibration of conceptual rainfall-runoff models: Optimization algorithms, catchment conditions, and model structure. Water Resour. Res. 32, 3513–3524.

Gan, Y., Duan, Q., Gong, W., Tong, C., Sun, Y., Chu, W., Ye, A., Miao, C., Di, Z., 2014. A comprehensive evaluation of various sensitivity analysis methods: A case study with a hydrological model. Environ. Model. Softw. 51, 269–285.

Garambois, P.A., Roux, H., Larnier, K., Castaings, W., Dartus, D., 2013. Characterization of process-oriented hydrologic model behavior with temporal sensitivity analysis for flash floods in Mediterranean catchments. Hydrol. Earth Syst. Sci. 17, 2305–2322.

Geem, Z.W., Roper, W.E., 2010. Various continuous harmony search algorithms for web-based hydrologic parameter optimisation. Int. J. Math. Model. Numer. Optim. 1, 213–226.

Goegebeur, M., Pauwels, V.R.N., 2007. Improvement of the PEST parameter estimation algorithm through Extended Kalman Filtering. J. Hydrol. 337, 436–451.

Gordon, N.J., Salmond, D.J., Smith, A.F.M., 1993. Novel approach to nonlinear/non-gaussian Bayesian state

estimation. IEE Proceedings, Part F Radar Signal Process. 140, 107–113.

Grant, J.P., Wigneron, J.-P., Van de Griend, A.A., Kruszewski, A., Søbjærg, S.S., Skou, N., 2007. A field experiment on microwave forest radiometry: L-band signal behaviour for varying conditions of surface wetness. Remote Sens. Environ. 109. doi:10.1016/j.rse.2006.12.001

Grayson, R.B., Western, A.W., Chiew, F.H.S., Blöschl, G., 1997. Preferred states in spatial soil moisture patterns: Local and nonlocal controls. Water Resour. Res. 33.

Gupta, V.K., Waymire, E., Wang, C.T., 1980. A representation of an instantaneous unit hydrograph from geomorphology. Water Resour. Res. 16, 855–862. doi:10.1029/WR016i005p00855

Gupta, H. V, Sorooshian, S., Yapo, P.O., 1998. Toward improved calibration of hydrologic models: Multiple and noncommensurable measures of information. Water Resour. Res. 34, 751–763.

Gutman, G., Ignatov, A., 1998. The derivation of the green vegetation fraction from NOAA/AVHRR data for use in numerical weather prediction models. Int. J. Remote Sens. 19. doi:10.1080/014311698215333

Hahn, S., Melzer, T., Wagner, W., 2012. Error assessment of the initial near real-time METOP ASCAT surface soil moisture product. IEEE Trans. Geosci. Remote Sens. 50, 2556–2565. doi:10.1109/TGRS.2012.2183877

Han, E., Merwade, V., Heathman, G.C., 2012. Implementation of surface soil moisture data assimilation with watershed scale distributed hydrological model. J. Hydrol. 416–417, 98–117.

Hayashi, S., Murakami, S., Xu, K.-Q., Watanabe, M., 2008. Effect of the Three Gorges Dam Project on flood control in the Dongting Lake area, China, in a 1998-type flood. J. Hydro-Environment Res. 2. doi:10.1016/j.jher.2008.10.002

Heim Jr., R.R., 2002. A review of twentieth-century drought indices used in the United States. Bull. Am. Meteorol. Soc. 83.

Hillel, D., 1998. Environmental soil physics: Fundamentals, applications, and environmental considerations. Academic Press., San Diego.

Hossain, F., Anagnostou, E.N., 2006. Assessment of a multidimensional satellite rainfall error model for ensemble generation of satellite rainfall data. IEEE Geosci. Remote Sens. Lett. 3. doi:10.1109/LGRS.2006.873686

Houser, P.R., Shuttleworth, J.W., Famiglietti, J.S., Gupta, H. V, Syed, K.H., Goodrich, D.C., 1998. Integration of soil moisture remote sensing and hydrologic modeling using data assimilation. Water Resour. Res. 34, 3405–3420.

Jacobs, J.M., Mohanty, B.P., Hsu, E.-C., Miller, D., 2004. SMEX02: Field scale variability, time stability and similarity of soil moisture. Remote Sens. Environ. 92. doi:10.1016/j.rse.2004.02.017

Jacquemin, B., Noilhan, J., 1990. Sensitivity study and validation of a land surface parameterization using the HAPEX-MOBILHY data set. Boundary-Layer Meteorol. 52, 93–134. doi:10.1007/BF00123180

Jakeman, A.J., Hornberger, G.M., 1993. How much complexity is warranted in a rainfall-runoff model? Water Resour. Res. 29, 2637–2649.

Jarvis, P.G., 1976. The interpretation of the variation in leaf Water Potential and Stomatal Conductance found in canopies in the field. Philos. Trans. R. Soc. Lond. B. Biol. Sci. 273, 593–610.

Jazwinski, A.H., 1970. Stochastic Processes and Filtering Theories. Academic Press.

Jeu, R.A.M.A.M., Wagner, W., Holmes, T.R.H.R.H., Dolman, A.J.J., Giesen, N.C.C., Friesen, J., 2008. Global soil moisture patterns observed by space borne microwave radiometers and scatterometers. Surv. Geophys. 29, 399–420. doi:10.1007/s10712-008-9044-0

Kalman, R.E., 1960. A New Approach to Linear Filtering amd Prediction Problems. Trans. ASME - J. Basic Eng. 82 (Series, 35–45.

Kerr, Y.H., Waldteufel, P., Richaume, P., Wigneron, J.P., Ferrazzoli, P., Mahmoodi, A., Al Bitar, A., Cabot, F., Gruhier, C., Juglea, S.E., Leroux, D., Mialon, A., Delwart, S., 2012. The SMOS soil moisture retrieval algorithm. IEEE Trans. Geosci. Remote Sens. 50. doi:10.1109/TGRS.2012.2184548

Kerr, Y.H., Waldteufel, P., Wigneron, J.-P., Martinuzzi, J.-M., Font, J., Berger, M., 2001. Soil moisture retrieval from space: The Soil Moisture and Ocean Salinity (SMOS) mission. IEEE Trans. Geosci. Remote Sens.

39. doi:10.1109/36.942551

Khakbaz, B., Imam, B., Hsu, K., Sorooshian, S., 2012. From lumped to distributed via semi-distributed: Calibration strategies for semi-distributed hydrologic models. J. Hydrol. 418–419, 61–77.

Kim, S., Liu, Y., Johnson, F.M., Parinussa, R.M., Sharma, A., 2015. A global comparison of alternate AMSR2 soil moisture products: Why do they differ? Remote Sens. Environ. 161. doi:10.1016/j.rse.2015.02.002

Kim, U., Kaluarachchi, J.J., 2009. Hydrologic model calibration using discontinuous data: An example from the upper Blue Nile River Basin of Ethiopia. Hydrol. Process. 23, 3705–3717.

Kirchner, J.W., 2009. Catchments as simple dynamical systems: Catchment characterization, rainfall-runoff modeling, and doing hydrology backward. Water Resour. Res. 45. doi:10.1029/2008WR006912

Kobayashi, S., Maruyama, T., 1976. Search for the Coefficients of the Reservoir Model with the Powell's Conjugate Direction Method. Trans. Japanese Soc. Irrig. Drain. Reclam. Eng. 65, 42–47.

Kornelsen, K.C., Coulibaly, P., 2013. Advances in soil moisture retrieval from synthetic aperture radar and hydrological applications. J. Hydrol. 476. doi:10.1016/j.jhydrol.2012.10.044

Kornelsen, K.C., Davison, B., Coulibaly, P., 2016. Application of SMOS Soil Moisture and Brightness Temperature at High Resolution with a Bias Correction Operator. IEEE J. Sel. Top. Appl. Earth Obs. Remote Sens. 9, 1590–1605. doi:10.1109/JSTARS.2015.2474266

Koster, R.D., Dirmeyer, P.A., Guo, Z., Bonan, G., Chan, E., Cox, P., Gordon, C.T., Kanae, S., Kowalczyk, E., Lawrence, D., Liu, P., Lu, C.-H., Malyshev, S., McAvaney, B., Mitchell, K., Mocko, D., Oki, T., Oleson, K., Pitman, A., Sud, Y.C., Taylor, C.M., Verseghy, D., Vasic, R., Xue, Y., Yamada, T., 2004. Regions of strong coupling between soil moisture and precipitation. Science (80-.). 305. doi:10.1126/science.1100217

Koster, R.D., Mahanama, S.P.P., Livneh, B., Lettenmaier, D.P., Reichle, R.H., 2010. Skill in streamflow forecasts derived from large-scale estimates of soil moisture and snow. Nat. Geosci. 3. doi:10.1038/ngeo944

Kumar, S. V, Reichle, R.H., Harrison, K.W., Peters-Lidard, C.D., Yatheendradas, S., Santanello, J.A., 2012. A comparison of methods for a priori bias correction in soil moisture data assimilation. Water Resour. Res. 48.

Kurum, M., O'Neill, P.E., Lang, R.H., Cosh, M.H., Joseph, A.T., Jackson, T.J., 2012. Impact of conifer forest litter on microwave emission at L-band. IEEE Trans. Geosci. Remote Sens. 50. doi:10.1109/TGRS.2011.2166272

Laiolo, P., Gabellani, S., Campo, L., Cenci, L., Silvestro, F., 2015. Assimilation of remote sensing observations into a continuous distributed hydrological model : impacts on the hydrologic cycle, in: 2015 IEEE International Geoscience and Remote Sensing Symposium (IGARSS), Milan,. pp. 1308–1311. doi:10.1109/IGARSS.2015.7326015

Laiolo, P., Gabellani, S., Campo, L., Silvestro, F., Delogu, F., Rudari, R., Pulvirenti, L., Boni, G., Fascetti, F., Pierdicca, N., Crapolicchio, R., Hasenauer, S., Puca, S., 2016. Impact of different satellite soil moisture products on the predictions of a continuous distributed hydrological model. Int. J. Appl. Earth Obs. Geoinf. 48. doi:10.1016/j.jag.2015.06.002

Leroux, D.J., Kerr, Y.H., Bitar, A.A., Bindlish, R., Jackson, T.J., Berthelot, B., Portet, G., 2014. Comparison between SMOS, VUA, ASCAT, and ECMWF soil moisture products over four watersheds in U.S. IEEE Trans. Geosci. Remote Sens. 52. doi:10.1109/TGRS.2013.2252468

Li, C.Z., Wang, H., Liu, J., Yan, D.H., Yu, F.L., Zhang, L., 2010. Effect of calibration data series length on performance and optimal parameters of hydrological model. Water Sci. Eng. 3, 378–393.

Li, H., Xu, C.-Y., Beldring, S., 2015. How much can we gain with increasing model complexity with the same model concepts? J. Hydrol. 527. doi:10.1016/j.jhydrol.2015.05.044

Li, Y., Grimaldi, S., Walker, J.P., Pauwels, V.R.N., 2016. Application of remote sensing data to constrain operational rainfall-driven flood forecasting: A review. Remote Sens. 8. doi:10.3390/rs8060456

Li, Y., Ryu, D., Western, A.W., Wang, Q.J., Robertson, D.E., Crow, W.T., 2014. An integrated error parameter estimation and lag-aware data assimilation scheme for real-time flood forecasting. J. Hydrol.

Lievens, H., De Lannoy, G.J.M., Al Bitar, A., Drusch, M., Dumedah, G., Hendricks Franssen, H.J., Kerr, Y.H., Tomer, S.K., Martens, B., Merlin, O., Pan, M., Roundy, J.K., Vereecken, H., Walker, J.P., Wood, E.F.,

Verhoest, N.E.C., Pauwels, V.R.N., 2016. Assimilation of SMOS soil moisture and brightness temperature products into a land surface model. Remote Sens. Environ. 180, 292–304. doi:10.1016/j.rse.2015.10.033

Lievens, H., Tomer, S.K.K., Al Bitar, A., De Lannoy, G.J.M.J.M., Drusch, M., Dumedah, G., Hendricks Franssen, H.-J.J., Kerr, Y.H.H., Martens, B., Pan, M., Roundy, J.K.K., Vereecken, H., Walker, J.P.P., Wood, E.F.F., Verhoest, N.E.C.E.C., Pauwels, V.R.N.R.N., 2015. SMOS soil moisture assimilation for improved hydrologic simulation in the Murray Darling Basin, Australia. Remote Sens. Environ. 168, 146–162. doi:10.1016/j.rse.2015.06.025

Lin, L.-F., Ebtehaj, A.M., Wang, J., Bras, R.L., 2017. Soil moisture background error covariance and data assimilation in a coupled land-atmosphere model. Water Resour. Res. 53. doi:10.1002/2015WR017548

Liu, Y.Y., Dorigo, W.A., Parinussa, R.M., De Jeu, R.A.M., Wagner, W., McCabe, M.F., Evans, J.P., Van Dijk, A.I.J.M., 2012. Trend-preserving blending of passive and active microwave soil moisture retrievals. Remote Sens. Environ. 123, 280–297.

Liu, Y.Y., Parinussa, R.M., Dorigo, W.A., De Jeu, R.A.M., Wagner, W., M. Van Dijk, A.I.J., McCabe, M.F., Evans, J.P., 2011. Developing an improved soil moisture dataset by blending passive and active microwave satellite-based retrievals. Hydrol. Earth Syst. Sci. 15. doi:10.5194/hess-15-425-2011

Loaiza-Usuga, J.C., Pauwels, V.R.N., 2008. Calibration and multiple data set-based validation of a land surface model in a mountainous Mediterranean study area. J. Hydrol. 356, 223–233.

Loaiza-Usuga, J.C., Poch, R.M., 2009. Evaluation of soil water balance components under different land uses in a mediterranean mountain catchment (Catalan pre-pyrenees NE Spain). Zeitschrift fur Geomorphol. 53, 519–537.

Lobell, D.B., Asner, G.P., 2002. Moisture effects on soil reflectance. Soil Sci. Soc. Am. J. 66.

Loizu, J., 2017. Taking advantage of SMOS L4 (1-km resolution) for improved distributed hydrological modeling. Water Resour. Res. To be subm.

Loizu, J., Álvarez-Mozos, J., Casalí, J., Goñi, M., 2016. Evaluation of TOPLATS on three Mediterranean catchments. J. Hydrol. 539, 141–161. doi:10.1016/j.jhydrol.2016.05.025

Loizu, J., Massari, C., Álvarez-Mozos, J., Tarpanelli, A., Brocca, L., Casalí, J., 2017. On the assimilation set-up of ASCAT soil moisture data for improving streamflow catchment simulation. Adv. Water Resour. Under revi.

Loosvelt, L., De Baets, B., Pauwels, V.R.N., Verhoest, N.E.C., 2014a. Assessing hydrologic prediction uncertainty resulting from soft land cover classification. J. Hydrol. 517, 411–424.

Loosvelt, L., Pauwels, V.R.N., Verhoest, N.E.C., 2015. On the significance of crop-type information for the simulation of catchment hydrology. Hydrol. Process. 29, 915–926. doi:10.1002/hyp.10204

Loosvelt, L., Pauwels, V.R.N.V.R.N., Cornelis, W.M.W.M., De Lannoy, G.J.M.G.J.M., Verhoest, N.E.C.N.E.C., 2011. Impact of soil hydraulic parameter uncertainty on soil moisture modeling. Water Resour. Res. 47, n/a-n/a. doi:10.1029/2010WR009204

Loosvelt, L., Vernieuwe, H., Pauwels, V.R.N., De Baets, B., Verhoest, N.E.C., 2014b. Local sensitivity analysis for compositional data with application to soil texture in hydrologic modelling. Hydrol. Earth Syst. Sci. 17, 461–478.

López López, P., Wanders, N., Schellekens, J., Renzullo, L.J.L.J., Sutanudjaja, E.H.E.H., Bierkens, M.F.P.M.F.P., 2016. Improved large-scale hydrological modelling through the assimilation of streamflow and downscaled satellite soil moisture observations. Hydrol. Earth Syst. Sci. 20, 3059–3076. doi:10.5194/hess-20-3059-2016

Lü, H., Crow, W.T., Zhu, Y., Ouyang, F., Su, J., 2016. Improving streamflow prediction using remotely-sensed soil moisture and snow depth. Remote Sens. 8. doi:10.3390/rs8060503

Lucau-Danila, C., Callens, M., Defourny, P., Verhoest, N.E.C., Pauwels, V.R.N., 2005. Vegetation parameter retrieval from SAR data using near-surface soil moisture estimates dereived from a hydrological model, in: Owe, M., D'Urso, G. (Eds.), Proceedings of SPIE - The International Society for Optical Engineering. pp. 597603-597603–12. doi:10.1117/12.627574

Maggioni, V., Anagnostou, E.N., Reichle, R.H., 2012. The impact of model and rainfall forcing errors on characterizing soil moisture uncertainty in land surface modeling. Hydrol. Earth Syst. Sci. 16, 3499–3515. doi:10.5194/hess-16-3499-2012

Maggioni, V., Houser, P., 2017. Soil Moisture Data Assimilation, in: Data Assimilation for Atmospheric, Oceanic and Hydrologic Applications (Vol. III),. p. pp.195-217.

Maggioni, V., Reichle, R.H., Anagnostou, E.N., 2011. The effect of satellite rainfall error modeling on soil moisture prediction uncertainty. J. Hydrometeorol. 12. doi:10.1175/2011JHM1355.1

Martínez-Fernández, J., Ceballos, A., 2003. Temporal Stability of Soil Moisture in a Large-Field Experiment in Spain. Soil Sci. Soc. Am. J. 67, 1647–1656.

Massari, C., Brocca, L., Tarpanelli, A., Moramarco, T., 2015. Data Assimilation of Satellite Soil Moisture into Rainfall-Runoff Modelling: A Complex Recipe? Remote Sens. 7, 11403–11433. doi:10.3390/rs70911403

Massmann, C., Holzmann, H., 2012. Analysis of the behavior of a rainfall-runoff model using three global sensitivity analysis methods evaluated at different temporal scales. J. Hydrol. 475, 97–110.

Matgen, P., Fenicia, F., Heitz, S., Plaza, D., de Keyser, R., Pauwels, V.R.N., Wagner, W., Savenije, H., 2012a. Can ASCAT-derived soil wetness indices reduce predictive uncertainty in well-gauged areas? A comparison with in situ observed soil moisture in an assimilation application. Adv. Water Resour. 44, 49–65. doi:10.1016/j.advwatres.2012.03.022

Matgen, P., Heitz, S., Hasenauer, S., Hissler, C., Brocca, L., Hoffmann, L., Wagner, W., Savenije, H.H.G., 2012b. On the potential of MetOp ASCAT-derived soil wetness indices as a new aperture for hydrological monitoring and prediction: A field evaluation over Luxembourg. Hydrol. Process. 26, 2346–2359.

Maybeck, P.S., Siouris, G.M., 1980. Stochastic Models, Estimation, and Control, Volume I, IEEE Transactions on Systems, Man, and Cybernetics. Academic Press, New York. doi:10.1109/TSMC.1980.4308494

McCabe, M.R., Alsdorf, D.E., Miralles, D.G., Uijlenhoet, R., Wagner, W., Lucieer, A., Houborg, R., Niko E. C. Verhoest, Trenton E. Franz, J.S., Gao, H., Wood, E.F., 2017. The Future of Earth Observation in Hydrology. Hydrology and Earth System Sciences (under review). Hydrol. Earth Syst. Sci. (under Rev.

Melone, F., Neri, N., Morbidelli, R., Saltalippi, C., 2001. A conceptual model for flood prediction in basins of moderate size. Appl. Simul. Model. In: Hamza, 461–6.

Merlin, O., Malbéteau, Y., Notfi, Y., Bacon, S., Er-Raki, S., Khabba, S., Jarlan, L., 2015. Performance metrics for soil moisture downscaling methods: Application to DISPATCH data in central Morocco. Remote Sens. 7. doi:10.3390/rs70403783

Merlin, O., Rüdiger, C., Al Bitar, A., Richaume, P., Walker, J.P., Kerr, Y.H., 2012. Disaggregation of SMOS soil moisture in Southeastern Australia. IEEE Trans. Geosci. Remote Sens. 50, 1556–1571.

Milella, P., Bisantino, T., Gentile, F., Iacobellis, V., Trisorio Liuzzi, G., 2012. Diagnostic analysis of distributed input and parameter datasets in Mediterranean basin streamflow modeling. J. Hydrol. 472–473, 262–276. doi:10.1016/j.jhydrol.2012.09.039

Milly, P.C.D., 1986. Event-based simulation model of moisture and energy fluxes at bare soil surface. Water Resour. Res. 22, 1680–1692.

Mohanty, B.P., Cosh, M.H., Lakshmi, V., Montzka, C., 2017. Soil moisture remote sensing: State-of-the-science. Vadose Zo. J. 16. doi:10.2136/vzj2016.10.0105

Mohanty, B.P., Skaggs, T.H., 2001. Spatio-temporal evolution and time-stable characteristics of soil moisture within remote sensing footprints with varying soil, slope, and vegetation. Adv. Water Resour. 24. doi:10.1016/S0309-1708(01)00034-3

Molero, B., Merlin, O., Malbéteau, Y., Al Bitar, A., Cabot, F., Stefan, V., Kerr, Y., Bacon, S., Cosh, M.H., Bindlish, R., Jackson, T.J., 2015. SMOS disaggregated soil moisture product at 1km resolution: Processor overview and first validation results. Remote Sens. Environ. doi:10.1016/j.rse.2016.02.045

Moradkhani, H., Hsu, K.-L., Gupta, H., Sorooshian, S., 2005a. Uncertainty assessment of hydrologic model states and parameters: Sequential data assimilation using the particle filter. Water Resour. Res. 41. doi:10.1029/2004WR003604

Moradkhani, H., Sorooshian, S., Gupta, H. V, Houser, P.R., 2005b. Dual state-parameter estimation of hydrological models using ensemble Kalman filter. Adv. Water Resour. 28, 135–147.

Moriasi, D.N., Arnold, J.G., Van Liew, M.W., Bingner, R.L., Harmel, R.D., Veith, T.L., 2007. Model evaluation guidelines for systematic quantification of accuracy in watershed simulations. Trans. ASABE 50, 885–900.

Morris, M.D., 1991. Factorial sampling plans for preliminary computational experiments. Technometrics 161–174.

Muñoz-Carpena, R., Shukla, S., Morgan, K., 2004. Field Devices for Monitoring Soil Water Content. Extension Bulletin, vol. 343.

Naeimi, V., Scipal, K., Bartalis, Z., Hasenauer, S., Wagner, W., 2009. An Improved Soil Moisture Retrieval Algorithm for ERS and METOP Scatterometer Observations. IEEE Trans. Geosci. Remote Sens. 47, 1999–2013. doi:10.1109/TGRS.2008.2011617

Nash, J.E., Sutcliffe, J. V, 1970. River flow forecasting through conceptual models part I - A discussion of principles. J. Hydrol. 10, 282–290.

Norton, J.P., 2009. Selection of Morris trajectories for initial sensitivity analysis, in: IFAC Proceedings Volumes (IFAC-PapersOnline). pp. 670–674. doi:10.3182/20090706-3-FR-2004.0431

NRCS-USDA, 2014. 12th Edition Keys to Soil Taxonomy.

Oakley, J.E., O'Hagan, A., 2004. Probabilistic sensitivity analysis of complex models: a Bayesian approach. J. R. Stat. Soc. Ser. B (Statistical Methodol. 66, 751–769. doi:10.1111/j.1467-9868.2004.05304.x

Ochsner, T.E., Cosh, M.H., Cuenca, R.H., Dorigo, W.A., Draper, C.S., Hagimoto, Y., Kerr, Y.H., Larson, K.M., Njoku, E.G., Small, E.E., Zreda, M., 2013. State of the art in large-scale soil moisture monitoring. Soil Sci. Soc. Am. J. 77. doi:10.2136/sssaj2013.03.0093

Oliva, R., Daganzo, E., Richaume, P., Kerr, Y., Cabot, F., Soldo, Y., Anterrieu, E., Reul, N., Gutierrez, A., Barbosa, J., Lopes, G., 2016. Status of Radio Frequency Interference (RFI) in the 1400-1427 MHz passive band based on six years of SMOS mission. Remote Sens. Environ. 180. doi:10.1016/j.rse.2016.01.013

Paik, K., Kim, J.H., Kim, H.S., Lee, D.R., 2005. A conceptual rainfall-runoff model considering seasonal variation. Hydrol. Process. 19, 3837–3850.

Paloscia, S., Pettinato, S., Santi, E., Notarnicola, C., Pasolli, L., Reppucci, A., 2013. Soil moisture mapping using Sentinel-1 images: Algorithm and preliminary validation. Remote Sens. Environ. 134. doi:10.1016/j.rse.2013.02.027

Parrens, M., Zakharova, E., Lafont, S., Calvet, J.C., Kerr, Y., Wagner, W., Wigneron, J.P., 2012. Comparing soil moisture retrievals from SMOS and ASCAT over France. Hydrol. Earth Syst. Sci. 16, 423–440.

Passerat De Silans, A., Vauclin, M., Bruckler, L., Bertuzzi, P., Brunet, Y., 1986. Numerical modeling of water and heat flows in unsaturated soils under atmospheric excitation. Comparison with field data, in: Heat Transfer, Proceedings of the International Heat Transfer Conference. pp. 2629–2634.

Paulik, C., Dorigo, W., Wagner, W., Kidd, R., 2014. Validation of the ASCAT soil water index using in situ data from the International Soil moisture network. Int. J. Appl. Earth Obs. Geoinf. 30, 1–8.

Pauwels, V.R.N., Balenzano, A., Satalino, G., Skriver, H., Verhoest, N.E.C., Mattia, F., 2009a. Optimization of soil hydraulic model parameters using Synthetic Aperture Radar data: An integrated multidisciplinary approach. IEEE Trans. Geosci. Remote Sens. 47, 455–467.

Pauwels, V.R.N., De Lannoy, G.J.M., 2009b. Ensemble-based assimilation of discharge into rainfall-runoff models: A comparison of approaches to mapping observational information to state space. Water Resour. Res. 45, n/a-n/a. doi:10.1029/2008WR007590

Pauwels, V.R.N., Hoeben, R., Verhoest, N.E.C., De Troch, F.P., 2001. The importance of the spatial patterns of remotely sensed soil moisture in the improvement of discharge predictions for small-scale basins through data assimilation. J. Hydrol. 251, 88–102.

Pauwels, V.R.N., Hoeben, R., Verhoest, N.E.C., De Troch, F.P., Troch, P.A., 2002. Improvement of TOPLATS-based discharge predictions through assimilation of ERS-based remotely sensed soil moisture values. Hydrol. Process. 16, 995–1013.

Pauwels, V.R.N., Wood, E.F., 1999. A soil-vegetation-atmosphere transfer scheme for the modeling of water and energy balance processes in high latitudes 2. Application and validation. J. Geophys. Res. D Atmos. 104, 27823–27839.

Pauwels, V.R.N.V.R.N., Verhoest, N.E.C.N.E.C., De Lannoy, G.J.M.G.J.M., Guissard, V., Lucau, C., Defourny, P., 2007. Optimization of a coupled hydrology-crop growth model through the assimilation of observed soil moisture and leaf area index values using an ensemble Kalman filter. Water Resour. Res. 43, n/a-n/a. doi:10.1029/2006WR004942

Pellarin, T., Mialon, A., Biron, R., Coulaud, C., Gibon, F., Kerr, Y., Lafaysse, M., Mercier, B., Morin, S., Redor, I., Schwank, M., Völksch, I., 2015. Three years of L-band brightness temperature measurements in a mountainous area: Topography, vegetation and snowmelt issues. Remote Sens. Environ. doi:10.1016/j.rse.2016.02.047

Perrin, C., Michel, C., Andréassian, V., 2001. Does a large number of parameters enhance model performance? Comparative assessment of common catchment model structures on 429 catchments. J. Hydrol. 242, 275–301. doi:10.1016/S0022-1694(00)00393-0

Perrin, C., Oudin, L., Andreassian, V., Rojas-Serna, C., Michel, C., Mathevet, T., 2007. Impact of limited streamflow data on the efficiency and the parameters of rainfall-runoff models. Hydrol. Sci. J. 52, 131–151.

Peters-Lidard, C.D., Zion, M.S., Wood, E.F., 1997. A soil-vegetation-atmosphere transfer scheme for modeling spatially variable water and energy balance processes. J. Geophys. Res. D Atmos. 102, 4303–4324.

Petropoulos, G., Carlson, T.N., Wooster, M.J., Islam, S., 2009. A review of Ts/VI remote sensing based methods for the retrieval of land surface energy fluxes and soil surface moisture. Prog. Phys. Geogr. 33. doi:10.1177/0309133309338997

Petropoulos, G.P., Ireland, G., Barrett, B., 2015. Surface soil moisture retrievals from remote sensing: Current status, products & future trends. Phys. Chem. Earth 83–84. doi:10.1016/j.pce.2015.02.009

Piles, M., Camps, A., Vall-Llossera, M., Corbella, I., Panciera, R., Rudiger, C., Kerr, Y.H., Walker, J., 2011. Downscaling SMOS-derived soil moisture using MODIS visible/infrared data. IEEE Trans. Geosci. Remote Sens. 49, 3156–3166.

Piles, M., Pou, X., Camps, A., Vall-Llossera, M., 2015. Quality Report: Validation of SMOS-BEC L4 high resolution soil moisture products, version 3.0 or "all weather."

Piles, M., Sánchez, N., 2016. Spatial Downscaling of Passive Microwave Data With Visible-to-Infrared Information for High-Resolution Soil Moisture Mapping, Satellite Soil Moisture Retrieval: Techniques and Applications. doi:10.1016/B978-0-12-803388-3.00006-1

Piles, M., Sánchez, N., Vall-Llossera, M., Camps, A., Martínez-Fernandez, J., Martinez, J., Gonzalez-Gambau, V., 2014. A downscaling approach for SMOS land observations: Evaluation of high-resolution soil moisture maps over the Iberian peninsula. IEEE J. Sel. Top. Appl. Earth Obs. Remote Sens. 7, 3845–3857. doi:10.1109/JSTARS.2014.2325398

Piles, M., Vall-Llossera, M., Camps, A., Talone, M., Monerris, A., 2010. Analysis of a least-squares soil moisture retrieval algorithm from L-band passive observations. Remote Sens. 2, 352–374.

Plaza, D.A., De Keyser, R., De Lannoy, G.J.M., Giustarini, L., Matgen, P., Pauwels, V.R.N., 2012. The importance of parameter resampling for soil moisture data assimilation into hydrologic models using the particle filter. Hydrol. Earth Syst. Sci. 16, 375–390.

Polcher, J., Piles, M., Gelati, E., Barella-Ortiz, A., Tello, M., 2016. Comparing surface-soil moisture from the SMOS mission and the ORCHIDEE land-surface model over the Iberian Peninsula. Remote Sens. Environ. 174. doi:10.1016/j.rse.2015.12.004

Powell, M.J.D., 1964. An efficient method for finding the minimum of a function of several variables without calculating derivatives. Comput. J. 7, 155–162. doi:10.1093/comjnl/7.2.155

Prata, A.J., 1996. A new long-wave formula for estimating downward clear-sky radiation at the surface. Q. J. R. Meteorol. Soc. 122, 1127–1151.

Press, W.H., Teukolsky, S.A., Vetterling, W.T., Flannery, B.P., 1988. Numerical Recipes in Fortran 77: The art of scientific computing. Cambridge University Press.

Quattrochi, D.A., Luvall, J.C., 1999. Thermal infrared remote sensing for analysis of landscape ecological processes: Methods and applications. Landsc. Ecol. 14. doi:10.1023/A:1008168910634

Rafieeinasab, A., Seo, D.J., Lee, H., Kim, S., 2014. Comparative evaluation of maximum likelihood ensemble filter and ensemble Kalman filter for real-time assimilation of streamflow data into operational hydrologic models. J. Hydrol.

Rahmoune, R., Ferrazzoli, P., Kerr, Y.H., Richaume, P., 2013. SMOS level 2 retrieval algorithm over forests: Description and generation of global maps. IEEE J. Sel. Top. Appl. Earth Obs. Remote Sens. 6. doi:10.1109/JSTARS.2013.2256339

Randrianasolo, A., Thirel, G., Ramos, M.H.H., Martin, E., 2014. Impact of streamflow data assimilation and length of the verification period on the quality of short-term ensemble hydrologic forecasts. J. Hydrol. 519, Part, 2676–2691. doi:http://dx.doi.org/10.1016/j.jhydrol.2014.09.032

RAO, S.S., 2009. Engineering optimization: theory and practice., 4th editio. ed. John Wiley and Sons Ltd, New Jersey. doi:10.1002/9780470549124

Ratto, M., Tarantola, S., Saltelli, A., 2001. Sensitivity analysis in model calibration: GSA-GLUE approach. Comput. Phys. Commun. 136, 212–224.

Rawls, W.J., Brakensiek, D.L., Saxton, K.E., 1982. Estimation of soil water properties. Trans. Am. Soc. Agric. Eng. 25, 1316–1320, 1328.

Reichle, R.H., 2004. Bias reduction in short records of satellite soil moisture. Geophys. Res. Lett. 31, L19501. doi:10.1029/2004GL020938

Reichle, R.H., Crow, W.T., Keppenne, C.L., 2008. An adaptive ensemble Kalman filter for soil moisture data assimilation. Water Resour. Res. 44.

Reichle, R.H., De Lannoy, G.J.M., Forman, B.A., Draper, C.S., Liu, Q., 2014. Connecting Satellite Observations with Water Cycle Variables Through Land Data Assimilation: Examples Using the NASA GEOS-5 LDAS. Surv. Geophys. 35. doi:10.1007/s10712-013-9220-8

Reichle, R.H., Koster, R.D., Liu, P., Mahanama, S.P.P., Njoku, E.G., Owe, M., 2007. Comparison and assimilation of global soil moisture retrievals from the Advanced Microwave Scanning Radiometer for the Earth Observing System (AMSR-E) and the Scanning Multichannel Microwave Radiometer (SMMR). J. Geophys. Res. 112, D09108. doi:10.1029/2006JD008033

Reichle, R.H., McLaughlin, D.B., Entekhabi, D., 2001. Variational data assimilation of microwave radiobrightness observations for land surface hydrology applications. IEEE Trans. Geosci. Remote Sens. 39. doi:10.1109/36.942549

Renzullo, L.J., van Dijk, A.I.J.M., Perraud, J.M., Collins, D., Henderson, B., Jin, H., Smith, A.B., McJannet, D.L., 2014. Continental satellite soil moisture data assimilation improves root-zone moisture analysis for water resources assessment. J. Hydrol.

Richter, B.D., Richter, H.E., 2000. Prescribing flood regimes to sustain riparian ecosystems along meandering rivers. Conserv. Biol. 14. doi:10.1046/j.1523-1739.2000.98488.x

Ridler, M.E., Madsen, H., Stisen, S., Bircher, S., Fensholt, R., 2014. Assimilation of SMOS-derived soil moisture in a fully integrated hydrological and soil-vegetation-atmosphere transfer model in Western Denmark. Water Resour. Res. 50, 8962–8981. doi:10.1002/2014WR015392

Ritter, A., Muñoz-Carpena, R., 2013. Performance evaluation of hydrological models: Statistical significance for reducing subjectivity in goodness-of-fit assessments. J. Hydrol. 480, 33–45.

Rodriguez-Alvarez, N., Bosch-Lluis, X., Camps, A., Vall-Llossera, M., Valencia, E., Marchan-Hernandez, J.F., Ramos-Perez, I., 2009. Soil moisture retrieval using GNSS-R techniques: Experimental results over a bare soil field. IEEE Trans. Geosci. Remote Sens. 47. doi:10.1109/TGRS.2009.2030672

Rogger, M., Kohl, B., Pirkl, H., Viglione, A., Komma, J., Kirnbauer, R., Merz, R., Blöschl, G., 2012. Runoff models and flood frequency statistics for design flood estimation in Austria - Do they tell a consistent story? J. Hydrol. 456–457. doi:10.1016/j.jhydrol.2012.05.068

Rosenbaum, U., Bogena, H.R., Herbst, M., Huisman, J.A., Peterson, T.J., Weuthen, A., Western, A.W., Vereecken, H., 2012. Seasonal and event dynamics of spatial soil moisture patterns at the small catchment scale. Water Resour. Res. 48. doi:10.1029/2011WR011518

Rötzer, K., Montzka, C., Bogena, H., Wagner, W., Kerr, Y.H., Kidd, R., Vereecken, H., 2014. Catchment scale validation of SMOS and ASCAT soil moisture products using hydrological modeling and temporal stability analysis. J. Hydrol. 519, 934–946.

Rudiger, C., Su, C.-H., Ryu, D., Wagner, W., 2016. Disaggregation of Low-Resolution L-Band Radiometry Using C-Band Radar Data. IEEE Geosci. Remote Sens. Lett. 13. doi:10.1109/LGRS.2016.2583433

Ryu, D., Crow, W.T., Zhan, X., Jackson, T.J., 2009. Correcting unintended perturbation biases in hydrologic data assimilation. J. Hydrometeorol. 10, 734–750.

Sabater, J.M., Jarlan, L., Calvet, J.-C., Bouyssel, F., De Rosnay, P., 2007. From near-surface to root-zone soil moisture using different assimilation techniques. J. Hydrometeorol. 8. doi:10.1175/JHM571.1

Sahoo, A.K., De Lannoy, G.J.M., Reichle, R.H., Houser, P.R., 2013. Assimilation and downscaling of satellite observed soil moisture over the Little River Experimental Watershed in Georgia, USA. Adv. Water Resour. 52, 19–33. doi:10.1016/j.advwatres.2012.08.007

Saltelli, A., 2002. Making best use of model evaluations to compute sensitivity indices. Comput. Phys. Commun. 145, 280–297.

Saltelli, A., Annoni, P., Azzini, I., Campolongo, F., Ratto, M., Tarantola, S., 2010. Variance based sensitivity analysis of model output. Design and estimator for the total sensitivity index. Comput. Phys. Commun. 181, 259–270.

Saltelli, A., Ratto, M., Tarantola, S., Campolongo, F., 2006. Sensitivity analysis practices: Strategies for model-based inference. Reliab. Eng. Syst. Saf. 91, 1109–1125.

Saltelli, A., Tarantola, S., Campolongo, F., 2000. Sensitivity Analysis as an Ingredient of Modeling. Stat. Sci. 15, 377–395.

Sanchez-Ruiz, S., Piles, M., Sánchez, N., Martínez-Fernández, J., Vall-llossera, M., Camps, A., 2014. Combining SMOS with visible and near/shortwave/thermal infrared satellite data for high resolution soil moisture estimates. J. Hydrol. 516, 273–283. doi:10.1016/j.jhydrol.2013.12.047

Sánchez, N., Martínez-Fernánadez, J., Scaini, A., Pérez-Gutierrez, C., 2012. Validation of the SMOS L2 soil moisture data in the REMEDHUS network (Spain). IEEE Trans. Geosci. Remote Sens. 50, 1602–1611. doi:10.1109/TGRS.2012.2186971

Sandholt, I., Rasmussen, K., Andersen, J., 2002. A simple interpretation of the surface temperature/vegetation index space for assessment of surface moisture status. Remote Sens. Environ. 79. doi:10.1016/S0034-4257(01)00274-7

Sayde, C., Gregory, C., Gil-Rodriguez, M., Tufillaro, N., Tyler, S., Van De Giesen, N., English, M., Cuenca, R., Selker, J.S., 2010. Feasibility of soil moisture monitoring with heated fiber optics. Water Resour. Res. 46. doi:10.1029/2009WR007846

Schaefer, G.L., Cosh, M.H., Jackson, T.J., 2007. The USDA Natural Resources Conservation Service Soil Climate Analysis Network (SCAN). J. Atmos. Ocean. Technol. 24. doi:10.1175/2007JTECHA930.1

Scipal, K., Drusch, M., Wagner, W., 2008. Assimilation of a ERS scatterometer derived soil moisture index in the ECMWF numerical weather prediction system. Adv. Water Resour. 31, 1101–1112. doi:10.1016/j.advwatres.2008.04.013

SCS - Soil Conservation Service., 1972. National Engineering Handbook, section 4. Washington D.C.

Senarath, S.U.S., Ogden, F.L., Downer, C.W., Sharif, H.O., 2000. On the calibration and verification of two-dimensional, distributed, Hortonian, continuous watershed models. Water Resour. Res. 36, 1495–1510. doi:10.1029/2000WR900039

Seneviratne, S.I., Corti, T., Davin, E.L., Hirschi, M., Jaeger, E.B., Lehner, I., Orlowsky, B., Teuling, A.J., 2010. Investigating soil moisture–climate interactions in a changing climate: A review. Earth-Science Rev. 99, 125–161. doi:10.1016/j.earscirev.2010.02.004

Seuffert, G., Gross, P., Simmer, C., Wood, E.F., 2002. The influence of hydrologic modeling on the predicted local weather: Two-way coupling of a mesoscale weather prediction model and a land surface hydrologic model. J. Hydrometeorol. 3, 505–523.

Shin, M.J., Guillaume, J.H.A., Croke, B.F.W., Jakeman, A.J., 2013. Addressing ten questions about conceptual rainfall-runoff models with global sensitivity analyses in R. J. Hydrol. 503, 135–152.

Shuttleworth, W.J., Zreda, M., Zeng, X., Zweck, C., Ferré, P.A., 2010. The COsmic-ray Soil Moisture Observing System (COSMOS): a non-invasive, intermediate scale soil moisture measurement network, in: British Hydrological Society (Ed.), BHS Third International Symposium, Managing Consequences of a Changing Global Environment. Newcastle.

Singh, V.P., Woolhiser, D.A., 2002. Mathematical modeling of watershed hydrology. J. Hydrol. Eng. 7. doi:10.1061/(ASCE)1084-0699(2002)7:4(270)

Sivapalan, M., Beven, K., Wood, E.F., 1987. On hydrologic similarity. 2. A scaled model of storm runoff production. Water Resour. Res. 23, 2266–2278.

SMOS-BEC Team, 2016. SMOS-BEC Ocean and Land Products Description. Technical Report,. Barcelona.

Sobol, I.M., 1993. Sensitivity estimates for nonlinear mathematical models. Math. Model. Comput. Exp. 1, 407–417.

Song, X., Zhang, J., Zhan, C., Xuan, Y., Ye, M., Xu, C., 2015. Global sensitivity analysis in hydrological modeling: Review of concepts, methods, theoretical framework, and applications. J. Hydrol. 523, 739–757. doi:10.1016/j.jhydrol.2015.02.013

Sorooshian, S., Gupta, V.K., 1983. Automatic calibration of conceptual rainfall-runoff models: The question of parameter observability and uniqueness. Water Resour. Res. 19, 260–268. doi:10.1029/WR019i001p00260

Spear, R.C., Grieb, T.M., Shang, N., 1994. Parameter uncertainty and interaction in complex environmental models. Water Resour. Res. 30, 3159–3170.

Stisen, S., Jensen, K.H., Sandholt, I., Grimes, D.I.F., 2008. A remote sensing driven distributed hydrological model of the Senegal River basin. J. Hydrol. 354, 131–148. doi:10.1016/j.jhydrol.2008.03.006

Sun, X.Y., Newham, L.T.H., Croke, B.F.W., Norton, J.P., 2012. Three complementary methods for sensitivity analysis of a water quality model. Environ. Model. Softw. 37, 19–29.

Tang, Y., Reed, P., Wagener, T., Van Werkhoven, K., 2007. Comparing sensitivity analysis methods to advance lumped watershed model identification and evaluation. Hydrol. Earth Syst. Sci. 11, 793–817.

Thiboult, A., Anctil, F., 2015. On the difficulty to optimally implement the Ensemble Kalman filter: An experiment based on many hydrological models and catchments. J. Hydrol. 529, 1147–1160. doi:10.1016/j.jhydrol.2015.09.036

Tian, S., Tregoning, P., Renzullo, L.J., van Dijk, A.I.J.M., Walker, J.P., Pauwels, V.R.N., Allgeyer, S., 2017. Improved water balance component estimates through joint assimilation of GRACE water storage and SMOS soil moisture retrievals. Water Resour. Res. 53. doi:10.1002/2016WR019641

Tolson, B.A., Shoemaker, C.A., 2007. Dynamically dimensioned search algorithm for computationally efficient watershed model calibration. Water Resour. Res. 43, n/a-n/a. doi:10.1029/2005WR004723

Topp, G.C., Davis, J.L., Annan, A.P., 1980. Electromagnetic determination of soil water content: Measurements in coaxial transmission lines. Water Resour. Res. 16. doi:10.1029/WR016i003p00574

Trudel, M., Leconte, R., Paniconi, C., 2014. Analysis of the hydrological response of a distributed physically-based model using post-assimilation (EnKF) diagnostics of streamflow and in situ soil moisture observations. J. Hydrol. 514, 192–201. doi:10.1016/j.jhydrol.2014.03.072

Tuttle, S., Salvucci, G., 2016. Atmospheric science: Empirical evidence of contrasting soil moisture-precipitation feedbacks across the United States. Science (80-.). 352. doi:10.1126/science.aaa7185

Utku, C., Le Vine, D.M., 2011. A model for prediction of the impact of topography on microwave emission. IEEE Trans. Geosci. Remote Sens. 49. doi:10.1109/TGRS.2010.2053936

Vachaud, G., Passerat De Silans, A., Balabanis, P., Vauclin, M., 1985. Temporal stability of spatially measured soil water probability density function. Soil Sci. Soc. Am. J. 49.

Van Griensven, A., Meixner, T., Grunwald, S., Bishop, T., Diluzio, M., Srinivasan, R., 2006. A global sensitivity analysis tool for the parameters of multi-variable catchment models. J. Hydrol. 324, 10–23.

van Werkhoven, K., Wagener, T., Reed, P., Tang, Y., 2008. Characterization of watershed model behavior across a hydroclimatic gradient. Water Resour. Res. 44, n/a-n/a. doi:10.1029/2007WR006271

Van Werkhoven, K., Wagener, T., Reed, P., Tang, Y., 2009. Sensitivity-guided reduction of parametric

dimensionality for multi-objective calibration of watershed models. Adv. Water Resour. 32, 1154–1169.

Verhoest, N.E.C., Lievens, H., Wagner, W., Álvarez-Mozos, J., Moran, M.S., Mattia, F., 2008. On the soil roughness parameterization problem in soil moisture retrieval of bare surfaces from synthetic aperture radar. Sensors 8. doi:10.3390/s8074213

Verhoest, N.E.C., Van Den Berg, M.J., Martens, B., Lievens, H., Wood, E.F., Pan, M., Kerr, Y.H., Al Bitar, A., Tomer, S.K., Drusch, M., Vernieuwe, H., De Baets, B., Walker, J.P., Dumedah, G., Pauwels, V.R.N., 2015. Copula-based downscaling of coarse-scale soil moisture observations with implicit bias correction. IEEE Trans. Geosci. Remote Sens. 53. doi:10.1109/TGRS.2014.2378913

Vrugt, J.A., Gupta, H. V, Bouten, W., Sorooshian, S., 2003. A Shuffled Complex Evolution Metropolis algorithm for optimization and uncertainty assessment of hydrologic model parameters. Water Resour. Res. 39, SWC11-SWC116.

Wagener, T., Kollat, J., 2007. Numerical and visual evaluation of hydrological and environmental models using the Monte Carlo analysis toolbox. Environ. Model. Softw. 22, 1021–1033. doi:10.1016/j.envsoft.2006.06.017

Wagner, W., Hahn, S., Kidd, R., Melzer, T., Bartalis, Z., Hasenauer, S., Figa-Saldaña, J., De Rosnay, P., Jann, A., Schneider, S., Komma, J., Kubu, G., Brugger, K., Aubrecht, C., Züger, J., Gangkofner, U., Kienberger, S., Brocca, L., Wang, Y., Blöschl, G., Eitzinger, J., Steinnocher, K., Zeil, P., Rubel, F., 2013. The ASCAT Soil Moisture Product: A Review of its Specifications, Validation Results, and Emerging Applications. Meteorol. Zeitschrift 22, 5–33. doi:10.1127/0941-2948/2013/0399

Wagner, W., Lemoine, G., Rott, H., 1999. A method for estimating soil moisture from ERS Scatterometer and soil data. Remote Sens. Environ. 70, 191–207.

Wainwright, H.M., Finsterle, S., Jung, Y., Zhou, Q., Birkholzer, J.T., 2014. Making sense of global sensitivity analyses. Comput. Geosci. 65, 94.

Wanders, N., Bierkens, M.F.P., de Jong, S.M., de Roo, A., Karssenberg, D., 2014a. The benefits of using remotely sensed soil moisture in parameter identification of large-scale hydrological models. Water Resour. Res. 50, 6874–6891. doi:10.1002/2013WR014639

Wanders, N., Karssenberg, D., Bierkens, M., Parinussa, R., de Jeu, R., van Dam, J., de Jong, S., 2012. Observation uncertainty of satellite soil moisture products determined with physically-based modeling. Remote Sens. Environ. 127, 341–356.

Wanders, N., Karssenberg, D., De Roo, A., de Jong, S.M., Bierkens, M.F.P., 2014b. The suitability of remotely sensed soil moisture for improving operational flood forecasting. Hydrol. Earth Syst. Sci. 18, 2343–2357. doi:10.5194/hess-18-2343-2014

Weerts, A.H.A.H., El Serafy, G.Y.H.G.Y.H., 2006. Particle filtering and ensemble Kalman filtering for state updating with hydrological conceptual rainfall-runoff models. Water Resour. Res. 42, n/a-n/a. doi:10.1029/2005WR004093

Wood, E.F., Roundy, J.K., Troy, T.J., van Beek, L.P.H., Bierkens, M.F.P., Blyth, E., de Roo, A., Döll, P., Ek, M., Famiglietti, J., Gochis, D., van de Giesen, N., Houser, P., Jaffé, P.R., Kollet, S., Lehner, B., Lettenmaier, D.P., Peters-Lidard, C., Sivapalan, M., Sheffield, J., Wade, A., Whitehead, P., E. Blyth, ... P. Whitehead E.F. Wood J.K. Roundy T.J. Troy L.P.H. van Beek M.F.P. Bierkens, 2011. Hyperresolution global land surface modeling: Meeting a grand challenge for monitoring earth's terrestrial water. Water Resour. Res. 47, W05301. doi:10.1029/2010WR010090

Wood, E.F., Sivapalan, M., Beven, K., Band, L., 1988. Effects of spatial variability and scale with implications to hydrologic modeling. J. Hydrol. 102, 29–47.

Wu, X., Walker, J.P., Rudiger, C., Panciera, R., Gao, Y., 2017. Intercomparison of Alternate Soil Moisture Downscaling Algorithms Using Active-Passive Microwave Observations. IEEE Geosci. Remote Sens. Lett. 14. doi:10.1109/LGRS.2016.2633521

Xie, X., Zhang, D., 2010. Data assimilation for distributed hydrological catchment modeling via ensemble Kalman filter. Adv. Water Resour. 33, 678–690.

Xu, X., Tolson, B.A., Li, J., Staebler, R.M., Seglenieks, F., Haghnegahdar, A., Davison, B., 2015. Assimilation of SMOS soil moisture over the Great Lakes basin. Remote Sens. Environ. 169, 163–175. doi:10.1016/j.rse.2015.08.017

Yan, H., Moradkhani, H., 2016. Combined assimilation of streamflow and satellite soil moisture with the particle filter and geostatistical modeling. Adv. Water Resour. 94, 364–378. doi:10.1016/j.advwatres.2016.06.002

Yang, G.J., Zhao, C.J., Huang, W.J., Wang, J.H., 2011. Extension of the Hapke bidirectional reflectance model to retrieve soil water content. Hydrol. Earth Syst. Sci. 15, 2317–2326.

Yapo, P.O., Gupta, H. V, Sorooshian, S., 1998. Multi-objective global optimization for hydrologic models. J. Hydrol. 204, 83–97.

Yapo, P.O., Gupta, H. V, Sorooshian, S., 1996. Automatic calibration of conceptual rainfall-runoff models: Sensitivity to calibration data. J. Hydrol. 181, 23–48.

Ye, L., Zhou, J., Zeng, X., Guo, J., Zhang, X., 2014. Multi-objective optimization for construction of prediction interval of hydrological models based on ensemble simulations. J. Hydrol. 519, 925–933.

Yilmaz, M.T., Crow, W.T., 2013. The Optimality of Potential Rescaling Approaches in Land Data Assimilation. J. Hydrometeorol. 14, 650–660. doi:10.1175/JHM-D-12-052.1

Young, P.C., 1978. Modeling, Identification and Control in Environmental Systems, in: Edited by: Vansteenkiste, G.C.N.H. (Ed.), . Amsterdam, pp. 103–135.

Zhang, C., Chu, J., Fu, G., 2013. Sobol''s sensitivity analysis for a distributed hydrological model of Yichun River Basin, China. J. Hydrol. 480, 58–68.

Zhang, D., Madsen, H., Ridler, M.E., Refsgaard, J.C., Jensen, K.H., 2015. Impact of uncertainty description on assimilating hydraulic head in the MIKE SHE distributed hydrological model. Adv. Water Resour. 86, 400–413. doi:10.1016/j.advwatres.2015.07.018

Zhang, X., Lindström, G., 1997. Development of an automatic calibration scheme for the HBV hydrological model. Hydrol. Process. 11, 1671–1682.

Zhang, X., Srinivasan, R., Zhao, K., Van Liew, M., 2009. Evaluation of global optimization algorithms for parameter calibration of a computationally intensive hydrologic model. Hydrol. Process. 23, 430–441.

Zreda, M., Shuttleworth, W.J., Zeng, X., Zweck, C., Desilets, D., Franz, T., Rosolem, R., 2012. COSMOS: The cosmic-ray soil moisture observing system. Hydrol. Earth Syst. Sci. 16. doi:10.5194/hess-16-4079-2012